SPECTROSCOPIC INVESTIGATION OF CURRENT ZERO ARC PROPERTIES

By

Saber Mohamed El-Kholy

A thesis submitted in accordance with the requirements of the University of Liverpool for the Degree of Doctor in Philosophy.

Department of Electrical Engineering and Electronics

June 1988

بسم الله الرحمن الرحيم

To my

Parents, Wife and Children

Shymaa, Mohamed, Hebh and Ahmed

ABSTRACT

The performance of a gas blast circuit breaker is governed by the extinction of the arc discharge which is formed between the contacts of the interrupter. The arc exists within the confines of a nozzle used to tailor a flow of gas for achieving the control and eventual extinction of the discharge. It has been long appreciated that measurements of the arc properties during its extinction in such a circuit breaker are important for understanding the role of various fundamental processes in causing arc extinction. However the inaccessible nature of the circuit breaker nozzle throat and complexity of the operating conditions have limited the use of sophisticated diagnostics in realistic interrupter test heads.

Spectroscopic measurements have been made during the few microseconds of the arc extinction period at the nozzle throat location where it is believed that the plasma recovery is most critical. This has been achieved through the use of an Optical Spectrum Analyser (OSA 500) capable of detecting low level light emission with microsecond exposure and with five simultaneously recorded line of sight measurements. Optical access into the confines of the interrupter nozzle without affecting the circuit breaker performance was achieved via a slot in the nozzle wall made gas tight by a window and gasket on the side remote from the arc.

Experimental investigations have thus been performed during the critical current zero period of a full power circuit breaker arc. The

significance of these results has been realised in evaluating the current zero temperature profiles and subsequently the energy conservation equation terms for severe circuit breaking conditions.

These investigations seek to exploit the results of these measurements to gain an improved understanding of the role of various physical processes during the arc extinction phase in the model interrupter.

ACKNOWLEDGEMENTS

I wish to express my sincere appreciation and gratitude to Dr. G.R. Jones, under whose supervision this work was carried out, for his guidance and encouragement throughout the project and the preparation of the thesis. My thanks extend also to Dr. M.T.C. Fang and Dr. A.N. Prasad for many interesting and stimulating conversation. Thanks are also due to Mr. B.J. Nevin and the technical staff of the Department of Electrical Engineering and Electronics of the University of Liverpool for their valuable assistance.

I wish to thank my parents, my wife, children and my family for their patience and understanding. I am very grateful to the Menoufia University, Egyptian Education Bureau in London and the Ministry of Higher Education, Egypt, for financial support.

CONTENTS

Abstract

List of figures

List of tables

Page

Chapter 1 Introduction 1

Chapter 2 Review of high current arc theory 6

2.1 Introduction 6

2.2 The LTE model 6

2.2.1 Deviation from the CTE 7

2.3 LTE relations 8

2.3.1 The relationship between the electron temperature and kinetic gas temperature 8

2.3.2 The conditions for equilibrium between the electron and excitation temperature 9

2.4 Theoretical models describing current zero arc behaviour 11

2.5 The description of the circuit breaker by empirically derived laws 40

Chapter 3 Spectroscopic diagnostic techniques 50

3.1 Introduction 50

Page

3.2 Local plasma temperature 51

3.2.1 The evaluation of suitable spectral lines 52

3.2.2 Estimation of the approximate plasma temperature during the current zero period 53

3.2.3 Plasma temperature measurements from the intensity ratio of CuI lines 54

3.2.4 Electron number density 55

3.3 Development of arc spectroscopic techniques 57

3.4 Continuum radiation 70

3.4.1 Introduction 70

3.4.2 Development of radiation power loss measurements 70

3.5 Concluding statement 74

Tables (3.1) & (3.2)

Chapter 4 Experimental apparatus and diagnostic Instrumentation 76

4.1 Introduction 76

4.2 High power SF_6 interrupter test facility 77

4.2.1 Significant properties of SF_6 78

4.2.2 Gas handling system 81

4.2.3 Pneumatic initiation facility 82

4.2.4 Test head geometry 82

4.2.5 Power supply circuit 84

Page

4.3 Instrumentation 85

4.3.1 Electrical measurements 85

4.3.2 Optical and spectroscopic measurement system 86

4.4 System control and timing sequences 88

4.4.1 Overall timing of the circuit breaker mechanism and arc current pulse 89

4.4.2 Timing of the diagnostic instrumentation particularly near current zero 90

Figs. (4.1) to (4.10)

Chapter 5 Spectroscopic measurements of the arc temperature and electron density 94

5.1 Introduction and survey spectra 94

5.2 Temperature measurements 97

5.2.1 Radially averaged spectra captured during the current zero period 97

5.2.2 Time variations of radially averaged arc temperature 98

5.2.3 Radially averaged temperature variation with current decay rates 99

5.2.4 Radially resolved arc spectra captured during the current zero period 100

5.2.5 Arc temperature profiles calculated from the radially resolved spectra 103

5.3 Occurrence of tungsten lines 108

Page

5.4 Electron density measurements 111

5.5 Chapter summary and concluding statement 112

Table (5.1)

Figs. (5.1) to (5.19)

Chapter 6 Analysis and discussion of experimental results 114

6.1 Introduction 114

6.2 The evaluation of radial temperature profiles from line of sight considerations 115

6.3 The arc behaviour before and after current zero 119

6.3.1 Introduction 119

6.3.2 The appearance of the arc column 120

6.3.3 Approximate performance trends with different pressure and different arc length 121

6.3.4 Quantitative implications of results 123

(i) The electrical conductance and core shape factors 123

(ii) LTE in the current zero arc column 128

6.3.5 Optical depth of a plasma 130

6.4 Definition of the energy conservation terms 131

6.5 The current zero energy balance 133

6.5.1 The electrical power input 134

6.5.2 The change in thermal energy stored in the arc column 135

6.5.3 Power loss due to radial thermal heat

Page

conduction across the core boundary 136

6.5.4 Power loss due to radiation 137

6.5.5 The power loss due to axial heat convection 138

6.5.6 The radial convection losses 140

6.5.7 The core power balance 141

6.6 Chapter summary and concluding statement 144

Tables (6.1) to (6.4)

Figs. (6.1) to (6.21)

Chapter 7 Summary and conclusions 148

References 153

Appendix (A.1) Computer programs 164

(A.2) Diagnostic instrumentation 167

(A.3) Optical depth 186

(A.4) Transport properties of SF_6 188

(A.5) Publications 189

(1) Optical spectra of SF_6 circuit breaker arcs during the current zero period 190

(2) Evaluation of the spectra of decaying arcs in gas blast circuit breakers 192

(3) Power dissipating processes in the current zero circuit breaker arc 194

(4) Spectral emission from copper and tungsten following high current arcing

Chapter 4 Experimental Apparatus and Diagnostic Instrumentation

Fig.4.1 Photographic view of the SF_6 test rig

Fig.4.2 Schematic diagram of the SF_6 test rig

Fig.4.3 Simplified schematic diagram of the SF_6 test rig

Fig.4.4 Schematic diagram of the SF_6 gas handling system

Fig.4.5 The test head geometry

Fig.4.6 The electrical test circuit

Fig.4.7 Schematic diagram of the general measurement system (spectroscopic system)

Fig.4.8 Optical system used for arc spectroscopy

(ai) Photography

(aii) Schematic diagram

(b) Capping shutter operation

(c) Vidicion camera details

(d) 2-dimensional scanning facility

Fig.4.9 General timing and triggering of the experimental system

(a) Arc current waveform and important timing points

(b) Schematic representation of the delay unit timing sequence

Fig.4.10 Timing system for current zero full power arc spectroscopy

(a) Schematic diagram

(b) Timing diagram.

Chapter 5 Spectroscopic measurements of the arc temperature and electron density

Fig.5.1 Arc spectrum CuI lines only

(a) Low di/dt

(b) Medium di/dt

(c) High di/dt

Fig.5.2 Arc spectrum Cu and W lines

Fig.5.3 Relative intensities of tungsten lines

Fig.5.4 Examples of radially averaged spectra for different instants during the current decay

(a) Low di/dt

(b) Medium di/dt

(c) High di/dt

Fig.5.5 Decay of the two spectral line intensities during the current zero period

Fig.5.6 Variation of radially averaged arc temperature under different arcing conditions

Fig.5.7 The variation of radially averaged temperature during the current zero period with the current decay rate (for two pressures 60 and 110 psig)

Fig.5.8 Radially resolved arc spectra during the current zero period (P = 110 psig)

(a) Low di/dt

(b) Medium di/dt

(c) High di/dt

Fig.5.9 Radially resolved arc spectra during the current zero period (P = 60 psig)

(a) Low di/dt

(b) Medium di/dt

(c) High di/dt

(d) & (e) After current zero, high di/dt

Fig.5.10 Computer flow diagram spectral analysis of shifted and asymmetric line profiles

Fig.5.11 Arc temperature profiles during the current zero period (p = 110 psig)

(a) Low di/dt (14 - 17 A/μs)

(b) Medium di/dt (18 - 21 A/μs)

(c) High di/dt (22 - 25 A/μs)

Fig.5.12 Arc temperature profiles during the current zero period (p = 60 psig)

(a) Low di/dt (14 - 17 A/μs)

(b) Medium di/dt (18 - 21 A/μs)

(c) Medium di/dt (18 - 21 A/μs) & after current zero

(d) High di/dt (22 - 25 A/μs) & after current zero

Fig.5.13 Comparison between the temperature profiles for the two pressures (p = 60 & p = 110 psig)

Fig.5.14 Time variations of the axis temperature profiles under different operating conditions

Fig.5.15 Time variations of the arc diameter under different operating conditions

Fig.5.16 Correlated results showing occurrence of W lines (p = 110 psig)

Fig.5.17 The appearance of tungsten lines during the current zero period

Fig.5.18 Correlated results showing occurrence of W lines (p = 60 psig)

Fig.5.19 The radially averaged electron density versus time, for different peak currents, during the current zero period

Chapter 6 Analysis and discussion of experimental results

Fig.6.1 (a) Representation of the cross-section of the plasma
(b) Measured and Abel inverted intensity profiles

Fig.6.2 The theoretical intensity variation of the principal diagnostic spectral lines with temperature

Fig.6.3 Conversion of the emissivity profile into a radial intensity histogram

Fig.6.4 Approximate performance trends, various upstream pressures and various gap between the two electrodes

Fig.6.5 Typical records of the time variation of current and voltage under full power conditions
(a) L_{arc} = 105 mm & p = 110 psig
(b) L_{arc} = 105 mm & p = 60 psig
(c) L_{arc} = 65 mm & p = 110 psig
(d) L_{arc} = 65 mm & p = 60 psig

Fig.6.6 Approximate performance trends, 35 mm throat nozzle, various nozzle materials, SF_6 and air, f = 78 Hz. (source Taylor et al (1982))

Fig.6.7 The overall conductance shape factor (Λ_c) variation with Nusselt number (Nu) for different arc types

Fig.6.8 The core conductance shape factor (λ_c) variation with Nusselt number (Nu) for different arc types

Fig.6.9 Justification of existence of L.T.E.

Fig.6.10 Optical depth of the plasma versus temperature for CuI diagnostic lines

Fig.6.11 Electrical power input variation with the time before and after current zero

Fig.6.12 Thermal energy stored variation with the time before and after current zero

Fig.6.13 Thermal heat conduction loss v time before and after current zero

Fig.6.14 Total radiation v instantaneous current (source Shammas private comm.) (p = 110 psig) slot 2 & slot 3

Fig.6.15 Total radiation v instantaneous current (source Shammas private comm.) (p = 60 psig) slot 2 & slot 3

Fig.6.16 The total radiation loss v time before and after current zero

Fig.6.17 Summary of temporal arc area and intensity decay during the current zero period (Source Lewis (1987))

Fig.6.18 The axial heat convection loss vs. time before current zero at different pressures and different di/dt

Fig.6.19 The radial heat convection loss vs. time before current zero at different pressures and different di/dt

Fig.6.20 Comparison of the various power loss terms during the current zero period

(a) p = 110 psig & di/dt = 15 A/μs

(b) p = 110 psig & di/dt = 20 A/μs

(c) p = 60 psig & di/dt = 15 A/μs

(d) p = 60 psig & di/dt = 20 A/μs

Fig.6.21 Variation of the power loss terms in the core power balance with di/dt and different pressures at the same time before current zero

(a) t = - 3 μs

(b) t = -10 μs

Appendix (A.1) Computer programs

Fig.A.1.1 Program structure for interpretation of data into radially averaged temperature and evaluation of theoretical line intensity and optical depth

Appendix (A.3) Optical depth

Fig.A.3.1 CuI and electron densities for different plasma composition (Source : Kinsinger unpublished)

Appendix (A.4) Transport properties of SF_6

Fig.A.4.1 The transport properties of SF_6 (p = 4 atm)

Fig.A.4.2 The transport properties of SF_6 (p = 2 atm)

Fig.A.4.3 Variation of sonic velocity in SF_6 with temperature at different pressures

LIST OF TABLES

Table (3.1) Atomic data for the spectral lines of CuI (Source : Kock and Richter (1968))

Table (3.2) Stark broadening of CuI lines

Table (5.1) Wavelength, Energy levels and gA values of tungsten atomic lines appear in the spectra

Table (6.1) Summary of the thermal transport properties used in this chapter

Table (6.2) Summary of the overall conductance shape factor and the core shape factor during the current zero period (p = 60 psig)

Table (6.3) The thermal transport properties (Reference Frost & Liebermann (1971))

Table (6.4) Summary of the power terms in the current zero energy balance for different operating conditions

(a) p = 110 psig

(b) p = 60 psig

CHAPTER 1

INTRODUCTION

In any electrical system there is always, at one time or another, the need to isolate a certain portion of the system from the rest. For example, one may need to deenergize a load or to isolate a faulted portion of the system so that the equipment or the line can be repaired. A switching device is needed to perform such a function. In some special applications this function can be served by semiconductor devices or by vacuum tubes. However, in the case of high power transmission and distribution systems, this function is served by an electromechanical device more commonly known as a switch or a circuit breaker. Because of the low impedance of such networks very high short-circuit currents can be produced which would damage the installation in a short time. It is the task of a circuit breaker to switch off quickly and with high reliability the faulted part of such a network.

The operation of such a device is well known. Fundamentally, there is a pair of electrical contacts, one movable and the other usually stationary. The movable contact is actuated by a mechanism. So that when the contacts are closed, the electric circuit is completed by metallic conduction. In order to interrupt the circuit, the movable contact is drawn away from the stationary one. During this process an electrical arc is formed between the contacts. Being a high tem-

perature ionized gas (plasma), the arc continues to carry the current. Until the arc is extinguished in one way or another, the electric circuit is not interrupted because of the finite electrical conduction of the plasma. Thus, the physical process of circuit interruption is one of changing a highly conducting plasma into an insulating gas in a controlled manner.

An important criterion when comparing different circuit breakers is the way in which the arc is treated. In the case of high voltage circuit breakers the arc is made to burn in a strong gas flow along the arc axis. This is achieved by igniting the arc in a nozzle with supersonic flow conditions. This serves the dual purpose of controlling the arc during the peak current phase and causing arc extinction at the current zero at the end of alternating current cycle, when the voltage inducing capacity of the inductive system is at its lowest. In the case of low voltage circuit breakers the arc is moved transverse to its axis by a transverse magnetic field driving the arc into a grid of metal plates where a relatively high voltage required to sustain the arc. This serves to limit the current flow and leads to subsequent arc extinction.

To achieve such a successful interruption, sufficient energy must be removed in order to keep the electrical conductance of the recovering arc in the contact gap as low as possible so that reignition due to joule heating caused by residual current flow is avoided. In addition a subsequent recovery of the insulation properties is required

to prevent dielectric breakdown by the voltage across the arcing gap produced by the network reaction to the current interruption.

For the above reasons the medium in which the arc is formed is important in determining the electrical performance limitations of a circuit breaker. Sulphur hexafluoride (SF_6) and air (or N_2) are the two most common working gases for gas blast arcs used in high voltage circuit breakers. Of the two, SF_6 has proven to be superior in its interrupting abilities against both thermal and dielectric reignitions (Ragaller (1978)). SF_6 has a much greater dielectric strength than air at the same pressure. These improvements are due mainly to the large electron attachment coefficient of the SF_6 molecule : thus the probability of an electron accelerated in an electric field causing ionisation and breakdown by fast collision is much reduced (Airey (1977)). The influence of the medium is manifest through its thermodynamic and aerodynamic properties prior to current zero, the first few microseconds thereafter, and its dielectric properties during the voltage restrike period. Thus as power system voltages have increased, the ability of a circuit breaker to interrupt increasing short circuit fault currents and withstand greater voltage has necessitated improving and changing circuit breaker designs.

Over the last 25 years the use of air has been further superseded by SF_6 gas as an arcing medium for the above reasons, the first SF_6 production breakers being developed by Westinghouse (Friedrich et al, 1957) and (Leeds et al, 1957). SF_6 also has a low ionisation energy and a high affinity for electrons during deionisation which

makes it an ideal arc quenching medium. These properties enable a lower pressure or a higher rating per break unit to be used compared to the equivalent air circuit breaker. SF_6 has therefore been used for all the experiments carried out in the present investigations.

The model circuit breaker, the power supply circuit and the measuring system employed are described in detail in Chapter (4). The power supply circuit provided peak sinusoidal currents in the range 34-64 KA at a frequency of 78 Hz. The model circuit breaker was of the two pressure monoflow SF_6 type using an upstream pressure of both 7.8 bar and 4.25 bar, and downstream pressure of 1 bar. The contacts of the circuit breaker were made from copper-tungsten, and the nozzle was made from PTFE. A 3 mm high slot situated at the nozzle throat permitted the arc radiation to be studied. This was achieved by focusing the radiation at the entrance slit of a monochromator to provide spectral resolution of the radiation. This monochromator had a 1 m focal length and a 0.82 nm/mm reciprocal dispersion. The width of the entrance slit of the monochromator was 28.5 μm. The spectrum on the exit plane of the monochromator was detected and recorded by an Optical Spectrum Analyser with Vidicon Camera SIT 500.

The aim of the present work has been to obtain the arc dimensions, to measure the radial temperature profile and electron density variations during the current zero period using the spectrally resolved radiation from the arc. From the radial temperature profile derived from these diagnostic techniques the transient variation of arc prop-

erties could be derived. The purpose of the electron density measurements has been mainly to establish whether local thermodynamic equilibrium (LTE) conditions exist in the arc plasma during the current zero period. Since the energy loss terms can, in principle, be related, through equilibrium calculations, to the temperature profile, the acquisition of this parameter is a major aid to the quantitative solution of the energy balance equation (Chapter 6). Additionally a quantitative evaluation of parameters used in theoretical arc models such as those based upon boundary layer integral analyses (Walmsly et al 1978(ii)) can be made.

This thesis contains 7 chapters. The literature on theoretical models describing current zero arc behaviour, the LTE model, and the description of the circuit breaker by empirical derived laws are reviewed in chapter (2). The development of arc spectroscopic techniques, and radiation power loss measurements are reviewed in chapter (3).

The spectroscopic investigation enabled direct localised arc column intensity measurements to be made with radial (and spectral) resolution and a time exposure of 1.6 μs such that radial temperature profiles during the current zero period could be derived. The instrumentation pertaining to this investigation is described in chapter (4) and the results obtained are presented in chapter (5). The analysis and discussion of experimental results are presented in chapter (6). This thesis is concluded by chapter (7) which outlines the more important aspects of this research.

CHAPTER 2

REVIEW OF HIGH CURRENT ARC THEORY

2.1 Introduction

This chapter presents a review of published work concerned with arcs burning in an accelerating flow of gas and particularly the current zero behaviour of the gas blast circuit breaker arc. It is divided into three main sections. The first is concerned with Local Thermal Equilibrium (LTE) model. The second is devoted to the evaluation of theoretical models describing the current zero arc behaviour. In the last section a review of interrupter design and development by means of empirical laws which were derived directly from experimentally observed phenomena are reported. The latter involves principally the measurement of overall arc parameters such as current and arc voltage. In particular, the development of optical measurements as a useful diagnostic technique and their significance with respect to interruptor development is considered.

2.2 The LTE model

The concept of local thermodynamic equilibrium (LTE) plays a vital role in plasma physics and particularly plasma spectroscopy. With the assumption of local thermodynamic (or thermal) equilibrium all particle densities - neutral particles as well as ions - can be calculated

from total densities and temperature. LTE is a special case of a more general problem related to the concept of (complete) thermodynamic equilibrium (CTE). If all the physical processes occurring inside an arc are reversible, the arc is said to be in CTE, which is characterised by :

(i) The velocity distribution of all particles is according to Maxwell-Boltzmann and the distribution of internal energy obeys Boltzmann's distribution.

(ii) The distribution of the atoms and their ionization products (ions and electrons) obeys the Saha-Eggert equation, which is a special case of the mass action law.

(iii) A unique temperature for all species inside the arc.

(iv) Radiation field within the arc follows Planck's law for black body

For an arc in LTE, all thermodynamic quantities are unique functions of two thermodynamic variables. Thus, an arc can be treated as an electrically conducting fluid. This forms the basis upon which the models described in section 2-4 are based and its consideration is important for the spectroscopic measurements presented later in this thesis. The LTE assumption is usually not valid for the region close to electrodes, where the electrical field strength is much higher than that of arc column (Zhang 1986).

2.2.1 Deviation from the CTE

However, the arc in CTE does not exist in practice although it can be a good approximation for certain arcs. Many factors make an arc

deviate from that in CTE : firstly an arc occupies a finite space. Thus, the radiation field is diluted at certain frequences at which the arc is optically thin. Secondly, there usually exists a net transport of mass, momentum and energy within the arc and with its surroundings. For example, the arc may be sustained by Ohmic heating in practice and the non-uniformity within the arc and the imposed gas motion leads to energy transfer. Thirdly, in many practical cases arc discharge conditions vary rapidly and the arc is in a transient state. Thus, some physical processes may not attain equilibrium. Fortunately, for high pressure (> 1 bar) arc columns, which are often encountered in industrial situations, the departure from CTE is not severe.

2.3 LTE relations

The purpose of this section is to detail working relationships for equilibrium between the electron energy distribution and the individual kinetic and internal energy distributions of the gas atoms and ions. For brevity we shall include calculations using the derived equations and the arc parameters given in chapters 5 and 6.

2.3.1 The relationship between the electron temperature and kinetic gas temperature

When the plasma is heated by electrons, the latter continuously gain surplus energy from the field and a total transfer of this energy to the gas atoms and ions (equilibrium) is never completely realised.

The electron temperature T_e will always be greater than the gas temperature T_g. A stationary state is reached when the temperature difference, $T_e - T_g$, is equal to the energy gain , λeE, from the field E where λ is the mean free path and e the electron charge. Lochte-Holtgreven (1968, p 147) has derived the following expression for the average elastic collision

$$(T_e - T_g)/T_e = [(\lambda eE)/(3KT_e/2)\ ]^2(m/4m_e) \qquad (2.1)$$

For a quantitative solution of equation (2.1) the mean free path is given by

$$\lambda = 1 / Q\ N_e \qquad (2.2)$$

Where Q is the electron/atom or electron/ion collision cross-section and can be obtained from the following equation (Airey 1977).

$$Q_{ie} = e^4/(KT_e)^2 Ln[(4KT_e) / (e^2N_e)^{1/3}] \qquad (2.3)$$

Where

N_e is the particle number density (m^{-3}).

2.3.2 The conditions for equilibrium between the electron and excitation temperature

The formulae for calculating the plasma temperature presented in this thesis are based upon the assumption of the existence of LTE in

the region of interest in the plasma. LTE may not exist in an optically thin plasma because the energetic emission of photons is not balanced by its inverse process (absorption). It is therefore desirable to be able to test for the existence of LTE in this case. This is possible through the application of certain LTE criteria to the arc plasma. Two criteria are discussed here, namely McWhirter's criterion and Griem's criterion.

In the case of the circuit breaker arc plasma of this investigation it is the electrons which are the major collision - causing particles. Thus it is the electron density and plasma temperature which form the two primary variables in the consideration of LTE criteria. The first of the two criteria which needs to be considered is McWhirter's criterion (Leonard (1965)). By considering the energy threshold for excitation of ions and the spontaneous transition probability of a photon with energy, ΔE_{mn}, McWhirter has derived the expression

$$N_e \geq 1.6 \times 10^{12} T_e^{1/2} (\Delta E_{mn})^3 \qquad (2.4)$$

Where the units of N_e and ΔE_{mn} are cm^{-3} and eV respectively.

The second criteria is provided by the Griem formulation (Lochte - Holtgreven, 1968). This is based upon the hypothesis that the collisional excitation rate should exceed the radiative decay rate by an order of magnitude. An expression is developed for each transition rate, one of which contains N_e, the electron density. An inequality is formed on the basis of the above hypothesis and the Boltzmann

equation is invoked to close the set of equation. The final formulation becomes :

$$N_e \geq 9 \times 10^{17} [E_2^{z-1,a} / E_H]^3 [KT / E_H]^{1/2} \qquad (2.5)$$

Where

N_e is the electron density (cm^{-3}).

$E_2^{Z-1,a}$ is the first excited level (upper resonance level eV)

E_H is the ionization energy (eV)

It is clearly that Griem's criterion (1964) represents the most severe test. The two criteria will be applied carefully and discussed in chapter (6).

2.4 Theoretical models describing current zero arc behaviour

In the early 1900's it was impossible to explain why, under similar conditions of KVA and system voltage, duplicate circuit breakers gave a wide variation in performance when installed in different circuits, even though they behaved relatively consistently when tested repeatedly on the same plant. It was not until 1927, when the cathode ray oscilloscope was first used in testing that these inconsistencies were attributed to high frequency voltage oscillations (" the transient restrike voltage"), following a current zero (Rieder 1972). Such tests showed that the frequency of this transient was determined by the shunt capacitance and the series inductance of the external circuit to which the breaker was coupled so that not surprisingly the re-

striking behaviour would vary with system design. In 1927 the relatively fast recording capability of the C.R.O. enabled these transients to be observed and the apparent anomaly explained in terms of post current zero severity.

The existence of such phenomena has been recognised for some years and various authors (reviewed by Flurscheim, 1935) have advanced theories that these transients could affect circuit breaker operation. The most notable of these was due to Slepian whose paper in 1928 marked the start of theoretical work on the description of arc interruption processes in a.c. circuit breakers.

Slepian's explanation, which became known as the " race theory " (Slepian, 1928 and 1930), suggested that the success of current interruption depended upon the result of a race between two independent voltages; the restriking voltage (dielectric strength) of the arc path after current zero, governed by the circuit breaker only, and the recovery voltage across the breaker, governed by the circuit only. The conditions of the arc gap at current zero were assumed to be solely dependent upon the circuit breaker and the inherent di/dt of the sinusoidal current. Although the " race " concept remains valid, Slepian's theory was disproved through the observation that circuit breakers could withstand a faster rate of rise of recovery voltage (large dielectric strength) than predicted by Slepian's theory. Slepian (1941) responded to this by accounting for the increased rrrv withstand by the molecular diffusion of cool material through turbulent mixing of the plasma.

In 1931 Prince and Skeats who, working independently of Slepian, advanced a theory which became known as the " displacement " or " wedge " theory. This theory stated that the criterion for successful current interruption was the occurrence of a finite break in the conducting plasma at some critical position in the arc column at current zero. The two resulting arc sections, each terminated on an electrode and each electrically conducting, were then assumed to be separated by a growing wedge of un-ionized dielectric. The maximum rrrv in volts per second, which could appear across the contact gap without causing reignition was therefore predicted as being equal to the impulse strength of the inserting dielectric, in volts per mm, multiplied by the relative velocity of the separating arc sections, in mm per sec. Although agreement was evident with cross blast circuit breakers, the theory was disproved by Slepian who cited the high speed photographs of Biermanns (1932) showing a continuous arc column at current zero (post arc current) which could not flow according to the displacement theory.

Cassie (1953) presented experimental evidence which invalidated Slepian's (1941) claims that turbulence played a major role in enhancing arc column recovery. Firstly, high speed photographs of the arc column around current zero showed that the arc maintained a narrow, continuous form, whereas at higher values of instantaneous arc current, the arc column sometimes appeared to break up. This suggested that if turbulence was important it appeared at larger arc diameters than those observed at current zero. Secondly, no corre-

sponding increase was observed in arc voltage in the period when turbulence had been observed.

The two theories described above could not accommodate the possibility of a continuous conducting channel giving rise to post current zero conductance. In (1939) Cassie proposed the first form of dynamic arc model to be followed by Mayr's (1943) alternative model, developed from a separate set of energy assumptions. These latter theories developed dynamic equilibrium energy equations describing arc gap conditions during the current zero period and hence allowing the form of the arc conductance decay to be predicted. Both models were based on the assumption that the arc conductance was a function of arc power input, arc power loss and time. Thus the general equation characterising both arc models can be written as:

$$1/R = f (W, N, t) \qquad (2.6)$$

Where

R is the arc resistance per unit length

W is the arc power input per unit length

N is the arc power loss per unit length

t is the time

Browne (1948) proceeded to show that both authors, in arriving at their respective final models, further assumed

$$1/R = F (Q) = F \left(\int_0^t (W - N) \, dt \right) \qquad (2.7)$$

Where

Q is the energy content per unit length

$$Q = \int_0^t (W - N) \, dt \qquad (2.8)$$

Equation (2.7) can be differentiated to establish a more general form for use in arc modelling

$$R \, (d/dt)[1/R] = (F'(Q)/F(Q)) \times (dQ/dt)$$
$$= (F'(Q)/F(Q)) \times (W - N) \qquad (2.9)$$

The specific form of this differential equation will now depend upon the particular forms selected for F(Q) and N, since W, will be specified by the product of instantaneous electric field and instantaneous arc current.

Cassie (1939) formulated his model with the following set of assumptions :

(1) The arc column is surrounded by an axial flow without any mutual interaction occurring.

(2) There is a heat flux from the arc to the surrounding gas flow in the radial direction only.

(3) The arc cylindrical column is regarded to have uniform temperature with constant electrical resistivity (δ) and energy content (q) per unit volume.

(4) The arc column is enclosed by a well defined boundary outside which the conductivity is zero.

(5) The arc cross-sectional area undergoes change to accommodate changes in current but the arc temperature remains constant.

(6) The power loss is proportional to the column cross-section thus

$$N = \lambda A$$

Where

λ is the power loss per unit volume

A is the column cross-sectional area

Therefore

$$W-N = (E^2/R) - \lambda A = (E^2 - \rho\lambda)/R \qquad (2.10)$$

Also

$$Q = qA = (q\rho)/R$$

Therefore

$$1/R = Q/q\rho = F(Q) \qquad (2.11)$$

which upon substitution into equation (2.9) gave Cassie's dynamic arc equation

$$R(d/dt)[1/R] = (\lambda/q)[(E^2/\lambda\rho) - 1]$$
$$= (1/\theta_c)[(E^2/\lambda\rho) - 1] \qquad (2.12)$$

Where

θ_c has units of time and is called the Cassie time constant.

Mayr (1943) based his model upon an alternative set of assumptions which were:

(1) There is no gas flowing around the arc.

(2) The arc column is cylindrically symmetrical with a constant area A in space and time.

(3) Thermal losses occur in a radial direction only and obey the Fourier Law of heat conduction.

(4) To accommodate changes in current the conductivity is allowed to vary with temperature according to a much simplified Saha equation, namely

$$1/R = K_1 \exp(-\alpha/T) \tag{2.13}$$

Where

K_1 and α are constants.

Introducing these assumptions into equation (2.9) gives Mayr's dynamic arc equation

$$R\,(d/dt)[1/R] = (N_o/Q_o)[(W/N_o) - 1]$$
$$= (1/\theta_M)[(W/N_o) - 1]$$

Therefore

$$R\,(d/dt)[1/R] = (1/\theta_M)[(E^2/RN_o) - 1] \tag{2.14}$$

Where

E is the instantaneous electric field.

N_o is the power dissipated by thermal heat conduction and is constant.

$\theta_M = Q_o/N_o$ is the Mayr time constant.

Q_o is constant.

Both Cassie and Mayr claimed good qualitative agreement between the form of the decaying arc conductance predicted by the energy balance equations and their respective experimental observations.

A composite arc model encompassing both the Cassie and Mayr equations was proposed by Browne (1948). This author indicated, by comparison with experiment, that Cassie's equation was superior in describing arc behaviour during the pre-current zero period whereas Mayr's equation became superior following current zero.

However, Browne's (1948) model was open to criticism in many ways. Initially, if the steady state condition is applied to the Cassie model before current zero (eq. 2.12) then the relationship $E = \sqrt{(\rho\lambda)}$ emerges with ρ and λ constant and independent of instantaneous current. Consequently the Cassie equation cannot predict the increase in electric field which occurs just before current zero in the case of a good interruption. Secondly, Browne (1948) defines his criterion for the critical electric field to cause reignition as being the instantaneous voltage required to hold the conductance constant, a condition synonymous with the dielectric definition quoted originally by Slepian (1930) rather than continuing the original theme of a power balance.

This criterion yielded incorrect values of critical electric field strength when either the Cassie or Mayr equation was applied to the real circuit breaking case. An original criticism of Browne's work came from Skeats (1948) who objected to the concept of describing arc behaviour before and after current zero by separate arc models derived from completely incompatible assumptions. It will be shown in chapter (5) that in practice both arc column area and arc temperature may collapse simultaneously during the final few microseconds before current zero.

In response to these criticisms Cassie and Mason (1956) proposed a new model which was based upon Cassie's original model with the inclusion of a constant power loss from the arc column by thermal conduction (Mayr's assumption). Although Cassie and Mason (1956) claimed to have obtained good agreement with experiment using this model, Browne (1959) however claimed it was too complex to be used as an efficient arc model. This author then continued to apply Mayr's arc equation in the post current zero period and, again using Slepian's definitions to characterise reignition, he obtained simple equations giving the critical reignition voltage in terms of the arc voltage, the Mayr time constant and the circuit time constant, for various types of recovery voltage waveform.

Browne's model, including Slepian's definition of critical electric field strength, was disproved when measurements showed that arcs could still be quenched despite the post zero conductance initially increasing during the imposition of the TRV. Thus the importance of

incorporating the electrical interaction processes between the arc and the external circuit was realised and dynamic arc models were augmented to include this effect. The first author to achieve a reasonable agreement with the real circuit breaker test results was Kopplin (1962) who used an analog computer to solve a pair of simultaneous non-linear differential equations, one describing the circuit, the other the arc (Browne's (1948) model). He presented his results in the form of two non-dimensionalised quantities representing a time constant and heat dissipation. Kopplin (1962) plotted these two quantities and defined a boundary on the plot which he claimed discriminated between thermal reignition and extinction. The agreement with experimental results was however limited.

Cassie's (1939) and Mayr's (1943) original equations have been used by other researchers in attempts to achieve closer agreement with the experimentally observed phenomena during the current zero period. However these have proved unsuccessful owing to over simplification leading to poor accuracy (when compared with experimental measurements) or the increment of prohibitive mathematical complexity (preventing the model from being capable of predicting interruptor behaviour during the current zero period). Clearly only limited success could be obtained by the use of these early models for interruptor behaviour predictions and superior methods of approach would be required if closer agreement with test results was to be obtained.

A good understanding of gas blast arc behaviour, both during the high current and current zero periods, have resulted from the application of boundary layer approximations to the conservation equations governing arc behaviour in an axial gas flow. A boundary layer formulation of the pertinent equations is considered acceptable only when the gradients of properties in the radial direction are much larger than those in the axial direction; a situation which exists in the gas blast arc.

The first authors to apply a boundary layer analysis to the energy equation of an arc in a circuit breaker nozzle were Swanson and Roidt. These authors develop in a series of papers (Swanson et al 1970, 1971, 1971a, 1972) and (Swanson and Roidt 1971, 1972) two equations which they claim define the maximum RRRV that can be applied across the arc gap of a gas blast circuit breaker, after current zero, without reignition taking place. The two equations are derived from separate assumptions regarding the functional relationship between electrical conductivity and heat flux potential within the arc core.

Swanson and Roidt (1971) started their analysis by assuming that the energy transfer processes cooling the arc column at each axial station between the nozzle throat and upstream electrode are :

(a) radial convection ($\rho v \partial h/\partial r$).

(b) axial convection ($\rho u \partial h/\partial x$).

(c) expansion cooling (assumed proportional to the material derivative of pressure) $[1-\rho(\partial h/\partial P)_T]u(dP/dx)$.

(d) radial diffusion $(1/r)(\partial/\partial r)[r((\mu/p_r)+(\rho_t\varepsilon_m/p_{rt}))(\partial h/\partial r)]$

(e) radiation (W(P,T)).

So that the energy equation takes the form

$$\rho(\partial h/\partial t) + \rho v(\partial h/\partial r) + \rho u(\partial h/\partial x) = [1-\rho(\partial h/\partial P)_T]u(dP/dx) - W(P,T) + (1/r)(\partial/\partial r)[r((\mu/p_r)+(\rho_t\varepsilon_m/ p_{rt}))(\partial h/\partial r)] + \sigma E^2 \qquad (2.15)$$

Where

the first term in equation (2.15) is the storage and the last term is the Joule heating.

ρ is the density.

h is the enthalpy.

v is the radial velocity.

u is the axial velocity.

p is the pressure.

W is the radiated power per unit volume.

ε_m is the eddy diffusivity for momentum.

P_{rt} is the turbulent Prandtl number.

σ is the electrical conductivity.

E is the voltage gradient.

Using boundary layer techniques (i.e. radial integration across the conducting arc core) their assumed energy equation is then transformed into a partial differential equation describing the axial distribution of dynamic arc radius within the upstream section of a

circuit breaker nozzle. Appearing within this equation are two coefficients which represent the ratio of

a) excess energy density stored in the arc column

b) magnitude of radial energy losses

to the energy loss due to axial convection. Each energy term is expressed as an integral evaluated across the conducting arc radius. To obtain a solution of the equation for arc radius Swanson and Roidt make two assumptions :

(1) The radial integrals which are contained in the coefficient of the radius terms are regarded constant for assumed average radial temperature profiles.

(2) The term accounting for radial energy losses N(x,t,R) is assumed to vary with R only. Consequently the change in thermally stored energy is accounted for by changes in arc radius only.

Incorporating the above assumptions and starting from a quasi-steady (d/dt=0) solution for the arc radius at peak current, the dynamic arc equation is solved for a linear current ramp to obtain the arc radius, within the nozzle throat , at current zero. Two separate solutions to this equation are obtained by firstly allowing only axial convection to be the dominant energy loss process and then secondly allowing axial convection to be augmented by radial losses. For both of these conditions the current zero arc radius is determined as equal to the peak current arc radius attenuated by certain heat transfer parameters. By substituting each of the solutions for the current zero arc radius at the nozzle throat, into the equation for the thermal time constant of an arc controlled by turbulent diffusion, (Frind 1960),

Swanson and Roidt (1971) propose two expressions claimed to represent the thermal time constant of the arc in the nozzle throat at current zero for

(a) the arc controlled by axial convection.

(b) the arc controlled by diffusion losses.

The proceeding expressions are used in a comparison paper (Swanson, Roidt and Browne, 1971) where interruption criteria are established for the case of short line faults (Rieder, 1972). In this publication the authors were concerned with the arc at the current zero period during which a linear RRRV is imposed.

Swanson et al (1971) make the assumption that during this post arc period energy loss from the narrow column is governed by turbulent and molecular diffusion and that axial convection may be neglected. They also state that energy growth in the arc column is by Joule heating (σE^2) which is proportional to the column conductivity (σ). Above 8000 °K the variation of electrical conductivity σ is taken as linear whereas the variation below 8000 °K is taken as exponential. Thus Swanson et al (1971) state that above 8000 °K the arc energy can be transformed into a " Cassie " type integral equation for post arc current whereas below 8000 °K the same equation can be transformed into a " Mayr " type equation for post arc resistance. The criterion for interruption to occur is that the time derivative of post arc current should reach zero at some instant after current zero. From this condition a critical thermal time constant is established. This is then equated to convection and a diffusion controlled arc time constant

obtained by Swanson and Roidt (1971) to determine the value of maximum RRRV which can be imposed without reignition occurring. From the Mayr type solution a criterion is also established whereby interruption must occur. This is that for successful interruption the time derivative the post zero arc resistance must reach zero at some instant. A critical time constant is thus established in a similar manner as indicated above in this case. By further equating this to the arc time constants derived by Swanson and Roidt (1971) another maximum value of RRRV is obtained. Swanson et al (1971) further conclude that from the Cassie and Mayr type equations the maximum RRRV shows the following relationships :

(1) approximately proportional to gas pressure.

(2) proportional to the effective nozzle arc length at current zero and to the number of nozzle arc gaps connected in series.

(3) proportional to the coefficients which are functions of the gas properties.

(4) inversely proportional to $(di/dt)^m$ where m = 3/2 for the Cassie type solution and m = 1 for the Mayr type solution.

A further publication (Swanson et al 1972) incorporates the basic concepts presented above with improved arc models. However, basic inconsistencies are still inherent in the overall approach. These include :

(1) The criterion involving a zero rate of change of post arc current is not in itself a necessary and sufficient condition for interruption. The criterion regarding the zero rate of change of post arc resistance is also erroneous.

(2) Chapman (1977) in his measurement of localised arc behaviour has shown that the definition of an effective nozzle length to be unrepresentative in the case of real circuit breaker arcs.

(3) The time constants used to define the maximum RRRV were derived by the use of different energy transport assumptions and originate from different time periods with respect to current zero.

(4) Unrealistic assumptions regarding radial distributions (Bessel functions) of arc properties are made which are mutually inconsistent and not representative of the true physical situation.

(5) The expression for the dynamic variation of heat flux potential is dependent on the dynamic resistance equation (Swanson and Roidt, 1972). Swanson (1977) proceeds to calculate arc radii and axial temperature from this pair of equations (Swanson, 1977) which is rigorously invalid.

(6) It will be shown experimentally in this thesis that to consider the arc temperature constant and allow the arc area to collapse alone is not representative of the case of a real circuit breaker arc (chapter 5). This is particularly true close to current zero and one effect of making the constant temperature assumption is to artificially increase the arc thermal time constant.

A further attempt to describe the transient behaviour of the low current arc burning in an accelerating gas flow has been made by Topham in a series of publications (Topham 1971, 1972a, 1972b and 1973). Topham (1971) formulated a theory on the basis of the following assumptions for a steady state, laminar flow arc in a constant pressure axial flow :

(1) Arcs at atmospheric pressure and above can be described by equilibrium thermodynamics and the continuum equations of fluid dynamics.

(2) Radiation power loss can be neglected.

(3) Self - magnetic pinch pressure is neglected.

(4) Electrode effects can be neglected. In practice these can never be eliminated and, although the regions directly affected by the anode and cathode may be small, the upstream electrode produces an aerodynamic wake which can significantly affect the arc voltage distribution. This is most noticeable when the arc diameter is smaller than the wake diameter. In addition, vaporised electrode material is also present which lowers the ionization potential of the gas. In practice, melting of the electrode sets a lower limit to the electrode diameter.

(5) The main flow is unchanged by the presence of the arc, which is axisymmetric and in a steady state with laminar flow throughout.

(6) The boundary - layer approximations are valid. These can be applied to situations in which the radial derivatives are large compared with the axial ones.

This author uses the dynamic arc energy equation standard integral from (Schlichting, 1958) and simplifies his analysis by assuming a linear - pressure - gradient distribution along the arc gap. Topham states that this simulates the pressure condition near the throat of a practical circuit breaker nozzle. The energy conservation equation was non-dimensionalized by dividing every parameter within each term

of the equation by its value at the 4000 °K boundary of the arc in pure nitrogen.

The solution of the final arc equation required on exact knowledge of the transient forms of the two non-dimensional integrals which in turn required a knowledge of the transient variations of the radial temperature and velocity profiles of the flow. Due to a lack of experimental data Topham (1971) derived a radial temperature profile from the Elenbaas-Heller equation which the author claims to be only slightly modified by axial convection. This profile is claimed to be a good approximation to the temperature profile of a circuit breaker arc below 100 A. The solution shows that the variation of arc voltage gradient with current is uniquely related to its variation with the flow conditions and arc length, the arc being represented by a single non-dimensional characteristic.

The analysis has been extended to the effect of pressure gradients on the arc characteristics by Topham (1972a). The flows discussed have a stagnation point at the origin, and the solutions are expressed in terms of the same non-dimensional parameters as for the constant pressure flow arc. In this analysis some additional assumptions are made :

(7) The calculations are performed for laminar flow, although the method can in principle be applied to turbulent flow .

(8) Viscous forces are small compared with the pressure and inertia forces.

(9) The kinetic energy of the flow is small compared to the thermal energy allowing the pressure work and viscous heating terms to be neglected in the energy equation.

Topham (1972b) attempted to adapt his analysis to the transient case of a circuit breaker arc in the current zero period. In this publication he further reduced the energy equation for the case of a linear pressure gradient and represented it in non-dimensional. To obtain simple solutions of the energy balance a number of drastic simplifications were made. The steady-state velocity and temperature profiles were used as approximations for the calculation of the non-dimensional integrals, which were further assumed to be a unique function of G^*, the non-dimensional electrical conductance.

With these assumptions the dynamic arc equation takes the form :

$$d(g_2^*)/dt^* + g_1^* = I^{*2}/ G^* \qquad (2.16)$$

Where

I^* is the non-dimensional current

t^* is the non-dimensional time

g_1^*, g_2^* } non-dimensional integrals representing heat loss and heat storage function respectively.

G^* is the non-dimensional conductance.

For certain analytical forms of the functions g_1^* and g_2^* equation (2.16) was reduced to the Bernoulli type equation. If the functions g_1^* and g_2^* are the linearly related power laws.

$$g_1^* = a_1 G^{*m}$$

$$g_2^* = a_2 G^{*m}$$

The arc energy equation becomes :

$$dG^*/dt^* = (1/a_2 m)(I^{*2}/G^{*m}) - (a_1/a_2 m)G^* \qquad (2.17)$$

Where

a_1, a_2 and m are constants.

Topham (1972b) was able to determine approximate values for a_1, a_2 and m which provided characteristics near those of the real gas. Topham also showed that the simple power law model embodied both Cassie's and Mayr's arc equation. These could be obtained simply by assigning specific values to the constants a_1, a_2 and m.

Using the power low model, and extending the non-dimensional scheme to include test circuit parameters, Topham (1972b) was able to solve for the transient variation of arc current and voltage during the current zero period in a simple busbar circuit. The results of these calculations showed good qualitative agreement with the known current zero behaviour of gas blast arcs, (Chapman et al 1975) and allowed a unique set of clearance / failure boundaries to be constructed. These curves represented all combinations of gas-flow variables and circuit values.

The lack of experimental data which existed when this model was developed forced the author into making drastic assumptions for the radial property profiles for the dynamic model. The work presented here (chapter 5) provides such much required data for SF_6 arcs and in particular establishes the shape of the temperature profile above the 5,500 °K isotherm of an SF_6 gasblast arc during the current zero period.

Topham (1973) has also presented a similar dynamic analysis for the case of a constant pressure flow arc. The dynamic equation obviously becomes simpler in this case since the axial flow velocity is constant everywhere and therefore $g_1^* = g_2^*$. However, the results obtained from these calculations cannot be used to describe gas blast circuit breaker operation since processes enhanced by gas acceleration are obviously not included in the analysis.

A numerical model to describe the pre current zero decay of the arc in a gas blast interrupter has been constructed by Kinsinger (1974). In this model consideration is given to the various processes Kinsinger regards as dominant during the interruption process. These processes are ohmic heating, radial thermal conduction, radial thermal convection, radiation transport and viscous heating.

In formulating his model Kinsinger (1974) obviously regards the radial loss processes to occur on a much smaller time scale than those processes associated with the axial flow gradients. Kinsinger commences his calculation at a current level of 200 A, decaying at a rate

of 20 A/μs implying that the radial loss processes dominate at 10 μs before current zero. Consequently Kinsinger's inclusion of turbulence to bring his theoretical predictions in line with experiment may not be totally justified.

Because of the arbitrary inclusion of turbulence it is difficult to accept Kinsinger's model as accurately describing arc behaviour during the pre current zero period. It is also difficult to draw any general conclusions regarding Kinsinger's predictions since only one value of di/dt has been examined

The Brown-Boveri group produced a series of publications in which they attempted to characterise the transient behaviour of the circuit breaker arc by initially describing the steady state behaviour (Hermann et al 1974a, b) and developing a theoretical model in conjunction with experimentally observed phenomena (Hermann et al, 1976 and Hermann and Ragaller, 1977). These authors have shown experimentally that the arc column sections upstream and downstream of the nozzle throat behave differently during the current zero period and therefore play different roles during the interruption process. The upstream high pressure section appears uniform and stationary with respect to the axis and the diameter decays continuously with decaying current. The downstream (low pressure) region appears irregular and erratic in cross-section with respect to the axis and the cross-section oscillates with decaying current.

The upstream and downstream regions are each characterised respectively by :

(1) Laminar flow conditions, with its properties determined mainly by the equilibrium between Ohmic heating and convective cooling.

(2) Turbulent flow conditions due to the formation of a shear layer between the low density arc column and the high density surrounding hot gas whereby energy loss is principally by radial transport (mainly turbulent mixing).

The following set of simplifications was used for the turbulent arc section (Hermann et al 1974b) :

(i) Axial heat conduction was neglected compared with convection.

(ii) Only the dominant term of the viscous stresses was included in the momentum equation.

(iii) The radial pressure variation across the boundary region of the arc is neglected compared with that in the axial direction.

In their model Hermann et al (1976) describe the total arc by a single cylindrical element with a length corresponding to that arc section which has been observed to determine the pertaining arc behaviour. It is assumed that in this model section all processes are effective although, in reality, they occur separately in the upstream and downstream arc regions. These processes are ohmic heating, energy transport by radiation, turbulent mixing, conduction, momentum transport by turbulent mixing, convection and friction. The pressure and mean axial velocity in the different transport terms is chosen according to the section in which the respective process is effective.

In the convective term the velocity is assumed to increase linearly (defined by a parabolic pressure drop, Hermann et al 1974b). In the radial direction the model arc section is subdivided into three zones :

(1) The electrically conductive arc column that determines the electrical parameters.

(2) An outer region of cold gas flow (T<1000 °K) that determines the pressure variation along the element.

(3) An intermediate zone (1000 < T < 4000 °K) which is important for describing the radial processes, principally turbulence i.e to act as an energy buffer.

The energy and momentum conservation equations are derived and solved in detail in a further publication (Hermann and Ragaller 1977). Solution is by radial integration assuming a parabolic temperature profile in the central zone and an exponentially decaying temperature profile in the intermediate zone. Hermann and Ragaller (1977) predict the thermal extinction limiting curves for air and SF_6 for various upstream stagnation processes, and the variation of post arc current with time and different RRRV for SF_6 at 21 bar and a single peak current.

The above model (Hermann et al, 1976) is claimed to be capable of predicting, through the solution of equations of conservation of energy, axial momentum and mass, the time variation of localised arc parameters such as axial electric field and radial temperature profile during the current zero period. It has also been used to compute the

interrupting capability of an arc burning in a supersonic nozzle flow as a function of arc current and RRRV, upstream stagnation pressure and the nature of the quenching gas. Good agreement between these computed results and experimental results of Frind and Rich (1974) is claimed although only one set of results is presented (Hermann et al, 1976).

Chapmann (1977) made the criticism that an increase in electric field strength should be evident further downstream where turbulence is more severe. Hermann et al (1976) explain this phenomenon by a widening of the arc column in this axial region. However the authors claim that an elongated downstream section to the nozzle throat enhances interruption capability. The latter claim is difficult to comprehenced in view of the variation of local electric field strength. Indeed such a variation itself implies that the critical area for arc interruption is near the nozzle throat. Experimental results presented by Lewis (1987) show that the arc column is uniform in appearance in the nozzle throat region which is indicative of an arc in a laminar flow.

In the same publication (Hermann et al 1976) claim to provide experimental evidence from which they obtain quantitative information regarding the upper limit of the average temperature. The technique used is a side on scanning method with a 1 μs (or greater) scan which exceeds the time constants which characterise their claimed turbulent energy removal mechanism. Indeed the computed temperature variation for an SF_6 arc during the current zero period is of

the order of 18,000 to 20,000 °K 3 μs before current zero (response to discussion on Hermann and Ragaller 1977) which appears close to the upper limits during the peak current phase and certainly higher than the experimental results presented in this thesis chapter (5).

An analytical approach to the problems of circuit breaker arc modelling was introduced in a series of papers (Cowley 1974, Cowley and Chan 1974 and Chan et al 1976) in which the analysis of electrical arcs by integral methods was described. In this method of arc analysis, (Cowley 1974, part I), the overall conservation equations relating to the electrical arc in a longitudinal gas flow arc expressed in terms of radial integrals. The equations are formulated such that integral quantities can be characterised by areas relating to specific electrical or thermodynamic properties which are physically meaningful. A standard area is then chosen, namely the thermal area, to which all the area terms defined in the analysis are normalised and the concept of shape factors obtained. The shape factors are thus defined as the ratio of a given area to the thermal area. To close the system of integral equations it was shown that the relations between the shape factors, especially the conductance shape factor (Λ_c) and some known arc characteristic is needed. Cowley (1974) relates the shape factors calculated from the full differential solution of the model gas equations to the non-dimensional form of the electrical power input (EI) for a fully developed arc and thus the set of integral equations could be closed.

An attempt to predict shape factor variation has been made with some success by (Cowley and Chan 1974 and Chan et al 1976). These authors regard the arc environment as consisting of an electrically conducting arc core surrounded by a cooler annular thermal region. This necessarily involves consideration of energy and momentum transport by diffusive processes at the core boundary and they correlate the variation in shape factors to the variation in radial heat transfer at the edge of the arc core. The value of this heat transfer is derived from the conservation equation for core energy.

The above method of shape factor prediction has proved remarkably successful for a range of model-gas arc situations (Chan et al 1976), but the authors state that it may well be restricted to cases where Fourier heat conduction is the dominant mechanism for thermal diffusion. The success of this method, however, implies that the overall conservation equations, the core energy equation and a knowledge of how shape factors are related to heat transfer at the core edge are adequate to predict arc behaviour.

In (1978ii) Walmsley and Jones realised the significance of correlating the shape factors with a parameter representing power loss. Characteristic " area " and " shape factor " values are presented for arcs and methods of correlating these parameters for different arcing conditions are examined. Curves are presented for conductance shape factor versus Nusselt number Nu and a further parameter χ, the dynamic power loss, for different arc types derived from a wide range

of operating conditions covered by previous authors. Significantly, a unique set of curves are obtained for δ_c versus Nu and χ.

In (1979) Fang and Brannen attempted the first current zero arc model based on the boundary layer integral method. This model is capable of predicting physical quantities of interest to circuit breaker engineers and deals with an arc in an orifice flow of air. Arc characteristic times are introduced to define quantitatively the current zero period and to describe the relative importance of the physical processes involved. As there were only a few experimental velocity profiles available for the calculation of shape factors, the following assumptions were made :

(1) The velocity profile is directly related to the enthalpy profile through the relationship $\rho\omega^2 = \rho_\infty\omega_\infty^2$ where the subscript ∞ relates to the values of quantities in the external flow. Thus the axial momentum conservation equation is discarded and the displacement area θ_d is equal to the momentum area θ_m. This is equivalent to assuming constant Mach number across the cross-section.

(2) The net radiation from the arc is neglected in comparison with the kinetic energy and enthalpy transport.

(3) The enthalpy area is equivalent to the thermal area and the enthalpy flux area is equivalent to the kinetic energy area.

When the above assumptions are incorporated the arc energy integral equation is reduced to :

$$(\partial/\partial t)[\rho_\infty h_o \theta_\delta] + (\partial/\partial z)[\rho_\infty \omega_\infty h_o \delta_h \theta_\delta] = i^2/(\sigma^* \delta_c \theta_\delta) \qquad (2.18)$$

where

ρ_∞ is the density of the external flow

h_o is the characteristic value of enthalpy

θ_δ is the thermal area

ω_∞ is the velocity of the external flow

δ_h is the enthalpy flux shape factor

i is the instantaneous current

σ^* is the characteristic value of electrical conductivity

δ_c is the conductance shape factor

This equation is then solved for a known δ_h and δ_c which are unique functions of dynamic power loss. The model is capable of predicting the axial electric field strength, the arc size, the axial temperature and the critical rate of rise of recovery voltage $(rrrv)_c$. The performance curves interms of $(rrrv)_c$ and the rate of change of current at current zero di/dt are presented and the effects of stagnation pressure on $(rrrv)_c$ are discussed. The model accommodates the imposition of arc circuit interaction through the distortion of the current waveform.

All the theoretical models described in this section have involved the use of empiricisms to various extents. Empirical formulae are derived from direct arc property measurement or circuit breaker testing. It is ultimate aim of theoretical arc modelling to minimise expensive full scale testing so that at least initial feasibility studies of a reliable

nature may be made without resorting to the use of industrial test facilities.

2.5 The description of the circuit breaker by empirically derived laws

This section reviews briefly the empirical results which have served to enhance the understanding and identification of the physical phenomena which govern arc extinction in the gas blast interrupter.

In (1946) it was realised that interruptor performance could be optimised by altering such design parameters as the ratio of the nozzle diameter to the arc length and the pressure differential across the nozzle throat.

In (1955) Hudson investigated the effect of nozzle geometry and circuit influence on arc performance. Hudson (1955) used a mass flow ratio, (the mass flow during arcing to the mass flow without an arc), and showed that this ratio could be expressed empirically as a function of arc current (I), nozzle diameter (d), and arc chamber pressure (P_o). By considering a critical value of this ratio, defined as the mid-point of the region where tests resulted in mixed clearances and failures of the circuit breaker, further switch and circuit variables were examined.

In (1964) Hudson extended his work to examine the relationship between the critical ratio and variables connected with the circuit breaker nozzle geometry, namely nozzle entry, length and exit. For

this investigation he developed a pressure coefficient, C_{pc}, defined as

$$C_{pc} = P_c / (I^{0.5} d^{0.6}) \qquad (2.19)$$

Where P_c is the mean critical value of P

From the latter investigations Hudson concluded :

(i) The breaker performance using a radiused entry nozzle was better than when using a sharp-edged entry nozzle.

(ii) The optimum nozzle length is between 1/2 and 1 inch.

(iii) The circuit breaker performance was not enhanced when using a divergent nozzle section. (this conclusion is misleading since other researchers have determined the nozzle divergence semi-angle optimum range to be less than 15° (the minimum value used by Hudson)). This also is governed by the nature of the gas i.e. SF_6, air.

(iv) The smallest possible upstream arc gap should be used (the limit being determined by the voltage insulation between nozzle and electrode).

In (1967) similar work by Zuckler, who measured gas throughput of a nozzle, as a function of the current pulse peak value and frequency. The dynamic back pressure is defined as the pressure required to reduce the mass-flow rate to that observed during arcing. Using high speed photographs Zuckler (1967) showed that improvements in interrupting capability could be achieved by increasing the

pressure with a good nozzle design. Zuckler (1969) extended his work to the problem of nozzle clogging where it was found that the mass-flow rate at current zero could be substantially reduced if the flow through the nozzle was choked at peak current.

Kopplin et al (1971) measured the performance of their experimental duo flow interruptor, using peak arc current as a variable and a fixed rrrv. These authors were able to show that the performance was increased when SF_6 rather than air was used as the arcing medium, and that an optimum inter-nozzle distance existed for both quenching gases.

Frind and Rich (1974) attempted an extensive investigation into the effect of the current decay rate (di/dt) and pressure upon the critical (rrrv). Tests were performed for air and SF_6 using upstream pressure of 100 to 600 p.s.i.a and di/dt in the range of 5 to 30 A/μs (peak current of 10 to 60 KA) for a 60 Hz current pulse. The throat diameter of the Laval nozzle was 1/2 inch with a 15° semi divergent angle whilst the ratio of upstream length to throat diameter approached one. These authors have shown that using a di/dt of 27 A/μs the critical rrrv varies with the upstream pressure as the first power for air and as the 1.4 power for SF_6. They have also shown that the $(rrrv)_c$ varies inversely as the square of (di/dt) for both air and SF_6 for a fixed upstream pressure of 550 p.s.i.a. The absolute of these characteristics confirm the superiority of SF_6.

A possible criticism of the experiments of Frind and Rich (1974) is that they arranged their tests to avoid the phenomenon of nozzle clogging by using a high frequency (1200 Hz) current pulse. The effect of peak arc current, and hence nozzle clogging, upon the type of results presented by these authors is unfortunately difficult to determine quantitatively without further experiments.

In (1980) Frind et al investigated the thermal reignition and the post arc current for a gas blast interruptor using air and SF_6 as arcing media. The interruptor used in their experiments was an orifice type with a throat diameter (0.5 in), thickness (0.125 in), and an electrode diameter (0.5 in). These authors used high speed photography to identify which arc section had the fastest transient response and to study the arc structure and its axial developments. The electrical power input during the thermal recovery period and the variation of arc resistance were determined using the voltage and the post arc current. The critical post-zero current depends very strongly on the rate of decay of current di/dt

$$I_{post,crit} \alpha (di/dt)^2$$

Frind et al (1980) concluded that :

(1) Thermal recovery speed was comparable to other nozzle configurations.

(2) The dominant arc section during the thermal reignition period was close to the throat. It's length was about 10 mm and this section showed a smooth decay but constricted sharply at current zero.

(3) Two modes of arc broadening were observed in the downstream flow. One was caused by arc instability and turbulence, the other by the interaction of the arc with a shock wave.

(4) The post zero current in the case of air and SF_6 was smaller than the values suggested by theory.

(5) In both gases, power loss during the thermal recovery period was much smaller than predicted theoretically.

An empirical equation of the thermal performance prediction calculation of SF_6 circuit breakers has been derived by the G.E.C. group (Ancilewiski et al 1984). The equation was obtained by examining test results for 2-pressure systems. This was for both air and SF_6 as a media. This equation gives the RRRV as a function of a number of parameters as follows :

$$RRRV = (axP^{n}xLxD_{t}xM^{q})/((di/dt)xA) \qquad (2.20)$$

Where

RRRV rate of rise of recovery voltage

P upstream pressure

L ratio between throat and gap

D_t throat diameter

M Mach number

di/dt rate of decay of current

A cross sectional area of the arc at current zero

a,n,q constants

These authors have derived another equation for the upstream arc diameter variation

$$D_c = (bxI^{0.63}xL_u^{0.25}) / (P^{0.25}xM^{0.25}) \qquad (2.21)$$

Where

D_c core diameter in cm

I instantaneous current in amps

L_u upstream arc length in cm

P upstream pressure in bar

M Mach number

b constant

Equation (2.21) can only be approximate since it implies zero arc diameter at current zero. These authors claim that the equation gives good agreement with test measurements above a current of 1 KA, but below this value increasingly deviate from a monotonic decay. The authors measured the cold flow velocity distribution through the nozzle using a particle tracing technique which the authors claim enables the radial pinch component of the flow to be evaluated. They also produced a series of performance curves for various values and conclude that a value of 25 % for the radial pinch component shows the best agreement between the calculated and measured performance.

Many difficulties exist in the utilisation of the empirical analysis of Ancilewski et al (1984) :

(1) Equation (2.20) has been derived from measurements made on a monoflow interruptor. It is not clear how the analysis should be applied to calculate the performance of a duoflow interruptor.

(2) The constants in equation (2.20) (a, n, q) have not been defined nor values given.

(3) No mention or description of the measurement technique employed to determine the arc diameter has been made so making a comparison with other authors difficult.

(4) Although measurements of the cold flow distribution have been made and unexpected flow properties demonstrated no measurements have been made under arcing conditions to confirm the effect, if any, upon the arc column.

An extensive investigation into the current zero electrical arc and the thermal performance of a model gas blast circuit breaker has recently been conducted at Liverpool as reported by Taylor et al (1982). Tests were performed under full and reduced power conditions. Full power conditions were produced with a ringing L-C circuit operating at voltage up to 6.3 KV (34 to 64 KA peak sinusoidal waveform), (di/dt in the range 14 to 26 A/μs).

Reduced power conditions were obtained using a D.C. holding current not exceeding 2 KA, ramped to zero at different decay rates in the range 14-60 A/μs. For the case of full power conditions the nozzle was a converging - diverging (12° semi - divergent angle) geometry coupled with an upstream tank pressure of 7.8 bar ensured sonic flow condition at the nozzle throat (diameter = 35 mm). The

nozzle materials were copper and PTFE and the upstream electrode materials were Cu/W and Carbon. In both cases approximately linear voltage restrikes could be sustained for a few microseconds after current zero so enabling the thermal limitation to the performance of the circuit breaker to be determined.

The circuit interruption performance of the test head was considered in terms of dv/dt : di/dt characteristics in both cases. The authors derived the following empirical relationships for the stated operating conditions :

Reduced power :

$$(dv/dt)_c = 3.3 \times 10^3 (di/dt)^{-2.8} \qquad (2.22)$$

Full power :

$$(dv/dt)_c = 4.6 \times 10^9 (di/dt)^{-7.5} \qquad (2.23)$$

The last two equations show that the test head performance measured under these two test conditions were different. At higher di/dt (high peak current in the full power tests), the power circuit performance was inferior to the ramp performance whereas at low di/dt the power circuit performance was at least as good as that of the ramp circuit if not marginally better.

Taylor et al (1982) calculated the arc conductance and instantaneous power input from which the authors calculated the Mayr arc time

constant as a function of time and di/dt and the critical peak post arc current and power loss for different operating conditions.

The authors concluded that :

(1) The existence of pressure transients for low di/dt values for the full power arcing condition indicated thermal nozzle blocking which did not affect the performance compared with the reduced power level.

(2) At higher values of di/dt (higher peak currents), which under full power conditions, an additional deterioration in performance was apparent. This was associated with severe nozzle ablation which was produced by radiant power transfer from the arc and the consequent generation of a substantial backflow of ablated mass into the upstream plenum. Consequently the performance at full power becomes additionally a function of nozzle material.

(3) The current zero arc conductance was found to be directly proportional to the current decay rate whilst the arc time constant was insensitive to di/dt.

(4) Small changes in the current zero arc conductance can produce relatively large changes in test head performance.

(5) Post arc currents and critical powers measured under these experimental conditions were in satisfactory agreement with those measured by Frind et al (1980).

In the above section it is clear that empirical investigations provide useful and directly applicable criteria whereby circuit breakers may be designed. These design parameters may be utilised in order to

produce an interruptor design to work at a lower or higher power rating provided the laws governing the scaling of the parameters are known.

CHAPTER 3

SPECTROSCOPIC DIAGNOSTIC TECHNIQUES

3.1 Introduction

To quantify the fundamental thermal properties and structure of the arc column, measurements must be made of arc temperature and species concentration, with spatial (radial and axial) and temporal resolution if the arc is in a transient state. This chapter therefore reviews different techniques which have enabled previous researchers to identify features of arc column structure and in some cases extinction criteria through both qualitative and quantitative analysis of their experimental measurements.

The branch of spectroscopy with which this thesis is concerned involves atomic spectra since at the temperatures of interest within an arc column most of the species are atomic in nature. With a knowledge of the physical principles governing atomic spectra, the theory may be applied to the plasma to derive the localised arc properties of temperature and species density. However, this analysis may be greatly simplified if certain assumptions regarding the thermodynamic state (Local Thermodynamic equilibrium) and optical depth of the plasma are shown to be valid. These are discussed in detail in chapters (2 and 6). Plasma, and in particular arc, spectroscopy in idealised situations has been used to confirm existing

theories and derive fundamental constants of certain materials (e.g. Koch and Richter, 1968 for copper). However the arc column in a circuit breaker departs in many ways from the above mentioned idealised situations, so that care must be taken when making spectroscopic measurements in such situations. As a result it is profitable to review the previously published work on arc spectroscopy.

3.2 Local plasma temperature

The intensity I_{mn} of an emitted spectral line from an optically thin plasma due to the relaxation of a bound electron from level m to level n is related to the population density N_m of the energy level m by

$$I_{mn} = (A_{mn}/\lambda_{mn})(hc/4\pi)N_m \qquad (3.1)$$

Where

A_{mn} is the transition probability from level m to level n transition

λ_{mn} is the wavelength of the emitted radiation

h is Planck's constant

c is the velocity of light

If the plasma is in LTE then N_m is related to the plasma temperature T and to the number density of the particular plasma species N_z by the Boltzmann equation

$$N_m/N_z = g_m \exp-(E_m/KT) \qquad (3.2)$$

Where

g_m is the statistical weight of the upper energy level

E_m is the energy bound level m (upper level)

K is Boltzmann's constant

Combining equations (3.1) and (3.2) yields

$$I_{mn} = N_z(A_{mn}g_m/\lambda_{mn}) \ (hc/4\pi)\exp-(E_m/KT) \qquad (3.3)$$

Thus for a particular emission line, since the first two bracketed terms are constant,

$$I_{mn} \propto N_z \exp-(E_m/KT)$$

Where N_z may be calculated from Saha's equation. For particular species it can be a strong function of temperature. Thus the temperature may be determined by measuring the absolute intensity of a particular spectral line.

3.2.1 The evaluation of suitable spectral lines

The choice of which spectral lines to use is determined by :

(1) The spectral line should maintain a consistent line profile, over the range of pressure variations within the plasma for the scope of the operating conditions studied.

(2) The line in question satisfies the optical density criteria (chapter 2) and shows no signs of self reversal.

(3) The line profile is not impeded by satellite emissions in the close neighbourhood spectral range to the extent that the line profile is distorted to give a false line width.

(4) The availability of reliable data for the constants required for equation (3.3).

If a line satisfies these requirements then it is possible to make spectroscopic measurements of temperature and electron density and thus compare the latter with a theoretical value of a given plasma pressure.

The lines selected for the present investigation were the CuI 510.5 nm line, the CuI 515.3 nm line and the CuI 521.8 nm line; the spectral constants are given in table (3.1).

3.2.2 Estimation of the approximate plasma temperature during the current zero period

Since the factors N_z and $\exp-(E_m/KT)$ in equation (3.3) are strong positive functions of temperature for particular lines over a limited temperature range then the presence of these spectral lines in survey spectra implies that the temperature conditions within the plasma are correct for their creation. Similarly the absence of particular lines implies that the plasma temperature is either too high or too low for the creation of these species and energy states. The strongest lines

will be those with the highest values of A_{mn} and G_m and the lowest values of E_m.

The data in table (3.1) present the most reliable values of transition probabilities found throughout the course of this work. By substituting these data into equation (3.3) the relative intensity of the two strongest lines representative of each species is obtained as a function of the plasma temperature. Although tungsten lines are present in the arc spectrum they have been used only for cross checking the temperature calculated from the copper lines.

3.2.3 Plasma temperature measurements from the intensity ratio of CuI lines

One advantage of using lines of the same species is that by measuring the ratio of the intensities of two or more lines, the factor N_z in equation (3.3) is cancelled. The ratio of two line intensities is given by

$$I_{mn1}/I_{mn2} = [(A_{mn1}g_{m1})/(A_{mn2}g_{m2})](\lambda_{mn2}/\lambda_{mn1}) \cdot \exp((E_{mn2}-E_{mn1})/KT) \qquad (3.4)$$

Where suffices 1 and 2 refer to the two lines under consideration (515.3 and 510.5) respectively. A knowledge of the atomic parameters A_{mn}, G_m, E_{mn} and the ratio of an appropriate pair of spectral lines allows the electron temperature T to be calculated. Inserting the

constants of the 515.3 nm and the 510.5 nm CuI lines from table (3.1) in equation (3.4) and rearranging yields

$$T = - 2.75x10^{4}[Ln(0.033)(I_{515}/I_{510})]^{-1} \qquad (3.5)$$

A program was developed to calculate the plasma temperature from the measured intensity ratio and atomic data for a pair of spectral lines (details in appendix 1). The relevant atomic data for CuI (A_{mn}, E_m, g_m) was obtained from Kock and Richter (1968). The temperatures derived in this manner need to be further assessed in terms of source and system geometry etc. in order to obtain radially resolved arc temperature profiles. This latter interpretive exercise is not related to fundamental spectroscopic theory and so is considered later.

3.2.4 Electron number density

The electron density of the arc was determined from the broadening of the spectral lines. The broadening of spectral lines can be caused by several processes which include pressure and Doppler effects. However in the case of a collision dominated high pressure arc plasma (as is the case in the present work) the principal broadening mechanism is Stark broadening. Another broadening mechanism which needs to be considered is that associated with the measuring instrument (instrument broadening). The slit width of the monochromator was maintained at 28.5 μm for the entire investigation of the present work which resulted in an instrument broadening of 0.03 nm.

The broadening of the spectral lines due to the Stark effect is given by Griem (1964) as

$$W_{total} = [\ 1 + 1.75\alpha(1 - 0.75r)]\omega \qquad (3.6)$$

Where

W_{total} is the total half width due to Stark broadening

ω is the electron impact width in angular frequencies

r is a correlation parameter defined by

r = (mean distance between ions) / (Debye radius)

$$= 6^{1/3}\pi^{1/6}(e^2/4\pi\varepsilon_o\ KT)^{1/2}N^{1/6}$$

N is the number density of perturbing ions (N_e)

$$\alpha = (\ C_\alpha\ F_o^{\ 2}/\omega\ )^{3/4}$$

F_o is the normal field strength

$$= (2.61/4\pi\varepsilon_o)\ N_e^{\ 2/3}$$

C_α is the quadratic Stark coefficient

Jenkins (private communication) has solved equation (3.6) using values of α, r and ω calculated by himself for different spectral lines of CuI and a range of N_e and temperature values. The results of these

calculations of selected spectral lines of interest are shown in table (3.2).

3.3 Development of arc spectroscopic techniques

The main parameter of interest in the present work is the radial temperature profile and this can be determined by measuring the intensity of one or more spectral lines. However, the information available from arc spectra is not limited to the temperature profile alone. Measurement of the line shapes can be interpreted to yield the electron number density (chapter 5) and survey spectra plates can be used to detect and evaluate the concentration of impurity species. Thus, in principle, a single spectroscopic measurement can yield a vast amount of information about local plasma conditions. This section reviews briefly the development of the arc spectroscopic techniques.

In (1971) Ito et al attempted a spectroscopic study of a high current arc which was developed between carbon electrodes. The authors used the gases H_2, SF_6, He, Ar and air as arcing media at an initial pressure higher than 2 atm. The current peak was above 5 KA and the duration of the current was 250 μs. The temporal and spatial changes of plasma parameters were measured by a time-resolved spectrograph and a high-speed framing camera. These authors estimated the electron density of the plasma from the Stark broadening of different lines.

Their observations show the following :

(1) The arc space was divided into two regions, the bright narrow core and the broad outer flame.

(2) The electron density of the core was estimated to be of the order of 10^{18} cm^{-3} and an electron temperature of the order of 10^4 °K was obtained at current peak.

(3) The electron density after current zero was of the order of 10^{17} cm^{-3} regardless of the kind of gas.

In (1972) Roberts and Prasad attempted one of the earliest spectroscopic investigations on the 10 KA free burning arc in air using copper electrodes. Spectra were taken with a Hilger medium spectrograph type E528 which could be used with glass or quartz optics. Ilford HP3 plates were used for the region 200.0 nm to 640.0nm and Long Range Spectrum plates to cover wavelengths up to 950.0 nm. Relative intensity calibration was performed with a step wedge and either the arc itself or a flashlamp at 1500 °K as the light source.

Spectra were taken in both streak and shuttered "snapshot" modes. An A.W.R.E streak camera system was used to enable streak records of up to 2 ms duration to be obtained. The shutter was a slotted aluminium disc rotated at 1400 r.p.m., giving an exposure time of 19 μsec. Measurements were also made using an EMI type 9529/B photomultiplier.

The authors used quite a large number of different methods for obtaining temperatures for the whole arc, the most accurate of which were :

(1) Relative intensity of the CuI lines (sensitive for $T_e \leq 14{,}000$ °K).

(2) Relative intensity of the CuII lines (sensitive for $T_e \leq 20{,}000$ °K).

(3) Relative intensity of the CuII to the CuI lines (sensitive for $T_e \leq 17{,}000$ °K).

(4) Line intensity variation of NI (sensitive for $T_e \leq 16{,}000$ °K).

(5) Relative intensity of the NII lines (sensitive for $T_e \leq 30{,}000$ °K).

A similar analytical approach to that of case (1) is used in this thesis and is discussed in chapter (6). The electron density, N_e was calculated from the Stark broadening of particular lines, a method which will be further described in chapter (5). Electron temperature and particle density distributions have been determined at various heights above the cathode. From these data, the conductivity, electric field and current density distributions in the arc have been evaluated.

The authors identified that the cathode root of the arc was observed to rotate continuously around the truncated surface of the electrode although the arc itself was stable. They also observed the presence of a copper vapour rich core at 10 KA which had a lower temperature than the rotating host plasma column owing to increased radiation losses around which the hotter host plasma column rotated. Approximately 63% of the power input to the arc column appeared to be lost by convection and about 36% lost by the radiation, 90% of the latter being by copper emission.

A spectroscopic study has been made of the effect of an efflux air flow on a 100 mm long, 10 KA arc between copper electrodes by Roberts and Cowley (1973). The spectroscopic equipment and techniques were exactly as described by Roberts and Prasad (1972). The authors considered first the no flow M = 0 (Mach number), case and compared their results with the above results. The authors found that the intensity of the copper lines was greater than reported above but the intensities of the nitrogen and oxygen lines were much less. Many of the strongest copper lines showed signs of re-absorption and self reversal.

When a flow with Mach number M = 0.7 was imposed, the main visible effect was in the anode region. The copper jet was also better defined. The main region of the arc was seen to have a rather wide flat temperature profile with steep temperature gradients of the edges, particularly nearer the cathode. Rotation of the arc was still apparent but again it was not a very prominent feature.

In (1978) Housby-Smith and Jenkins extended spectroscopic investigations to an arc in an orifice air flow. The air flow was generated by upstream pressures of 3.5, 6.9, 10.9 and 13.3 bars. Results have been obtained with four different upstream cathode materials - carbon, copper, mild steel and elkonite (copper-tungsten mixture) - both upstream and downstream of the orifice throat. The arc column was sustained by a triangular current pulse having a rise time of 1.3 ms and decay times > 5 ms with peak arc currents of 3 and 8 KA.

The authors used a Hilger medium spectrograph type E528 fitted with quartz optics to obtain the arc spectra. Short - time exposure 34 μs records could be obtained by means of a rotating shutter mounted in front of the vertical entrance slit of the spectrograph. A 90° image rotator was incorporated into the optical arrangement so that a radial segment of the arc was rotated and imaged along the spectrograph entrance slit. Spectra were recorded at three axial stations one upstream, 6.5 mm from the upstream edge of the orifice and two downstream, being located 2 mm and 9 mm from the downstream edge of the orifice.

The lines chosen were CuI 330.7 nm, 282.4 nm, CuII 276.9 nm downstream; CuI 249.2 nm, CuII 248.9 nm upstream and NII 399.4 nm, 444.7 nm, 453.0 nm and 463.0 nm at the downstream station.

Electron temperatures were determined from measurements of relative intensity of two copper lines. The more accurate method involving the relative intensity of CuII to CuI lines was employed using N_e, the oscillator strengths from Kock and Richter (1968) for CuII lines and Corliss (1970) for CuI lines. Electron temperature in the region where NII emission occurs were determined from the intensity ratio of the NII lines. These calculations assumed LTE and were based upon Abel inverted spectral emissions for the cases when cylindrical asymmetry was apparent. Electron densities were determined from measurements of the half-widths of spectral lines having known Stark broadening parameters.

Housby-Smith and Jenkins concluded that the arc was similar to the previously investigated free burning and efflux arcs in that there existed two principal emitting species (N and Cu) which were non-coaxial and at different temperatures. The number and intensity of the copper lines was found to be higher in the orifice arc implying a higher radiation loss from the copper core, and lower in the free burning arc. Their results also indicated that the optical diameter and the half width of the electron density profile were smaller than for the other arcing conditions, but the electron density was higher.

Airey (1977) presented a spectroscopic investigations of a pulsed high current, high pressure, SF_6 arcs, 100 mm long burning between Cu/W electrodes. The current range examined was 1 KA to 45 KA, the pulses were half sine waves with durations of 6 ms to 12 ms and the gas pressures were 6.5 bar upstream (anode) and 3.1 bar downstream (cathode).

The author used a Rank Hilger Monospek 600 combination grating spectrograph and Czerny-Turner monochromator model D460 for most of the spetroscopic investigations. The internal optical arrangement of the spectrometer consisted of the collimating and focusing mirrors and the plane grating. In the monochromator mode the output was dispersed across the focal plane of the exist slit, which selected the emergent wavelength and bandwidth according to the settings of the direct reading head and the width of the exit slit. The focal length and effective aperture of the instrument were 0.6 m and f/6 respec-

tively. Using a grating of 1200 lines/mm a linear dispersion of 1.36 nm/mm was obtained which was adequate for their investigations.

Airey's (1977) measurements were initially made radially integrated at a station 37 mm downstream of the anode which was also downstream of the nozzle exit. Photoelectric snapshots of 100 μs exposure were used to measure the line intensity and width of CuI 510.5 nm, 529.3 nm and 515.3 nm lines from which the average electron temperature and density were calculated. Further measurement of radially resolved spectra were performed on a section 25 mm downstream of the anode which were viewed through a cutaway section of the nozzle. The copper vapour concentration was low in this region for the currents below 200 A so it was necessary for the author to estimate the radial temperature distribution from the intensity ratio of the FI 624.0 nm and SII 545.4 nm lines. An Abel inversion procedure was incorporated in this calculation.

For arc currents below the metal vapour core formation level, (around 20 KA), the temperature profile exhibits a parabolic shape with an axis temperature of 20,000 °K down to about 11,000 °K. At the peak of a 24.5 KA current pulse the mean temperature, as measured using CuI lines, oscillated between 17,000 °K and a maximum value of 31,000 °K. The SF_6 plasma surrounding the core shows no spectroscopic change either in line widths or intensity and it was, therefore, concluded that the outer plasma temperature was the same as before core formation.

The author further concluded that conditions of LTE were satisfied for instantaneous current values below 20 KA but could break at higher values. The radially-averaged electron number density determined from FI and SII and CuI lines exhibited a value of 3.2×10^{23} m^{-3} at 6 KA. The latter value, together with the measured arc temperature of 17,000 °K, predicted a total equilibrium plasma pressure of 2.25 bar which was in good agreement with that value of 2.0 bar predicted from gas flow calculations. The copper vapour density in the arc was found to rise slowly with current and exhibited values of 1 % and 5 % at 7 KA and 13 KA respectively. However, at 19 KA peak the impurity concentration was 20 % and increased with time and with falling current to about 35 % at 10 KA.

Using high speed photographs the author identified globular motions of the copper plasma which appeared to merge into a continuous motion. This observation was similar to the phenomenon described by Walmsley et al (1976) and could account for the local temperature oscillations. However Airey (1977) did not relate these observations to those of Roberts and Prasad (1972) or Roberts and Cowley (1973) but rather believed them to be associated with temperature fluctuations. Also the author did not indicate to what extent the cutaway section of the nozzle effected flow patterns downstream which could seriously affect local and overall parameters.

In (1980) Okuda et al presented a spectroscopic approach to the analysis of high current arcs in SF_6. Spectroscopic observations were carried out on transient free-burning arcs drawn by separating Cu/W

electrodes and the peak current was varied up to 60 KA. The arc was observed with a high speed framing camera running at 5000 frames/s. The camera also had a maximum transmission at the wavelength of 648.5 nm with a half-width of 2.5 nm. In order to obtain the radial distribution of the composition of the arc, snapshot spectra were taken by means of an Ebert-type spectrograph with the entrance slit at right angle to the arc axis. A slit connected to the moving electrode was used as a blind shutter and the spectrum was detected by Kodak 103a-f plates in the range of wavelength from 350.0 nm to 700.0 nm.

A series of snapshot spectra were taken at various axial positions and at various current levels by Okuda et al (1980). The spectra were classified into three types :

(1) This type was observed at the instantaneous current higher than 10 KA. Continuum dominated the spectrum and no emission lines of sulfur and fluorine were observed. Copper and tungsten lines were strongly self-absorbed and some of them were self-reversed.

(2) This type was observed when the current was falling from 10 KA to zero. Continuum was weak and emission line spectra of copper and tungsten were observed. No emission lines of sulfur nor fluorine were observed.

(3) This type was observed when the current was rising from zero to 10 KA. The emission lines of FI and SII were observed and they were not coaxial with the continuum and the metal lines.

Okuda et al (1980) proposed a new method using the continuum for measuring the parameters of high current arcs. The method was based upon the following assumptions :

(1) The plasma was cylindrically symmetric.

(2) The plasma was in local thermodynamic equilibrium.

(3) The temperature decreased monotonically in the radial direction.

(4) The radial component of the pressure gradient was balanced with the radial component of the magnetic pinch force.

(5) The plasma was optically thin at the continuum dominated wavelength used.

The authors summarised their results as follows :

(i) The composition of the arc changed significantly at the critical instantaneous current of 10 KA independent of the peak value of the arc current and the opening phase of the electrodes.

(ii) Electrode vapour was the principal ingredient of the arc in the range of current above 10 KA. The spectral lines were self-absorbed and merged in the strong continuum.

(iii) A new method was developed to estimate the temperature and pressure profile of the arc by making use of the continuum.

(iv) The arc contained the conductive SF_6 gas at the current below 10 KA.

Further spectroscopic results of gas flow arcs under similar, but not identical, conditions to those investigated by Airey (1977) were presented by Ikeda et al (1982). Peak arc currents of 30 KA and above were investigated so extending the range above the threshold

for the formation of the arc plasma core. The arc was confined to burn along the nozzle axis by a flow of gas discharged from a high pressure reservoir of about 7 bar to a low pressure reservoir at 1 bar. The nozzle possessed a throat diameter of 50 mm and a length of 30 mm. The host gas used in the tests was SF_6, the upstream electrode was made from carbon or copper-tungsten and the nozzle material was either copper or PTFE.

The authors recorded the spectra with a Hilger-Watt 1000 prism spectrometer. A mechanical shutter was used to limit the exposure time to 0.5 ms at peak arc current when the arc was in a quasi steady condition. The arc spectra were recorded photographically and the optical density variations across the spectral lines measured using a Hilger-Watt microphotometer. The spectral lines selected for analysis were FI 623.9 nm, SII 545.39 nm , SII 532.07 nm, CuI 578.31 nm, CuI 529.26 nm, and CuI 510.55 nm.

The authors confirmed the evaluation of a copper core above an instantaneous current value of 18 KA which was in agreement with Airey (1977). Their results indicated a somewhat lower copper temperature in arc core (15,000 °K) compared with the surrounding host plasma (20,000 °K). The electron density values were calculated from line broadening and yielded an average value of 1.8×10^{24} m^{-3} upstream compared with 1.5×10^{24} m^{-3} downstream. The copper vapour concentration 1 mm downstream of the orifice exit was about 70 % and was considerably greater than that deduced by Airey (1977) (20%).

It is unfortunate that the upstream temperature, electron density etc. could not be calculated owing to reabsorption etc. which could have also enabled axial gradients of parameters to be determined. It is also unfortunate that, owing to the extreme experimental conditions encountered that the Abel inversion technique could not be employed and a more accurate radial temperature distribution derived.

In (1978) Smith et al reported the first spectroscopic investigation which included the current zero period of arcs in an orifice flow. The arc was sustained by a sinusoidal current pulse, (frequency 85 Hz) with peak current values of 3 and 8 KA. The arcs burned between copper electrodes and the host arcing medium was air or SF_6 with an upstream reservoir pressure of 7.8 bar. All upstream measurements were taken at a site 2 mm upstream of the orifice entrance plane, whereas downstream measurements were taken 1 mm from the orifice exit plane.

A Hilger Watts spectrograph type E528 fitted with quartz optics was used to obtain all the spectral records. Most of the upstream measurements were recorded on HP3 photographic plates, whereas the downstream measurements were recorded with the single channel scanning attachment E720, having variable exit slits, fitted with an IP22 photomultiplier. The photographic plates were exposed for 6 us snapshots during the current zero period whereas the photoelectric detection system enabled a continuous timewise record of a given spectral line to be obtained during the final 25 μs before current zero. An electro mechanical shutter was used to prevent the relatively in-

tense light levels which pre-dominated during the high current phase from affecting the current zero recording instrumentation.

The authors determined the electron temperatures both upstream and downstream of the orifice from measurements of the relative intensity of two copper lines as outlined in Griem (1964). The lines used for the upstream measurements were 319.4 nm, 309.9 nm and 330.7 nm whereas the lines used for the downstream measurements were 510.5 nm 515.3 nm, 578.2 nm, 521.8 nm and 570.0 nm. The electron density 2 mm upstream from the orifice inlet was determined from the Stark broadening of the CuI 330.7 nm line at 70 and 50 μs before current zero. The authors used the values of electron density and temperature to confirm the existence of LTE up to 50 μs before current zero.

For SF_6 no upstream temperature results were presented, although the temperatures in this region are similar to those at downstream stations during the current zero period. It is unfortunate also that the authors used different electrode geometries for different measurement locations since this makes comparison of their own results from different axial regions difficult let alone comparison with different authors. Furthermore no radial energy distribution detail could be deduced so that no evaluation of the current zero energy conservation equation could be obtained.

3.4 Continuum radiation

3.4.1 Introduction

Spectroscopic measurements have been reviewed previously and it has been shown how they can provide valuable information regarding overall arc as well as detailed local arc column structure. This information is useful for calculating important energy transport terms in the energy balance and it will be explained in detail in chapter (6). A brief review of some radiation power loss techniques is included since, they can provide additional valuable information to that already obtained with spectroscopic methods.

3.4.2 Development of radiation power loss measurements

An extensive investigation into the total radiation being transmitted remotely from an arc column has been made by Strachan (1973 a,b), (1974), (1975 a,b) and Strachan et al (1977 a). This radiation is the difference between the emitted radiation and the absorbed in the arc environs. In (1973 a,b) Strachan measured the radiation for free burning arcs burning between copper electrodes which were fixed at a 100 mm separation and with a peak current in the range 10 KA to 23 KA. The arc was viewed at several axial locations using a 3 mm width collimating slot laterally situated along the arc diameter. The author measured radiation loss as a function of time and axial distance and calculated the fraction of local power loss by radiation to local electrical power input using the probe measurements of Barrault et al (1972). The author showed how the presence of electrode vapour

can greatly enhance the radiation power loss in the free burning arc. In (1974, 1975 a) Strachan showed that radiation loss provided a major contribution to the total energy loss from the free burning arc column.

Strachan (1975 b) and strachan et al (1977 a) extended the work on the free burning and efflux flow arcs to the more realistic circuit breaking conditions of the orifice flow geometry. The authors investigated the effects of varying upstream pressure (4.46 to 14.1 bar), upstream electrode material (copper, carbon, elkonite, tungsten and mild steel) and peak current (3, 8 and 13 KA) upon the radiation power loss. The authors concluded that the radiation loss with various electrode materials increased in the order carbon, copper, mild steel, elkonite.

Strachan et al (1977 a) derived the following empirical law :

$$Q = \alpha_r . I . E . \sqrt{p} \qquad (3.7)$$

Where

Q is the total radiation power loss.

I is the instantaneous current.

E is the local electric field strength.

p is the local gas pressure.

α_r is a constant depending upon the host arcing medium and the upstream electrode material.

The authors have shown the significance of the radiation loss in terms of the energy balance (up to 30 % of the power dissipated is lost radiatively). However the sensitivity of their detector did not enable the authors to make a similar investigation during the current zero period, thus the significance of radiation loss could not be quantified during this period.

In (1982) Leclerc and Jones extended the above work about radiation power loss measurements for arcs in the peak current range 20 to 100 KA burning in a 50 mm diameter radiussed orifice. The authors used elkonite and carbon as electrode materials, copper and PTFE as nozzle materials and air and SF_6 as a host arcing medium. The flow through the nozzle was sustained by an upstream pressure of about 7 bar and a downstream pressure of 1 bar. The total radiation losses were measured at two axial locations, one 1 mm upstream of the nozzle inlet and the other 1 mm downstream of the nozzle outlet. The total radiation was measured using an RCA 4328 photomultiplier.

Leclerc and Jones (1982) identified the dominant influence on radiation loss as the arc current followed by the local static pressure. However under some operating conditions the general trends may be severely affected by areodynamically induced pressure transients, the formation of an electrode vapour core and the ablation of the nozzle wall resulting from excessive radiative loading. The authors estimated the total radiated power from the entire arc length at a peak current of 90 KA to be of the order of 10 MW. However the authors did not extend their investigation to include the current zero period, there-

fore a quantitative statement of the significance of radiation power loss during this period was not possible.

In (1982) Shammas and Jones attempted the first measurements of the arc energy loss component due to optical radiation close to current zero under conditions relevant to circuit interruption. Reduced power arcing conditions were investigated and the arc current was ramped from a holding (0.35 - 2.5 KA) level to zero with a current decay rate in the range 12 to 46 A/μs. The authors used different nozzle materials (copper and PTFE) and upstream electrode materials (copper-tungsten and carbon). The host arcing medium was SF_6 with an upstream tank pressure of 8.5 bar. Radiation measurements were made through a slot in the circuit breaker nozzle which was at the downstream end of the parallel throat section (a detailed description of this experimental test facility is included in chapter (4) of this thesis). The detector was an RCA photomultiplier type 60 ER (4832) situated sufficiently far (2m) from the arc to validate the inverse square law which was necessary to determine the total radiated power.

Shammas and Jones (1982) derived the following empirical relationships between the radiative losses and the electrical parameters :

(1) Under the quasi-steady state the empirical law governing radiation loss (corresponding to equation (3.7)) with constant pressure is proportional to instantaneous current as

$$L = 0.0143 \, (i - 300) \qquad \text{for } i > 300 \text{ A} \qquad (3.8)$$

Where

L is the equivalent radiative loss in volts ($L = Q_r / 99$).

Q_r is the radiative power loss.

i is the instantaneous current in amperes.

(2) During the transient current decay period ($i < 150$ A) the relationship between the radiative loss at the nozzle throat and the instantaneous current (i), the holding current (i_o), di/dt becomes

$$L = A\, i^{1.05} + B(i_o)^{1.1}\, (di/dt)^{2.37} \qquad (3.9)$$

Where

$A = 4.9 \times 10^{-3}$ $\qquad$ $B = 2.61 \times 10^{-8}$

di/dt is the current decay rate during the final 2 μs before current zero.

(3) The decay of radiation after current zero is given approximately by

$$\tau = 0.174\ (di/dt - 17)$$

for $di/dt > 24$ A/μs and $i_o = 1.55$ KA

Where τ is the time for the radiation to decay to a negligibly small value (μs).

3.5 Concluding statement

In this chapter it has been shown that extensive spectroscopic investigations can be used to calculate local arc parameters which are fundamental for describing the arc column condition and structure.

A detailed knowledge of such parameters further enables the energy transport terms to be calculated. It is the objective of the present experimental investigation to improve the technique of Smith et al (1978) in order to obtain a detailed spectroscopic investigation of an SF_6 nozzle flow circuit breaker arc during the current zero period.

Also in this chapter it has been shown that the total radiation power loss measurements at peak current or during the quasi-steady arcing phase plays an important part in the energy balance during this period. However a lack of reported experimental data makes such an estimation during the current zero period impossible although some unpublished data by Shammas and Jones does exist and will be used later in this thesis (chapter 6) in the quantitative solution of the current zero energy balance.

λ_c nm	A_{mn} S^{-1}	G_m	E_m eV	E_{mn} eV
510.5	0.2×10^7	4	3.82	2.43
515.3	6.04×10^7	4	6.19	2.4
521.8	7.5×10^7	6	6.19	2.37

Table (3.1) Atomic data for the spectral lines of CuI
(Source : Kock and Richter (1968)).

λ_c : Centre wavelength (nm)

A_{mn} : Transition probability (S^{-1})

G_m : Statistical weight of upper energy level

E_m : Energy value of upper energy level (eV)

E_{mn} : Energy difference between levels m and n (eV)

Centre Wavelength nm	Temp. °K / Ne cm^{-3}	Half width at half height (nm)		
		10^{16}	10^{17}	10^{18}
515.3	5,000	1.189×10^{-2}	1.189×10^{-1}	8.855×10^{-1}
	10,000	1.297×10^{-2}	1.326×10^{-1}	1.16
	20,000	1.355×10^{-2}	1.404×10^{-1}	1.34

Centre Wavelength nm	Temp. °K / Ne cm^{-3}	Half width at half height (nm)		
		10^{16}	10^{17}	10^{18}
510.5	5,000	3.55×10^{-4}	3.57×10^{-3}	3.43×10^{-2}
	10,000	4.52×10^{-4}	4.59×10^{-3}	4.59×10^{-2}
	20,000	6.15×10^{-4}	6.25×10^{-3}	6.37×10^{-2}

Centre Wavelength nm	Temp. °K / Ne cm^{-3}	Half width at half height (nm)		
		10^{16}	10^{17}	10^{18}
521.8	5,000	1.22×10^{-2}	1.22×10^{-1}	9.08×10^{-1}
	10,000	1.33×10^{-2}	1.36×10^{-1}	1.19
	20,000	1.39×10^{-2}	1.44×10^{-1}	1.37

Table (3.2) Stark broadening of CuI lines

CHAPTER 4

EXPERIMENTAL APPARATUS AND DIAGNOSTIC INSTRUMENTATION

4.1 Introduction

Fundamental arc measurements are usually made in small scale discharge tubes under relatively easily controlled steady state conditions. To obtain the same degree of control in a full scale circuit interrupter geometry operating at high currents and gas pressures, and under pulsed current and flow conditions, makes severe demands upon the electrical and mechanical design of the test facility. Moreover, existing diagnostic instrumentation, which is suitable for steady state measurements, can no longer be used in a time dependent situation without major modifications.

This chapter is divided into three main sections, the first of which describes the test facility, SF_6 gas properties, the gas handling system, the arc initiation technique, the test head geometry and the power supplies. The second section is principally concerned with the development of the diagnostic instrumentation used to measure both the electrical and spectroscopic arc parameters. Finally the third section is concerned with the system control and timing sequences.

4.2 High power SF_6 interrupter test facility

Details of the experimental test facility have been previously reported by Strachan et al (1977 b). Only a brief description, is therefore presented here.

The interrupter test facility was constructed to enable experiments to be carried out at realistic electric power levels, with full scale interrupter geometries, under controlled gas flow and arcing conditions. This facility is basically of the " two-pressure " type in which gas is allowed to expand from a high pressure upstream reservoir tank into a region of lower pressure. The upstream pressure vessel which is situated at the base of the test rig has a maximum working pressure of 500 psig at temperatures below 150 °F, has a capacity of 5 cubic feet and is made of carbon steel. A photograph of the test rig is given in figure(4.1). The downstream pressure vessel, situated at the top of the rig, has a maximum working pressure of 200 psig at a temperature of 150 °F, with a capacity of 10 cubic feet and is made of carbon steel.

The high pressure upstream reservoir tank was connected via a blast valve, a honeycomb, flow straightener, the test head and a cylindrical outlet pipe to the downstream pressure reservoir. The blast valve is a modified Reyrolle 275kv O.B. circuit breaker valve, having a 3.75 inch diameter outlet. The maximum working pressure of the blast valve is 450 psig. The flow straightener was made of PTFE. The upstream pressure was initially set to 110 and 60 psig and

the downstream pressure to just below atmospheric for the whole series of investigations.

A schematic of the overall test rig layout is shown on Figs.(4.2) & (4.3). Fig. (4.2) shows the test head which was isolated electrically from the remainder to the test rig and which consisted of a mild steel block into which nozzles of various geometries could be inserted and whose vertical sides could be sealed with glass ports so that optical access was readily available. The arc chamber is designed to have a considerable degree of flexibility in operation. It can easily be removed from the rig and the removable flanges greatly facilitate modifications, the changing of electrodes, cleaning and general servicing. Removal of the test head, or any other part of the test section is facilitated by the use of hydraulic jacks under the upstream pressure vessel.

4.2.1 Significant properties of SF_6

Sulphur hexafluoride is a colourless, odourless, tasteless gas. It is non-flammable and non-toxic. At atmospheric pressure the boiling point is -60 °C and the mass density at 20 °C is 6.1 Kg/m^3. The critical point is 45.6 °C at 38 atm and the gas may therefore be stored in liquid form at room temperature. The gas may be liquefied by compression, which simplifies production, but the case of liquefication causes problems in outdoor circuit breakers using high pressure particularly under arctic conditions.

SF_6 is chemically inert up to 150 °C, decomposing at higher temperatures into numerous fragments (Liebermann and Chen (1977)). Some of the fragments are chemically active, attacking metal, glass and some plastics.

The metal fluorides produced during arcing between metal electrodes can cause severe irritation to the skin, eyes and throat of maintenance personnel. SF_6 is rigorously dried to avoid the presence of moisture and the possible formation of HF at high temperatures. For similar reasons hydrocarbons in general are excluded from the internal parts of SF_6 circuit breakers. Recombination of the fragments occurs as the temperature falls, the time scale being of the order 10^{-5} to 10^{-7} second.

SF_6 has a much greater dielectric strength than air at the same pressure and temperature. The exact improvement factor depends both upon the thermodynamic state of the gas and the electrical test waveform, but is about 3 for 50 Hz power withstand tests. However the arc quenching capability of SF_6 is exceptional and derives from a combination of factors.

Under high power conditions the arc temperature is at least 10,000° K leading to an electrical conductivity of above 2000 $\mho$, comparable with copper vapour. This leads to lower power dissipation within the circuit breaker than for air, and consequently reduced heating of the bulk gas and less damage to parts of the interrupter (Jones (private communication)). Furthermore the nett radiation

emission from an SF_6 arc at a given current is lower than from an air arc, again reducing the damage to the nozzle and temperature rise of the surrounding gas.

The dissociation and recombination of SF_6 noted earlier has considerable significance for current zero arc recovery. The molecular bond energy is such that the recombined molecules at about 2000 °k have much less energy than the dissociated fragments at only slightly higher temperatures (Shimmin 1986). There is therefore a peak in the specific heat capacity Cp at 2000 °K, and also in the thermal conductivity K. During thermal recovery after a high current arc it is possible for radial thermal diffusion to dissipate much of the stored energy of the arc across the 2000 °K isotherm (Jones (private communication)). Since this temperature is below the electrical conduction minimum in SF_6 the presence of a recombination sink at 2000 °K does not degrade the thermal recovery performance, although the dielectric recovery performance may be impaired (Mahajan et al (1984)).

The major energy removal process for high power axial flow arcs is by convection along the axis. The power loss by this method depends upon the quantity ($\rho w h$), i.e the product of mass density, velocity and enthalpy (Frost and Liebermann (1971)). In spite of the reduction in mass density at high temperatures the increase in sonic velocity and enthalpy leads to an increase in enthalpy flow as the temperature rises. Once again the recombination effect, causing a high thermal capacity Cp at 2000 °K, leads to a significant value for

enthalpy in the temperature range 2000-3500 °K. There is therefore a substantial enthalpy flux in this temperature range, which is below the minimum for electrical conduction. The combination of good thermal conductivity and enthalpy flux over this temperature range, combined with efficient radiation transport within the higher temperature conducting arc core, leads to a steep-edged temperature profile for the Sf_6 arc at high currents (Airey (1977)).

4.2.2 Gas handling system

For all the reasons mentioned above SF_6 was used as the arcing medium for all the investigations of the present work. The principal components of the gas handling system are a vacuum pump, compressor and refrigerator together with their associated valves, filters, gauges, reservoirs, bursting discs etc. A schematic diagram of the system is given on Fig.(4.4).

As indicated by Fig.(4.4) a compressor is employed to pump gas from the low pressure to the high pressure reservoirs in the test section following an operation of the main blast valve BV. In addition, the compressor is used to pump the SF_6 gas back, via the refrigeration and cooling systems, into storage cylinders. It is a KH25 type air cooled, three stage high pressure pump manufactured by Worthington-Simpson Ltd. Driven by a 15 H.P. three phase S.C. motor, the compressor delivers gas at 600 psig maximum pressure at up to 20 cubic feet per minute running at 800 R.P.M.

Also shown on Fig.(4.4) is a rotary vacuum pump used to evacuate the system, prior to the admission of SF_6 gas, to a base pressure of typically $2x10^{-1}$ torr in 10 minutes. The pump is an Edwards type CNS-02556-ES2000 modified by the supplier for the recirculation of SF_6 gas. More details may be found in Strachan et al (1977b).

4.2.3 Pneumatic initiation facility

Studies of pulsed high current arcs in a flowing gas require a rapid and reliable method of arc initiation. Arc initiation was achieved by striking a low current (300 - 800 A) d.c arc between the two arcing electrodes. This was achieved by keeping the main arcing electrodes fixed and pneumatically driving an auxiliary electrode (a 0.187 inch diameter silver steel rod) through the hollow downstream electrode from it's initial rest position in contact with the upstream electrode. The time taken for the rod to fully retract into the electrode was made small compared to the duration of the d.c initiation such that electrical and flow conditions just prior to the main arcing period were quasi- steady. The efficient operation of the pneumatic initiation arrangement was ensured by the use of a vacuum latch and initiator gas supply vessel. More details may be found in Strachan et al (1977(b)).

4.2.4 Test Head geometry

The geometry of the circuit breaking test head is shown on figure(4.5). The nozzle consisted of an upstream convergent section

45° connected to a 12° diverging section via a 1.0 cm long parallel sided throat section of 35 mm diameter. The material of the nozzle was PTFE, representing an electrically insulating nozzle. A specially designed nozzle with the same flow profile was used for viewing the arc. This nozzle carried a (3 mm) slot which was located at the nozzle throat. The slot was sealed by a slotted rubber gasket compressed against a 15 mm thick glass viewing window so preventing the leakage of gas from the nozzle through the slot. This was an important measure both diagnostically and with regard to electrical performance since leakage of gas could cause image distortion and perturbation or shock waves in the gas flow.

The upstream contact of the model circuit breaker consisted of a 32.0 mm diameter, hemispherically tipped electrode with it's tip 17.0 mm upstream of the upstream edge of the nozzle throat section. The upstream electrode material was 10-W3 elkonite (a sintered copper tungsten mixture). The downstream electrode was of similar shape to the upstream electrode and carried a hollow bore which housed the auxiliary initiation electrode. The downstream electrode tip was fixed at distances of 78, 68, 58 and 48 mm downstream of the downstream edge of the nozzle throat resulting in overall gap lengths of 105, 95, 85, 75 and 65 mm respectively. The downstream electrode material was identical to that of the upstream electrode.

4.2.5 Power supply circuit

The arc current pulses were obtained from a tuned, series connected inductance / capacitance (LC) discharge circuit. The full power circuit (figure (4.6)) consisted of a capacitor bank (35.5 mF, at 6.3 Kv) tuned to a frequency 78 Hz with 90 μH inductors. The capacitor source was switched using two ignitron valves I_2 & I_3 connected back to back to provide smooth current commutation at current zero. Control of the peak current was via the magnitude of the capacitor bank charging voltage, which resulted in varying current decay rates before current zero. A low current (300 - 800 A) initiating arc was used to enable the electrodes to be fully parted before the main power half cycle was triggered. This low current arc was switched with the initiation ignitron I_1 in series with a current limiting resistor R_1 (4 - 6 - 8 Ω).

The voltage restrike (rrrv) immediately after current zero was provided by the natural circuit response. The rate of rise of recovery voltage was governed by the charging voltage of the capacitor bank which was determined by the peak current required. An additional branch in parallel with the main capacitor bank C_1 was provided so that excess energy remaining on the capacitor bank following the full arcing sequence was rapidly drained by diverting the current via a low value resistance to earth by means of an ignitron valve (I_4).

With this arrangement the current peak value was varied in the range 34 to 64 KA, resulting in a current zero decay rate (di/dt)

range of 14 to 27 A/μs. Further details of the full power circuit are given by Strachan et al (1977(b)).

4.3 Instrumentation

4.3.1 Electrical measurements

The parameters measured during the present tests were the peak current, the current zero and the overall gap voltage of the test head. The current shunt used for the measurement of the arc current was a co-axial type with a resistance of 1 mΩ and a (1 μs) risetime. This enabled accurate measurements to be made of the arc current during the current zero period. The lower value of shunt resistance was used to avoid excessive power dissipation and to prevent saturation of the oscilloscope preamplifiers by the excessive voltage developed across the shunt. This was preferred to a fuse protection technique (Taylor et.al.(1982)) in order to reduce electromagnetic noise problems when undertaking delicate spectroscopic measurements (section 4.3.2)

The overall voltage across the test gap was measured with two Tektronix P6015 high voltage probes (bandwidth of 50 MHz) operating differentially between the upstream and downstream electrodes (Figure 4.7). The voltage and current were recorded both during the peak current phase and during the current zero period using two Tektronix 468 digital storage oscilloscopes and a Tektronix 556 oscilloscope (registered photographically respectively).

All the above instrumentation was earthed to a single point located on the " earth side " of the current shunt (the experimental or signal earth) as shown on Fig. (4.7). This was to avoid the occurrence of current loops through the earth connections which could have profound effects on both instrumentation and data for the magnitude of arcing currents in question. Overall calibration of this particular measurement system was performed by Taylor et al (1982).

4.3.2 Optical and spectroscopic measurement system

The optical system (shown photographically on figure (4.8a(i)) and schematically on figure (4.8a(ii))) was used to view full power arcs. This system consisted of a focusing arrangement, a capping shutter (figure (4.8b)), a spectral resolving instrument (monochromator) and a detector / analyser system.

Collimated light emerging from the slot situated on the nozzle throat was focused by an f/2, f=20 mm biconvex lens onto a first reflecting surface of the 90° image rotator. The image rotator consisted of a mirror / prism arrangement which performed a 90° rotation of an image in the plane normal to the optical axis through it. After the subsequent 90° image rotation the light was focused onto the entrance slit of the monochromator such that the whole of the internal collimating mirror of this instrument was illuminated.

A double action capping shutter (close - open - close) (figure 4.8b) was incorporated in the light path, situated close to the

monochromator entrance slit. This prevented light from being incident on the entrance slit for up to 100 μs before and after current zero. The latter precaution was taken in the case of arc reignition which could cause overloading of the optical detection equipment.

The monochromator was a Hilger Watts monospek 1000 grating (1200 line / mm) spectrometer type D400 - 352 fitted with an F1497 slit on the entrance plane. The slit width was set to 28.5 μm resulting in a dispersion of about 0.7 nm/mm at about 500 nm.

The detector camera was a vidicon SIT 500 which enabled a spatial resolution to be achieved in two dimensions by virtue of it's multi-element diode array photo detector surface or target (figure (4.8c)). One dimension in this case was occupied by wavelength due to dispersion by the monochromator. The other dimension represented image dimensions across the entrance slit which in this case corresponded to the diameter of the arc. The camera operation was such that the diode array could be split into 5 lateral segments. These segments therefore corresponded to 5 segments along the arc diameter (figure (4.8d)). After intensification and resolution the information stored on the diode surface (target) was synchronously scanned off the target by an electron beam which took 32 ms to scan the whole target and 1.2 ms to flyback and restart.

The information collected off the target in this manner was instantaneously converted into an analogue signal and transferred to the parent OSA 500 system to be digitally processed. For the entire

spectroscopic investigation the SIT 500 camera was operated in " gated " mode. This meant that an internal electronic shutter allowed light to be incident on the vidicon target for a preset exposure time (1.6 μs). The operational limitations of the camera were such that this exposure time had to coincide with the scan flyback period. The gate pulse (-1 KV) for the shutter was provided by an external unit. After the information was recorded on the camera target in this manner the scanning electron beam required three full scans to fully transfer the information into the OSA 500 memory. This meant that some background (dark current) noise would be accumulated with each scan which could subsequently be removed using one of the OSA 500 controls (or call programs (Appendix 2)). In addition the OSA 500 (consists of 30 memories) controlling the scanning sequence and other operational parameters of the camera. A summary of these is given in appendix (2).

This system enabled 1.6 μs snapshots of arc spectra at selected wavelengths to be taken with radial averaging and radial resolution at different instants during the decay of the arc current to zero and also after current zero in the case of the arc reigniting.

4.4 System control and timing sequences

During the operation of the model circuit breaker many events were required to occur in a precise sequence. Thus the timing of such events was important to ensure reliable and reproducible arcing con-

ditions. It is convenient to divide the timing sequences into two categories.

(i) The overall timing of the circuit breaker mechanism and the arc current pulse.

(ii) The precision (microsecond or submicrosecond) timing during the current zero period (before and after current zero) of all the associated diagnostic instrumentation.

4.4.1 Overall timing of the circuit breaker mechanism and arc current pulse

There are essentially three main mechanical events, namely, the operation of each of the magnetic valves M.V.1, M.V.2 and M.V.3. These valves operate, respectively, the main blast valve B.V which provides the required gas flow through the arcing arrangement, the high pressure supply to the actuator piston, and the vacuum supply to the actuator piston. The pulses required to operate these valves were provided in the correct sequence by a rotary cam-timer device which gave sufficiently accurate and reproducible timing for these purposes. The steady flow of gas through the test head could be sustained for hundreds of milliseconds in this manner which provided sufficient time for the arcing events to occur.

The timing of the arcing events required greater accuracy than the gas flow sequence but a knowledge of the latter remained essential to ensure reproducible arcing conditions. It was essential to ensure the inception of flow of arc initiation current before the initiation rod

was pneumatically lifted off the upstream electrode and electrical contact lost. The initiation ignitron (figure (4.6)) was fired by an auxiliary pulse unit which was triggered initially from the 200 V output of a Culham delay unit at the instant t_i (figure (4.9a)). Sufficient time elapsed for the initiation rod to wholly retract into the hollow downstream electrode before the main arc current pulse was triggered to ensure reproducible arc length. The 1st main ignitron was triggered at the instant t_1 (figure (4.9b)) via an auxiliary pulse unit which was in turn triggered by a 200 V Culham delay unit pulse, and the main arcing sequence initiated. The main current pulse had a half period of 6.45 ms (figure (4.9a)). About 250 μs before current zero the 2nd main ignitron was fired in a similar manner which would facilitate a smooth commutation of current through zero in the event of arc reignition. The dump ignitrons were triggered at some preset time after current zero to remove the remnant charge remaining on the capacitor bank. Using this configuration all the arcing events could be timed to an accuracy of about 1 % or better.

4.4.2 Timing of the diagnostic instrumentation particularly near current zero

Microsecond or sub-microsecond time resolution was required for an accurate investigation of the current zero period plasma processes. For this reason the timing of the diagnostic instrumentation and recording sequences needed to be of microsecond accuracy or better. A more sophisticated method of timing was required in the full power case. The reason for this was that once the first ignitron valve was

triggered the resulting half cycle of arcing had a duration of 6.45 ms ± 0.05 ms regardless of the instant at which the second ignitron was triggered. This ± 50 μs fluctuation in the half period clearly did not meet the required current zero timing specification. Thus it was more convenient to trigger the diagnostic instrumentation off the falling current waveform as it approached zero (figure (4.10a)).

The timing requirements for the spectroscopic diagnostic system were similar to those described by Lewis (1987) for the photographic investigation of the full power arcing case. Similar principles were employed in the electronic technique for the measurement system and shutter. However owing to differences in the mode of operation of the OSA 500 system the techniques were applied in a different manner.

The continuous scanning operation of the SIT 500 meant that the timing sequence of the rest of the experiment would have to be synchronised to the scanning period of the camera rather than conversely. The time taken for the camera to complete one scan of the diode matrix (scanning period) was 33 ms which was followed by a 1.2 ms flyback interval. It was necessary to record the required information on the camera target during the 1.2 ms flyback period so that the current zero period needed to coincide with this flyback period. The camera could then be gated during this time. An electronic coincidence was used to achieve this timewise coincidence (figure (4.10a)). Pulses of 1.2 ms duration (corresponding to the flyback period) with a period of 33 ms were provided by an electronic pulse shaping unit. The pulses were input to the coincidence unit

which was externally triggered from a Culham delay unit (figure (4.9b)) so enabling the unit for a duration of 33 ms (figure (4.10a)). A pulse appeared on the output immediately after receiving the first pulse at the camera input when the unit was enabled. The output pulse was then used to trigger the ignitron valves with the correct delay settings to ensure that the current zero instant coincided with the next pulse at the camera input of the coincidence unit i.e. during the camera flyback period (figure (4.9b)).

The vidicon camera was gated (exposed) by a -1 KV pulse applied to the cathode of the tube whose duration corresponded to the exposure time and which was supplied by an external vidicon gate pulse generator (figure (4.10a)). The gate pulse was generated at different instances during the arc current decay by using the gate output of the current measuring oscilloscope. The gate out pulse was further shaped and delayed by variable amounts (0 to 10 μs) by an auxiliary delay unit which ultimately triggered the vidicon gate pulse generator (figure (4.10a)).

The shutter, whose physical characteristics were discussed in section 4.3.2 above (figure (4.8b)) was triggered following the output pulse from the coincidence unit. The delays were set so that the shutter would expose the camera fully at about 20 or 30 μs before current zero (figure (4.10b)).

With this experimental configuration, consistent simultaneous records of arc voltage, current and spectra during the current zero period could be obtained.

The descriptions given in this chapter show the complexity of the experimentation and instrumentation. Considerable effort was required to ensure reliable and reproducible operation to permit the substantial number of experimental records described in chapter (5) to be obtained.

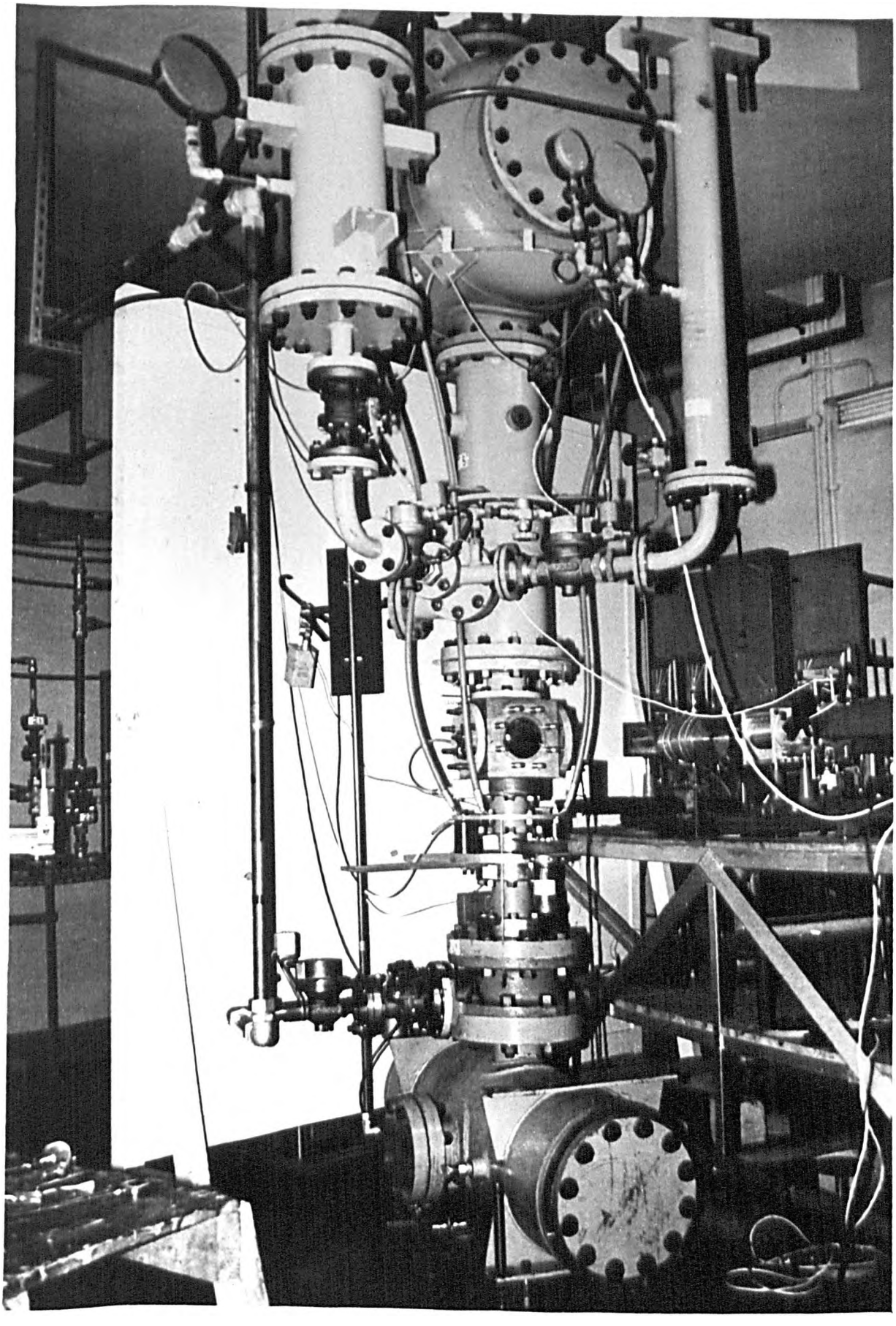

Fig. (4.1) A photographic view of the SF_6 test rig

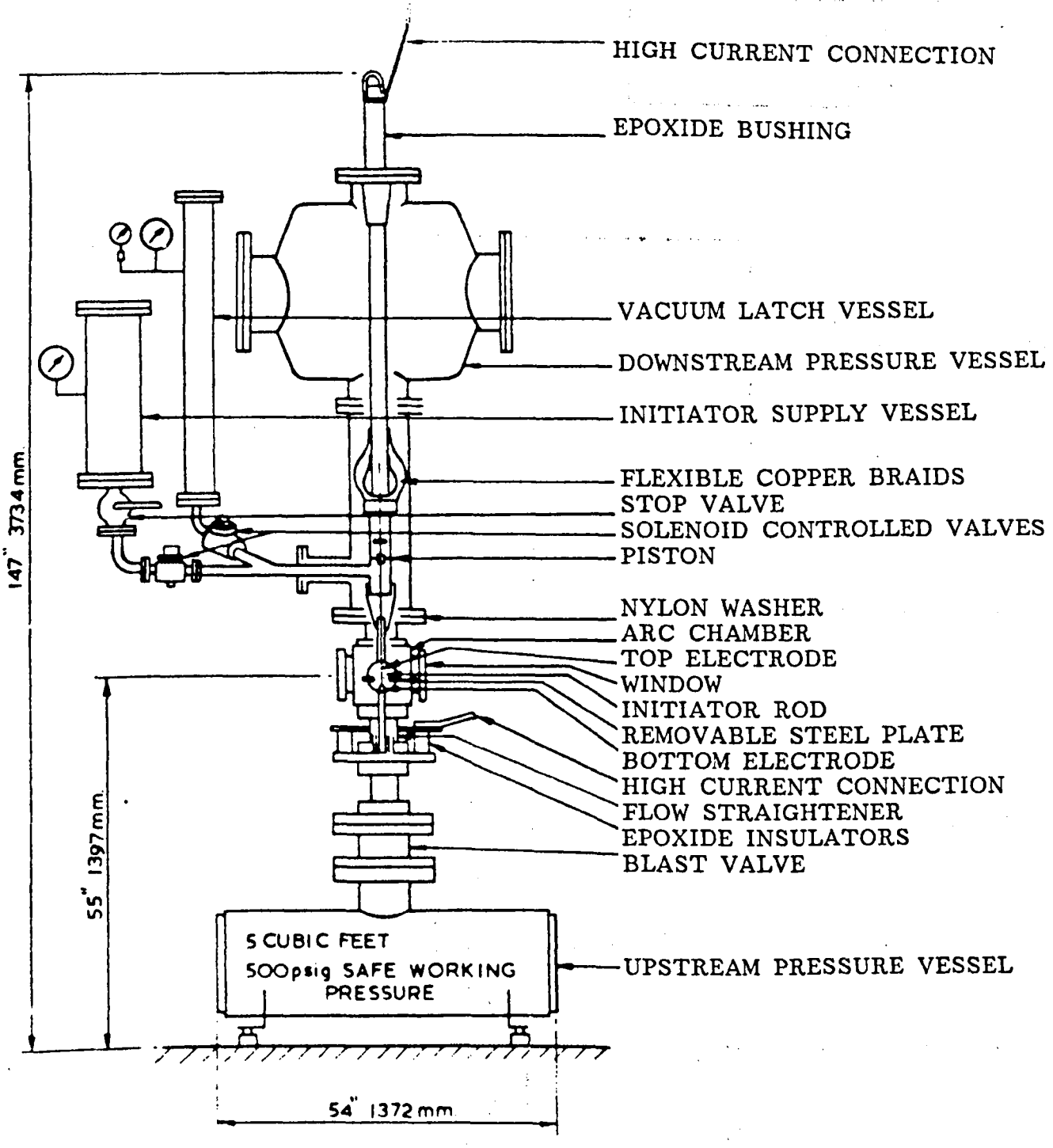

Fig. (4.2) Schematic diagram of the SF_6 test rig

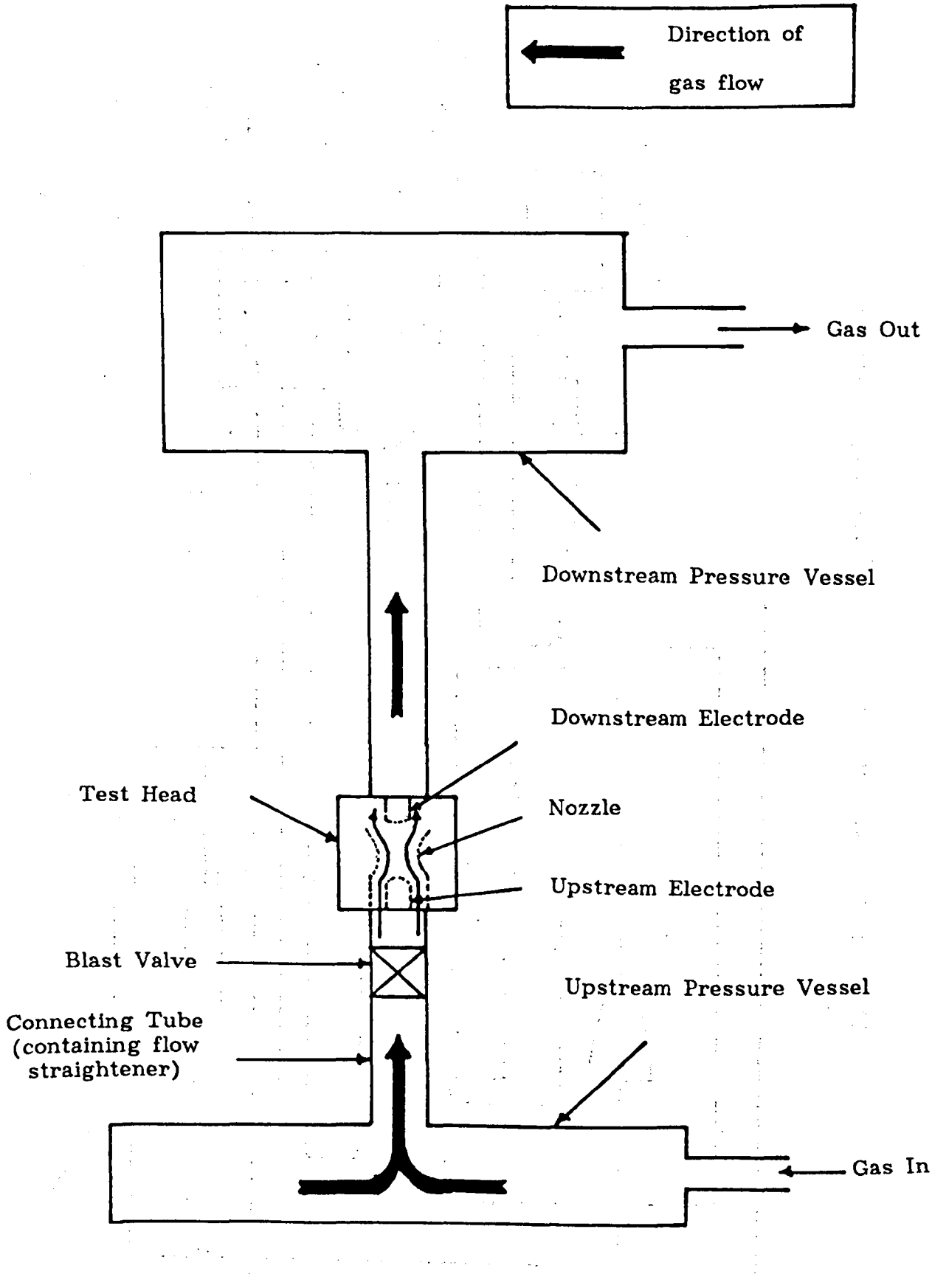

Fig. (4.3) Simplified schematic diagram of the SF_6 test rig

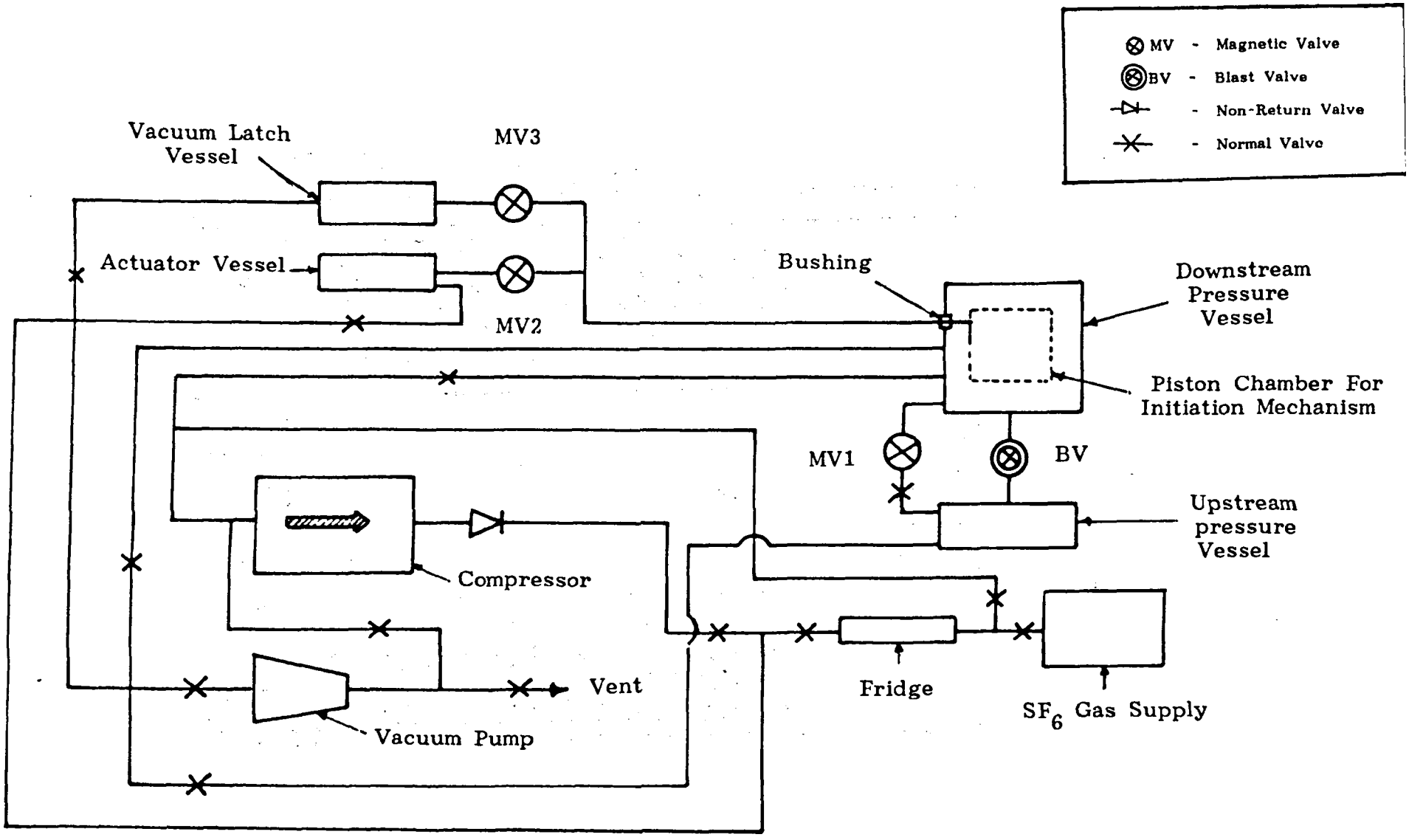

Fig (4.4) Schematic diagram of the SF_6 gas handling system

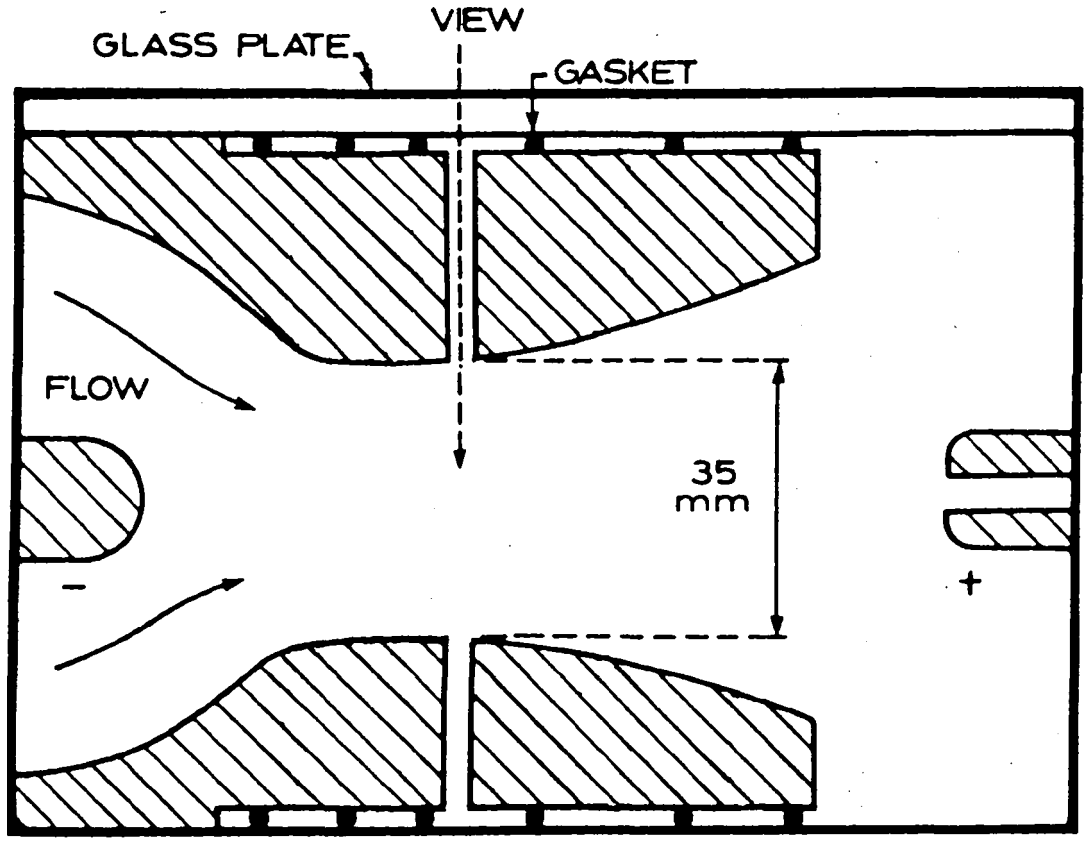

Fig. (4.5) The test head geometry

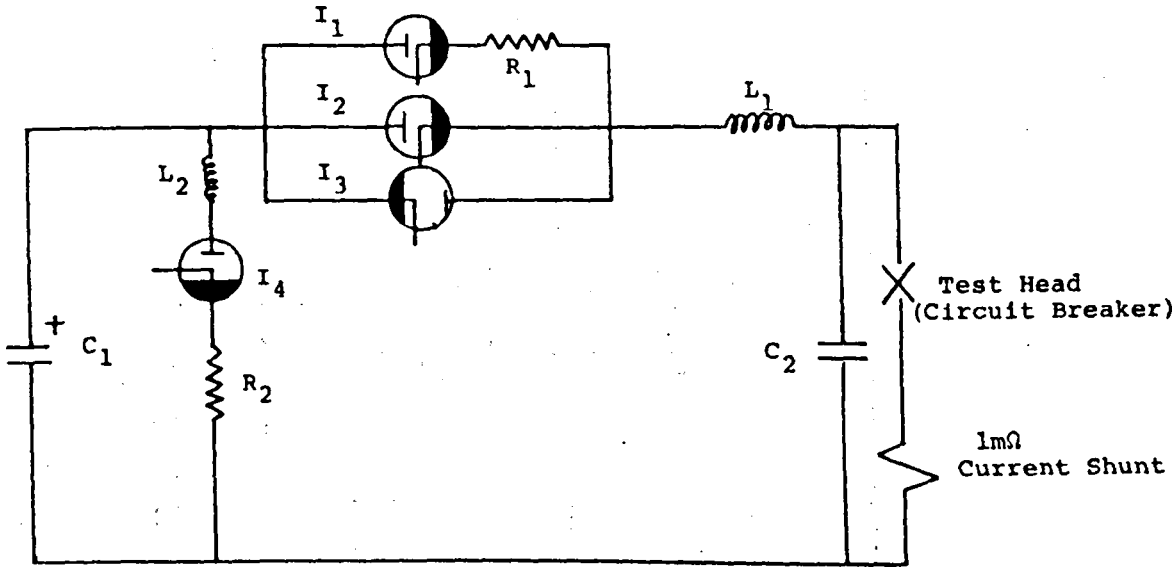

R_1 = 4 to 8 Ω

R_2 = 0.36 Ω

C_1 = 35.5 mF, 6.3 KV

C_2 = Stray capacitance > 1000 pF

L_1 = 90 μH (for 78 Hz operation)

L_2 = 24 μH

I_1 low current forward ignitron BK488

I_2 high current forward ignitron BK488

I_3 high current reverse ignitron BK488

I_4 high current dump ignitron BK488

Fig. (4.6) The electrical test circuit

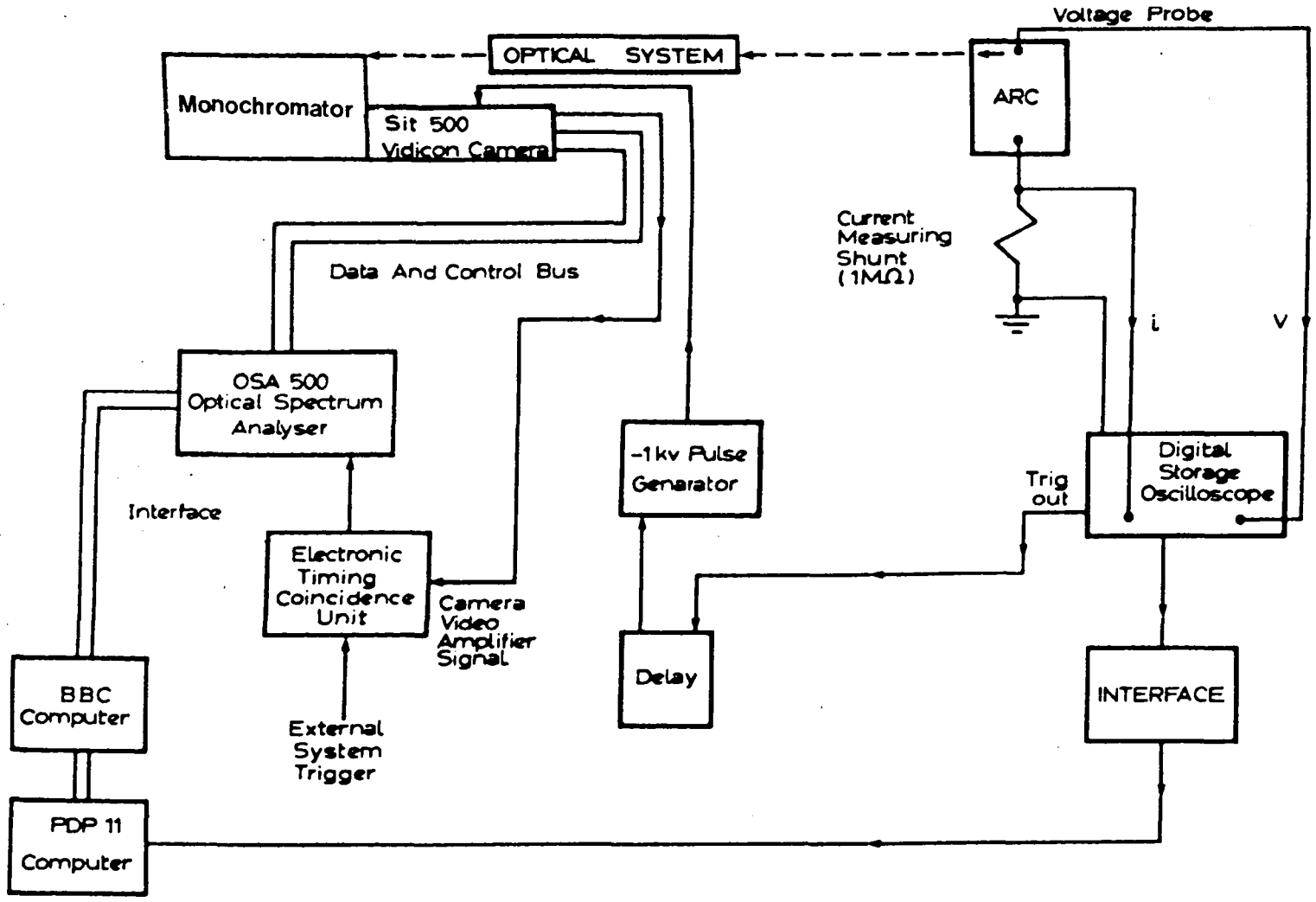

Fig. (4.7) Schematic Diagram of the General Measurement System

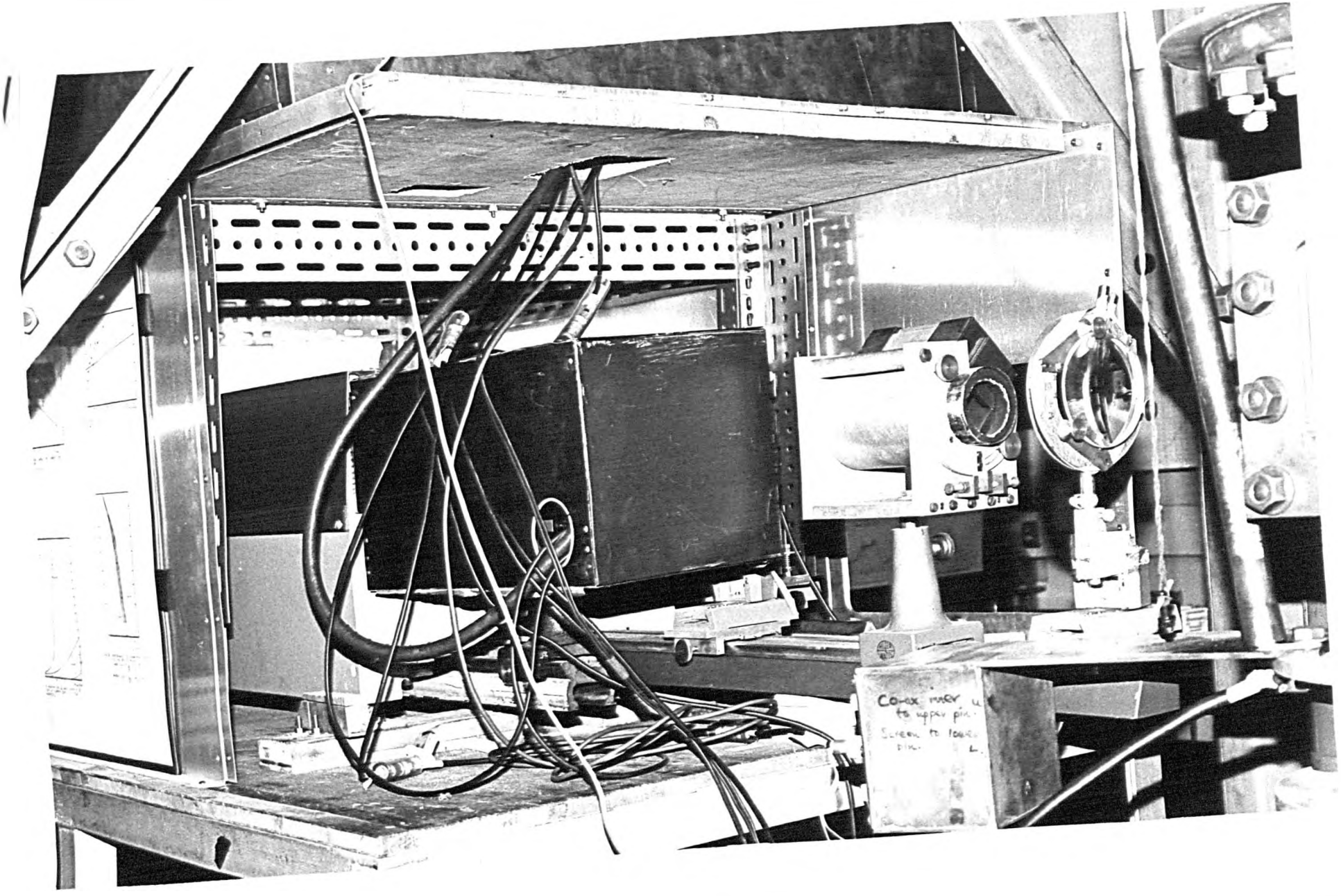

Fig. (4.8) a(i) A photographic view of the optical system

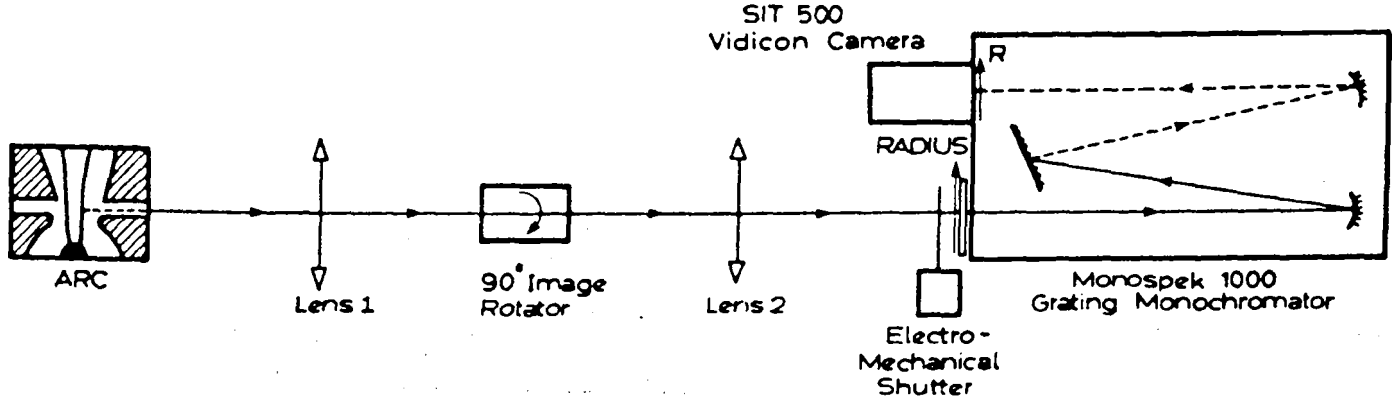

Fig. (4.8) a(ii) Schematic diagram

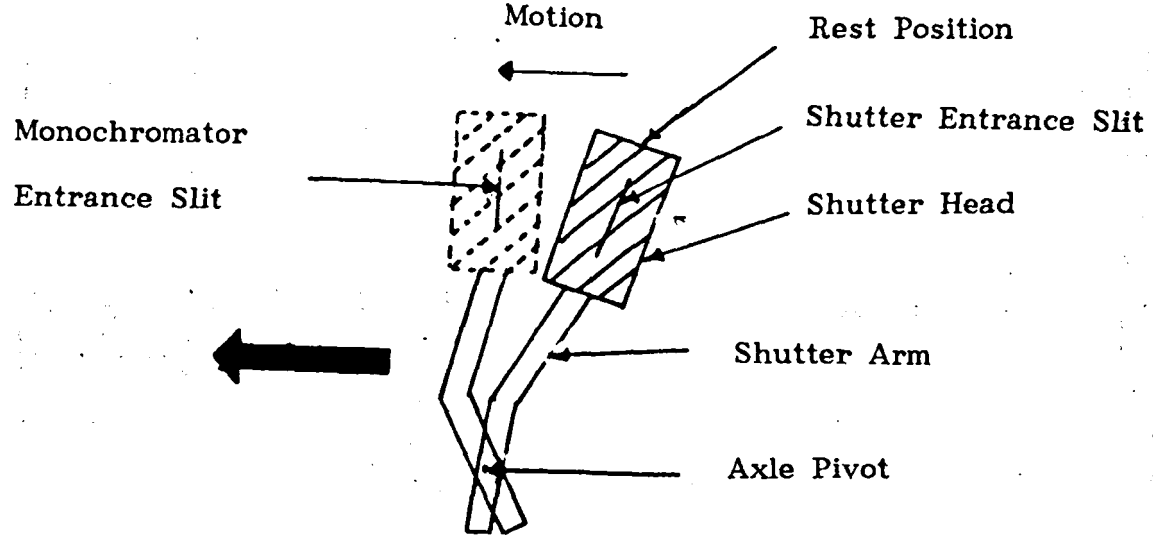

Fig. (4.8) (b) Capping shutter operation

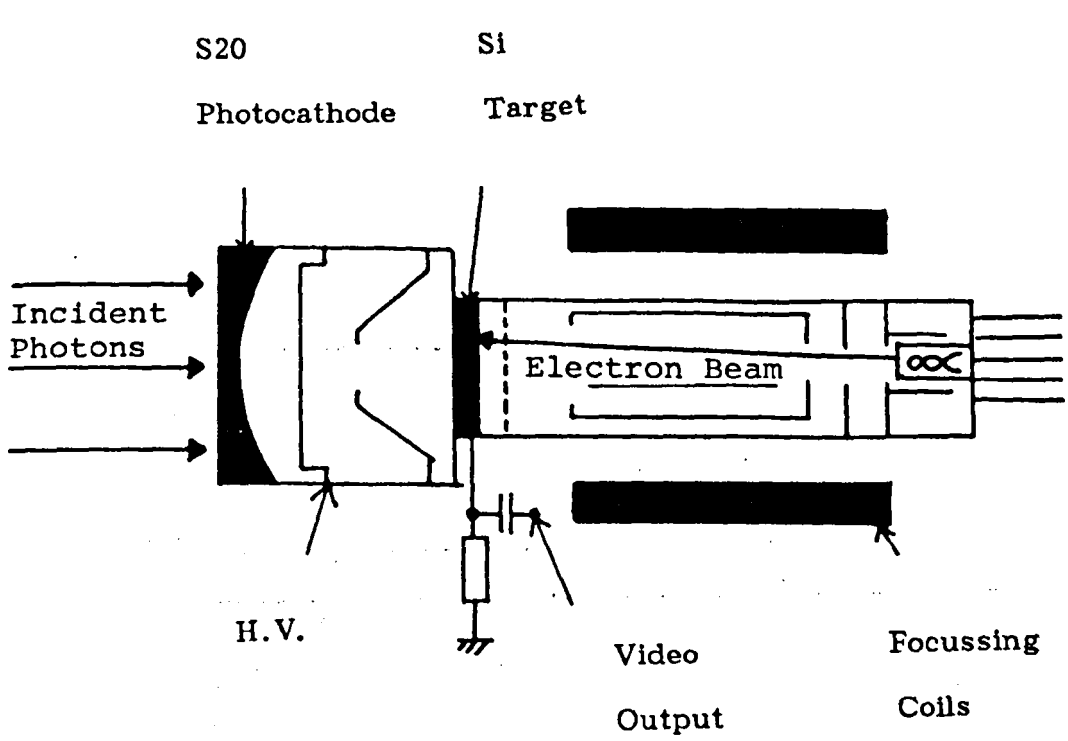

(c)

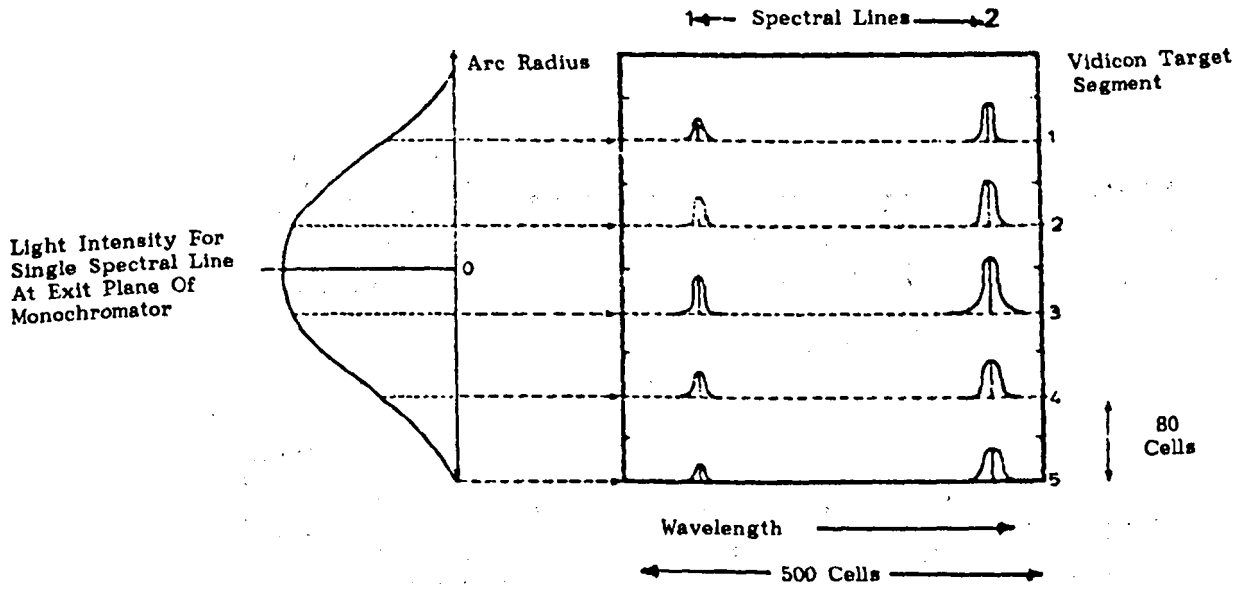

Fig.(4.8) (c) Vidicon camera details

(d) 2-dimensional scanning facility

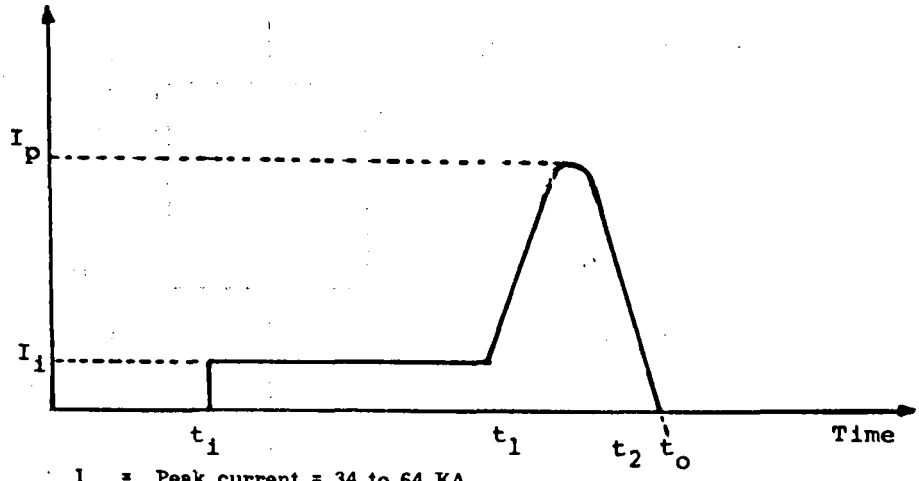

I_p = Peak current = 34 to 64 KA

I_i = Initiation current = 300 - 800 A

t_i = Instant of Firing Initiation Ignitron

t_1 = Instant of Firing First Ignitron

t_2 = Instant of Firing Second Ignitron

t_o = Current Zero Instant

$t_o - t_i$ 50 to 100 ms

Current zero scopes and image converter or vidicon cameras triggered off the falling current waveform

(a)

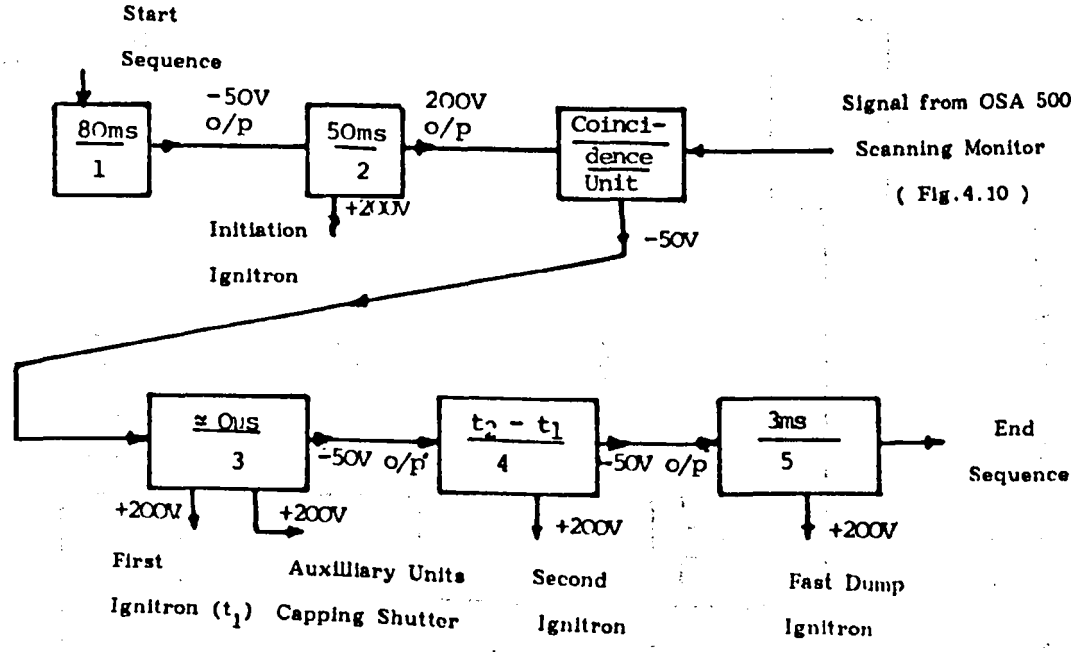

(b)

Fig. (4.9) General timing and triggering of the experimental system

(a) Arc current waveform and important timing points

(b) Schematic representation of the delay unit timing sequence

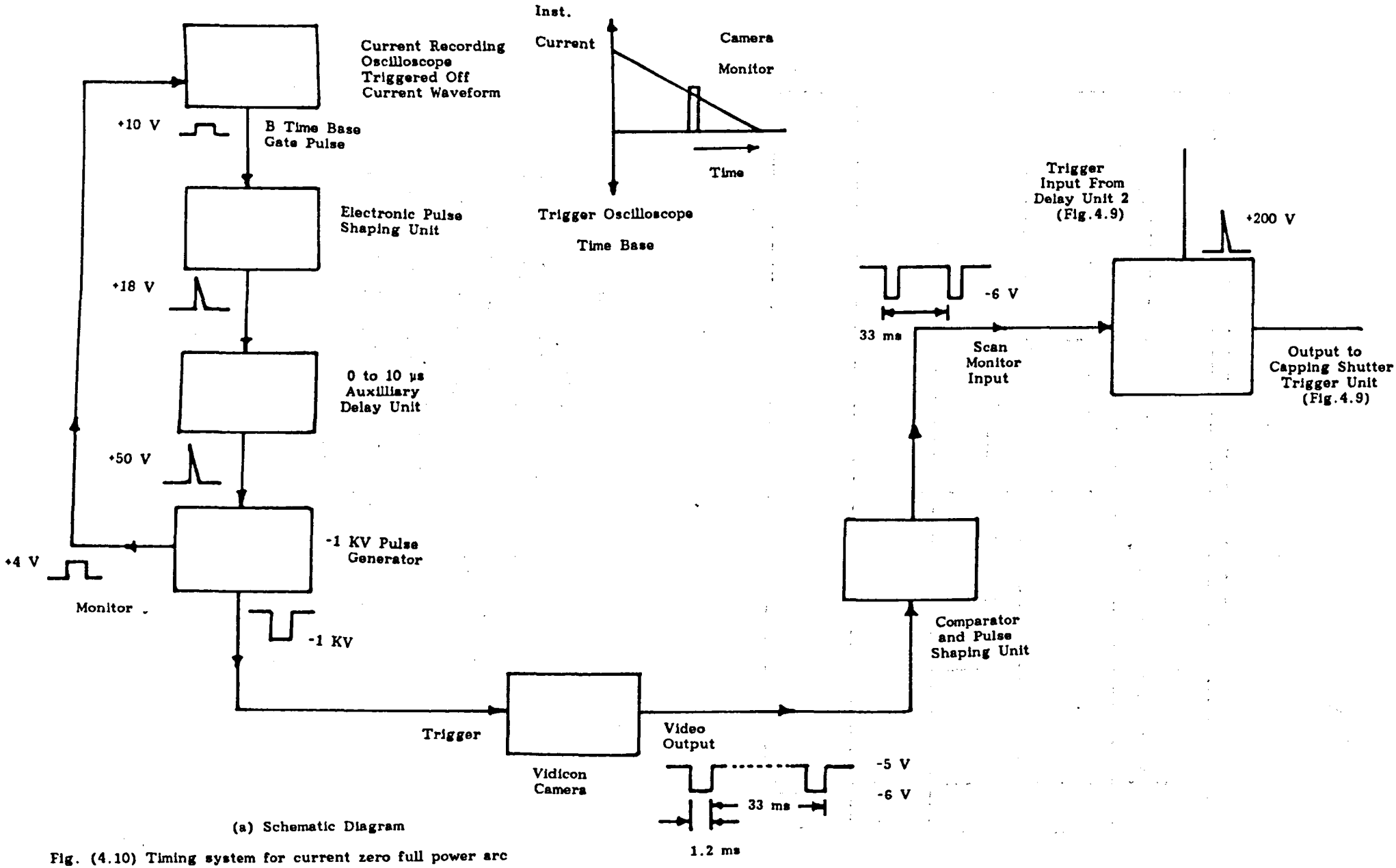

(a) Schematic Diagram

Fig. (4.10) Timing system for current zero full power arc spectroscopy

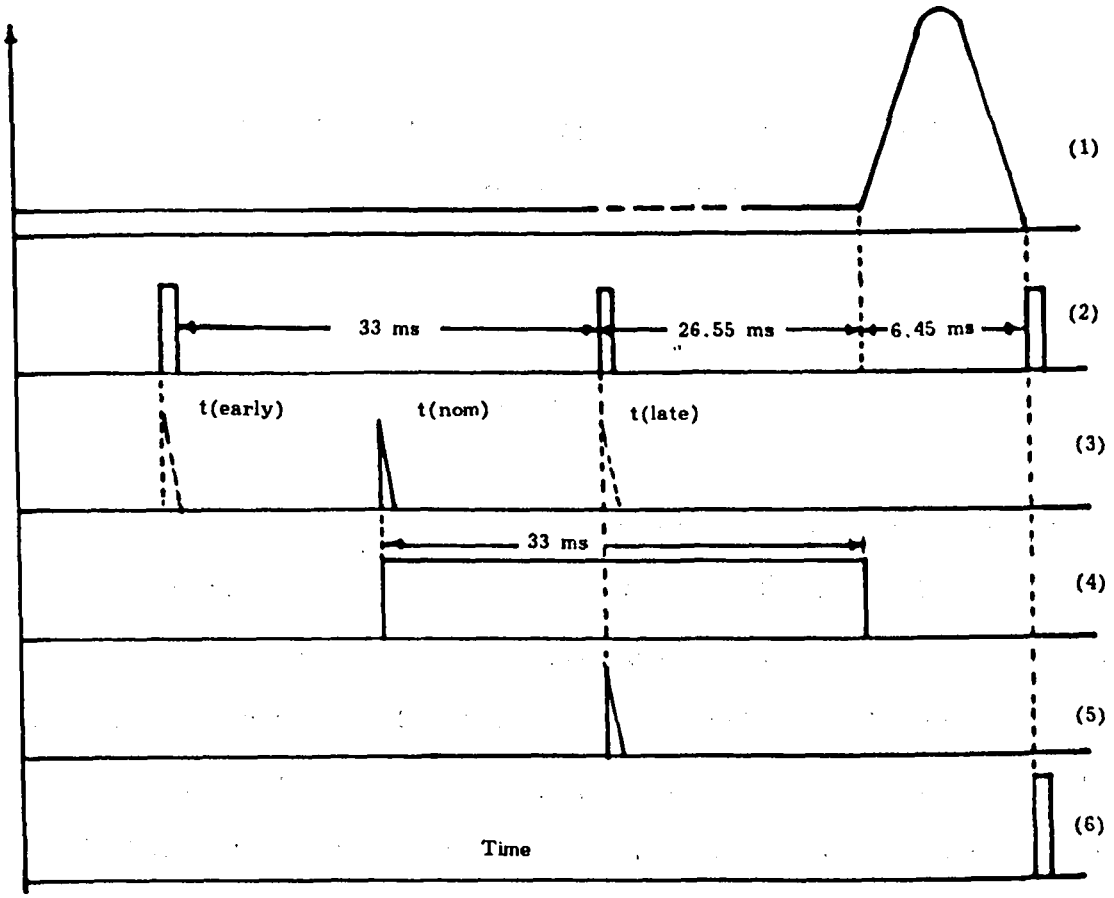

Key

(1) Arc Current Waveform

(2) Vidicon Video Output Scanning Monitor Signal

(3) Pulse from Delay Unit 2 to Trigger Coincidence Unit (Fig. 4.9) - Instant of Occurrence was Variable wrt Waveform (2)
t(early) - Earliest Possible Instant of Occurrence wrt (2)
t(late) - Latest Possible Instant of Occurrence wrt (2)
t(nom) - Nominal Occurrence Instant

(4) Gate Pulse of Coincidence Unit - for which duration the Coincidence Unit is Enabled (33 ms)

(5) Trigger out of Coincidence Unit - Triggers the Capping Shutter Trigger Unit and Latter the 1st Ignitron

(6) Capping Shutter Exposure Characteristic

Fig. (4.10) (b) Timing diagram

CHAPTER 5

SPECTROSCOPIC MEASUREMENTS OF THE ARC TEMPERATURE AND ELECTRON DENSITY

5.1 Introduction and survey spectra

A knowledge of temperature within the electrical core of a gas blast arc near current zero is an important parameter for determining the dominant loss mechanisms which govern arc extinction and reignition. In this chapter time and space resolved spectra of the decaying arc column during the current zero period are presented. The spatial resolution of the arc spectra corresponds to the arc diameter at the single axial location near the nozzle throat and was limited only by the resolution of the optical system and the vidicon camera scan capability as explained in chapter (4). The temporal resolution for all the results is 1.6 μs (exposure time) which was governed by the camera gate time (chapter 4) and limited by the amount of light incident upon the camera aperture. Snapshot spectra (1.6 μs exposure) are presented at different instants during the final 20 μs before and after current zero for two different pressures and a given set of operating conditions.

To obtain meaningful temperature results during the transient arc column decay during the current zero period, two fundamental conditions need to be satisfied :

(1) The spectral lines under observation must satisfy many conditions applied by the physical nature of the source.

(2) Adequate time resolution must be achieved to identify important transient current zero arc processes.

The first of these conditions has been discussed in chapter (3) and the second is wholly a function of the overall system sensitivity. So it is important that adequate light intensity exists during the current zero period to enable short duration exposures. The intensity requirement is made more severe by the requirement for radial resolution.

Figures (5.1) and (5.2) show typical spectra of high current circuit breaker arcs during the current zero period with the operating conditions as indicated on the diagrams. The axes correspond to intensity (vertical) and wavelength (horizontal). The spectral peaks are associated with emission from various elements. Analysis of these spectra involves an identification of the more intense lines i.e. to establish the dominant wavelength and from tables the elements producing the line.

In Figs. (5.1 a,b and c) there are only two lines apparent and these have been identified by Lewis et al (1985 a) to be two copper lines, CuI 510.5 and CuI 515.3 nm. This group of copper lines CuI 510.5, 515.3 and 521.8 nm is particularly conspicuous in this region and have been used by many authors, (e.g. Smith et al (1978)), since

the identification being certain. Thus, the position of the CuI 510.5 and 515.3 nm lines were used to calibrate the wavelength scale.

In Fig. (5.2) many smaller peaks appear between the two copper lines. Although relatively accurate estimates of the wavelengths of these smaller peaks have been obtained by using the two known copper lines to calibrate the wavelength scale, nevertheless an error of ± 0.05 nm still existed and this uncertainty can lead to some identification problems. Although several possible spectral lines could exist in the range 512.8 to 513.15 nm (e.g. Harrison et al (1952)), the most likely elements to be present in the arc plasma are those deriving from the arced gas or component materials. These include W, Cu, S, F, C and H. W and Cu may be produced from the arc electrodes, S, F from the dissociated SF_6 gas and C, H, F from the PTFE nozzle. Spectral lines not associated with these elements can therefore be excluded. Also within the wavelength range considered there are no significant transition associated with the elements S, F and H. The temperature of the arc has been estimated as lying between (7,000 - 10,000 °K) so that, almost all molecules have been dissociated, impling that no significant vibration and rotation transition will exist. Therefore the spectral band heads can also be excluded.

The degree of atomic ionization is also low at these temperatures so there will not be any significant ionization lines. As a result we conclude that the smaller peaks belong to tungsten. The spectral constants of these tungsten atomic spectral lines - which were taken

from Corliss and Bozman (1962) - are given in table (5.1). With these data the relative intensity of these tungsten lines may be estimated. Fig. (5.3) shows the intensity ratio of these lines, which should assist in estimating the species temperature.

5.2 Temperature measurements

5.2.1 Radially averaged spectra captured during the current zero period

The radially averaged, time resolved spectra of the decaying arc column are shown on Figs. (5.4 a,b and c) for different peak current values 34, 46 and 53 KA (corresponding to current decay rates di/dt of 15 A/μs, 18 A/μs and 22 A/μs). Spectral records for the two lines 510.5 and 515.3 nm show that these particular lines are free from any of the deleterious effects outlined in chapter (3) section (3.3.1).

Figure (5.5 a) represents the intensity decay of the two principal diagnostic lines used in this investigation (515.3 nm and 510.5 nm) during the current zero period. These values were derived from the results of Fig. (5.4 a) by a computational analysis of the respective spectrograms. Two distinct regions may be identified corresponding to two different decay rates.

Figure (5.5 b) represents the radially averaged intensity decay of the arc column during the current zero period of a medium di/dt = 18 A/μs (corresponding to 46 KA peak current). Sufficient information is available from the two lines investigated to allow extensive

temperature and electron density information to be extracted. Also this figure shows two distinct time intervals but with a slightly higher intensity decay rate during period I which is not the case for the same two spectral lines on Fig. (5.5 a). Also period I extends closer to current zero before the rapid intensity decay occurs.

The corresponding intensity variation with a peak current of 53 KA (di/dt = 22 A/μs) is plotted on Fig. (5.5 c). Also in this case the threshold between the two periods is even closer to current zero than the 34 and 46 KA cases. By comparing Figs. (5.5 a,b and c) it is clear that the intensity of the 515.3 nm line is generally higher in the 53 KA case throughout the current zero period.

Arc spectra during the current zero period have been captured for a wide range of arcing conditions and their resulting temporal intensity variations presented. However timewise intensity variations of spectral lines in this manner can be misleading owing to their unique intensity : temperature characteristics chapter (6). A more meaningful physical representation of the arc column would be a timewise variation of temperature rather than intensity.

5.2.2 Time variations of radially averaged arc temperature

Radially averaged arc temperatures have been calculated from the data presented in the above section. The method of calculation is described in full in chapter (3) section (3.3.3). The temperature was

deduced from the ratio of two CuI (510.5, 515.3 nm) line intensities using the spectral constants of table (3.1) and equation (3.5).

Figure (5.6) shows the temporal variation of the radially averaged arc temperature at the nozzle throat during the current zero period for three cases of peak arcing current (34, 53 and 60 KA). There are two sources of uncertainty involved in these temperature measurements. The first is the scatter produced by experimental test to test variation, the second, is the uncertainty in atomic data values e.g. transition probabilities which can be as high as 20 % in some cases. These uncertainties represent a total uncertainty of about ± 500 °K which is shown in Fig. (5.6) as an error bar. A second outstanding feature of these results is the slow temperature decay until the last 3 μs after which the temperature falls sharply as current zero itself is approached. Also it can be seen from this figure that the temperature is proportional to the peak current.

5.2.3 Radially averaged temperature variation with current decay rates

Figure (5.7) shows the variation of radially averaged temperature during the current zero period with current decay rate for the two pressures 60 and 110 psig. Because of the lack of intensity of the spectral lines at the current zero instant for the lower peak current case a plot of radially averaged arc temperature at the current zero instant would be of limited value. The most striking feature of these

results is the sharp rise in current zero period temperature above a di/dt value of about 20 A/μs and also the temperature is higher for the case of higher pressure. For example, at the lower di/dt (15 A/μs), the radially averaged temperatures lie in the range $6.75X10^3$ °K to $7.75x10^3$ °K; in the medium di/dt case (20 A/μs) the range of temperature values is $7.0x10^3$ °K to $8.0x10^3$ °K whereas at higher di/dt (24 A/μs) the range of temperature values is $7.8x10^3$ °K to above $9.0x10^3$ °K. It is notable that the value of di/dt at which the radially averaged temperature rises more sharply is 20 A/μs which corresponds to the di/dt values at which the arc column axis intensity (measured photographically (Lewis 1987)) and the total radiation power loss show a similar increase.

The nature of these radially integrated results clearly can only provide an approximate insight into arc temperature changes. More detailed and reliable information can be derived from radially resolved measurements.

5.2.4 Radially resolved arc spectra captured during the current zero period

Two types of spectroscopic results were obtained during the current zero period. The first type was a radially integrated result whereby light was gathered from the whole extent of the arc diameter and has been discussed in section 5.2.1 Figs.(5.4 a,b and c). The second type was a radially resolved result whereby light from 5 seg-

ments situated diametrically through the recorded as shown on Figs. (5.8 a,b and c) and Figs. (5.9 a-e). In the latter case the radial resolution of the spectral lines was obtained by dividing the photosensitive area of the camera into five equally proportioned strips as described in chapter (4). Each of these strips represents 1 mm of the arc column diameter.

Figures (5.8 a,b and c) represent the radially resolved arc spectra of 3 cases of peak current 34 KA, 46 KA and 53 KA at the viewing position near the nozzle throat and upstream pressure of 110 psig. In every record two CuI spectral lines are presented (510.5 nm and 515.3 nm CuI emission), centred on about 513.0 nm. These spectra were recorded at different instants during the current zero period and were representative of similar records taken at different times before and after current zero for each case of peak current.

The radially resolved spectra presented in Fig. (5.8) provide useful information regarding the arc radial intensity variation even before temperatures are calculated. A comparison of Figs. (5.8 a and b) reveals that the luminous diameter of the arc has increased from 4 mm to 5 mm with an increase in peak current from 34 KA to 46 KA. Also a comparison of Figs. (5.8 a and b) shows that the spectral line intensity is higher in the case of higher di/dt which means that the latter has a higher temperature value at its periphery. It is worth noting in this case that the emission in the centre viewing portion of (5.8 b) (I_p = 46 KA) is also higher than (5.8 a) (I_p = 34 KA) which

is indicative of a higher temperature existing in the centre portion of the latter arc column.

Figures (5.9 a-e) show the radially resolved arc spectra of 5 cases of peak current in the range of 34 to 60 KA captured before and after current zero and for an upstream pressure of 60 psig. A comparison of Figs. (5.9 b and c) reveals that the luminous diameter of the arc has increased from 5 mm to 6 mm with an increase in peak current from 46 KA to 53 KA. Also a comparison of Fig. (5.8 b) (p=110 psig.) and Fig. (5.9 b) (p=60 psig.), shows that the light intensity in the higher pressure case is greater especially in the middle track. This is indicative that the axis temperature (centre portion of the arc column) is higher in the case of higher pressure (p=110 psig.), Fig. (5.7). A comparison of Fig. (5.8 c) (p=110 psig.) with Fig. (5.9 c) (p=60 psig.) at the same di/dt shows that the arc diameter is wider in the case of the lower pressure.

Figures (5.9 d and e) represent the spectrograms centred at a wavelength of 513.0 nm captured 6.6 and 7.3 μs after current zero in the case of reignition. A comparison of Figs. (5.9 d and e) (after current zero) with Figs. (5.9 a,b and c) (before current zero) show that the light intensities are higher before current zero than after current zero. Also the spectrograms of Figs. (5.9 a,b and c) show that differences in the intensities (above the continuum) exist over the whole extent of the arc diameter for different di/dt. These results are in good agreement with the radially averaged results obtained at corresponding peak current values and instants before current zero.

At low di/dt values (15 A/μs) the contribution of the continuum, particularly near the periphery was low. However as the di/dt value increases a significant amount of continuum was detected near the periphery where spectral line emission may be present. The increase in continuum may give rise to a luminous region near the periphery of an arc photograph.

Radially resolved arc spectra have been presented which have enabled a comparison to be made with the radially averaged spectra. Also certain qualitative features regarding the radial profiles of spectral light intensity have been identified. However the radial distribution of the spectral intensity of the arc enables the calculation of the arc temperature profile to be made. The calculation of this profile further enables the physical properties of the arc column to be determined in a quantitative manner.

5.2.5 *Arc temperature profiles calculated from the radially resolved spectra*

Whilst the radially integrated temperature measurements are extremely valuable for the derivations of gross arc properties, accurate predictions of transport properties can be obtained only from a detailed knowledge of the radial temperature profile. During experimentation it become clear that the arc column could suffer both lateral shifts off the axis of symmetry and also suffer asymmetric radial distortions. An analytical scheme for interpreting the experimental

results of the form shown on figures (5.8) and (5.9) therefore needs to take account of such disturbances. For this reason a computer programme was developed for calculating the intensity of the 515.3 nm and 510.5 nm lines from various radial profiles of emissivity and also for different radial displacements of the arc column.

Form the experimental data the intensities of the 515.3 nm and 510.5 nm lines were determined using the computer programme shown in appendix (1). On the other hand the calculated intensity from a known radial emissivity profile for different arc radius (R) was determined and given by appendix (1). The experimental and the theoretical results were compared to check if there was a shift or an asymmetry of the arc column or both. After obtaining the correct shift, the shape of the 515.3 nm and 510.5 nm lines could be drawn. A simplified flowchart of the computer programme is shown on figure (5.10).

The arc temperature profiles calculated from the radially resolved spectra are presented on Figs. (5.11), (5.12) and (5.13). A temperature profile is presented for different peak currents in the range (34 KA - 60 KA) (di/dt 14 -25 A/μs) at various times before and after current zero and also for two cases of pressure (p=60 and p=110 psig.).

The temperature profiles of Fig. (5.11 a) show the arc to have a central axis temperature in the range of 8,000 °K to 8,500 °K and to have a 5,500 °K isotherm at a radius (1.7 to 2.25 mm) for the case

of low di/dt (14 - 17 A/μs). The operating condition for these curves are shown on Fig. (5.11 a) for the case of p=110 psig. The profiles show that there is a shift of the central viewing axis in the range of 0.05 mm to 0.2 mm as shown on Fig. (5.11 a) but there is no asymmetric radial distortion. The radially averaged temperature results of Fig. (5.6) show reasonable correlation with the temperature profile at the corresponding current level. The radial positions of the 5,500 °K isotherm also show reasonable correlation with the photographic luminous area measurements by Lewis (1987), which indicates a luminous radius of about 2.5 mm at the same axial viewing station.

Figure (5.11 b) represents the temperature profiles captured at 3.6, 5.3, 10 and 7.6 μs for the current decay rates of 20, 20, 18.5 and 20 A/μs respectively. The profiles in this case indicate an arc with a slightly higher axis temperature in the range of (8,250 to 9,000 °K). These profiles also show a 5,500 °K isotherm at a radius (2 - 2.4 mm).

The temperature profiles at 6, 2.8, 4.2 and 14.6 μs before current zero for the current decay rates of 22.2, 24, 25 and 24 A/μs respectively are shown on Fig. (5.11 c). The axis temperature for this case is higher (in the range of 8,750 to 10,250 °K) with a 5,500 °K isotherm radius in the range of (2 - 2.5 mm). These temperature profiles are again consistent with the radially averaged measurements of Fig. (5.6) for equivalent arcing conditions. The temperature profiles presented on Fig. (5.11 c) have a steep temperature gradient at the 5,500 °K isothermal boundary which plays an important role in

the justification of the boundary layer approximation of the integral analysis, chapter (6).

The temperature profiles at 1.2, 3.2 and 11.5 μs after current zero at very high current (di/dt = 25 A/μs) (peak current about 60 KA) are shown on Fig. (5.11 d). The profiles in this case indicate an arc with a central axis temperature in the range of 8,500 to 9,500 °K and with a 5,500 °K isotherm at a radius (1.4 - 2.2 mm).

Figures (5.12 a,b,c and d) show the temperature profiles in the case of low pressure (p=60 psig.) for four cases of peak current and for different operating conditions. Fig. (5.12 a) shows the case of low current (di/dt 14-17 A/μs), curve 1 corresponds to operating conditions, di/dt=16 A/μs and to a time 12.8 μs before current zero and pressure of 60 psig. The axis temperature is 8,500 °K and the profile has a smooth parabolic shape down to a temperature of about 5,500 °K at a radius of 2.5 mm. Curve 2 corresponds to the same operating conditions for curve 1 but for the case of high pressure p=110 psig. By comparing curve 1 and curve 2, the first one shows a wide flat temperature but the second one shows a steeper temperature profile. The temperature profile has a higher axis temperature in the case of high pressure, by about 250 °K for the above two cases. Similar temperature profiles were obtained for the case of low pressure (p=60 psig.), medium and high current before and after current zero as shown on figures (5.12 b,c and d).

Figure (5.13) shows a comparison between the temperature profiles for the two cases (high and low pressures p=60 & p=110 psig.). Curve 1 corresponds to operating conditions, di/dt = 15.5 A/μs and to a time 5.6 μs before current zero and pressure of 60 psig. The axis temperature for this case is about 8,000 °K with a 5,500 °K isotherm radius of about 2 mm. By comparing the profile (curve 1) and the profile (curve 2) - which has the same operating conditions but for p=110 psig. - one can conclude that the axis temperature is higher in the case of high pressure and the radius of the arc is wider in the case of low pressure.

A final observation on the radially resolved arc spectra of Figs. (5.8) and (5.9) is that the spectral lines do not appear in the same set of viewing tracks from test to test. This indicates that the arc column moves from shot to shot by as much as a column diameter. Apart from making such spectra difficult to capture in successive tests, this indicates an arc which is prone to eccentric movement about a central axis.

The time variations of the axis temperature profiles under different operating conditions are shown on Fig.(5.14). This figure shows that the axis temperature is higher in the case of high pressure. Also the axis temperature relating to the 34 KA (di/dt = 15 A/μs) case occupy a range generally lower than the corresponding 53 KA (di/dt = 22 A/μs) values throughout the current zero period. Also from temperature profiles the time variations of the arc diameter under different operating conditions were determined as shown on Fig. (5.15).

These variations of the arc diameter show reasonable correlation with the photographic luminous area measurements by Lewis (1987) for the same operating conditions.

5.3 Occurrence of tungsten lines

Analysis of several recorded spectra showed that tungsten lines did not always occur in the spectrum despite the appearance of strong copper lines. For instance, Lewis (1987) did not find tungsten lines in his experiments although the arc temperatures were certainly high enough for these to be apparent. Conversely the arc temperature was estimated to be lower, but nonetheless strong tungsten lines occurred. Also rather strong tungsten lines may be recorded in one experiment, but not in successive experiments under identical conditions. It therefore seems that the occurrence and intensity of the tungsten lines has no regular pattern. However, after statistical analysis of all experimental records, it has been found that there are two main factors which affect the occurrence of the tungsten lines. One of these factors is the value of the current decay rate (di/dt) at current zero, and the other is the time before current zero (or after current zero if arc reignition occurs) at which the spectrum was recorded.

Figure (5.16) summarises the occurrence or absence of tungsten lines from a series of 95 experiments at a pressure of 110 psig. (7.8 bar). The horizontal axis in this figure represents the instant of time at which the spectrum was recorded (t=0 indicates current zero)

whilst the vertical axis represents the current decay rate (di/dt). In this figure the plus sign represents cases in which tungsten lines appeared whilst the minus sign represents cases in which tungsten lines are absent. Results for conditions when the arc was extinguished at current zero are of course confined to the sector before current zero (to the left of the vertical axis corresponding to t=0).

The results shown on Fig. (5.16) may be divided into three zones as indicated by the two dashed lines. In the zone above the two dashed lines tungsten lines are always identifiable in the spectrum. In the zone below the two dashed lines, no tungsten lines have been identified in the spectrum. In the zone between the two dashed lines, the occurrence or absence of tungsten lines varies from one experiment to another. The existence of this zone of uncertainty may be due to the following reasons : Firstly, there is no absolute standard for judging the appearance of any tungsten line, but simply to decide approximately by comparing the relative intensities of the tungsten and copper lines El-Kholy et al (1987) (app. 5). Thus it is not clear whether on some records, the noisy nature of the spectrum between the two copper lines (e.g. Fig. (5.1 b)) is due to instrument noise or due to low intensity tungsten lines. Secondly there are error limitations in the measurement of di/dt and t. The error of di/dt is about 0.4 A/μs whilst the error of t is about 0.2 μs. Thirdly, perhaps the most important reason is that, some random factors may occur during testing which strongly affect the appearance of tungsten lines. For instance, tungsten lines are not usually apparent even at high currents when the circuit breaker contacts are new. This is because the

vaporisation of copper from the copper-tungsten sintered contact material occurs preferentially and as a result the temperature of contacts is prevented from rising sufficiently to promote tungsten evaporation El-Kholy et al (1987) (app. 5). For contacts which have suffered arcing several times, the tungsten content in the surface layer may be greatly increased, so that tungsten evaporation is enhanced. This behaviour is consistent with the observation from the present experimentation that the tungsten lines appear in the approximate order 514.5, 513.8, 512.95, 512.4, 512.0, 511.75 and 510.95 nm as shown on figure (5.17).

The dashed lines on Fig. (5.16) show that the tungsten lines appear only at high values of di/dt except for longer times before current zero. In other words the larger the di/dt and t, the higher the probability of appearance of tungsten lines. This implies that the appearance of tungsten lines is related to energy, because higher di/dt imply higher peak currents and more energy dissipation in the system. Longer times imply a higher instantaneous current and more power input into the system at the moment of recording the spectrum.

Figure (5.18) shows the experimental results for an upstream pressure of 60 psig. (4.25 bar). This shows a similar trend for the boundaries between the appearance and non appearance of the tungsten lines. However in the lower pressure case the occurrence boundaries are shifted to lower value of di/dt implying that the tungsten entrainment persists more extensively in the latter case. Temperature estimates for the arcs at both these pressures indicate

that the higher pressure arc possesses a higher plasma temperature. A simple correlation between the occurrence of tungsten in the arc with a higher plasma temperature therefore does not exist. Arc cross section estimates indicate the lower pressure arcs to have a greater diameter than the higher pressure arcs so suggesting less severe axial convection effects. This suggests that the occurrence or otherwise of the tungsten in the arc plasma is more strongly dependent upon axial convection rather than temperature in the arc.

5.4 Electron density measurements:

The electron density in the arc plasma was calculated using a formula which describes the Stark broadening of a particular spectral line (chapter 3, section 3.4). Use was made of Stark broadening coefficients (Jenkins, private communication) for the diagnostic spectral lines in this formula. Errors due to effects such as lower energy state broadening contribution may be avoided through a careful choice of spectral lines.

From the analysis of the line half width at half height due to Stark broadening for the 515.3 nm line yields electron densities in the range $3\text{-}8\text{x}10^{17}$ cm^{-3} during the current zero period as shown on figure (5.19). These electron densities are consistent with $5\text{-}8\text{x}10^{17}$ cm^{-3} measured by Smith et al (1978) for an orifice flow arc in SF_6 during the current zero period following an 8 KA peak current. Fig. (5.19) shows the variation of the radially averaged electron density during

the current zero period following the three different peak arc currents investigated. These electron density values were derived from the same spectra as the temperature results of figure (5.6).

5.5 *Chapter summary and concluding statement*

Arc spectra captured during the current zero period of a full power arc have been presented. The spectra were both time and space resolved (along the arc diameter). Furthermore these spectra have enabled both the radially averaged arc temperature and electron density to be calculated. The spatially resolved spectra have also allowed detailed arc temperature profiles to be measured during the current zero period.

The conclusions drawn from these results may be summarised as :

(1) The temperature profile of the arc used in this chapter has been determined from the ratio of intensities of two copper lines (CuI 515.3 nm and 510.5 nm) and is independent upon line profile and whether or not tungsten lines are present.

(2) Axis temperature estimates for the arc at different pressures indicate that the higher pressure arc possesses a higher plasma temperature.

(3) A simple correlation between the occurrence of tungsten in the arc with a higher plasma temperature therefore does not exist

(4) Arc cross section estimates indicate the lower pressure arcs to have a greater diameter than the higher pressure arcs.

(5) This suggests that the occurrence or otherwise of the tungsten in the arc plasma is more strongly dependent upon reduced convection being incapable of removing the persisting tungsten flowing entrainment during the peak current phase.

Wavelength nm	Spectrum	Energy levels K	gA 10^8 /sec
511.036	WI	15070-34633	0.057
512.424	WI	14976-34486	0.055
513.011	WI	23965-43452	0.59
513.840	WI	28233-47689	2.2
514.577	WI	20983-40411	0.33

Table (5.1) Wavelength, Energy levels and gA values of tungsten atomic lines appear in the spectra

I_o = - 10.4 μs di/dt = 14.2 A/μs T_{gate} = 1.6 μs Press. = 110 psig

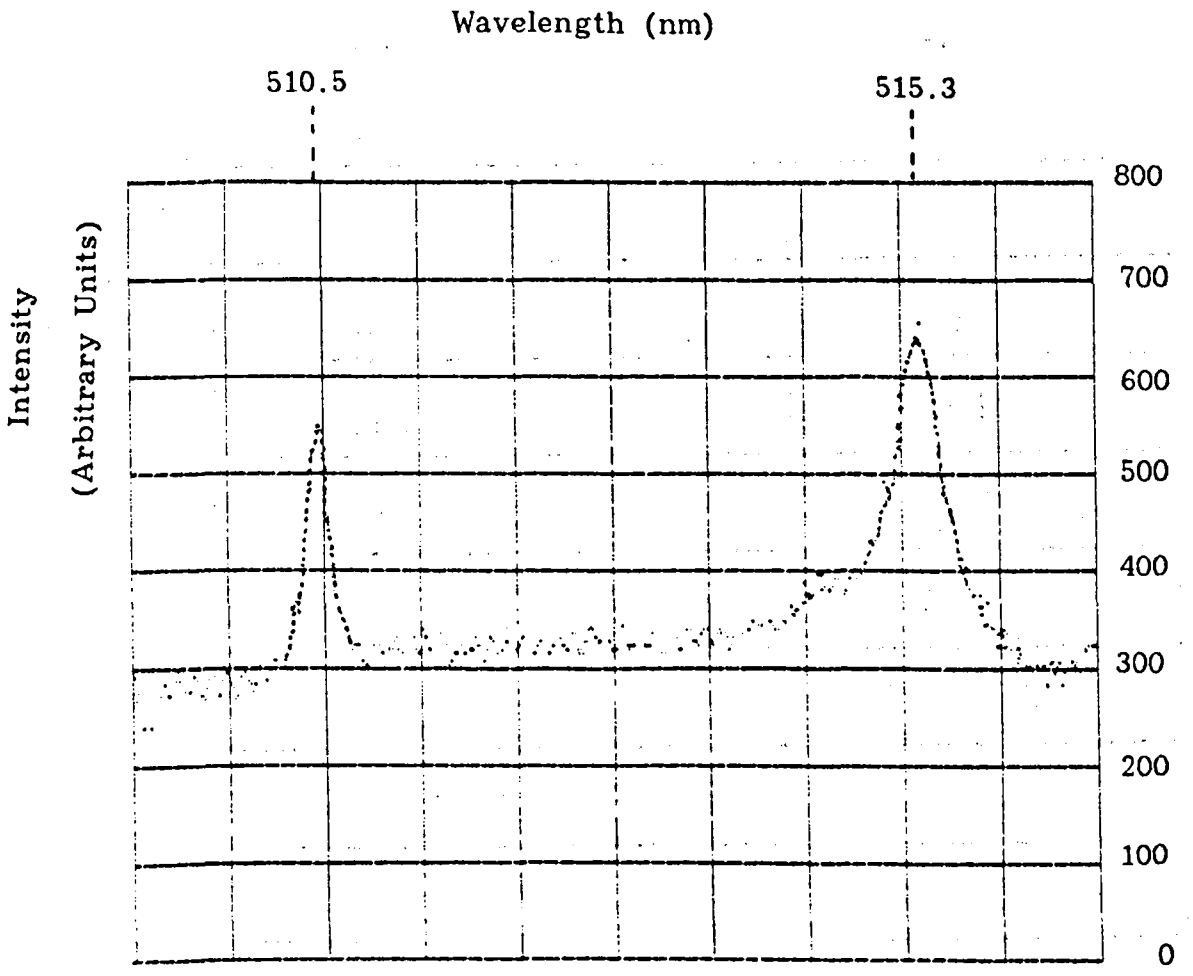

(a) Low di/dt

Fig. (5.1) Arc spectrum CuI lines only

I_o = - 10 μs di/dt = 18 A/μs T_{gate} = 1.6 μs Press. = 110 psig

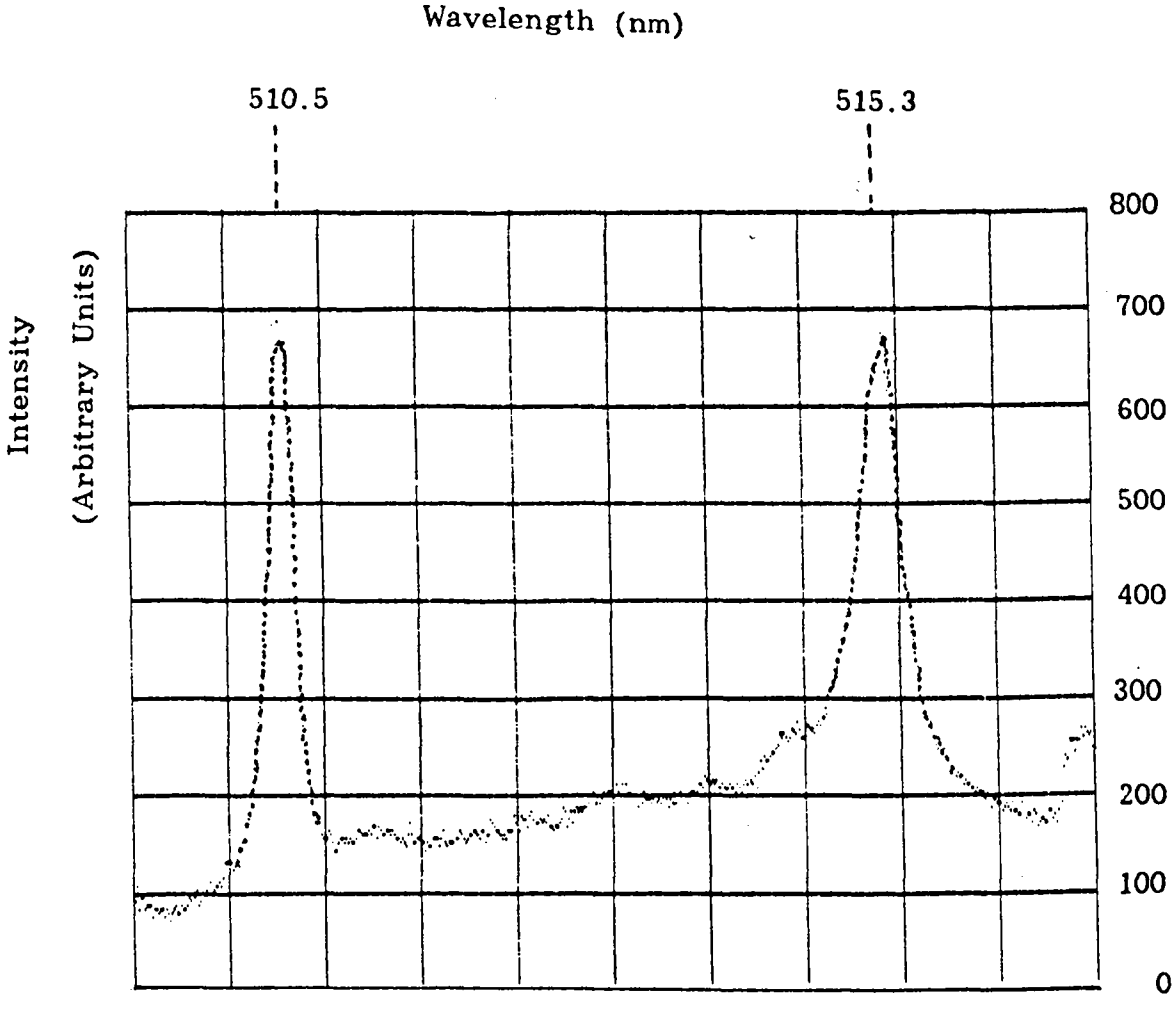

Fig.(5.1) (b) Medium di/dt

I_o = - 5.3 μs di/dt = 21 A/μs T_{gate} = 1.6 μs Press. = 110 psig

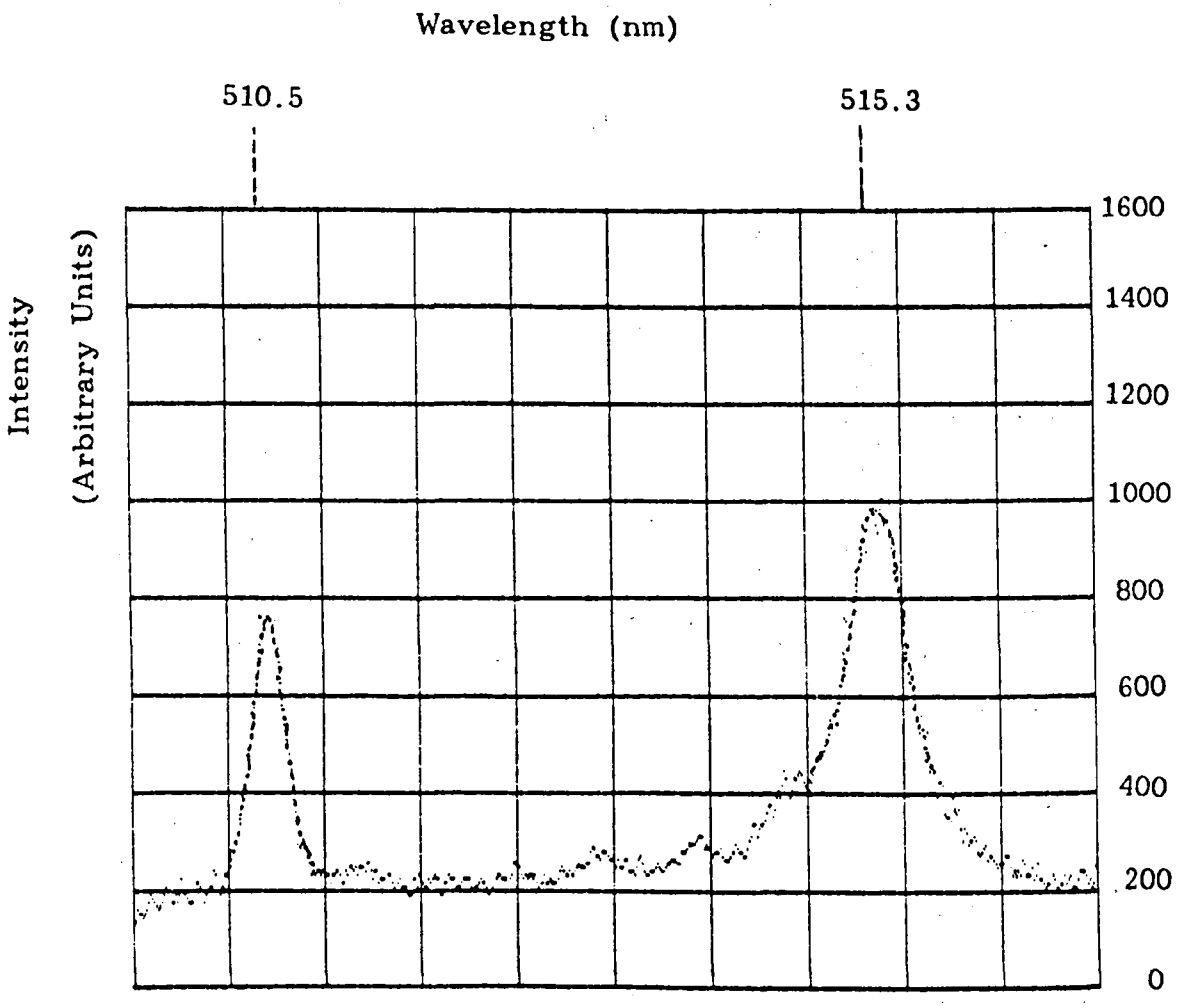

Fig. (5.1) (c) High di/dt

I_o = - 7.2 μs di/dt = 20 A/μs T_{gate} = 1.6 μs Press. = 60 psig

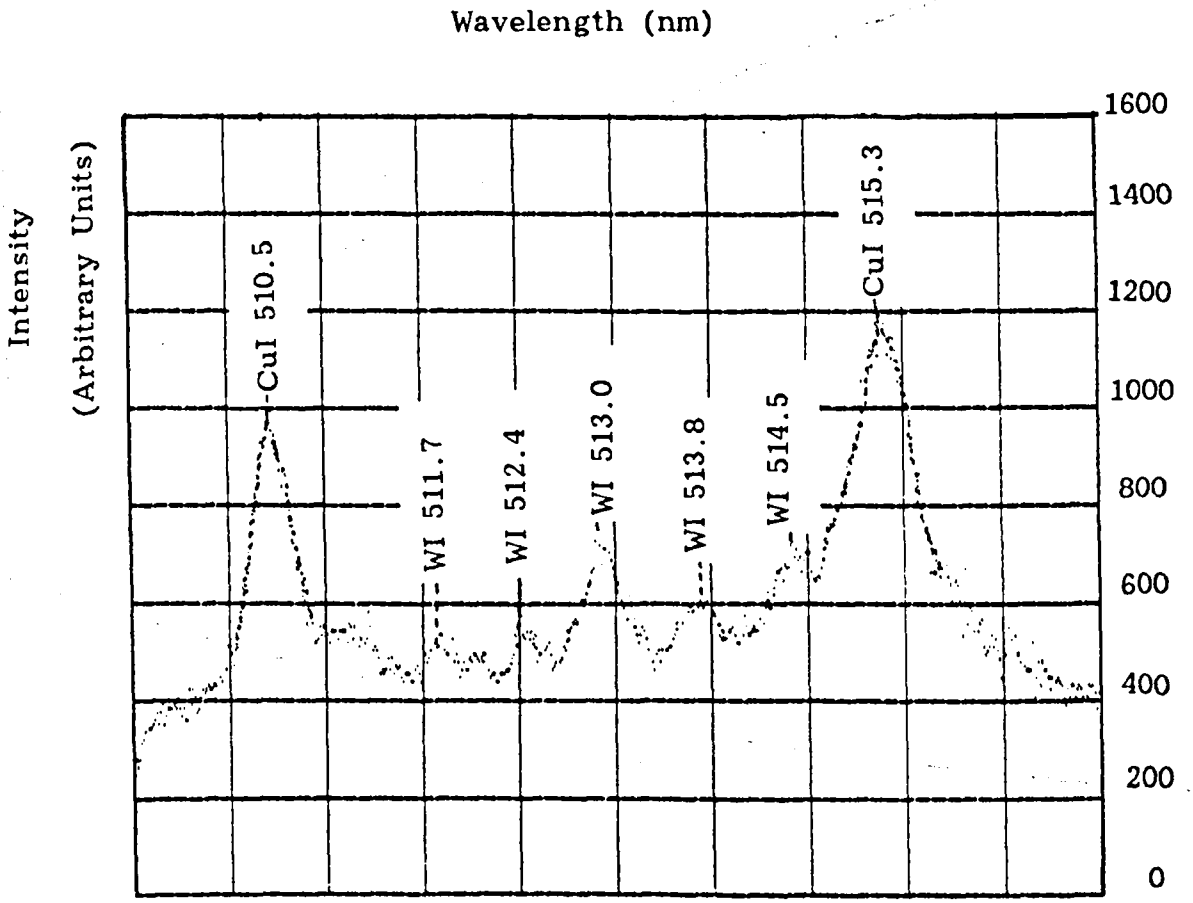

Fig. (5.2) Arc spectrum CuI and WI lines

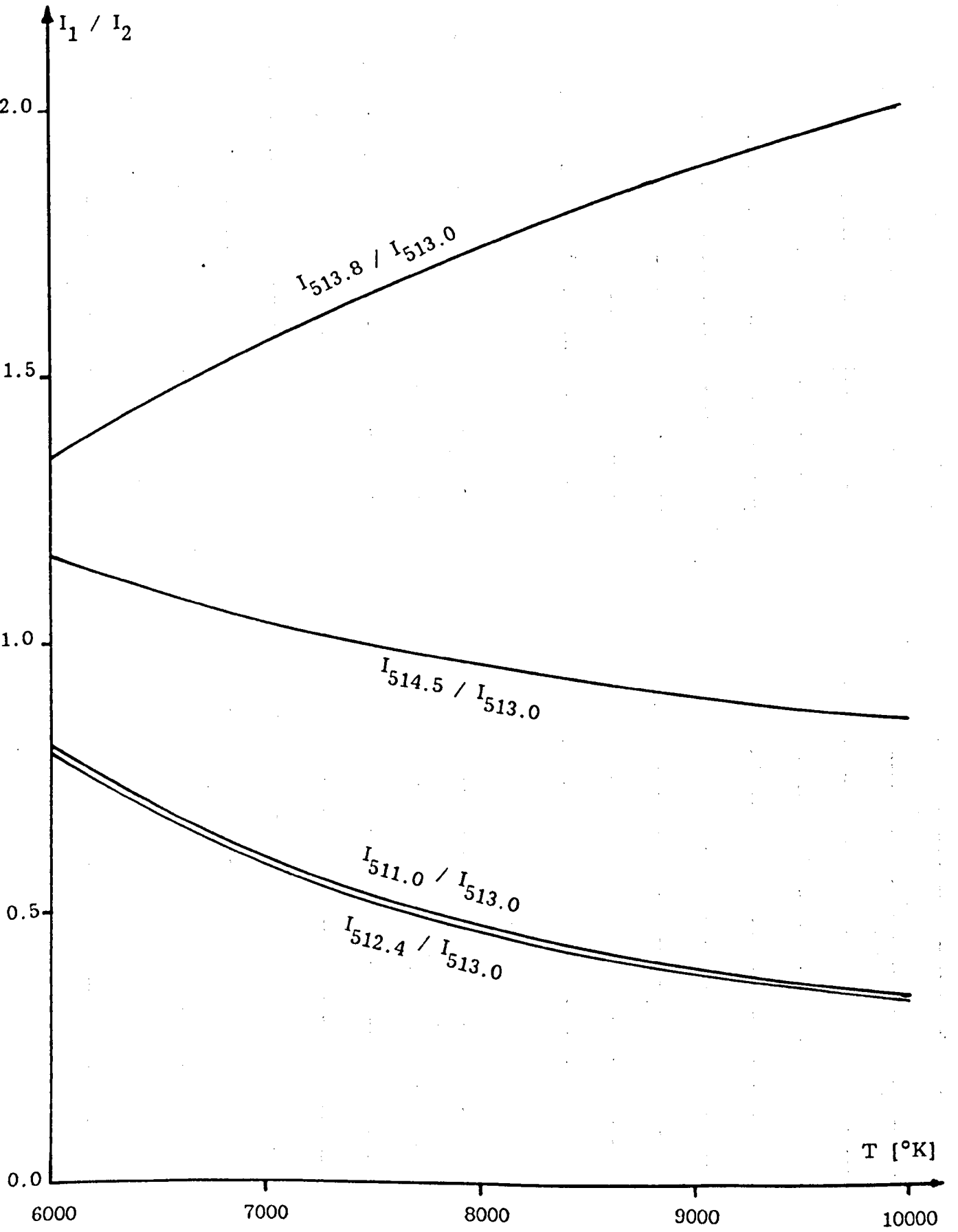

Fig. (5.3) Relative intensities of tungsten lines

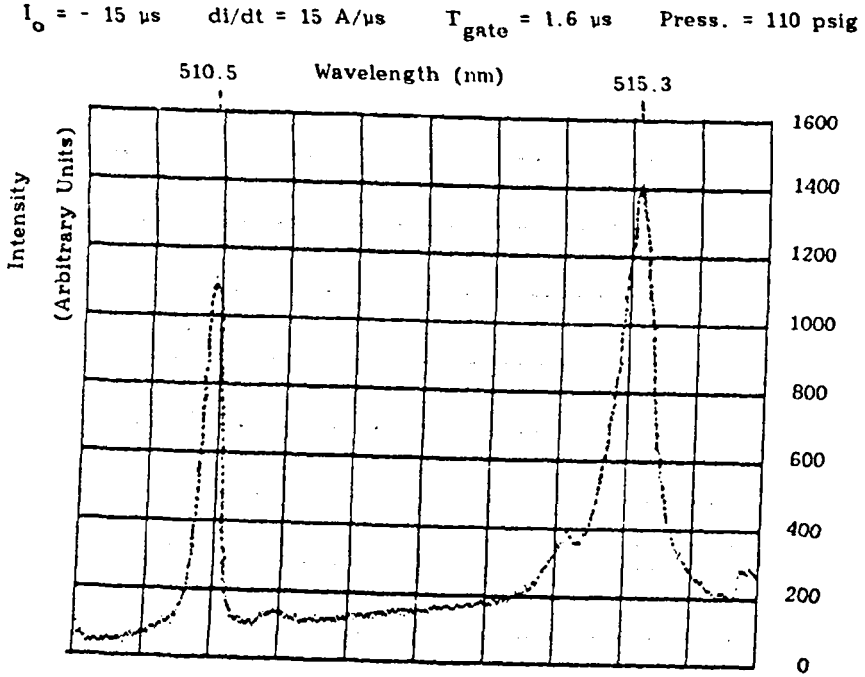

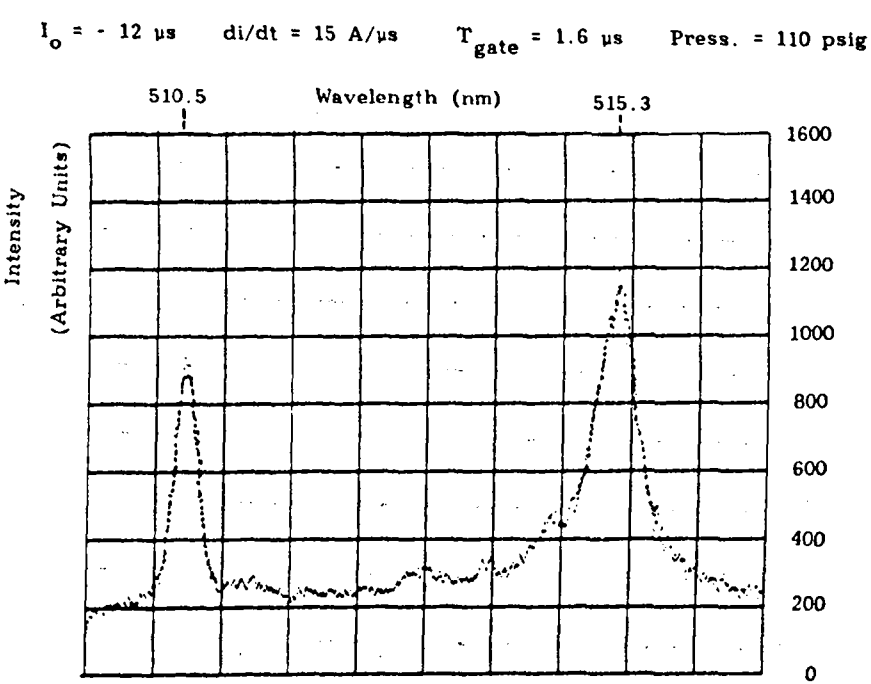

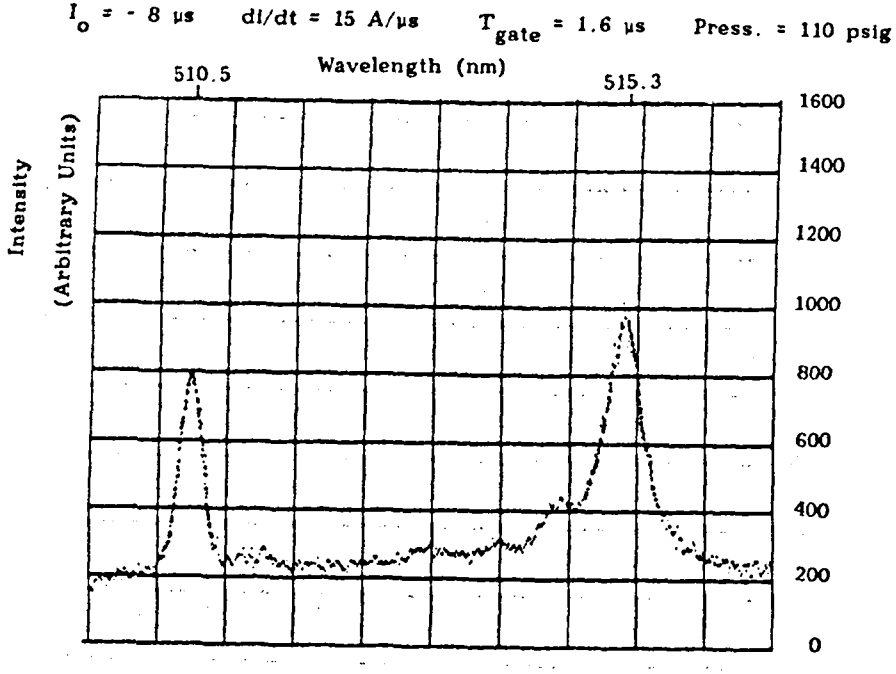

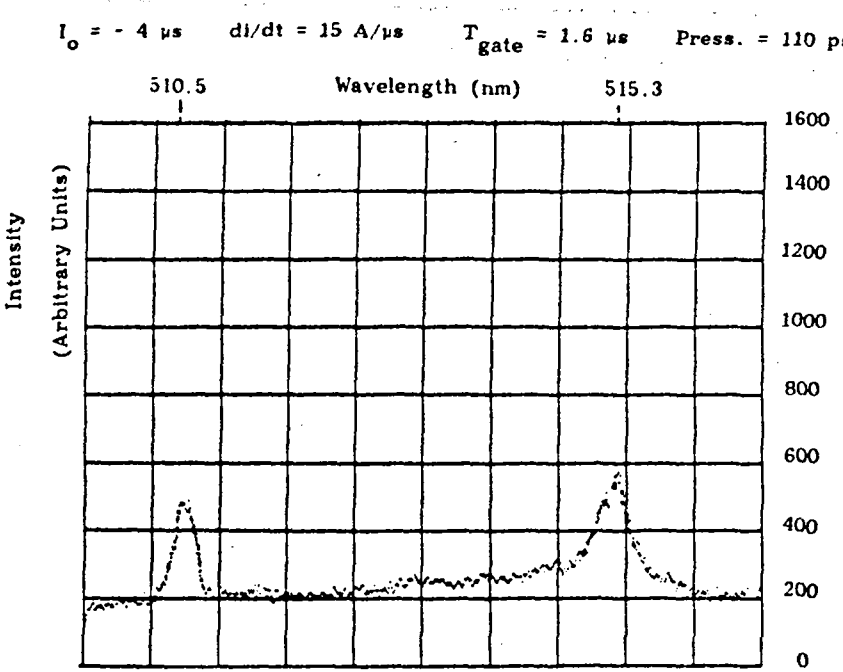

Fig. (5.4) Examples of radially averaged spectra for different instants during the current decay.

Fig.(5.4) (b) Medium di/dt

Fig. (5.4) (c) High di/dt

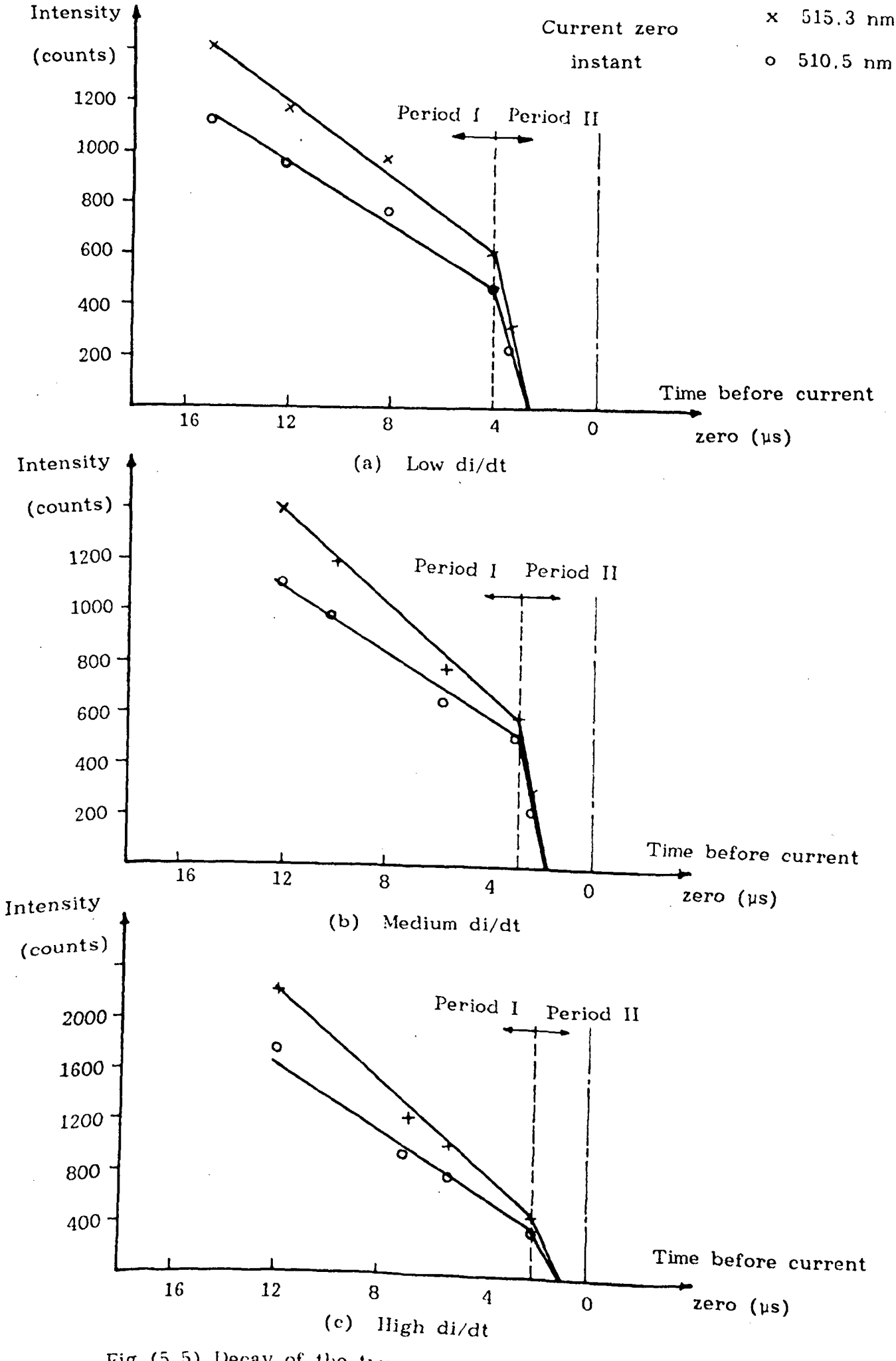

Fig.(5.5) Decay of the two spectral line intensities during the current zero period

Curve 1-- di/dt = 24 A/μs (I_p = 60 KA)

Curve 2-- di/dt = 22 A/μs (I_p = 53 KA)

Curve 3-- di/dt = 15 A/μs (I_p = 34 KA)

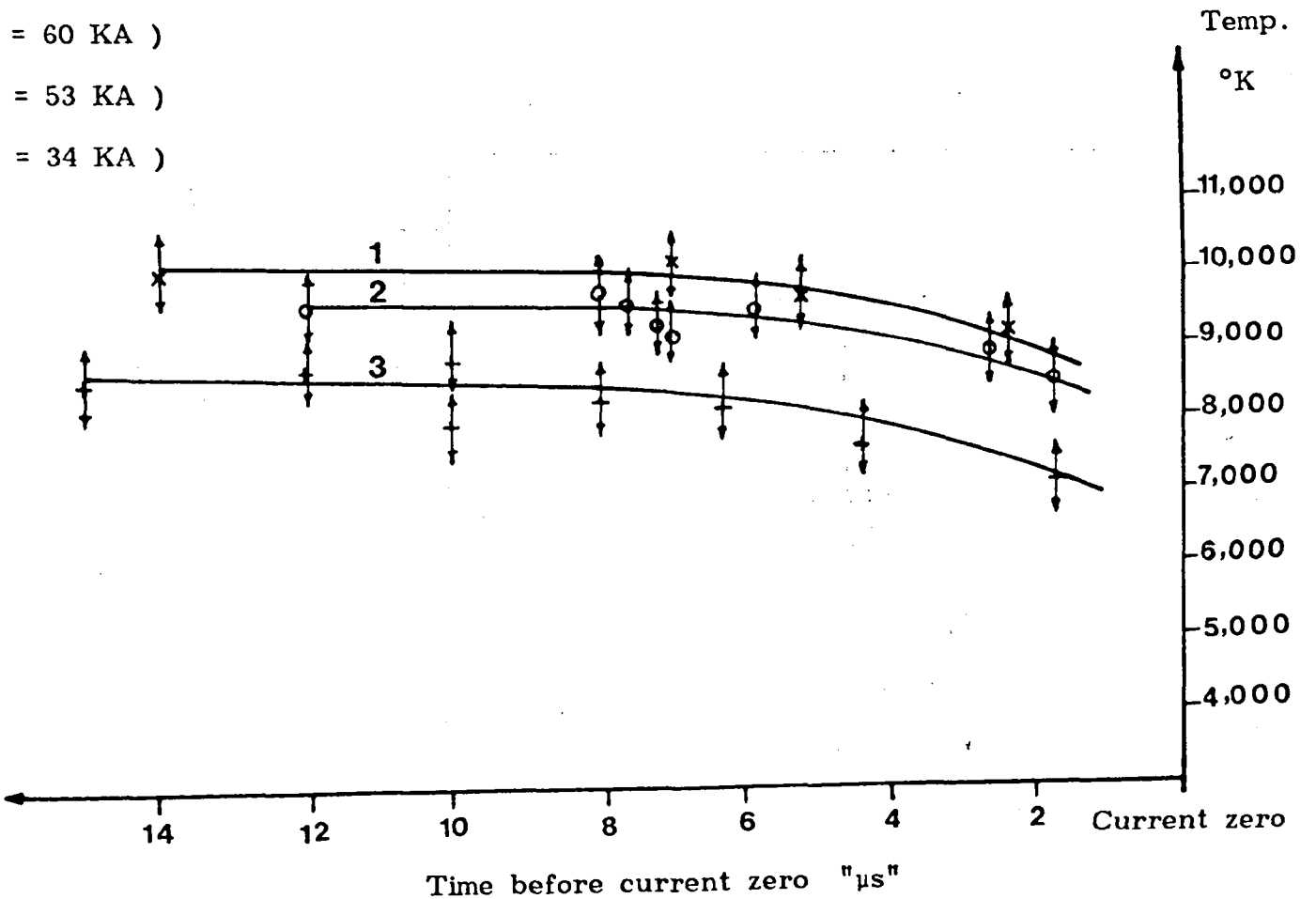

Fig.(5.6) Variation of radially averaged arc temperature under different arcing conditions.

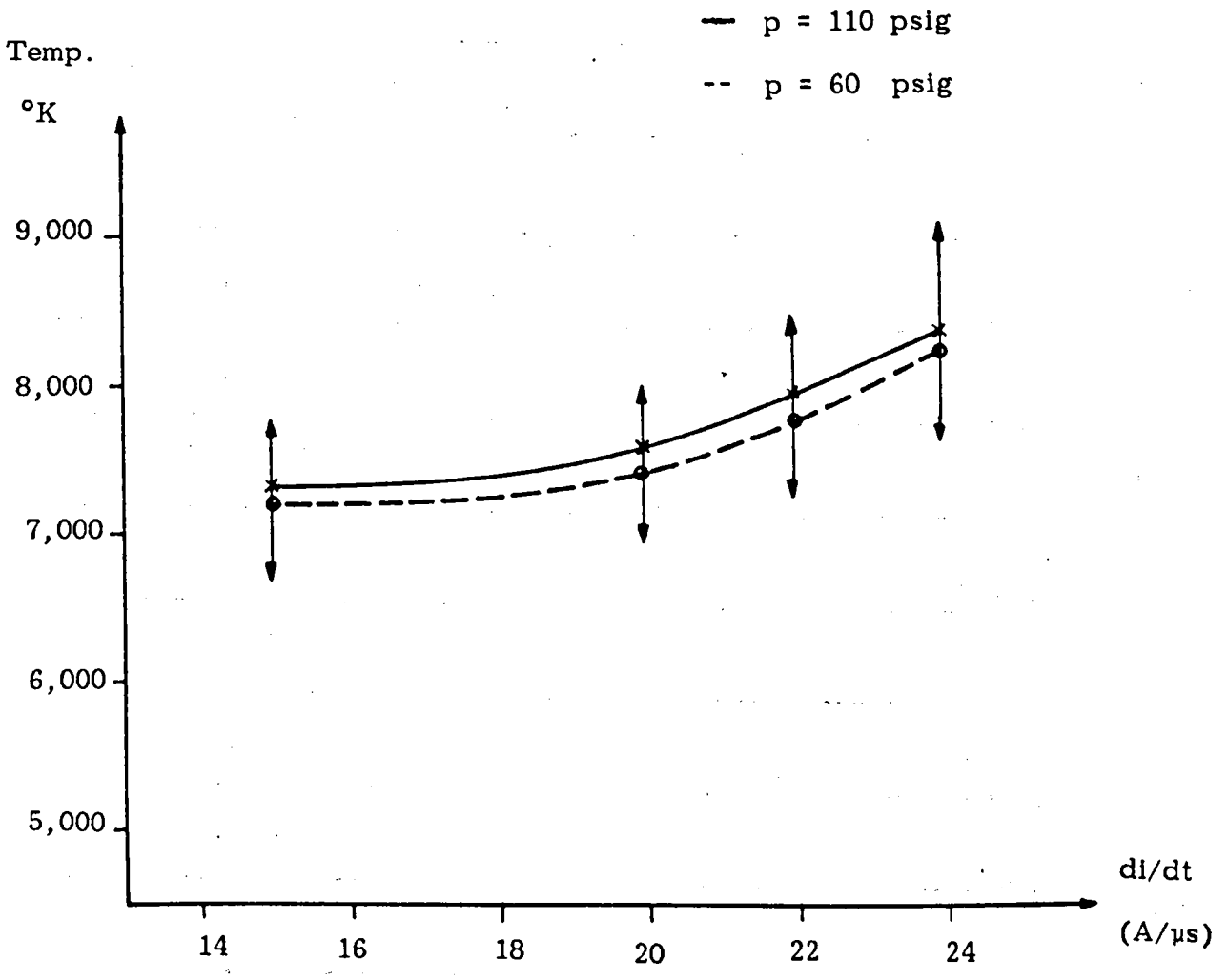

Fig.(5.7) The variation of radially averaged temperature during the current zero period with the current decay rate (for two pressures 60 and 110 psig.)

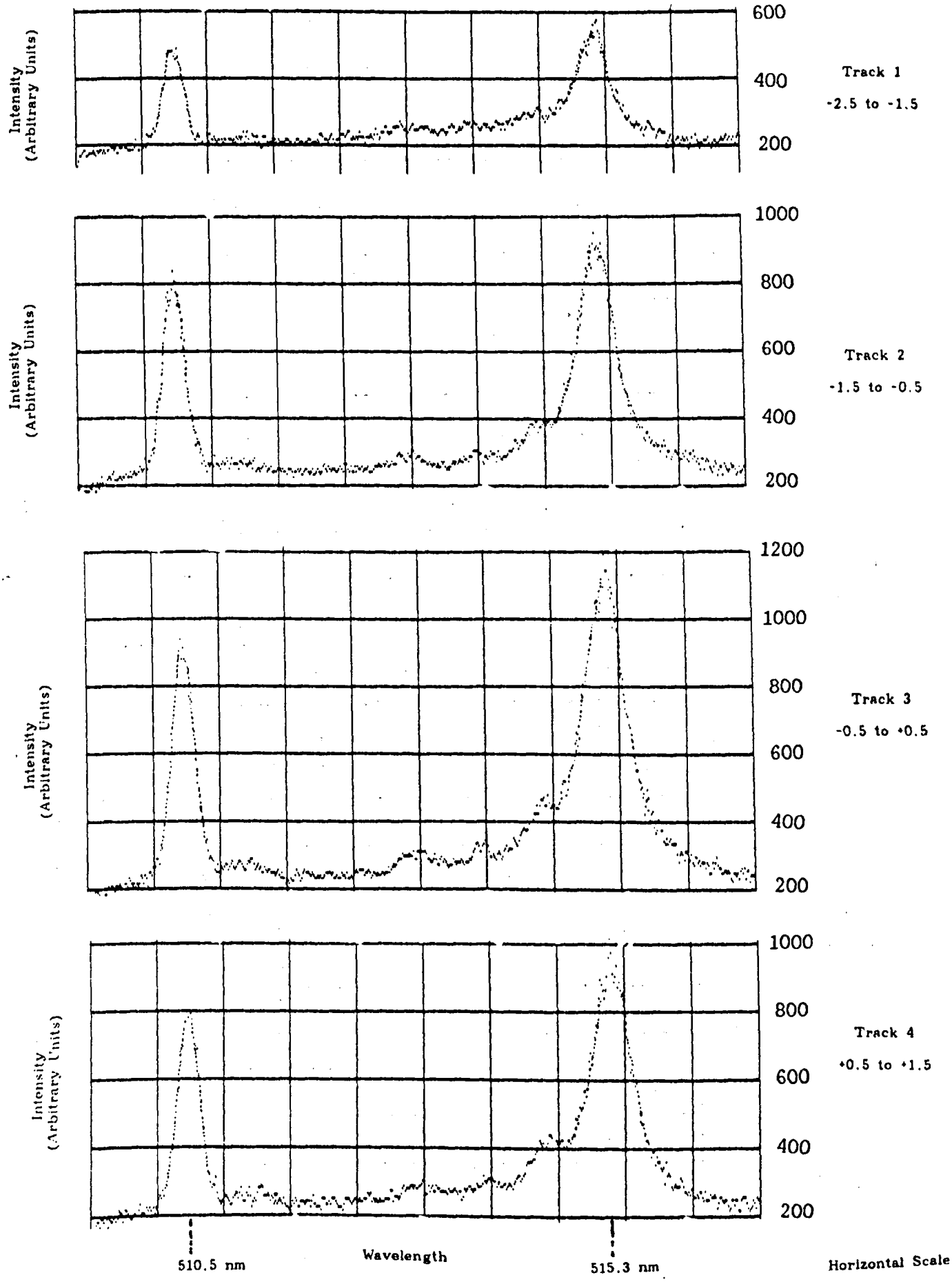

Operating Conditions	
Pressure = 110 psig	Time before current zero = 8 μs
di/dt = 16 A/μs	Exposure time = 1.6 μs

Fig.(5.8) Radially resolved arc spectra during the current zero period (p = 110 psig)

(a) Low di/dt

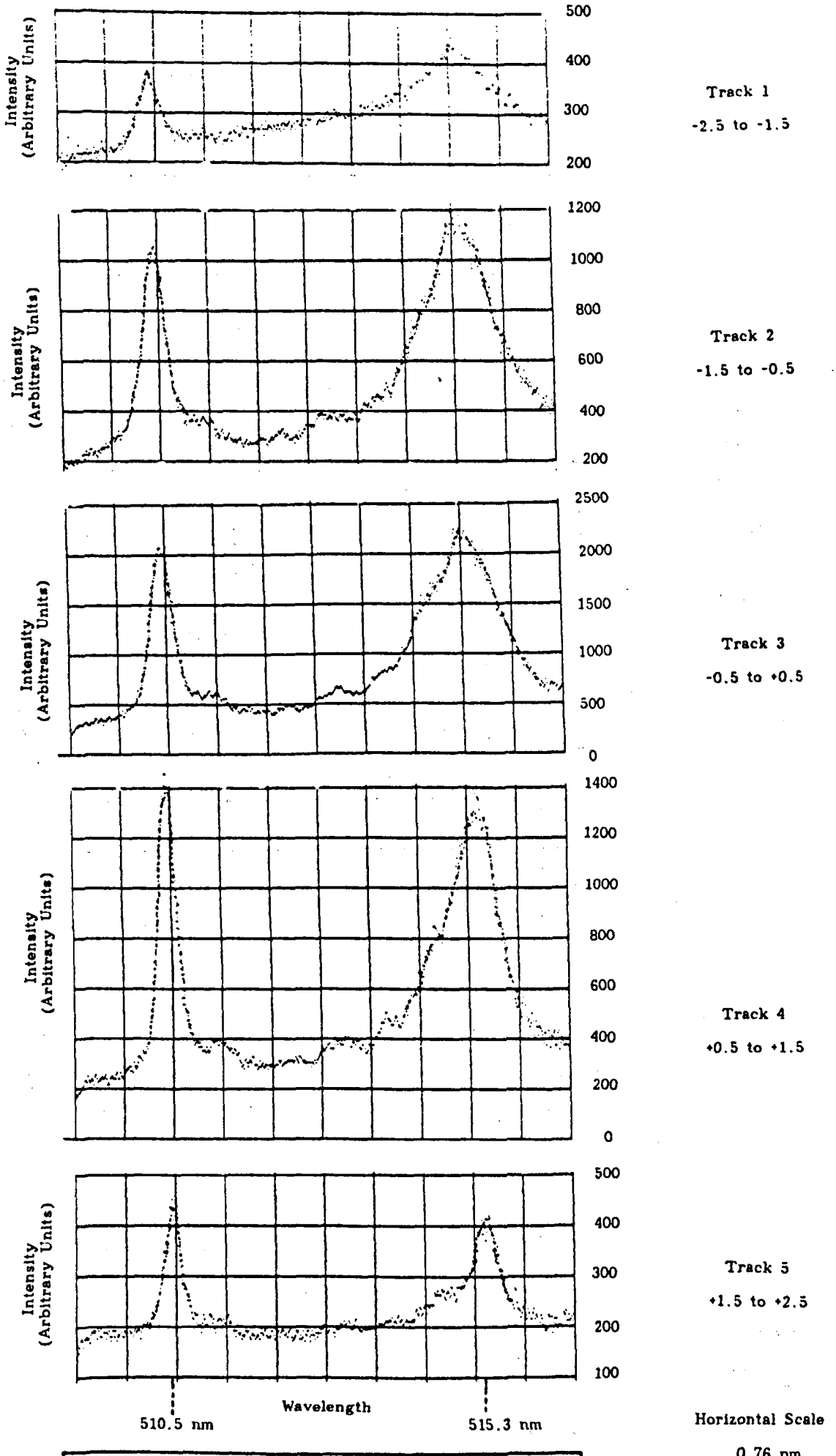

Operating Conditions	
Pressure = 110 psig	Time before current zero = 10 μs
dI/dt = 18 A/μs	Exposure time = 1.6 μs

Fig. (5.8) (b) Medium dI/dt

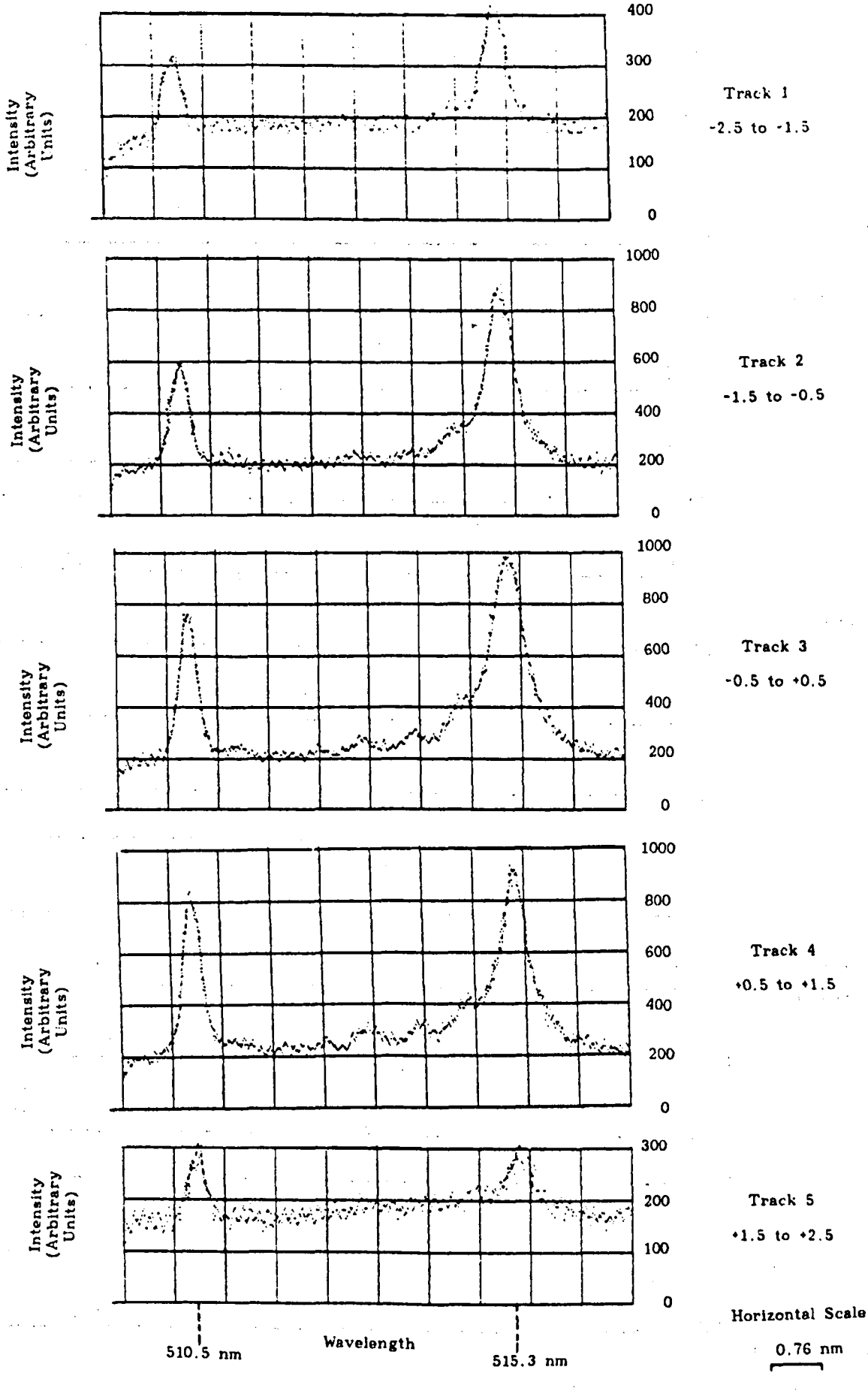

Operating Conditions	
Pressure = 110 psig	Time before current zero = 5.3 μs
di/dt = 22 A/μs	Exposure time = 1.6 μs

Fig. (5.8) (c) High di/dt

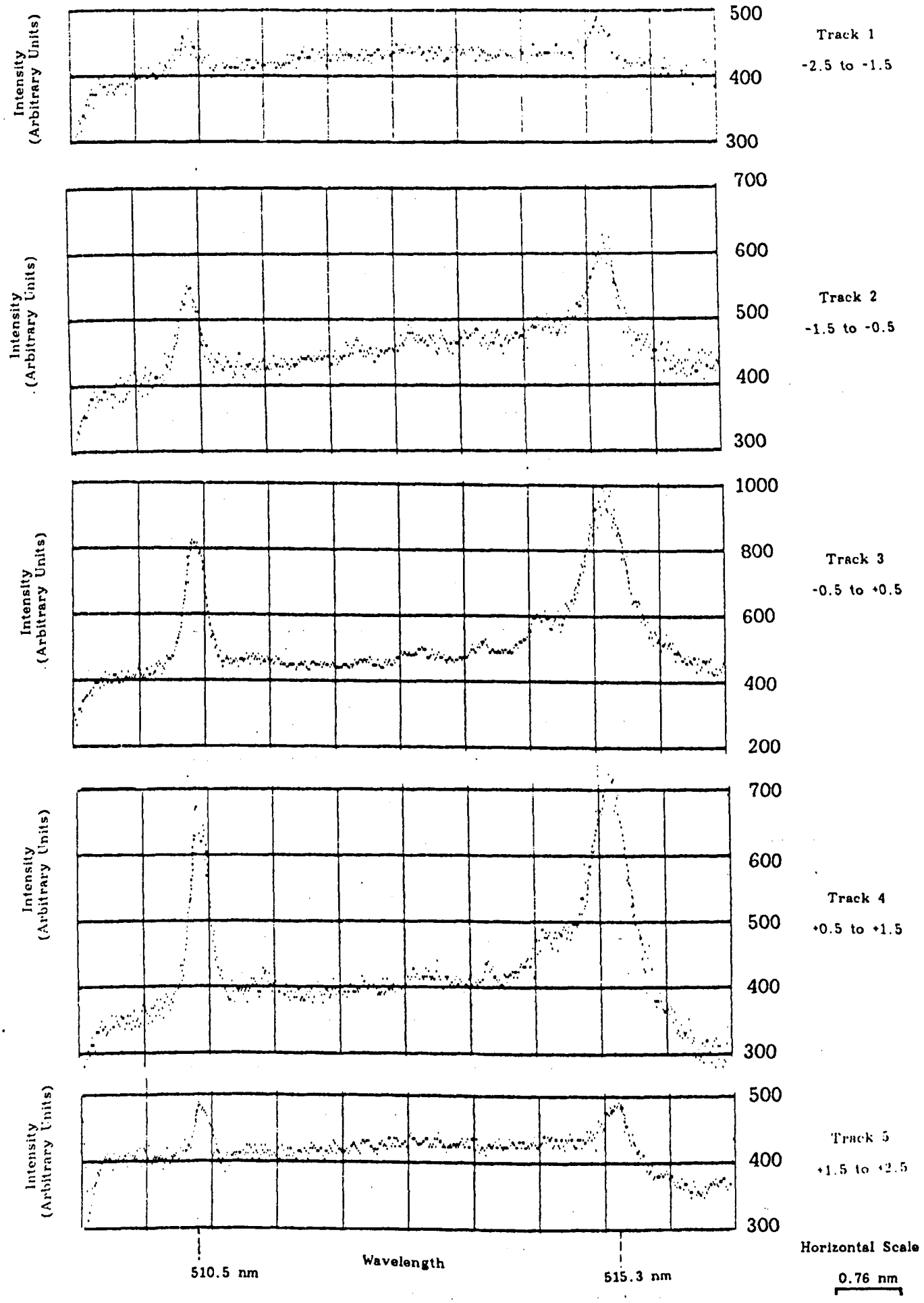

Operating Conditions	
Pressure = 60 psig	Time before current zero = 9.6 μs
dI/dt ≈ 16.5A/μs	Exposure time = 1.6 μs

Fig.(5.9) Radially resolved arc spectra during the current zero period (p = 60 psig) (a) Low dI/dt

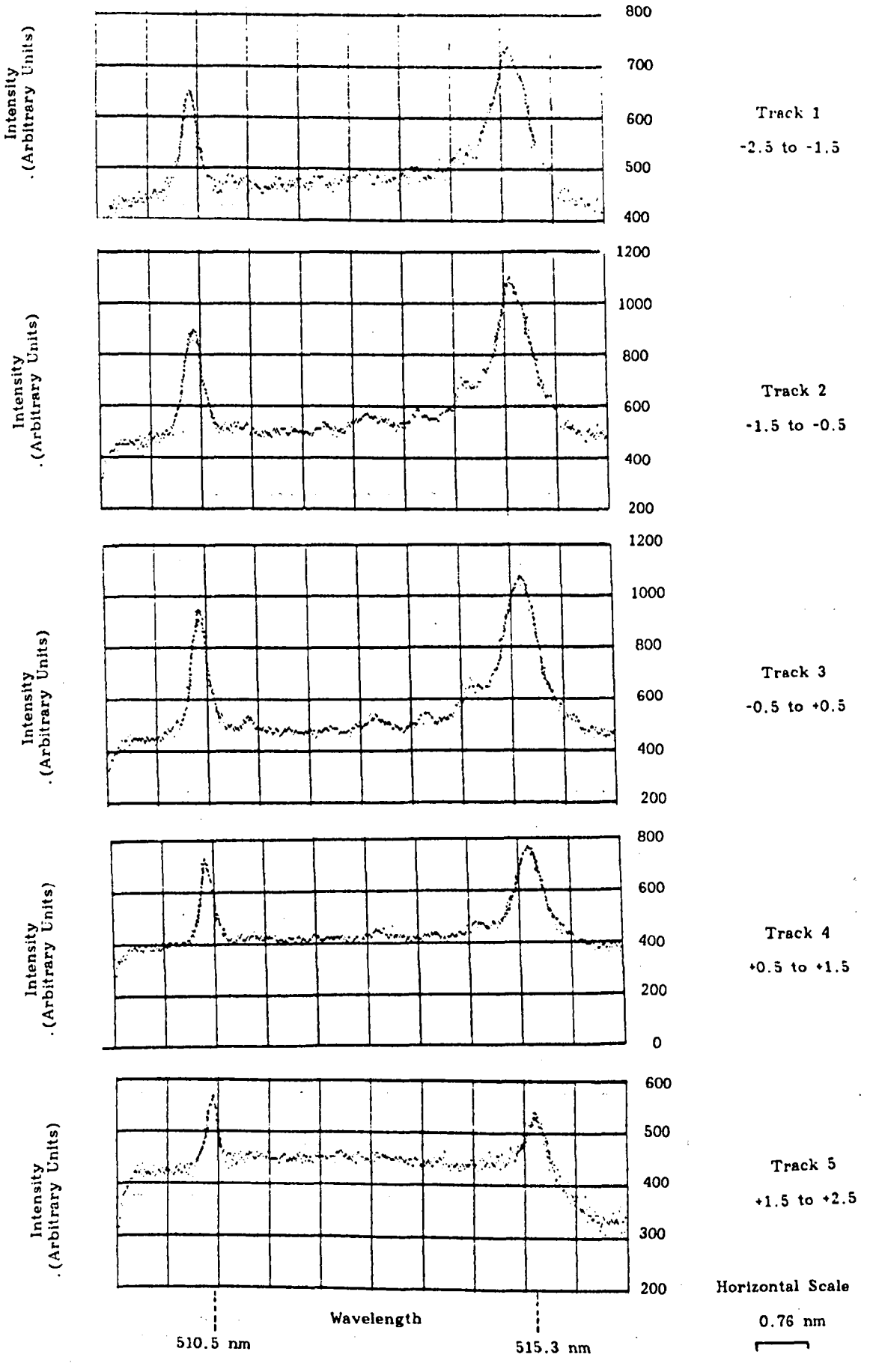

Operating Conditions	
Pressure = 60 psig	Time before current zero = 8.8 μs
di/dt = 19.5A/μs	Exposure time = 1.6 μs

Fig. (5.9) (b) Medium di/dt

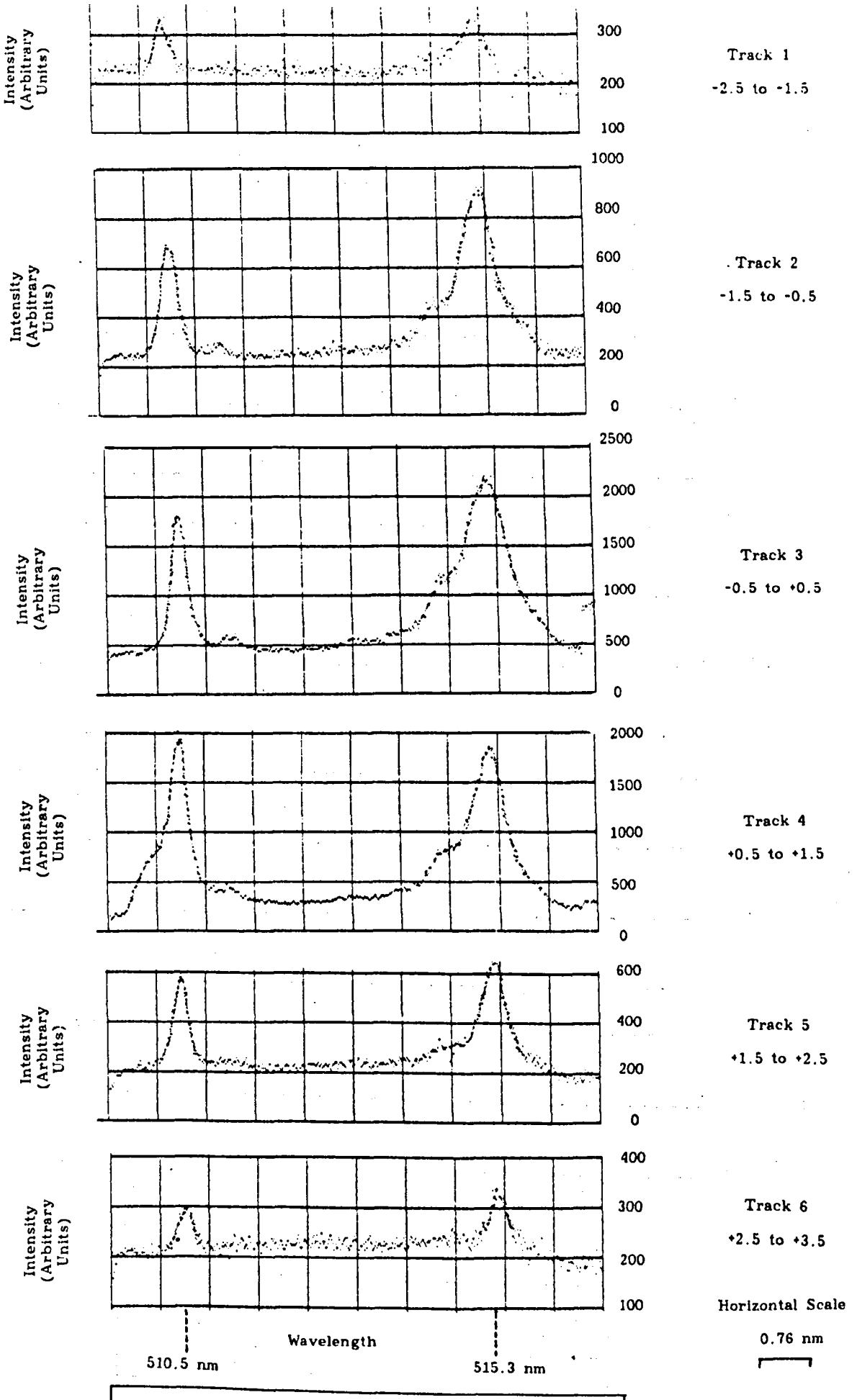

Operating Conditions	
Pressure = 60 psig	Time before current zero =12.6 μs
di/dt = 22 A/μs	Exposure time = 1.6 μs

Fig.(5.9) (c) High di/dt

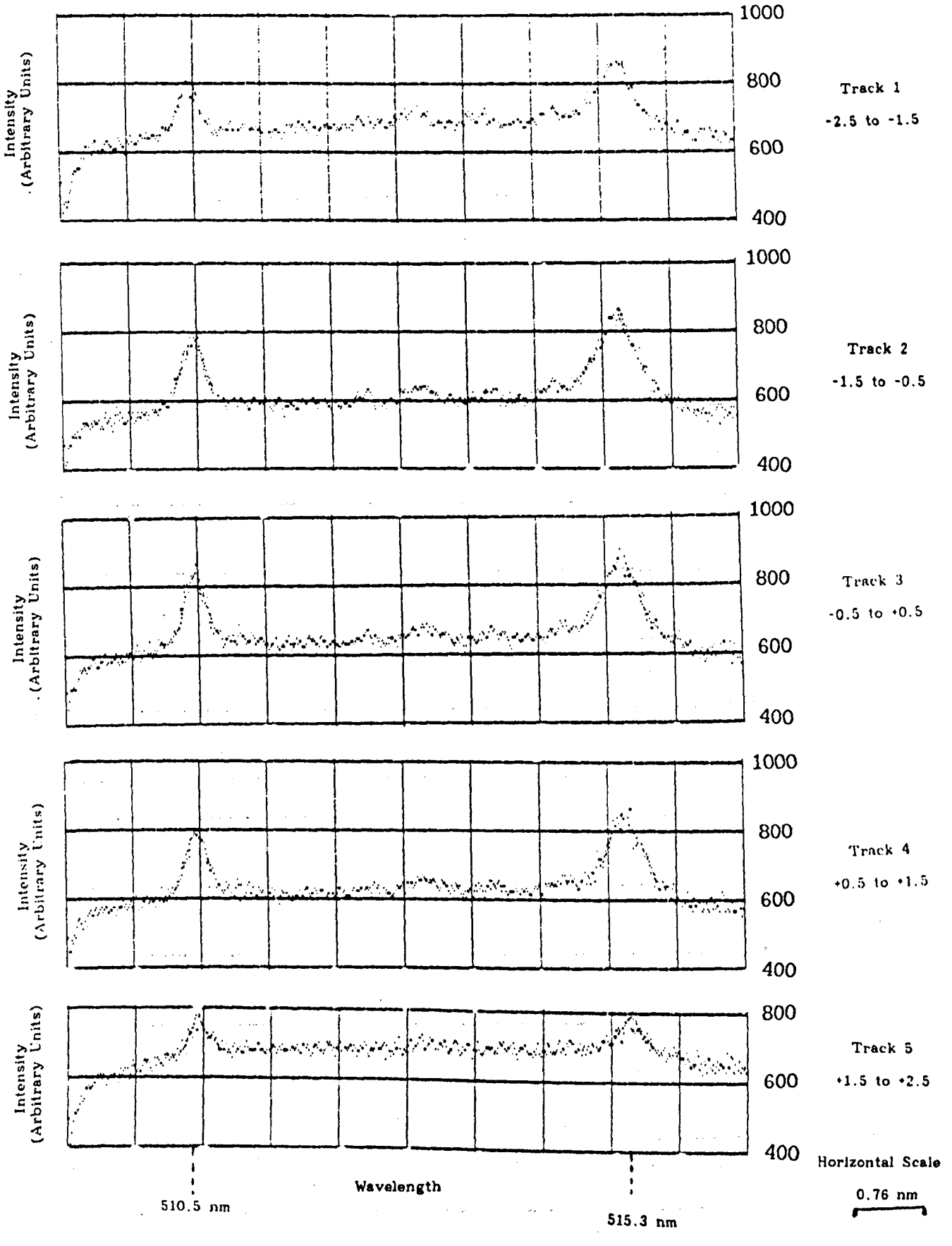

Operating Conditions	
Pressure = 60 psig	Time after current zero = 6.6 μs
di/dt = 23 A/μs	Exposure time = 1.6 μs

Fig.(5.9) (d) High di/dt & After current zero

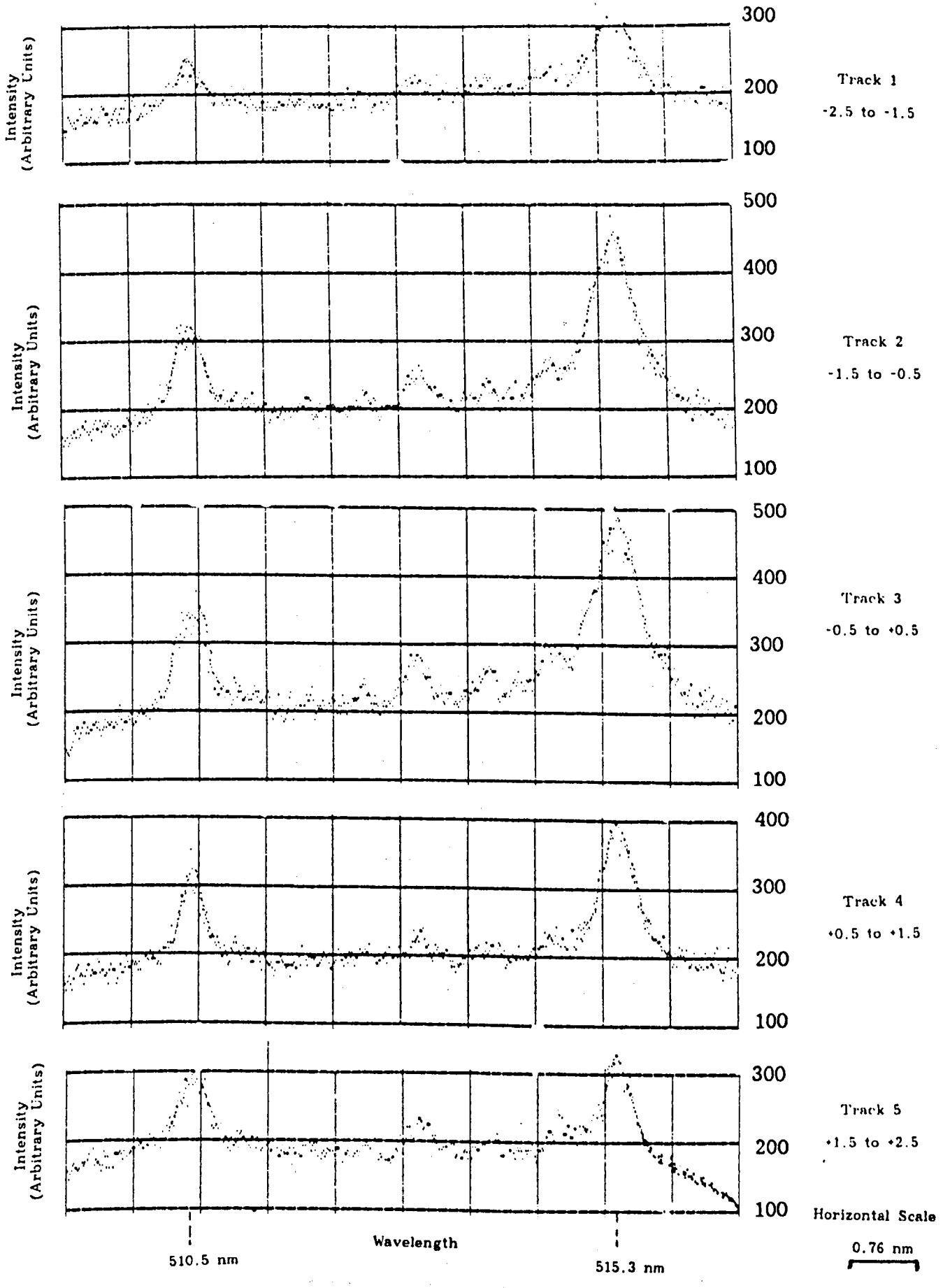

Operating Conditions	
Pressure = 60 psig	Time after current zero = 7.3 μs
di/dt = 23 A/μs	Exposure time = 1.6 μs

Fig.(5.9) (e) High di/dt & After current zero

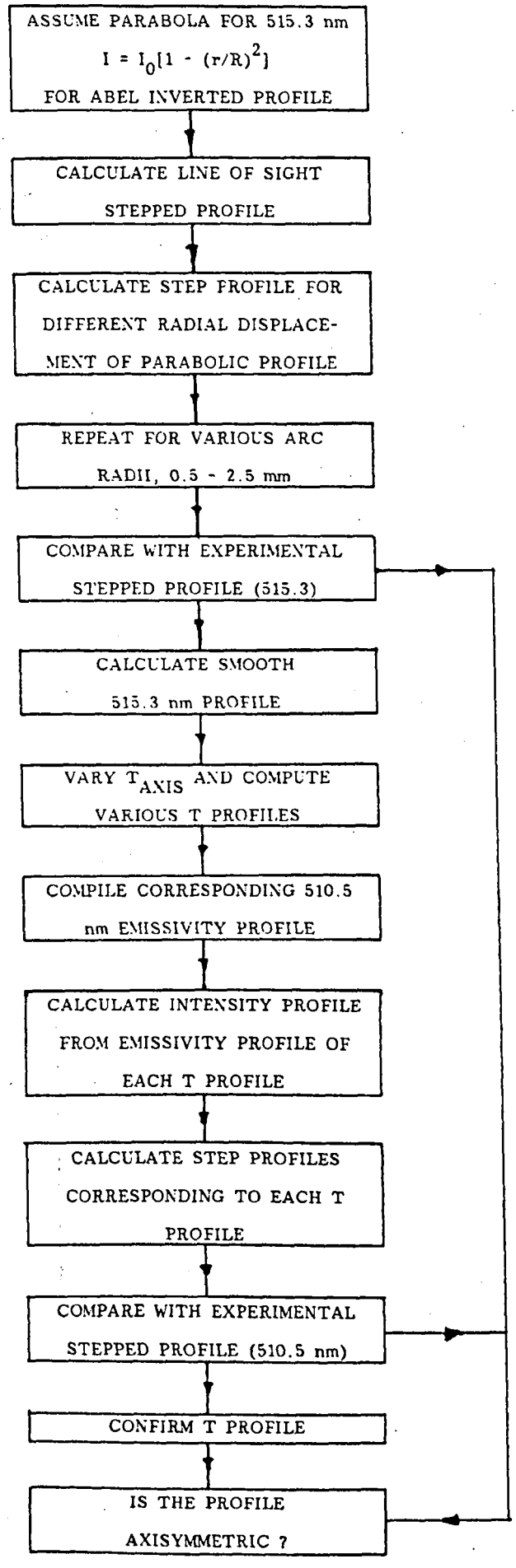

Fig. (5.10) Flow diagram for the analysis of laterally shiffted spectral line distributions.

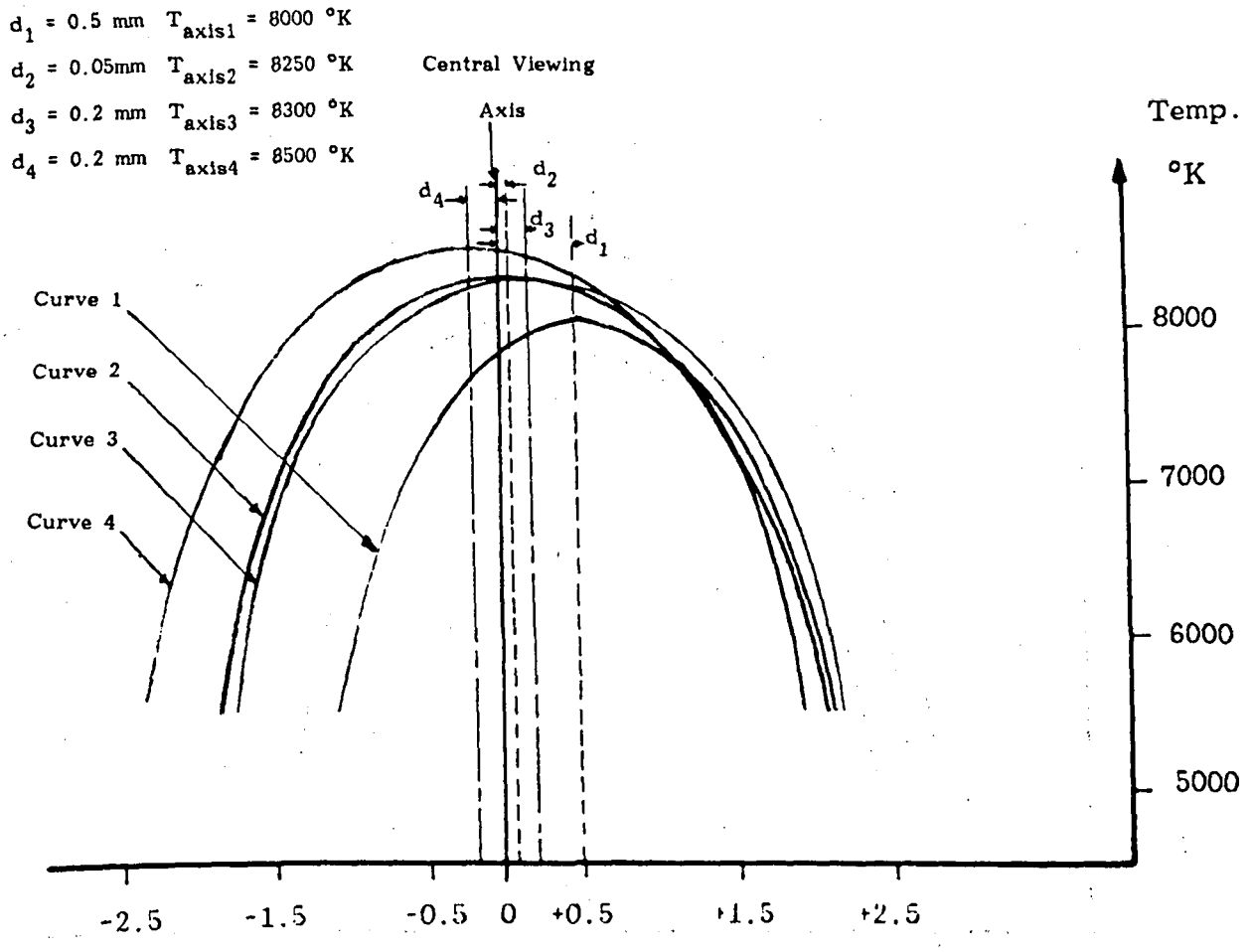

(a) Low di/dt (14-17 A/μs)

Operating conditions	Time before C.Z. μs	di/dt A/μs	Exposure time (μs)	pressure psig
Curve 1	- 6	15	1.6	110
Curve 2	- 8	16	1.6	110
Curve 3	-10.5	14.5	1.6	110
Curve 4	-13.4	14.8	1.6	110

Fig.(5.11) Arc temperature profiles during the current zero period

(p = 110 psig)

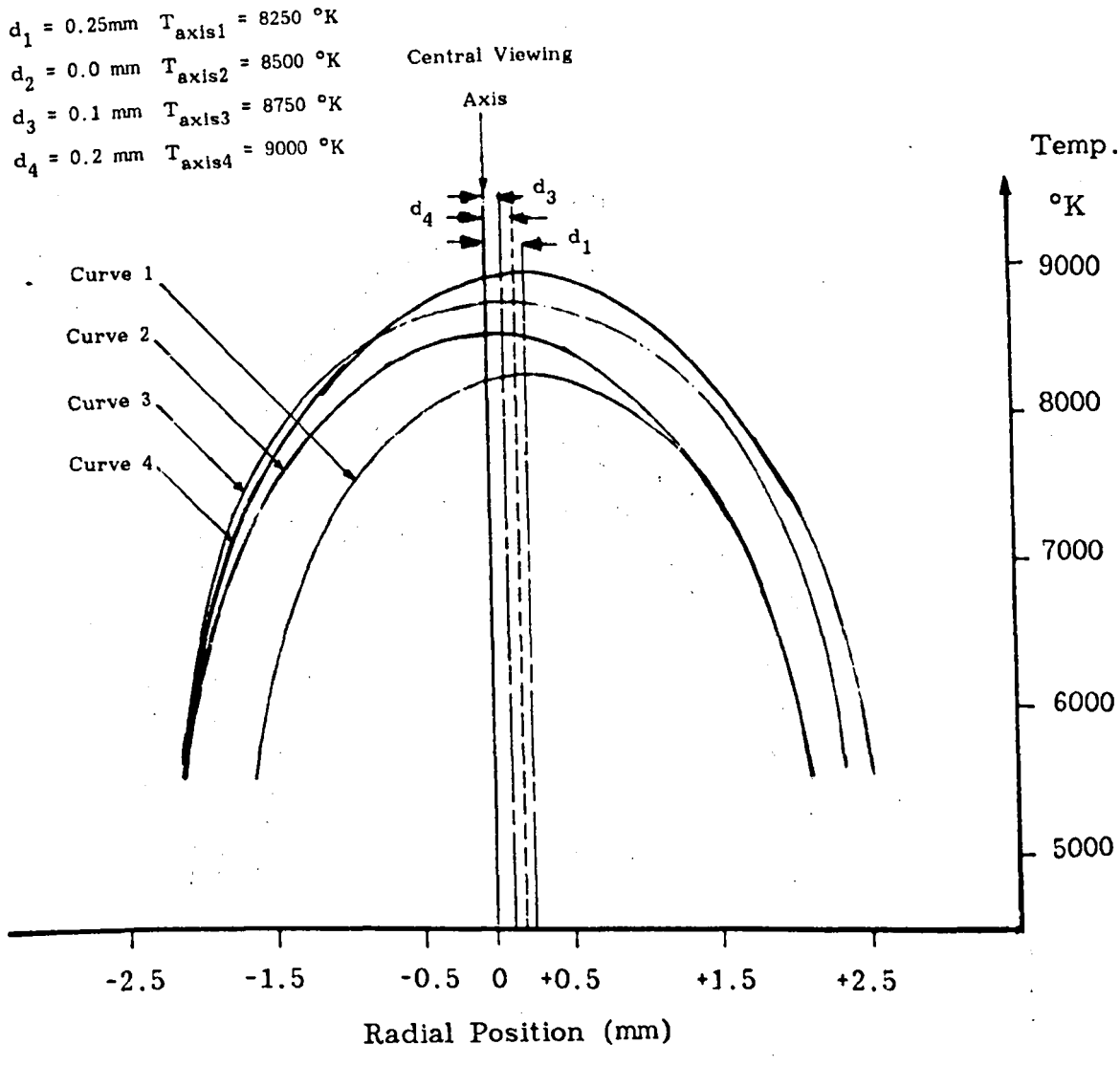

Fig.(5.11) (b) Medium di/dt (18-21 A/μs)

Operating conditions	Time before C.Z. μs	di/dt A/μs	Exposure time (μs)	pressure psig
Curve 1	- 3.6	20	1.6	110
Curve 2	- 5.3	20	1.6	110
Curve 3	- 10	18.5	1.6	110
Curve 4	- 7.6	20	1.6	110

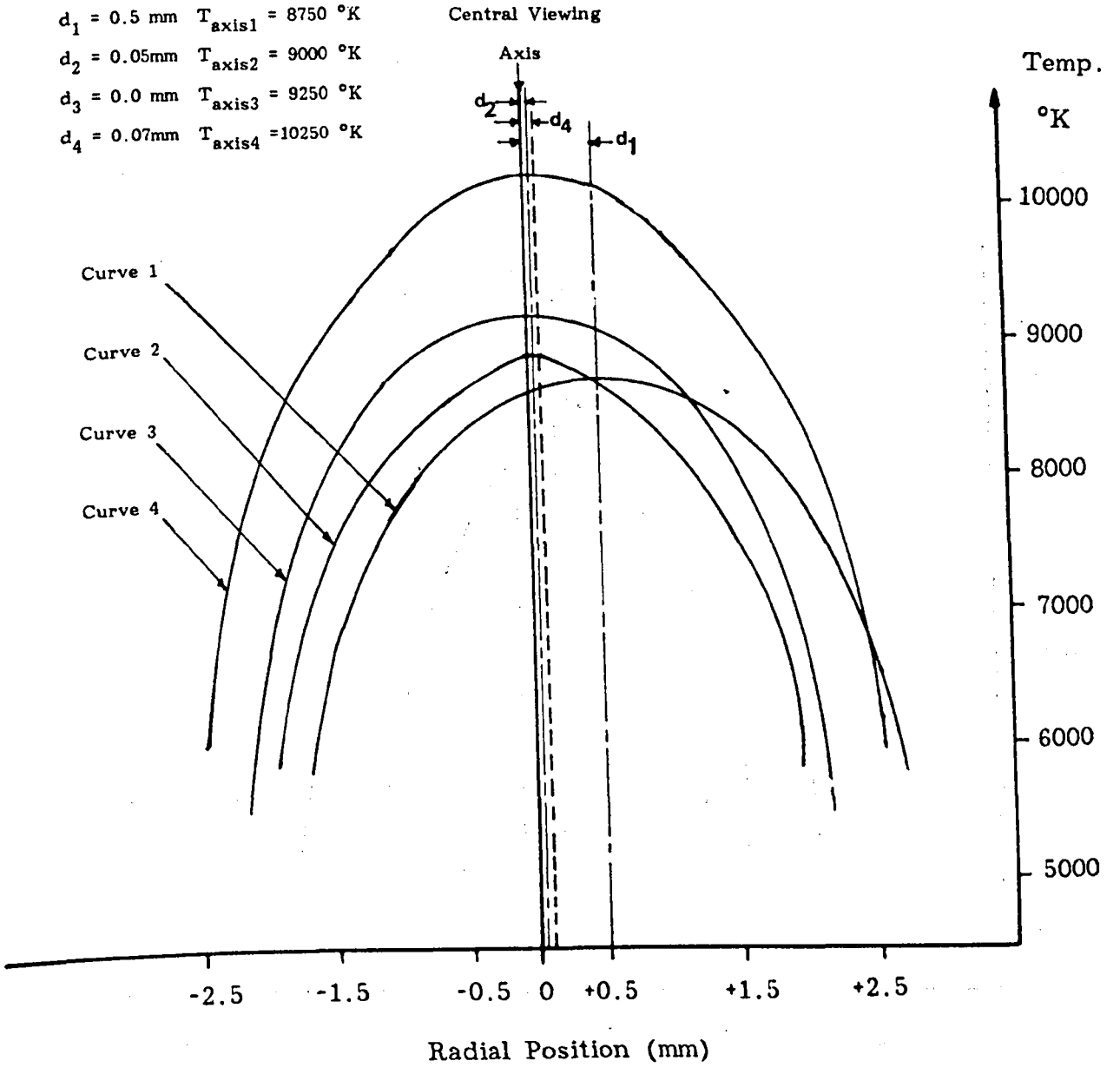

Fig.(5.11) (c) High di/dt (22-25 A/μs)

Operating conditions	Time before C.Z. μs	di/dt A/μs	Exposure time (μs)	pressure psig
Curve 1	- 6	22.2	1.6	110
Curve 2	- 2.8	24	1.6	110
Curve 3	- 4.2	25	1.6	110
Curve 4	-14.6	24	1.6	110

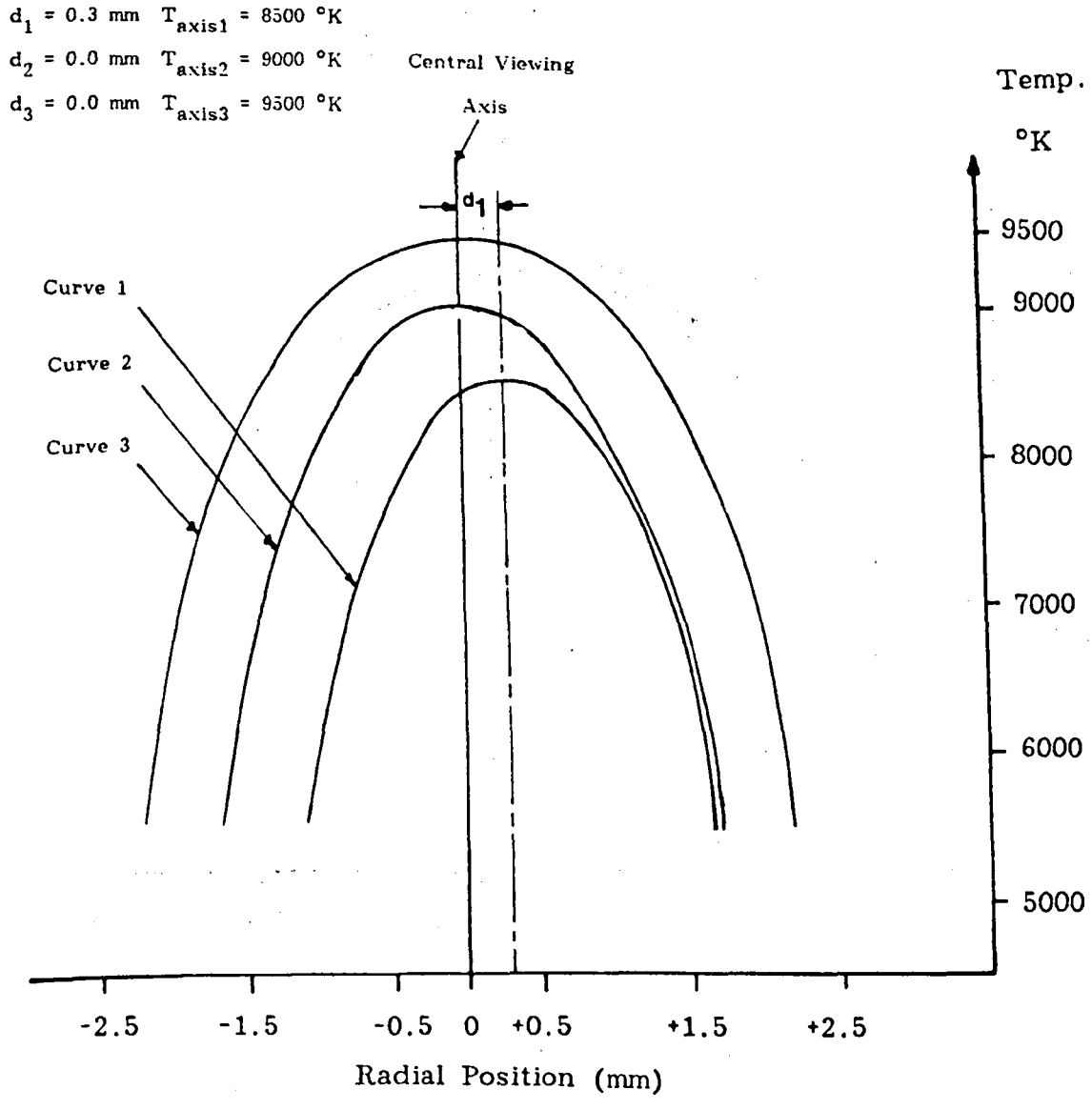

Fig.(5.11) (d) High di/dt (22-25 A/μs) & After current zero

Operating conditions	Time after C.Z. μs	di/dt A/μs	Exposure time (μs)	pressure psig
Curve 1	+ 1.2	25	1.6	110
Curve 2	+ 3.2	25	1.6	110
Curve 3	+11.5	25	1.6	110

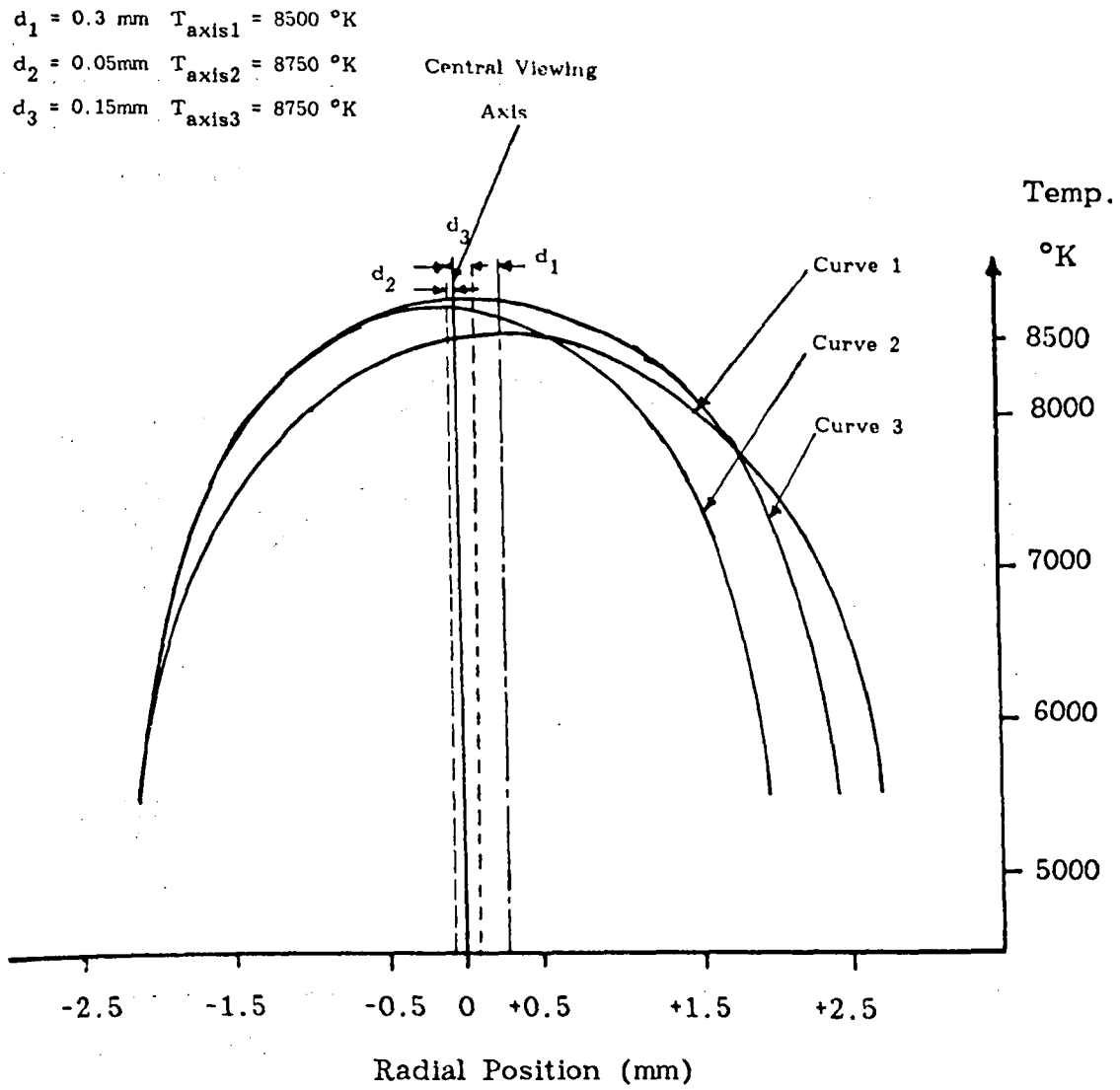

(a) Low di/dt (14-17 A/μs)

Operating conditions	Time before C.Z. μs	di/dt A/μs	Exposure time (μs)	pressure psig
Curve 1	-12.8	16	1.6	60
Curve 2	-12.4	16	1.6	110
Curve 3	-18.5	15	1.6	60

Fig.(5.12) Arc temperature profiles during the current zero period

(p = 60 psig)

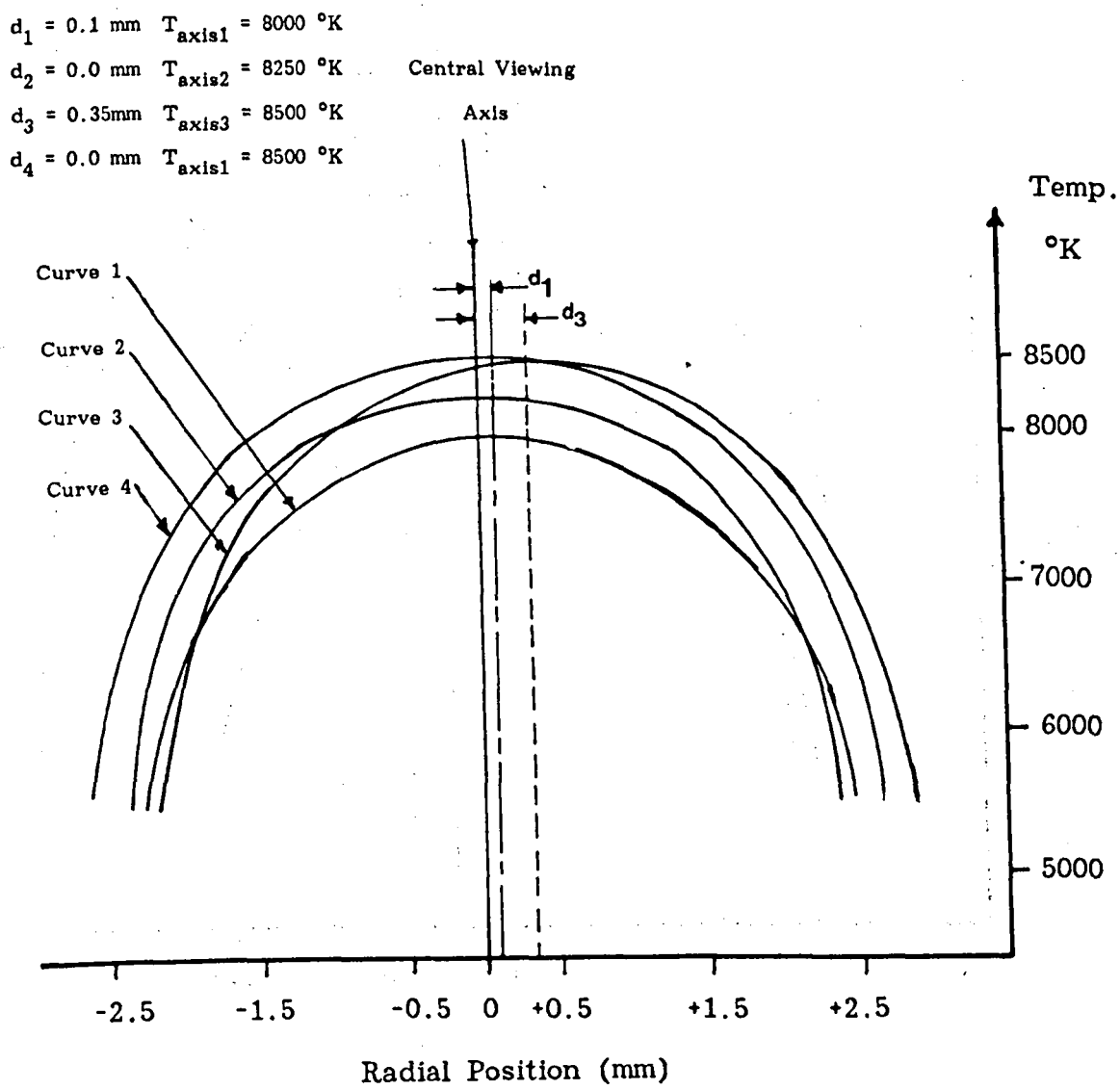

Fig.(5.12) (b) Medium di/dt (18-21 A/μs)

Operating conditions	Time before C.Z. μs	di/dt A/μs	Exposure time (μs)	pressure psig
Curve 1	- 3	18	1.6	60
Curve 2	- 4	20	1.6	60
Curve 3	- 8.8	19.5	1.6	60
Curve 4	- 9.6	20	1.6	60

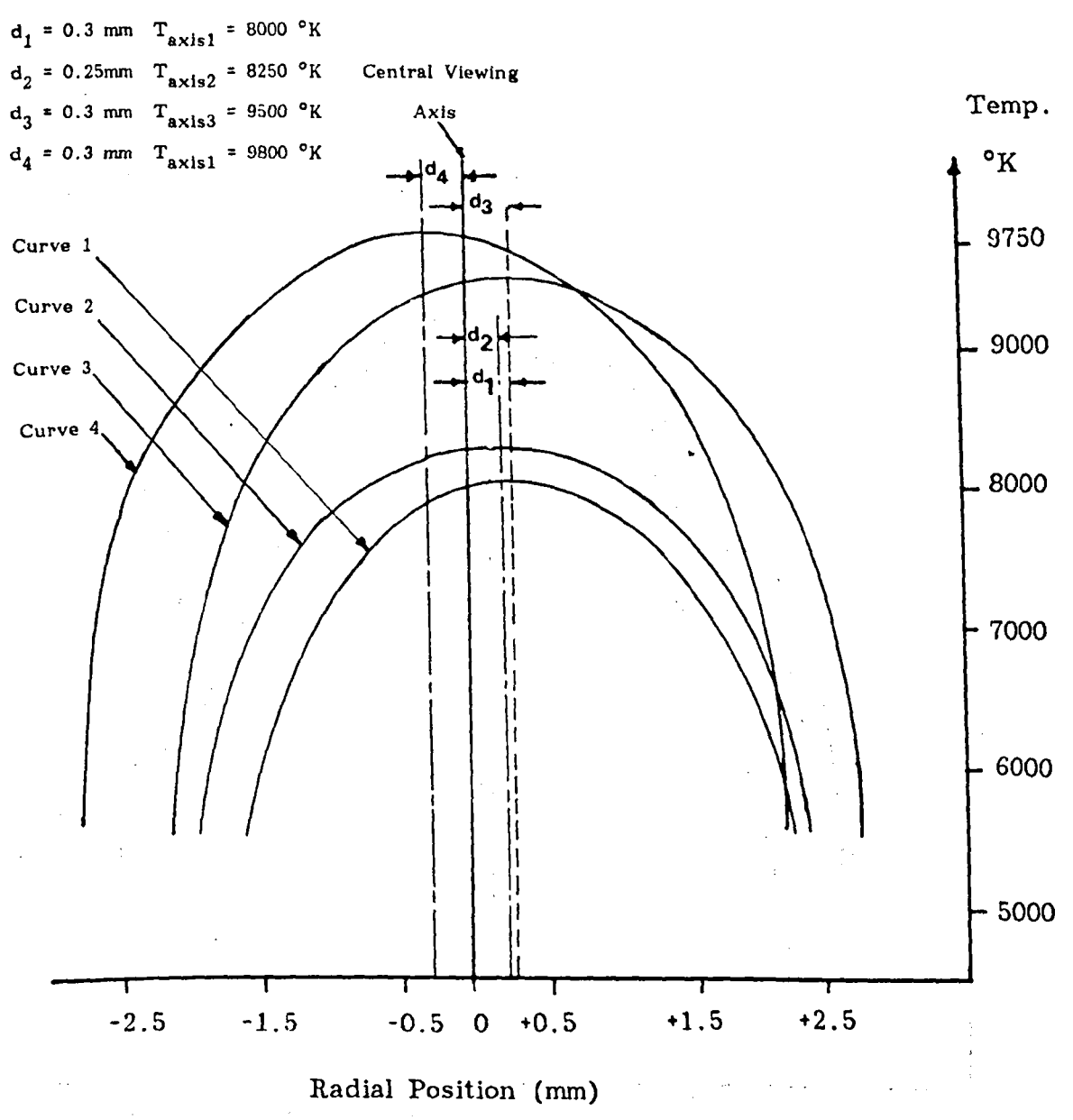

Fig.(5.12) (c) Medium di/dt (18-21 A/μs) & After current zero

Operating conditions	Time after C.Z. μs	di/dt A/μs	Exposure time (μs)	pressure psig
Curve 1	+ 4.6	20	1.6	60
Curve 2	+ 15	18	1.6	60
Curve 3	+ 22	21	1.6	60
Curye 4	+ 30	21.5	1.6	60

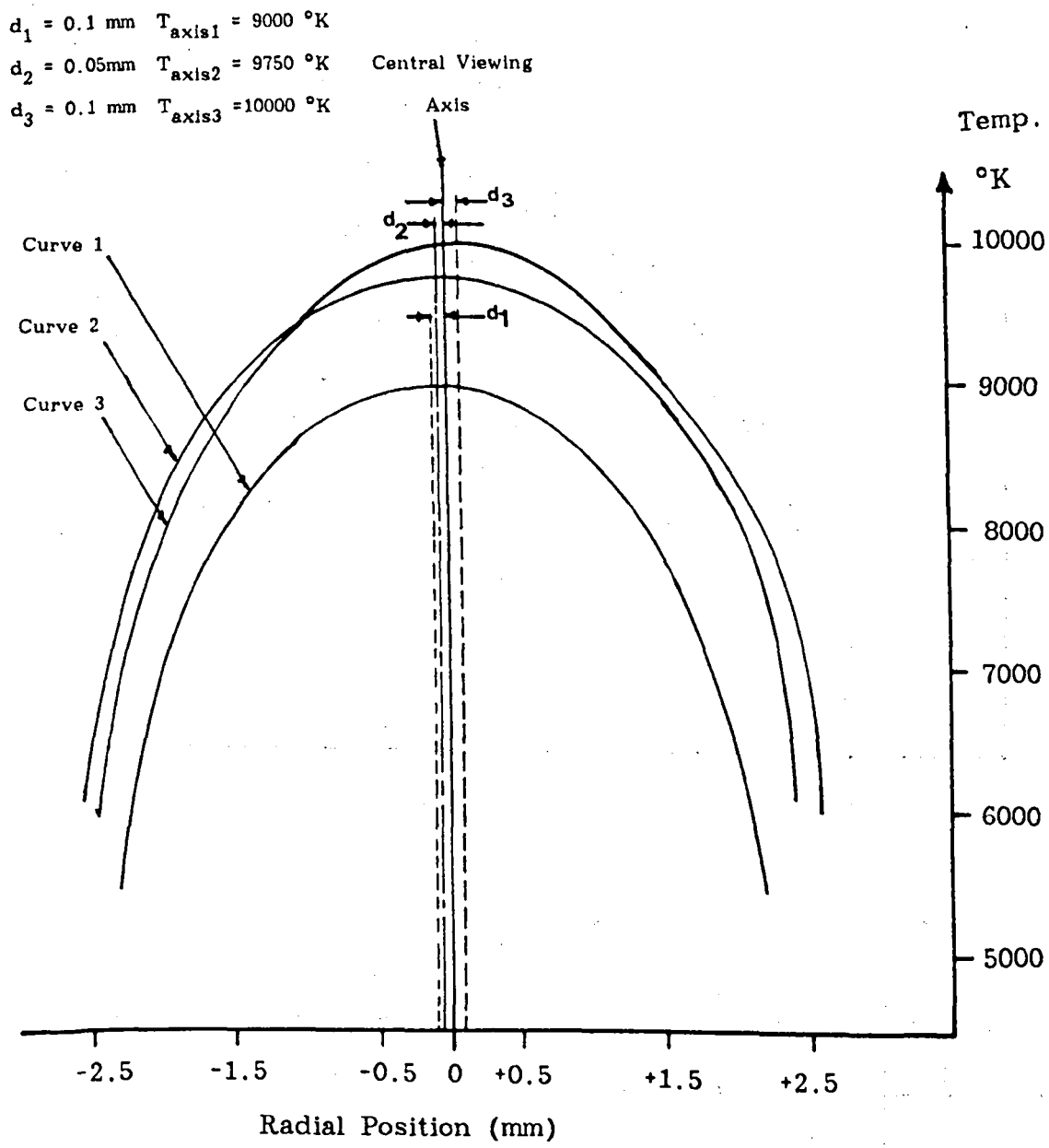

Fig.(5.12) (d) Medium di/dt (22-25 A/μs) & After current zero

Operating conditions	Time after C.Z. μs	di/dt A/μs	Exposure time (μs)	pressure psig
Curve 1	+ 7.3	23	1.6	60
Curve 2	+ 19	25	1.6	60
Curve 3	+ 47	23	1.6	60

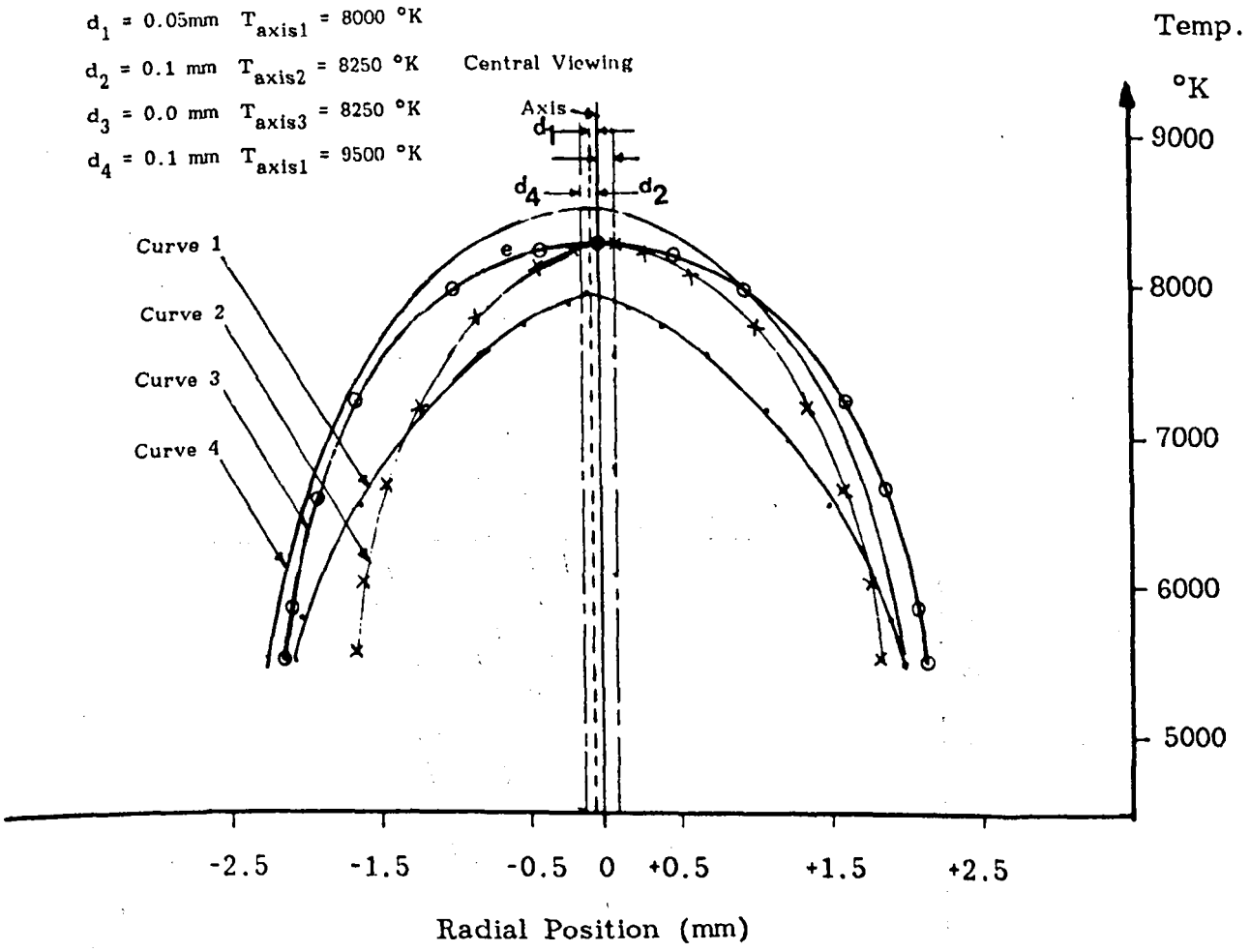

Operating conditions	Time before C.Z. μs	di/dt A/μs	Exposure time (μs)	pressure psig
Curve 1	- 5.6	15.5	1.6	60
Curve 2	- 4.4	16.5	1.6	110
Curve 3	- 9.6	15	1.6	60
Curve 4	- 9.6	15.8	1.6	110

Fig.(5.13) Comparison between the temperature profiles for the two cases high and low pressures (p=60 & p=110 psig)

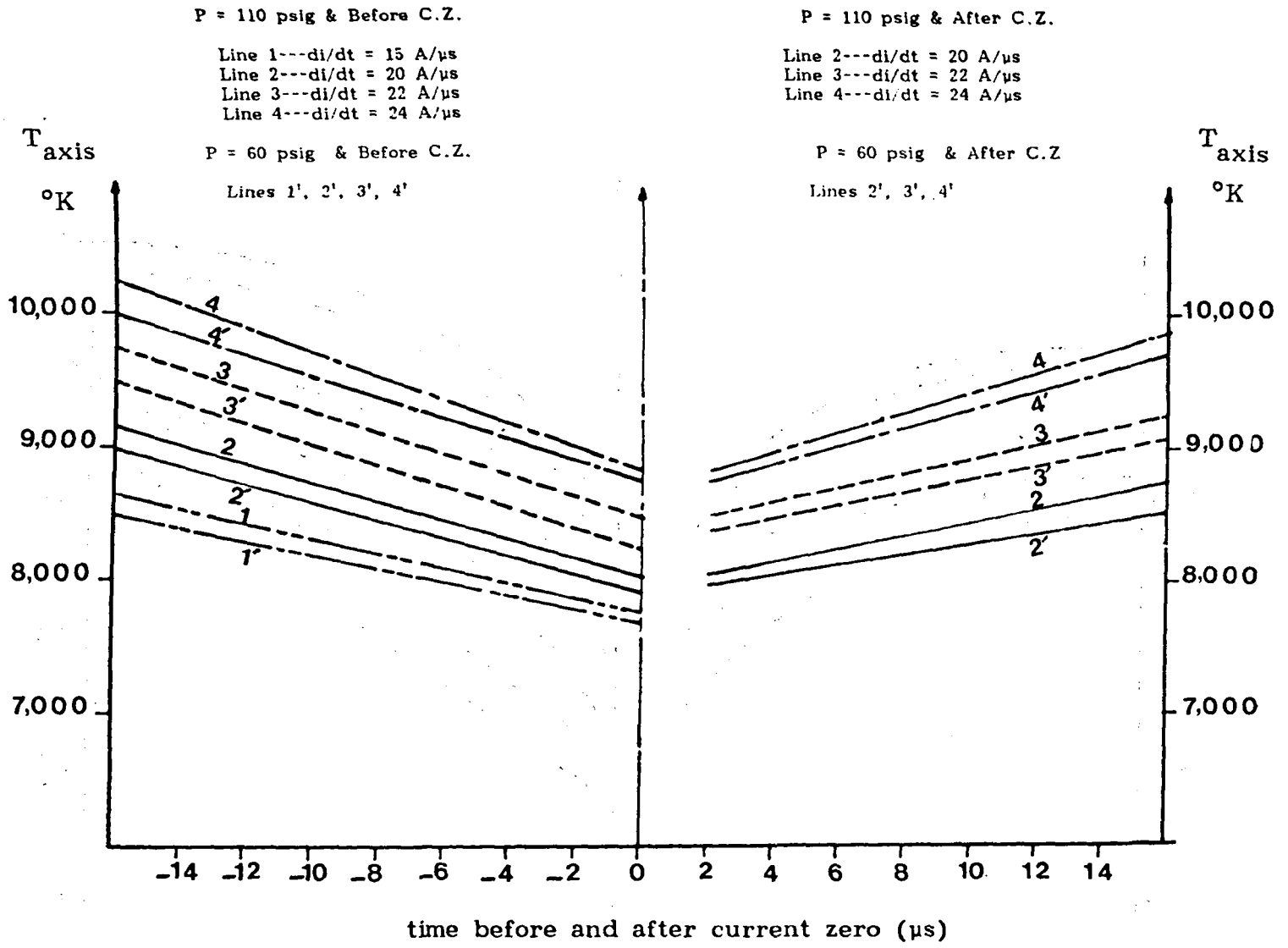

Fig.(5.14) Time variation of the axis temperature profile under different operating conditions

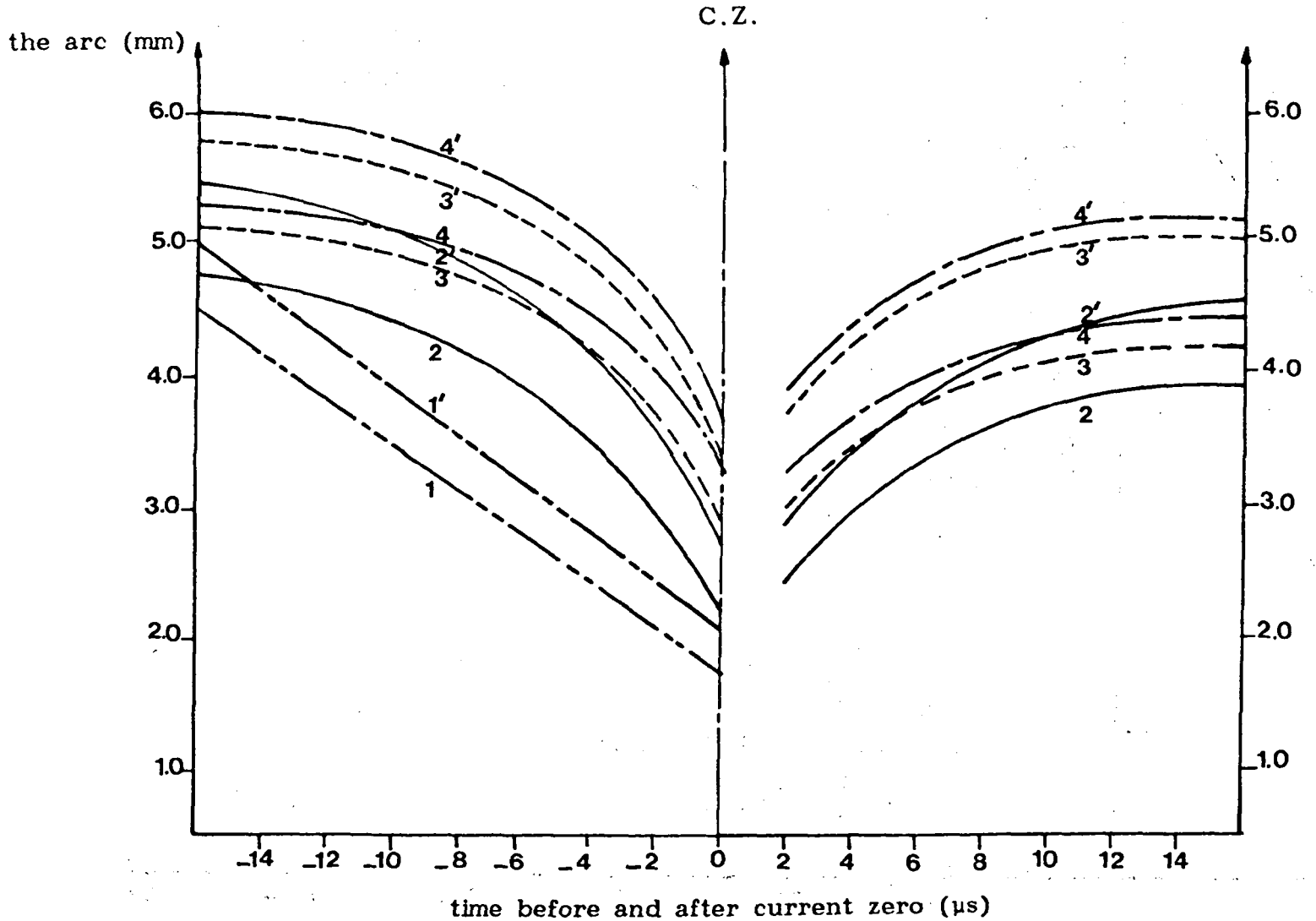

P = 110 psig & Before C.Z.

Curve 1---di/dt = 15 A/μs
Curve 2---di/dt =16.5A/μs
Curve 3---di/dt =20.5A/μs
Curve 4---di/dt = 24 A/μs

P = 60 psig & Before C.Z.

Curves 1', 2', 3', 4'

P = 110 psig & After C.Z.

Curve 2---di/dt = 18 A/μs
Curve 3---di/dt = 21 A/μs
Curve 4---di/dt = 24 A/μs

P = 60 psig & After C.Z

Curves 2', 3', 4'

Fig. (5.15) Time variation of the arc diameter under different operating conditions

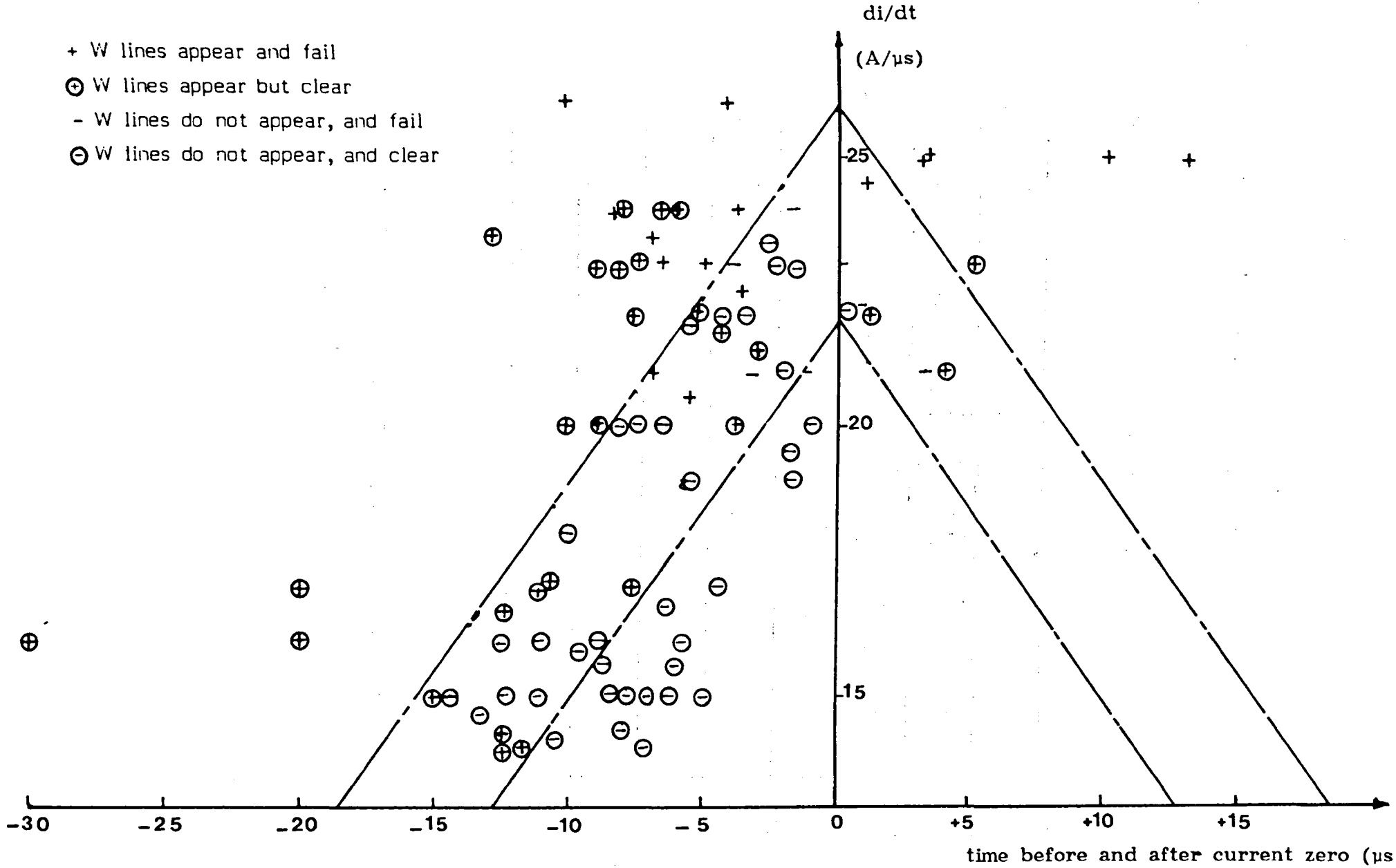

Fig.(5.16) Correlated results showing occurrence of W lines

(p = 110 psig)

I_o = + 3.2 μs di/dt = 25 A/μs T_{gate} = 1.6 μs Press. = 110 psig

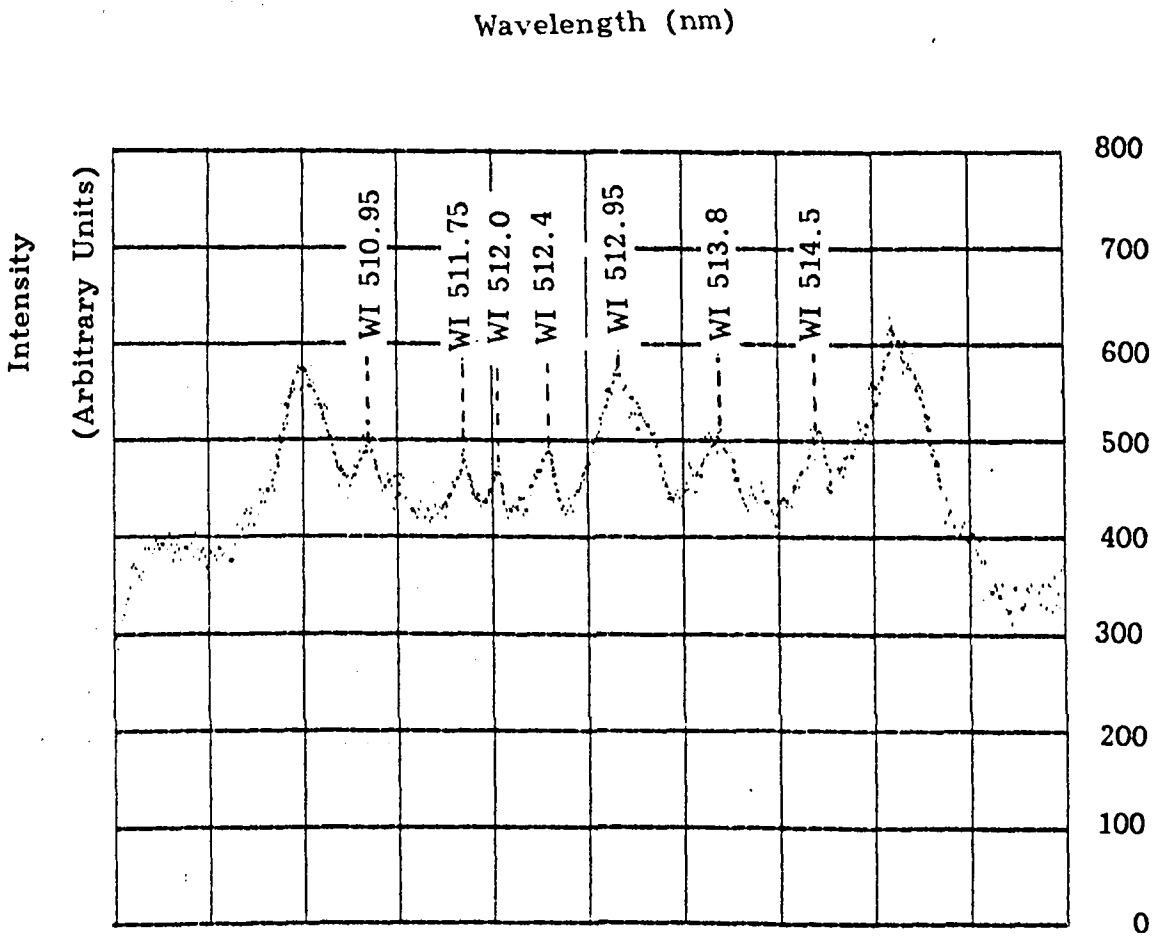

Fig.(5.17) The appearance of tungsten lines during the current zero period

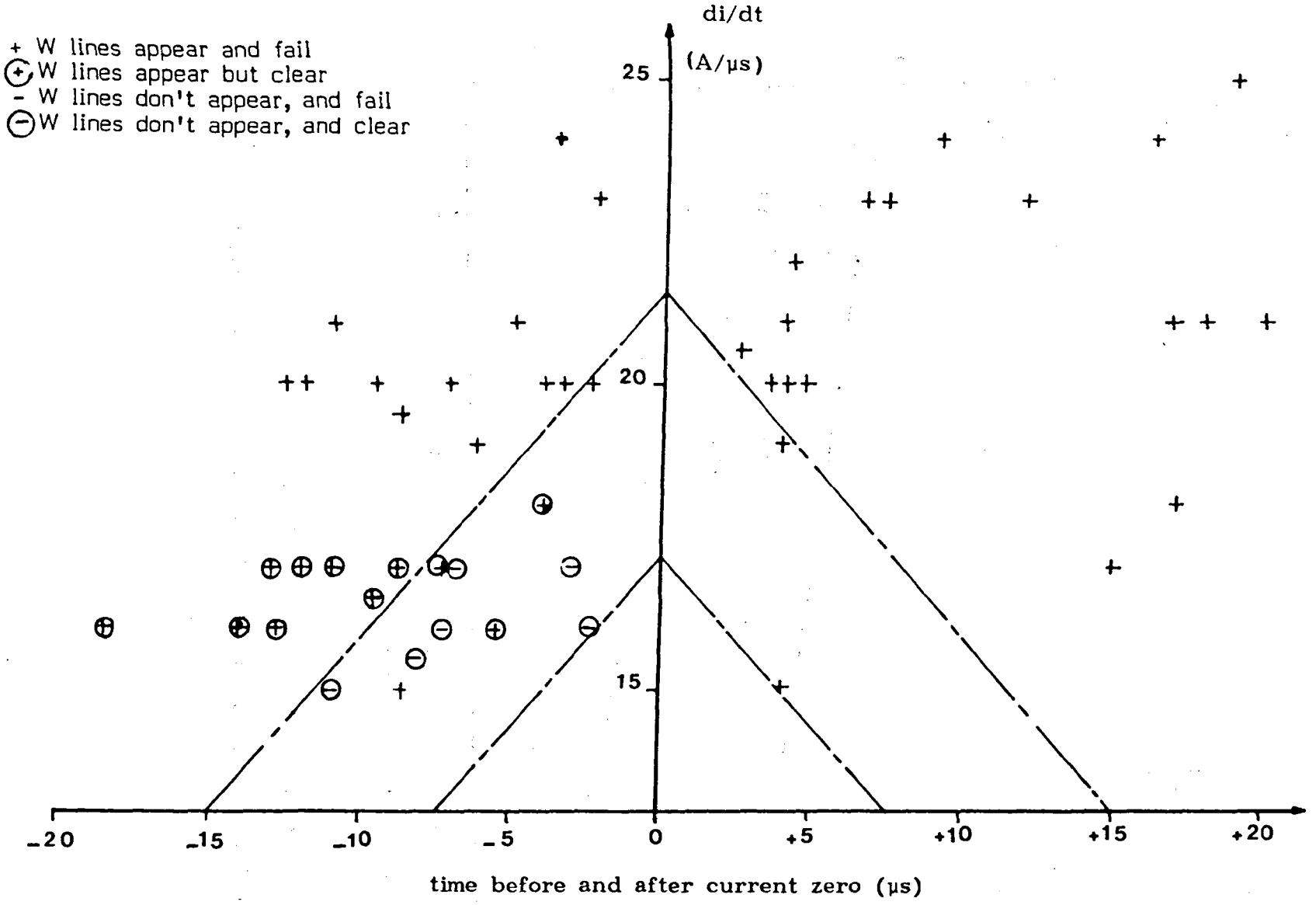

Fig. (5.18) Correlated results showing occurrence of W lines

(p = 60 psig)

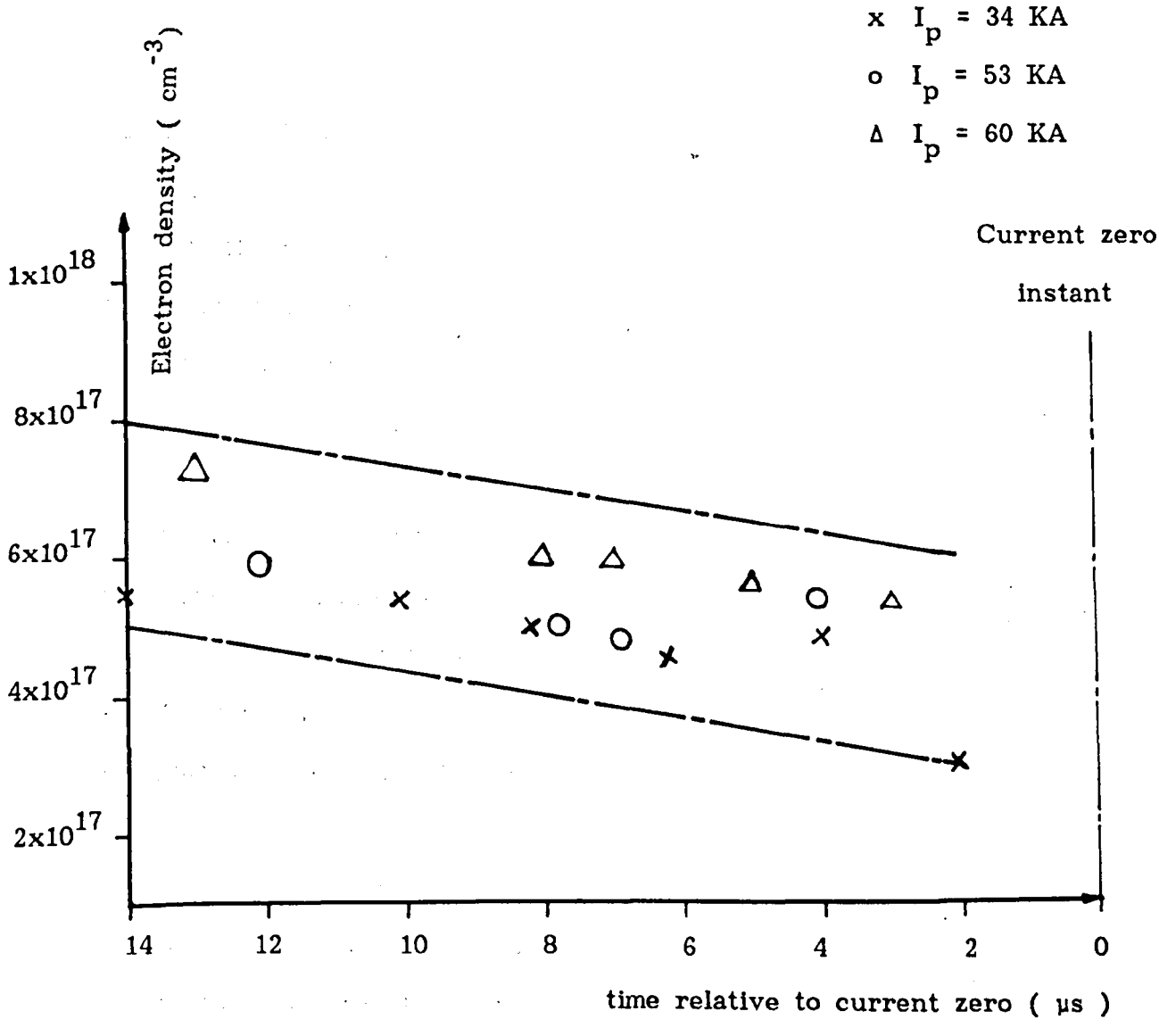

Fig. (5.19) The radially averaged electron density versus time, for different peak currents, during the current zero period.

CHAPTER 6

ANALYSIS AND DISCUSSION OF EXPERIMENTAL RESULTS

6.1 Introduction

It is the aim of this chapter to provide a quantitative insight into the processes governing arc thermal reignition. That aim may only be achieved through careful analysis of the results of chapter (5) in conjunction with theoretical arc considerations.

The first section of this chapter deals with the evaluation of radial temperature profiles from line of sight considerations. A method has been developed whereby the raw spectral data captured by the optical spectrum analyser (OSA 500) can be subjected to computational analysis and converted to a continuous radial temperature profile.

The second section of this chapter is concerned with the arc behaviour before and after current zero. Particular attention is paid to the appearance of the arc column, the shape factors of the integral analysis, and the optical depth of the plasma. Two criteria have been discussed from which the existence of LTE in the plasma may be assessed.

The third section of this chapter is concerned with the definition of the terms in the dynamic arc energy conservation equations and the current zero energy balance calculations.

6.2 The evaluation of radial temperature profiles from line of sight considerations

Since the arc plasma column is essentially a distributed cylindrical source the recorded spectrum needs to be corrected for its line of sight nature. A standard technique for making such a correction is the Abel inversion (Lochte Holtgreven, pp. 184, 1968). Fig. (6.1 a) represents the cross-section of a cylindrical arc source. The received intensity profile at a given displacement on the Y axis from the centre will be due to emission from a number of microscopic sources along the line of sight such as AA' in figure (6.1 a). In order to derive a radial intensity profile (along the Y axis of Fig. (6.1 a)) it is necessary to be able to analyse a continuous received radial intensity profile. Such a received profile was available in the form of the measured photographic intensity profiles (Lewis 1987). Fig. (6.1 b) represents such a measured profile when an interference filter centred on a wavelength of 521.8 nm was used (this was of wide enough bandwidth to include the whole CuI line emission centred on λ=521.8 nm).

The received intensity profile was subjected to the above mentioned Abel inversion for which it was assumed that the cylinder (or its cross-section) could be subdivided into 5 concentric shells (or rings

). Lines of sight were drawn (such as AA' in Fig. (6.1 a)) at five equi-spaced radial positions for the received intensity profile of Fig. (6.1 b) which corresponded to the radius of the innermost shell with the innermost line of sight being at a "Y" displacement of $r_1/2$ (Fig. (6.1 a)). Also shown on Fig. (6.1 b) is the Abel inverted intensity profile derived from the measured (or received) intensity profile discussed above. The computer program relating to the method of calculating of the inverted profile ("ABEL") is described in appendix (1). The Abel inverted profile of Fig. (6.1 b) corresponds closely to a parabolic shape. This profile is referred to hereafter as the emissivity profile and forms the basis for the interpretation of the radially resolved arc spectra (from which the radial temperature profiles are determined).

In chapter (4) the mode of operation of the OSA which yielded radially resolved arc spectra was discussed. This radial resolution corresponds to a splitting of the arc diameter into 5 viewing strips of equal width (i.e. radial dimension). Five strips across the diameter would give insufficient resolution to perform a proper Abel inversion for obtaining an emissivity profile directly. Also since these viewing strips are fixed with respect to the nozzle central axis small radial arc movements could further complicate such a direct interpretation, so resulting in major errors.

A more convenient and more accurate method of obtaining the temperature profile could be implemented if the emissivity profile was known and the inverse of the Abel inversion performed in order to

predict the received line intensity. This method would be particularly attractive in the case where two spectral lines are captured simultaneously which is the case in the spectra of figures (5.8) & (5.9) in chapter (5). The emissivity profile obtained by the Abel inversion of the photographic intensity profile shown on Fig. (6.1 b) was centred on λ = 521.8 nm for the CuI line. The two lines on Figs. (5.8) & (5.9) are centred on 510.5 nm and 515.3 nm. The theoretical line intensity variation with temperature for each of the above mentioned spectral lines calculated from equation (3.3) chapter (3) is shown on Fig. (6.2). It is clear from Fig. (6.2) that throughout the temperature range 6,000 to 12,000 °K the intensity values of the 521.8 nm and 515.3 nm emission differ only by a constant factor. Consequently the ratio of intensities of the two lines will remain constant within this region and be independent of temperature. In other words these two lines cannot be used to derive a radial temperature profile on account of their identical temperature dependence.

With the known parabolic emissivity profile of the 515.3 nm line the arc was divided into three concentric rings with the outermost ring forming the 6,000 °K boundary as shown on Fig. (6.3). Also shown on Fig. (6.3) are the 5 lines of view along which the arc diameter is observed by the optical spectrum analyser. The situation for an arc diameter of 6 mm is shown although the same would apply to any arc diameter. It is of significance however that, regardless of this diameter, the width of the viewing strips remains constant. In the case of Fig. (6.3) areas are produced by the intersection of the rings with the lines of view. The area enclosed by two rings re-

presents an area of homogeneous emissivity. This is representative of an average value of emissivity over the radius interval in question. Also shown on Fig. (6.3) is a typical arc emissivity profile (shown in arbitrary units).

It is possible for the emissivity profile extent (radius) to change with changing arc radius as well as the position of the profile centre with respect to the fixed line of sight, due to arc movement.

A program has been developed which predicts the effect of the above changes on the recorded intensity. In this program the areas described above are calculated according to a given arc radius and displacement from the central viewing axis. The recorded intensities are calculated according to a similar fixed emissivity profile of the arc column to that described above. Thus a number of predicted recorded intensities are generated for a single arc emissivity profile (515.3 nm line) which correspond to different arc radii and displacement from the central axis. These recorded intensities are in the form of radially resolved histograms and the program which calculates these is called " I515N " and is described in detail in appendix (1).

The radially resolved arc spectra centred at the 515.3 nm wavelength captured by the OSA are normalised to the highest line intensity value and an experimentally measured radial histogram is obtained. This histogram is then compared with the family of histograms calculated by the above method. A best fit of the experimental data is then obtained which enables the radial shift of the arc

axis and the arc radius to be determined. The method also enables asymmetry about the central axis to be incorporated in the calculations. For instance parabolas of different radii on opposite sides of a common central axis may occur in some cases.

The experimental data of chapter (5) often included not only the line emission at 515.3 nm but also the 510.5 nm spectral peak on the same record. The temperature variations of the intensity of these lines calculated from equation (3.3) is shown in Fig. (6.2). It is clear from this figure that the temperature variation for the 510.5 nm spectral line intensity is different from that of the 515.3 nm line. Thus for a given temperature profile a unique emissivity profile will exist for the 510.5 nm line. The same procedures which followed for the case of the 515.3 nm line to obtain the histograms are applied for the 510.5 nm line. Also the recorded intensities are in the form of radially resolved histograms and the program which calculates these is called " I510N " and is described in detail in appendix (1).

Thus a method has been developed whereby the raw spectral data captured by the OSA 500 can be subjected to computational analysis and converted to a continuous radial temperature profile.

6.3 The arc behaviour before and after current zero

6.3.1 Introduction

The performance of the circuit breaker investigated in this thesis is represented by a band region on a di/dt : dv/dt characteristic

which segregates the positive clearance and failure regimes (Taylor et al, 1982). In this band the circuit breaker may clear or fail in successive tests under identical operating conditions. When a circuit breaker fails under such conditions the reignition is referred to as a critical arc reignition. This failure occurs shortly after current zero during the period when the rate of rise of the recovery voltage can be sustained. This implies that failure occurs during the thermal recovery period i.e. due to Joule heating of the remnant arc column, i.e the reignition is dependent upon the thermal state of the arc channel (thermal reignition) and for SF_6 usually occurs within 3 or 4 μs after the current zero.

6.3.2 The appearance of the arc column

The physical appearance of the arc column during the current zero period gives an important insight into which energy transfer processes may dominate at different axial locations.

It was established by Lewis (1987) that in the case of full power arcing, although the luminous arc diameter exhibited some oscillatory characteristics, no arc column splitting or swirling was evident (particularly upstream of and near the nozzle throat). Arc column splitting probably indicates substantial turbulent flow conditions. The arc photographs by Lewis (1987) also indicated that the arc column downstream of the nozzle throat was generally more diffuse in nature than the upstream column during the current zero period. It is therefore likely that upstream of and in the nozzle throat vicinity the

arc appears to be surrounded by laminar flow conditions whereas further downstream turbulent conditions may exist in some cases.

It is of importance that no arc splitting or prominent turbulent effects are in evidence at the localities at which the arc temperature profile is measured so that energy flow calculations may be applied radially and axially without complication and in compliance with the boundary layer approximations. Also the continuous nature of the radial arc intensity profile allows the above mentioned boundary layer formulations to be applied to the dynamic arc equations.

6.3.3 Approximate performance trends with different pressure and different arc length

The variation of the peak current under 100% clearance with different pressures and different arc lengths for a 35 mm throat nozzle (PTFE), with SF_6 as the arcing medium and a waveform frequency of 78 Hz is shown on Fig. (6.4). This figure shows that the gap length between the two electrodes has a pronounced effect upon the performance of the circuit breaker. For example, the test head failed to interrupt the peak currents above 55 KA in the case of a 105 mm (gap between two electrodes), but this value reduced to 41 KA in the case of a 65 mm gap for the same pressure (p = 110 psig).

Results also given on Fig. (6.4) show a similar influence of the upstream pressure on the performance of the circuit breaker. The low pressure produces a poorer performance than the case of high pres-

sure. In this case the difference between the high pressure performance and that of the low pressure is less pronounced than with different arc lengths (55 KA with high pressure compared with about 51 KA with low pressure for the same arc length).

Some typical records of the time variation of current and voltage under full power conditions are shown on Figs. (6.5 a-d). The voltage and current were recorded both during the peak current phase and during the current zero period using two Tektronix 468 digital storage oscilloscope and a Tektronix 556 oscilloscope (registered photographically respectively) as described in chapter (4). Fig. (6.5 a) corresponds to a peak current of about 53 KA with an upstream pressure of 110 psig and arc length of 105 mm. This figure shows that the test head succeeded in interrupting the current whilst Fig. (6.5 b) shows that the test head failed to interrupt a 51 KA for the same arc length but for different pressure (p = 60 psig). For the conditions shown on Figs. (6.5 c and d), which correspond to peak currents of 47 KA and 36 KA respectively, the test head failed to interrupt the current, for the same arc length (65 mm) and different pressures.

A similar study was conducted by Taylor et al (1982) to study the effect of the nozzle material and the gas upon the circuit breaker performance. The results of their investigations are summarised on Fig. (6.6) for both air and SF_6 as the arcing media and with PTFE, copper, steel and carbon as the nozzle materials for the same pressure and the same arc length. Their results for SF_6 as the arcing medium

suggested that the performance with copper, steel and carbon nozzles were all similar with the clear/fail transition occurring at a peak current of approximately 60 KA at 78 Hz. However a PTFE nozzle produced a deterioration in test head performance indicated by the clear/fail transition occurring at the lower peak current of 53 KA, which is approximately the same value found from the present investigations (55 KA). Results also given on Fig. (6.6) show a similar influence of nozzle material on performance with air as the arcing medium, whereby PTFE produces a poorer performance than the other materials.

6.3.4 Quantitative implications of results

i) The electrical conductance and core shape factors

The boundary layer integral approach (e.g. Cowley and Chan (1974), Chan et al (1974), Topham (1971, 1972 a, b)) provides a powerful analytical technique for correlating and predicting the behaviour of gas blast arcs under different conditions. These integrals have units of area and were thus called characteristic areas. One of these integrals is the conductance area, θ_c. According to the integral analysis of Cowley (1974) the conductance area is represented by :

$$\theta_c = \int_0^{\infty} (\sigma_{(r)}/\sigma^*) 2\pi r dr \qquad (6.1)$$

where

$\sigma_{(r)}$ = the local radial electrical conductivity ($\mho$/m)

r = the radial position (m)

σ^* = the characteristic electrical conductivity ($\mho$/m)

In this thesis the characteristic values of electrical conductivity were chosen to be those values corresponding to a temperature of 6,000 °K in SF_6 which are equal to 236.3 $\mho$/m and 304.6 $\mho$/m at 4 atm and 2 atm pressure respectively (Frost & Liebermann 1971). These values were chosen on the basis of a comparison with other authors who used similar characteristic values in nitrogen. Walmsley and Jones (1978 ii) gave a value of σ^* = 366 $\mho$/m for nitrogen. For their working pressure this corresponds to a temperature of about 5,500 °K (Shayler and Fang, 1976). The conducting radius for nitrogen is defined according to many authors working on both theoretical and empirical arc models (e.g. Topham, 1971) as being at a radius defined by an isotherm whose value usually lies between 4,000 °K and 5,000 °K. The value of 5,500 °K deduced from Walmsley et al's (1978 ii) work therefore lies above the temperature at which the electrical conductivity becomes significant. All the transport properties of SF_6 used in this chapter are summarised in table (6.1).

The conductance area θ_c may be evaluated using the measured temperature profiles Figs. (5.11), (5.12) and (5.13) and equation (6.1). These calculations have been made for different di/dt and different time before and after current zero for the upstream pressure of 60 psig. For the purpose of these calculations the core boundary (R_c) was defined as the 5,500 °K isotherm. The results of these calculations are summarised in table (6.2).

The area chosen for such normalising purposes is usually the thermal area which then yields the primary shape factor Λ_c of Chan et al (1974), where

$$\Lambda_c = \theta_c / \theta_\delta \tag{6.2}$$

and

$$\theta_\delta = \int_0^\infty [\, 1 - (\rho_{(r)} / \rho_\infty)] \, 2\pi r dr \tag{6.3}$$

Where

$\rho_{(r)}$: local gas density

ρ_∞ : cold flow density

θ_δ : thermal area

To a first approximation the thermal area may be equated to the area which would be obtained from a shadowgraph measurements θ_s. According to Lewis (1987) this area can be calculated as

$$\theta_\delta = \theta_s \simeq \pi(6.5)^2 \text{ mm}^2 \tag{6.4}$$

Using the above equation and the data from table (6.2), the overall conductance shape factor Λ_c was calculated and summarised in table (6.2).

These values of Λ_c may be correlated to the results of other authors with different operating conditions through a universal correlation parameter. Such a parameter is the Nusselt number which represents the non-dimensional heat loss conduction across the arc

core boundary. Calculation of this parameter requires a knowledge of the temperature gradient at the core boundary which the temperature profiles of Figs. (5.11), (5.12) and (5.13) provide. The Nusselt number is defined as (Walmsley and Jones (1978 ii)).

$$Nu = (Cp^{*}/K^{*}h^{*})\ (K_c/Cpc)\ R_c\ (dh/dr)_{r=R_c} \qquad (6.5)$$

Where

Cp^{*} = specific heat capacity (characteristic value)

K^{*} = thermal conductivity (characteristic value)

h^{*} = specific enthalpy (characteristic value)

K_c = thermal conductivity (at core edge)

Cpc = specific heat capacity (at core edge)

R_c = radius of core edge

All the above values are given in table (6.1). The Nusselt number was then computed using the values of table (6.1) and $(dh/dr)_{r=Rc}$ obtained from the temperature profiles of Figs. (5.11), (5.12) and (5.13) for different di/dt and different times before and after current zero at a pressure of 60 psig. The results of these calculations are summarised in table (6.2). The values of Λ_c corresponding to these values of Nu are shown on Fig. (6.7) and compared with results for other operating conditions. These results correlate well with previously reported results.

Another comparison with the previously results may be made for the core shape factor (λ_c). The core shape factors are determined

as ratios involving integration not to infinity but rather to the core boundary (Chan et al, 1976).

Thus the core thermal area is defined as :

$$\phi_\delta = \int_0^{R_c} [\, 1 - (\rho/\rho_c)] \, 2\pi r dr \qquad (6.6)$$

Where

R_c is the radius of the electrical core and

ρ_c is the gas density at R_c.

Walmsley and Jones (1978 ii) also defined the equivalent shadow area referred to the core as

$$\phi_s = \int_0^{R_c} 2\pi r dr = \pi R_c^{\,2} \qquad (6.7)$$

Thus by restricting the integration to the core both ϕ_c (equivalent to θ_c) and ϕ_s may be determined more accurately from the present results. Also by making the Cowley (1974) approximation that ϕ_s and ϕ_δ are equivalent, the conductance shape factor referred to the core boundary is then :

$$\lambda_c = \phi_c / \phi_\delta = \theta_c / \phi_s = \theta_c / \pi R_c^{\,2} \qquad (6.8)$$

The results of the above equation are summarised in table (6.2). Fig. (6.8) shows the values of λ_c plotted against the Nusselt number along with other values of λ_c obtained from different arcing conditions

(Walmsley and Jones 1978 ii). These results show a good correlation within experimental scatter with the previously reported results.

ii) LTE in the current zero arc column

Two criteria were established in chapter (2) which allowed the existence of LTE to be confirmed in the current zero arc column. The results of chapter (5) were used to evaluate both of these criteria in turn and the implications of these are discussed in this section.

The first of the two criteria which needs to be considered is McWhirter's criterion :

$$Ne \geq 1.6\times10^{12}\ T_e^{1/2}\ (\Delta E_{mn})^3 \qquad (6.9)$$

Where all the symbols were defined in chapter (2) equation (2.16) and ΔE_{mn} = 2.73 eV for a CuI line.

The temperature value (T_e) required for the right hand side of equation (6.9) was taken as the experimentally measured radially averaged arc temperature. Fig. (6.9) shows the variation of the product on the right hand side of equation (6.9) for the different arcing conditions investigated in this thesis. Also shown in this figure the values of electron densities obtained experimentally from the Stark broadening calculations based upon the spectroscopic data of chapter (5). It is clear from this data that the McWhirter criterion for the existence of LTE is satisfied by more than an order of magnitude.

Fig. (6.9) shows also the values based on similar calculation but with T = 5,500 °K to test the existence of LTE at the 5,500 °K radial isotherm.

The second of these two criteria was Griem's criterion which was discussed in chapter (2) and was stated as follows :

$$Ne \geq 9\times10^{17} \, (E_2^{z-1,a}/E_H)^3 \, (KT/E_H)^{1/2} \qquad (6.10)$$

Where all the symbols were defined in chapter (2), equation (2.17) and E_H and $E_2^{z-1,a}$ take the values 7.724 eV and 3.82 eV respectively for a CuI line. Fig. (6.9) also shows that this criterion is comfortably satisfied (in the worst case by a factor 7), these results show that the Griem criterion is a more severe test of LTE existence.

Thus the two criteria for testing LTE existence derived in chapter (2) have been evaluated using the experimental data of chapter (5). Comparison with measured values of electron density Ne from chapter (5) shows that LTE exists in the circuit breaker arc throughout the current zero period. Furthermore a comparison of the same formulae using a value of 5,500 °K with the measured electron densities shows that LTE exists within the confines of the 5,500 °K isotherm i.e. the conducting radius.

6.3.5 Optical depth of a plasma

In order to ensure accurate interpretation of spectral results it is essential to ascertain the transparency of the plasma to the various emission lines. The test adopted for plasma transparency is that postulated by Airey (1977). This involves comparing the intensity of a diagnostic line with the " black body " intensity at the same wavelength and temperature. If the line intensity exceeds the black body limit in any region of the line profile, then the line shape will saturate by redistributing its energy within a larger bandwidth. This in turn enhances the probability of self absorption by particles of the same type as the emitter and in the limit leads to the total loss of emission at the line centre. Such lines cannot then be used for diagnostic purposes. The test gives the conditions under which absorption might first be observed and therefore constitutes a severe transparency test.

The optical depth for no self absorption , 2r, is given by (appendix (3)).

$$2r = [24\pi Z(T)\Delta\lambda_{mn}((C_1/\lambda^5)(\exp(C_2/\lambda T)-1)^{-1})]/[Nz(T)A_{mn}g_m \Delta E_{mn}e^{-(Em/KT)}] \quad (cm) \qquad (6.11)$$

The optical depth variation with temperature (T) according to equation (6.11) is shown on Fig. (6.10) for some of the CuI diagnostic lines used in this investigation. The program for this calculation is listed in appendix (1).

Another method for determining whether the current zero arc plasma is optically thin involves an inspection of the shape of particular spectral lines. If the plasma departs from being optically thin then re-absorption of the radiation at a wavelength corresponding to the line centre occurs. The effect of this is to give the line an increasingly flattened appearance and, in the extreme, self reversal occurs whereby the line profile shows a dip at the centre wavelength. It was beyond the capability of the present optical system to detect the CuI resonance lines (which are centred in the U.V. part of the spectrum), so that it was not possible to detect whether self reversal occurred for these lines. The profile of the spectral lines centred 515.3 and 510.5 nm lines (results of chapter (5)) show no indication of flattening at the centre wavelengths. Consequently the arc plasma may be considered to be optically thin.

6.4 Definition of the energy conservation terms

Energy conservation for the core of axisymmetric electric arcs has been considered interms of radial integrals by Chan et al (1976). These authors applied the boundary layer assumptions to the core energy equation, which included radial diffusive transport terms (i.e. radiation and heat conduction). By substituting for the mass flow rate crossing the arc boundary (which was derived from the mass flow continuity equation) into the core energy equation and then introducing the energy equation for the external flow, the authors were able to write the complete energy equation for the arc core. For the boundary layer analysis applied in this case, we may set $P_I = P_\infty$

(where P_I is the pressure at the core boundary, P_∞ the cold flow pressure) i.e. pressure balance is assumed.

The core energy equation of Chan et al (1976) can be written in the following form :

Electrical power input to the core	+	Rate of decay of the stored energy in the core	= +	Radial heat conduction from the core	+	Axial heat convection from the core

Net power loss due to radiation from the core	-	Radial heat convection from the core	(6.12)

Equation (6.12) corresponds to

$$E.i + (d/dt)[\int_0^{r_{arc}} \rho_{(r)} h_{(r)} \; 2\pi r dr] = + \int_0^{r_{arc}} (1/r)(\partial/\partial r)[Kr(\partial T/\partial r) \; 2\pi r dr] + (\partial/\partial x)[\int_0^{r_{arc}} (\rho_{(r)} h_{(r)} C_{(r)}) \; 2\pi r dr] + Q_r - m_e h_\infty \qquad (6.13)$$

For which the following assumptions have been made :

(1) The enthalpy at the core edge is much greater than the square of the local axial flow velocity. Thus

$$h_{r\ arc} >> W_{r\ arc}^2$$

(2) Radial pressure balance exists.

(3) Radial heat conduction occurs according to the Furrier Law.

(4) The work done against shear stress is discarded.

Thus with a knowledge of the temperature profile the terms of equation (6.12) can be individually evaluated (except for Q_R).

6.5 *The current zero energy balance*

The dynamic core energy balance of an axially blown arc during the current zero period may be written :

Electrical power input	=	Losses due to thermal convection from core	+	Loss due to radial heat conduction from core	+	Loss due to radiation from core
	+	Power dissipated by thermally stored energy changes in the arc core				(6.14)

In equation (6.14) it is assumed that the following energy transfer terms are negligible and can therefore be ignored :

(a) turbulence (b) axial heat conduction

In this section the terms in equation (6.14) are evaluated individually for the current zero period, using the experimental data of chapter (5), and their relative significance determined. Each term

will be evaluated for different times before and after current zero and for different di/dt and also for different upstream pressures.

6.5.1 The electrical power input

The Joule heating input power, Q_E, is obtained from :

$$Q_E = E \, . \, i = (V_{arc} / L_g) \, . \, i \qquad (6.15)$$

Where

i : instantaneous current (A)

E : overall arc electric field strength (V/m)

V_{arc} : instantaneous arc voltage (volts)

L_g : overall gap length = 105 mm

In this case the value of E is taken as the arc voltage divided by the overall gap length. This is representative of an average value of E for the whole arc column. Arc voltage and current values have been determined from the oscillograms (Fig. (6.5)). The results of these calculations are plotted on figure (6.11) as a function of time before and after current zero for different di/dt. These results show that during the pre current zero period the energy input decreases monotoincally, is approximately independent of current decay rate. There is however a significant pressure dependence whereby the input power increases with pressure and the decrease with time before current zero is more severe.

6.5.2 The change in thermal energy stored in the arc column

The rate of change of stored energy in the arc core is defined as:

$$Q_s = (d/dt)\left[\int_0^{r_{arc}} \rho_{(r)} h_{(r)}\, 2\pi r dr\right] \qquad (6.16)$$

Where

$\rho_{(r)}$: Local radial value of gas density

$h_{(r)}$: Local radial value of enthalpy

r : radial position

With a knowledge of the radial temperature profile (chapter (5) Figs. (5.11), (5.12) and (5.13)) the integral in equation (6.16) can be evaluated for different times before and after current zero and also for different di/dt. The results of these calculations are shown on Fig. (6.12). The values of ρ and h for different temperatures at the two pressures p = 4 atm and p = 2 atm were obtained from Frost and Liebermann (1971) (table (6.3)) and the products $\rho_{(r)} \times h_{(r)} \times r$ were computed for the radial temperature profiles corresponding to these cases of Figs. (5.11), (5.12) and (5.13). Fig. (6.12) shows that the pressure has a pronounced effect upon the rate of change of the thermal energy stored, the gradient being much greater for the higher pressure.

To evaluate the time derivative term in equation (6.16) two temperature profiles at different times before and after current zero for every di/dt must be used. The results of these calculations are given

in table (6.4). These results show that the change in thermal energy stored (Q_s) increases with pressure and di/dt. For example, Q_s is equal to 2.4 Mw/m in the case of higher pressure and di/dt = 20 A/μs but Q_s decreases to 1.1 Mw/m in the case of lower pressure at the same of operating conditions.

6.5.3 Power loss due to radial thermal heat conduction across the core boundary

The power loss by radial thermal conduction is defined as

$$Q_{co} = \int_0^{r_{arc}} (1/r)(\partial/\partial r)\ [Kr(\partial T/\partial r)\ 2\pi r dr] \qquad (6.17)$$

Where

k : the thermal conductivity

The temperature profile of Figs. (5.11), (5.12) and (5.13) with the transport properties data of Frost and Liebermann (1971), (table (6.3)), were used to evaluate the integral of equation (6.17) over the arc diameter. Care was taken to measure the dT/dr value at the core boundary since this formed the most significant contribution to the integral value. The results of these calculations are shown on Fig. (6.13). These results suggest that the boundary thermal conduction loss decreases more rapidly with time for the higher pressure case suggesting that the current zero losses are less for the higher pressure case than for the lower pressure.

6.5.4 Power loss due to radiation

The radiation loss at the arc core boundary is difficult to calculate in detail since the radiative emission and absorption characteristics of the arc plasma and surrounding heated gas are complicated functions of wavelength and temperature. However it is possible to establish a lower limit for the radiative transfer by measuring the total radiation remote from the arc. (The radiative loss at the arc core boundary is of course given by the sum of this radiation remote from the arc and that absorbed by the surrounding heated gas).

The decay of the total visible radiation power loss (400 to 900 nm) wavelength range was measured simultaneously (Shammas, private communication) with the photographic records presented by Lewis (1987). Thus instantaneous radiation power loss was measured throughout the current zero period for a number of di/dt levels corresponding exactly to the operating conditions of the investigation of this thesis. The results of Shammas (private comm.) are shown on Figs. (6.14) & (6.15) for the total radiation loss in (volts) as a function of the instantaneous current for different di/dt at the two locations, slot 2 and slot 3. To convert the total radiation values from (volt) to (w/mm) a clibration factor (99) (Shammas and Jones (1982)) was used. This method was explained in detail in chapter (3).

These results have been used to evaluate the net radiation loss from the arc for two pressures p=60 & p=110 psig and for different

di/dt during the current zero period. The results of these calculations are shown on Fig.(6.16). These results show that the radiation losses increase with pressure. The results may also be compared with estimates from the modelling by Airey (1977) using the equation

$$Q_R = 20.1\ \pi\ p\ r_c^{1.684} \quad \text{(w/mm)} \tag{6.18}$$

Where p is the pressure in bar and r_c the radius in mm. The agreement between the present results and the above equation is reasonable.

6.5.5 The power loss due to axial heat convection

The power loss by axial heat convection is defined as :

$$Q_{CA} = (\partial/\partial x)\ [\int_0^{R_c} \rho_{(r)}\ h_{(r)}\ C_{(r)}\ 2\pi r dr] \tag{6.19}$$

Where

$C_{(r)}$ - the axial component of the flow velocity.

Since under normal operating conditions sonic flow was arranged downstream of the nozzle throat (e.g. Taylor (1983)), the gas velocity was assumed sonic across the section of the arc at the nozzle throat during the current zero period under investigation. Using the temperature profiles represented in chapter (5) (Figs. (5.11), (5.12) and (5.13)) and the values of ρ, h and C (the sonic velocity) from Frost and Libermann (1971), the integral in equation (6.19) can be

calculated. In order to estimate the axial gradient, use was made of results obtained through two adjacent viewing slots (slot 2 and slot 3). Fig. (6.17) shows a summary of temporal arc area and intensity decay during the current zero period. These results were used to estimate changes in both the luminous crossection of the arc (yielding the diameter of the 5,500 °K isotherm) and the peak (axial) intensity of the optical emission (indicating approximately changes in the axis temperature through approximate calibration).

The measurements of local axial gas pressure of Taylor (1983) have provided the knowledge of the axial pressure distribution which is necessary to evaluate the local values of the transport properties. It is necessary that radial pressure balance exists at the axial location of interst. Departure from pressure balance at slot 3 is unlikely (Taylor (1983)). The axial separation of slots 2 and 3 is 10 mm. The axial pressure profile in this region is close to linear (Taylor, 1983). Thus the axial derivative in equation (6.19) is calculated as the difference between two integrals (one for each slot) divided by the interslot separation (10 mm). The results of these calculations are shown on Fig. (6.18). These results show that the axial heat convection contributes a significant amount of power loss term especially in the case of the higher pressure. Also the axial heat convection loss is higher in the case of a higher di/dt. Fig. (6.18) also shows that the axial heat convection loss decreases more rapidly with time before current zero for the higher pressure case.

6.5.6 The radial convection losses

The power loss by radial convection is defined as :

$$Q_{CR} = m_e \, h_\infty \qquad (6.20)$$

where

m_e - the radial mass flow rate.

h_∞ - the enthalpy at 5,500 °K isotherm.

The radial mass flow rate (m_e) may be determined from the mass conservation equation (e.g. Fang and Brannen (1979)).

$$(\partial/\partial t)\left[\int_0^R \rho_{(r)} 2\pi r dr\right] + (\partial/\partial x)\left[\int_0^R \rho_{(r)} C_{(r)} 2\pi r dr\right] - m_e = 0 \qquad (6.21)$$

The above equation (6.21) involves both a time derivative term and an axial derivative term. These terms were evaluated in a similar manner to that described above for the axial convection term (equation (6.19)) and the change in stored thermal energy (equation (6.16)). The results of these calculations are shown on Fig. (6.19) for different pressures and different di/dt. Fig. (6.19) shows that the radial convection losses are greater at the higher pressure and increase in the case as current zero is approached. However at the lower pressure this latter trend is not apparent.

6.5.7 The core power balance

The terms in the core energy conservation equation (6.14) have thus been evaluated for different pressures and different current decay rates during the current zero period. These results are summarised on table (6.4) and shown on figures (6.20 a, b, c and d).

Figure (6.20 a) shows the values calculated at two instants (10 μs and 3 μs) before current zero following a peak arc current of 34 KA (di/dt = 15 A/μs)for the high pressure case (p = 110 psig). These results show that the dominant power loss mechanisms during this period are the axial and radial convection (Q_{CA}), (Q_{CR}) with the radiation loss (Q_R) also contributing significantly. On the other hand the thermal conduction term (Q_{co}) is insignificant contributing only about 1 % of the total power loss. Furthermore the axial convection and radiation losses decrease significantly within the time period studied but the radial convection losses increase with time.

Figure (6.20 a) also shows the power input terms Q_E and Q_s . The change in stored thermal energy Q_s is greater than the electrical power input Q_E close to current zero although both are of the same order of magnitude at 10 μs before current zero. Of course at current zero itself the electrical power input must decrease significantly to zero. Fig. (6.20 a) also shows the total power input and the total power losses are equal to within 10 % at 3 μs and 2.5 % at 10 μs before current zero.

In the case of low di/dt (15 A/μs) and at 3 μs before current zero the total electrical power input as calculated from the overall arc voltage and current is 42 KW. This corresponds to an arc length of 105 mm. The corresponding total radiation loss is 0.35 KW/mm. The length of the arc from the upstream electrode to slot 2 is 25 mm. Thus since the bulk of the radiation loss occurs in this region it may be reasonable to deduce that a lower limit for the arc radiation power loss is given by the local loss per unit length at slot 2 multiplied by the upstream arc length i.e. 25x0.35 = 8.75 KW. Thus the total radiation power loss as a percentage of electrical power input is 20.8 %. This closely cortesponds to the figure of total radiation power loss as the percentage of electrical power input presented by Shammas and Jones (1982) for reduced power arcing i.e. for a low level (600 A) steady current ramped to zero at the appropriate rate. This value also agrees with the results of Lewis (1987) for full power arcing conditions.

Figure (6.20 b) shows the power terms values calculated at two instants (10 μs and 3 μs) before current zero following a peak arc current of 53 KA (di/dt = 20 A/μs) at p = 110 psig. A comparison of Figs. (6.20 a and b) shows that each of the power loss terms is greater in the case of higher current decay rate (di/dt = 20 A/μs). Fig. (6.20 b) also shows that the power loss mechanisms at 3 μs before current zero may be ordered in terms of magnitude as follows, radial convection, axial convection and radiation. Thermal conduction is again insignificant contributing only about 1 % of the total power loss. This figure shows further that the total power input (Q_E + Q_s) and the total power loss are equal to within 15 % at 3 μs and

3.5 % at 10 μs before current zero. The agreement between the total power input ($Q_E + Q_s$) with the total losses ($Q_{co} + Q_{CA} + Q_{CR} + Q_R$) at both values of di/dt is therefore good so confirming the self consistency of the calculations.

Similar results are shown on Figs. (6.20 c and d) but for the case of the lower pressure (p = 60 psig). A comparison of Figs. (6.20 a, b, c and d) shows that the power loss terms are greater in the case of the higher pressure. The exception is the radial heat conduction term which contributes about 2 % of the total power loss in the case of lower pressure. These results show that the radial heat conduction is greater in the lower pressure case since the rate of change of arc area is greater than that in the high pressure case very close to current zero. These results also show that the radial heat conduction (Q_{co}) is higher in the case of higher di/dt since the arc has a higher axis temperature and thus steep sided temperature profile at the 5,500 °K isotherm. In the case of the lower pressure the balance between the total power input and the total power loss are in the range of 3.6 % to 28 % for the different operating conditions.

It is interesting to observe radial convection results more closely since they do show different trends to the other losses. Thus at the higher pressure level (110 psig) for both di/dt investigated this loss increases as current zero is approached. All the other losses decrease so suggesting that radial convection becomes increasingly dominant. At the lower pressure of (60 psig) the trend for the radial con-

vection to increase is quite severely moderated consistent with the poorer interruption performance at this pressure.

The variation of the power loss terms in the core power balance with di/dt and different pressures at the same time before current zero (3 & 10 μs) are shown on Figs. (6.21 a and b). The solid lines show the case of higher pressure and dashed lines show the case of lower pressure. These results show that the total power loss is greater in the case of the higher pressure and also in the case of higher di/dt. These figures show that the radiation loss is greater in the higher pressure case than the lower pressure case. However in the lower pressure case and higher di/dt (at 10 μs before current zero) the radiation power loss in this region corresponds to the greatest energy removal mechanism, and the percentage of the total power input in this case is 38 %.

6.6 Chapter summary and concluding statement

The results of chapter (5) have been used to make a quantitative evaluation of many important aspects of the current zero arc column.

A method has been developed whereby the raw spectral data captured by the optical spectrum analyser (OSA 500) can be subjected to computational analysis and converted to a continuous radial temperature profile.

It is of importance that no arc splitting or prominent turbulent effects are in evidence at the localities at which the arc temperature profile is measured so that energy flow calculations may be applied radially and axially without complication and complies with the boundary layer approximations.

The shape factors (overall and core) of the integral analysis have been evaluated for the current zero period for different di/dt and P = 60 psig. They have been compared with the work of others which have used widely different operating conditions through a universal correlation parameter, the Nusselt number. The good agreement found between these results and the shape factors of other workers is an important result since it shows for the first time that the current zero arc column conditions fit the general description established with the boundary layer integral analysis.

Two criteria have been discussed from which the existence of LTE conditions in the plasma can be investigated using the values of electron density and temperature presented in chapter (5).

A further investigation has also been conducted into the optical thickness of the arc plasma. Two methods for testing and determining the optical depth have been discussed. These have been used in conjunction with the results of chapter (5) to confirm that the arc plasma near current zero is generally optically thin. This implies that no self absorption of the visible spectral lines occurs which would invalidate to the calculations of electron temperature and density.

An evaluation of each term appearing in the core energy conservation equation has been made using the experimentally measured core temperature profiles. The agreement between the total power input (Q_E + Q_s) with the total losses (Q_{co} + Q_{CA} + Q_{CR} + Q_R) at different di/dt and different pressures is good so confirming the self consistency of the calculations. These calculations have shown that the combination of axial and radial convection losses dominate the recovery of the arc plasma column even close to the instant when the fault current passes through zero. The results also show a number of important trends :

(1) The power input term due to thermally stored energy is about 70 % of the total power input in the case of the higher pressure arc and about 50 % in the case of the lower pressure arc.

(2) The power dissipated due to the release of stored energy is greater in the higher pressure case than the lower pressure case. It is also greater than the radiation loss term during the current zero period.

(3) The dominant power loss mechanisms during the current zero period are the axial and radial convection (Q_{CA}) & (Q_{CR}) with the radiation loss (Q_R) also contributing significantly.

(4) The radial heat conduction term (Q_{co}) is insignificant contributing only about 1 % of the total power loss in the case of higher pressure and about 2 % in the case of lower pressure even close to current zero.

(5) The total radiation power loss as a percentage of electrical power input is 20.8 % in the case of low di/dt and very close to current zero (3 μs before current zero).

(6) The total power input and the total power loss are equal to within 10 % at 3 μs and 2.5 % at 10 μs before current zero in the case of higher pressure.

(7) In the case of lower pressure the balance between the total power input and the total power loss are in the range from 3.6 % to 28 % for different operating conditions.

Quantity	Symbol	Characteristic value at	
		P=4 atm	P=2 atm
Electrical Conductivity	σ^*	236 ℧/m	304 ℧/m
Enthalpy	h^*	20.31×10^6 J/Kg	20.34×10^6 J/Kg
Thermal Conductivity	K^*	0.48 W/m°K	0.502 W/m°K
Specific Heat Capicity	Cp^*	1080 J/Kg°K	1100 J/Kg°K

(i) Characteristic values

Quantity	Symbol	Value at conducting core edge	
		P=4 atm	P=2 atm
Thermal Conductivity	Kc	0.346 W/m°K	0.35 W/m°K
Specific Heat Capicity	Cpc	1060 J/Kg°K	1050 J/Kg°K

(ii) Value at core edge

Table (6.1) Summary of the thermal transport properties used in this chapter

di/dt A/μs	15	16	18	19	20
Time ±C.Z μs	-9.6	-8.8	-3.0	-6.3	-9.6
θ_c mm^2	43.6	43.6	45.0	66.28	71.76
ϕ_s mm^2	14.5	14.5	17.35	20.43	21.06
$\lambda_c = \theta_c/\phi_s$	3.0	3.0	2.59	3.24	3.4
Nu	0.57	0.59	0.51	0.67	0.75
$\Lambda_c = \theta_c/\theta_\delta$	0.32	0.32	0.34	0.49	0.54

di/dt A/μs	15	16	19	20	21	23	24	25
Time ±C.Z μs	-12.8	-18.5	-8.8	-4.0	+22	+7.3	+6.6	+19
θ_c mm^2	61.3	63.0	67.35	52.7	87.0	63.19	69.3	103.6
ϕ_s mm^2	18.09	17.0	20.0	18.09	18.09	15.9	18.0	20.4
$\lambda_c = \theta_c/\phi_s$	3.38	3.7	3.36	2.9	4.8	3.97	3.85	5.07
Nu	0.66	0.69	0.74	0.68	1.03	0.63	0.66	1.02
$\Lambda_c = \theta_c/\theta_\delta$	0.46	0.46	0.50	0.39	0.65	0.47	0.52	0.77

Table (6.2) Summary of the overall conductance shape factor and the core shape factor during the current zero period (p=60 psig)

T 10^3 °K	ρ 10^{-1} Kg/m	h 10^6 J/Kg	K 10^{-1} w/m°K	ρh 10^5 J/m	σ 10^2 ʊ/m	c 10^2 m/s
4	2.593	16.81	2.977	43.58	0.007	14.69
5	2.039	18.17	2.785	37.04	0.355	17.85
6	1.696	19.23	3.462	32.6	2.36	19.71
7	1.451	20.31	4.8	29.35	6.5	20.97
8	1.266	21.52	6.72	27.24	12.32	21.84
9	1.117	22.99	9.51	25.67	19.2	22.56
10	0.991	24.88	13.21	24.65	26.56	23.40
11	0.883	27.27	16.31	24.08	33.97	24.49

P = 4 atm

T 10^3 °K	ρ 10^{-1} Kg/m	h. 10^6 J/Kg	K 10^{-1} w/m°K	ρh 10^5 J/m	σ 10^2 ʊ/m	c 10^2 m/s
4	1.286	16.98	2.654	21.84	0.016	15.02
5	1.018	18.19	2.74	18.5	0.569	17.97
6	0.847	19.24	3.523	16.3	3.046	19.69
7	0.725	20.34	5.02	14.75	7.59	20.81
8	0.632	21.62	7.2	13.66	13.65	21.58
9	0.556	23.26	10.62	12.93	20.58	22.3
10	0.491	25.44	13.95	12.49	27.58	23.25
11	0.435	28.17	16.58	12.25	34.48	24.49

P = 2 atm

table (6.3) The thermal transport properties

(Reference Frost & Liebermann (1971)).

Power input terms	Power loss terms
$Qe = 4.0 \times 10^5$ w/m	$Qr = 3.5 \times 10^5$ w/m
$Qs = 1.1 \times 10^6$ w/m	$Qco = 1.0 \times 10^4$ w/m
	$Qca = 6.0 \times 10^5$ w/m
	$Qcr = 7.0 \times 10^5$ w/m

(1) di/dt = 15 A/μs t = - 3 μs before C.Z.

Power input terms	Power loss terms
$Qe = 4.6 \times 10^5$ w/m	$Qr = 5.0 \times 10^5$ w/m
$Qs = 1.4 \times 10^6$ w/m	$Qco = 1.75 \times 10^4$ w/m
	$Qca = 8.0 \times 10^5$ w/m
	$Qcr = 9.3 \times 10^5$ w/m

(2) di/dt = 20 A/μs t = - 3 μs before C.Z.

Power input terms	Power loss terms
$Qe = 1.2 \times 10^6$ w/m	$Qr = 6.8 \times 10^5$ w/m
$Qs = 1.6 \times 10^6$ w/m	$Qco = 2.3 \times 10^4$ w/m
	$Qca = 1.4 \times 10^6$ w/m
	$Qcr = 5.9 \times 10^5$ w/m

(3) di/dt = 15 A/μs t = - 10 μs before C.Z.

Power input terms	Power loss terms
$Qe = 1.4 \times 10^6$ w/m	$Qr = 1.2 \times 10^6$ w/m
$Qs = 2.4 \times 10^6$ w/m	$Qco = 4.6 \times 10^4$ w/m
	$Qca = 1.8 \times 10^6$ w/m
	$Qcr = 6.2 \times 10^5$ w/m

(4) di/dt = 20 A/μs t = - 10 μs before C.Z.

Table (6.4) Summary of the power terms in the current zero energy balance for different operating conditions

(a) p = 110 psig.

Qe = Electrical power input

Qs = Change in thermally stored energy

Q_r = Radiation power loss

Qco = Radial conduction loss

Qca = Axial heat convection

Qcr = Radial heat convection

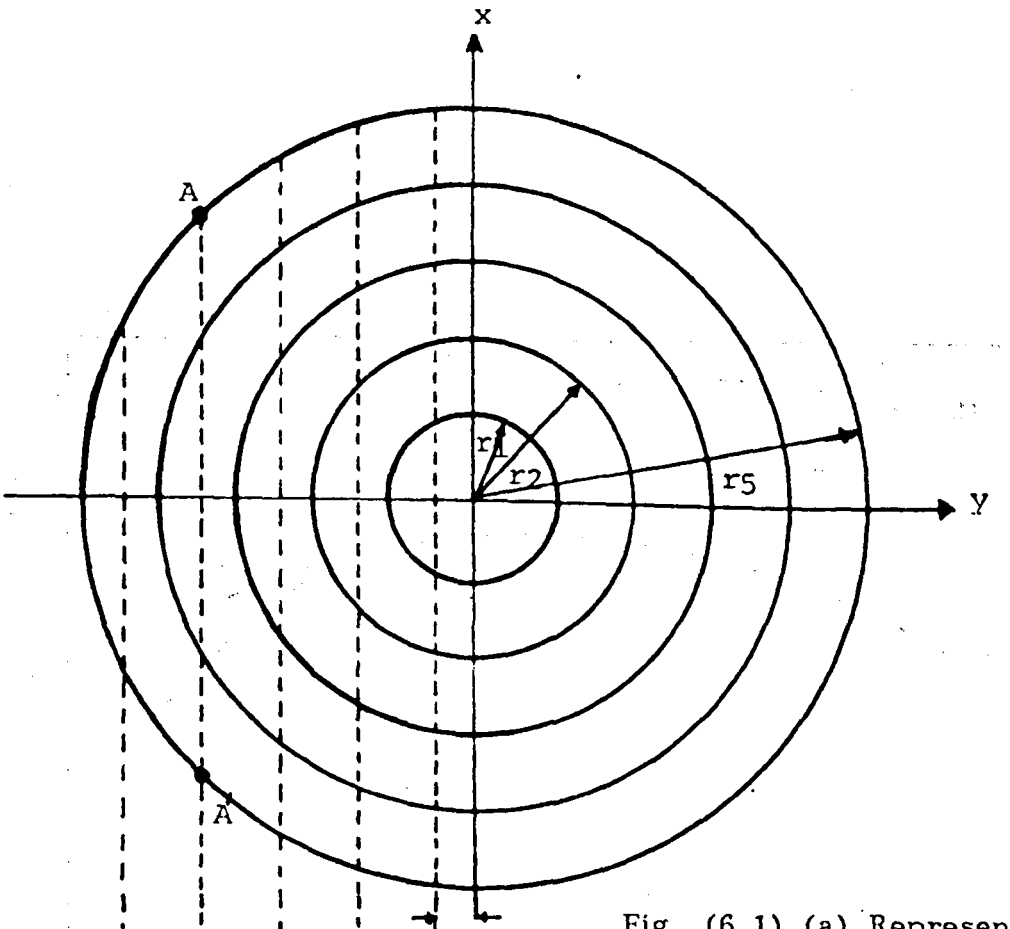

Fig. (6.1) (a) Representation of the cross-section of the plasma

$r_1/2$

r_1

Operating conditions
time before current zero = 5.2 μs
di/dt = 18 A/μs

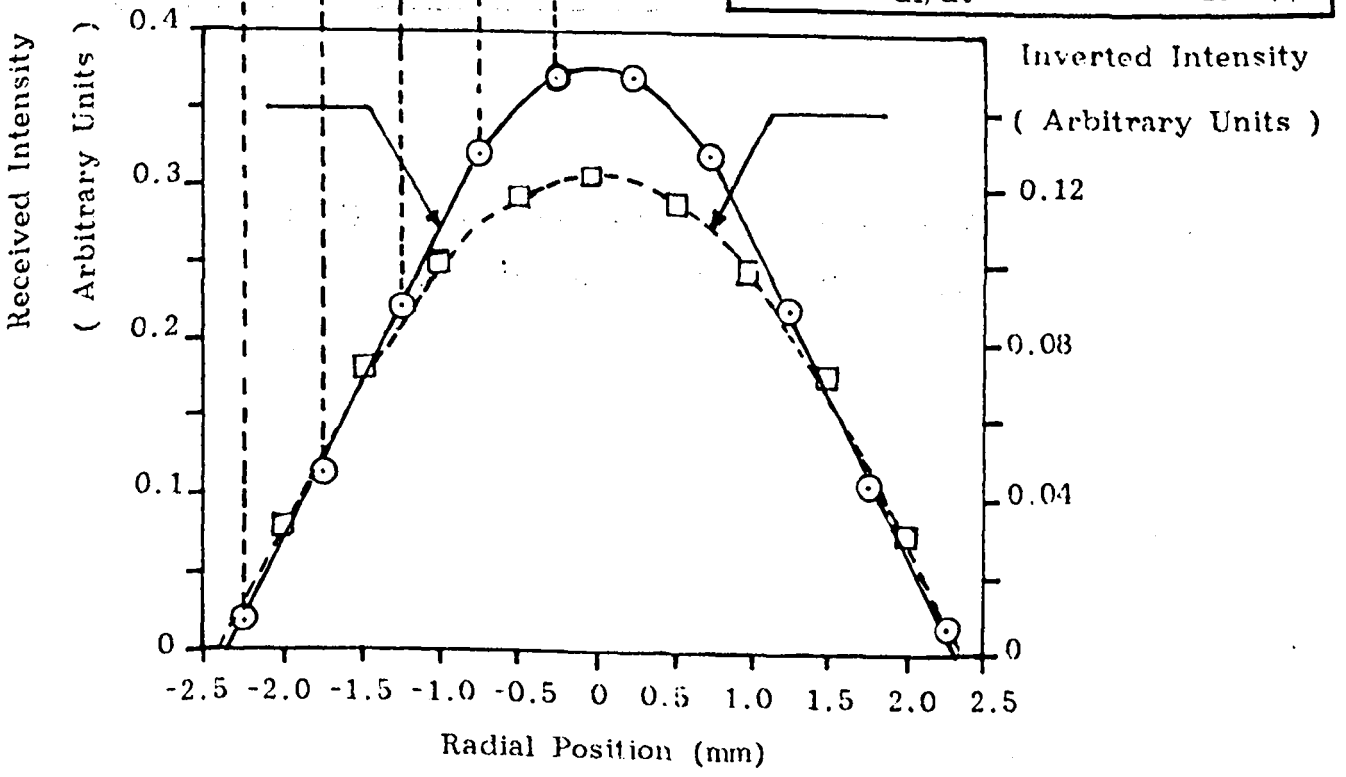

□ represents theoretical parabola $i_{(r)}=0.12(1-r^2/(2.35)^2)$

Fig. (6.1) (b) Measured and Abel inverted intensity profiles

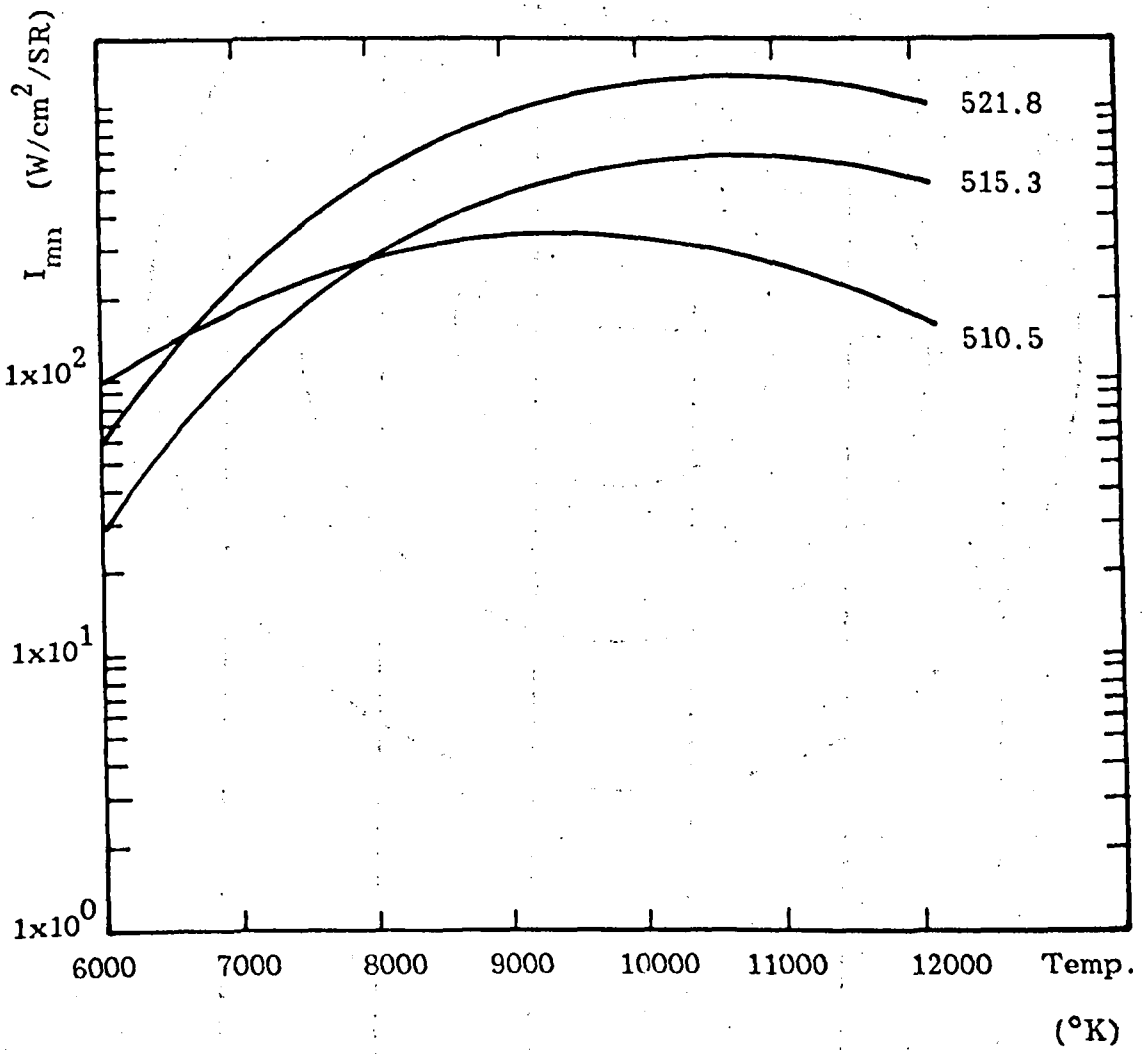

Fig. (6.2) The theoretical intensity variation of the principal diagnostic spectral lines with temperature

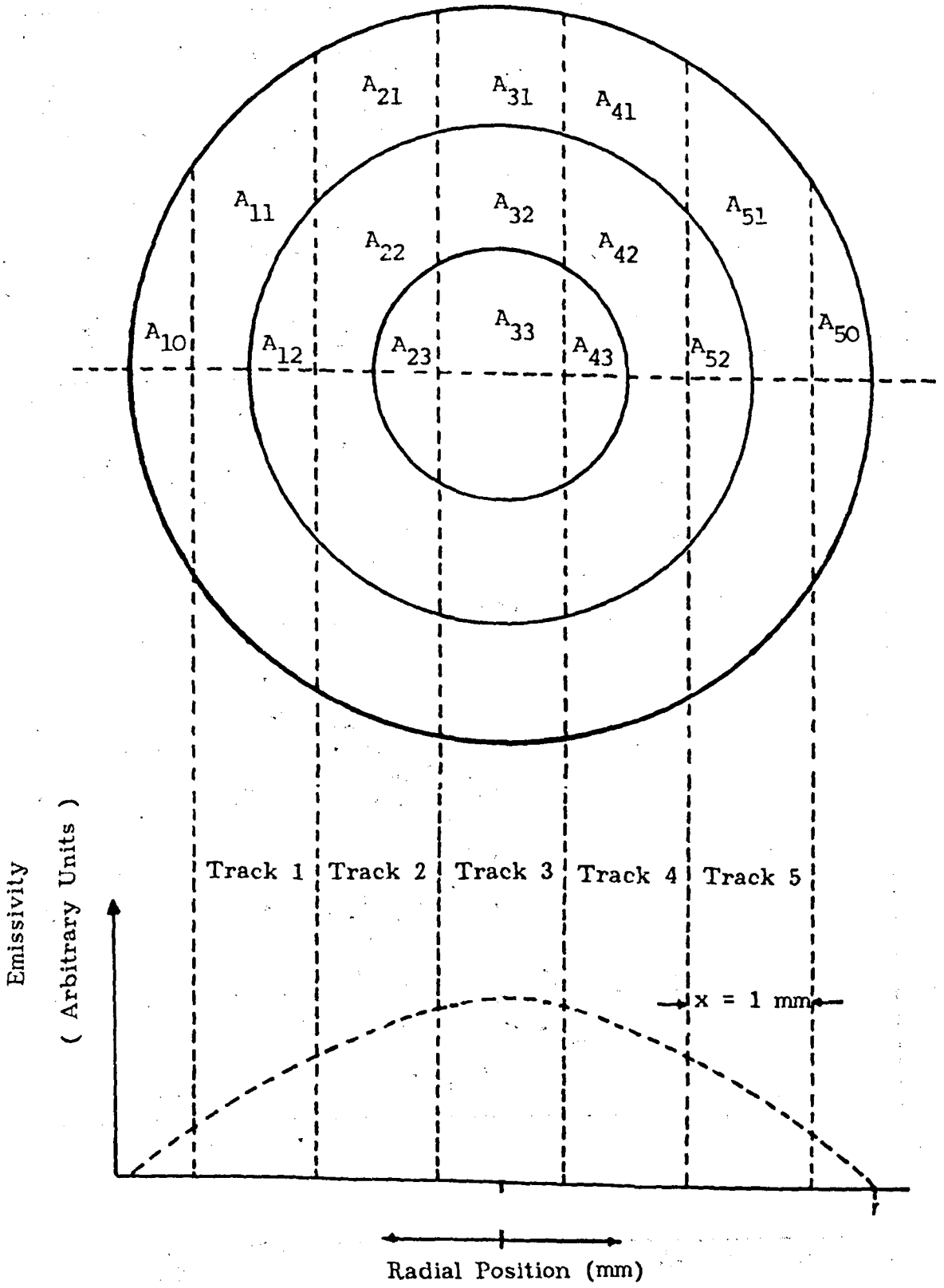

Fig. (6.3) Conversion of the emissivity profile into a radial intensity histograms

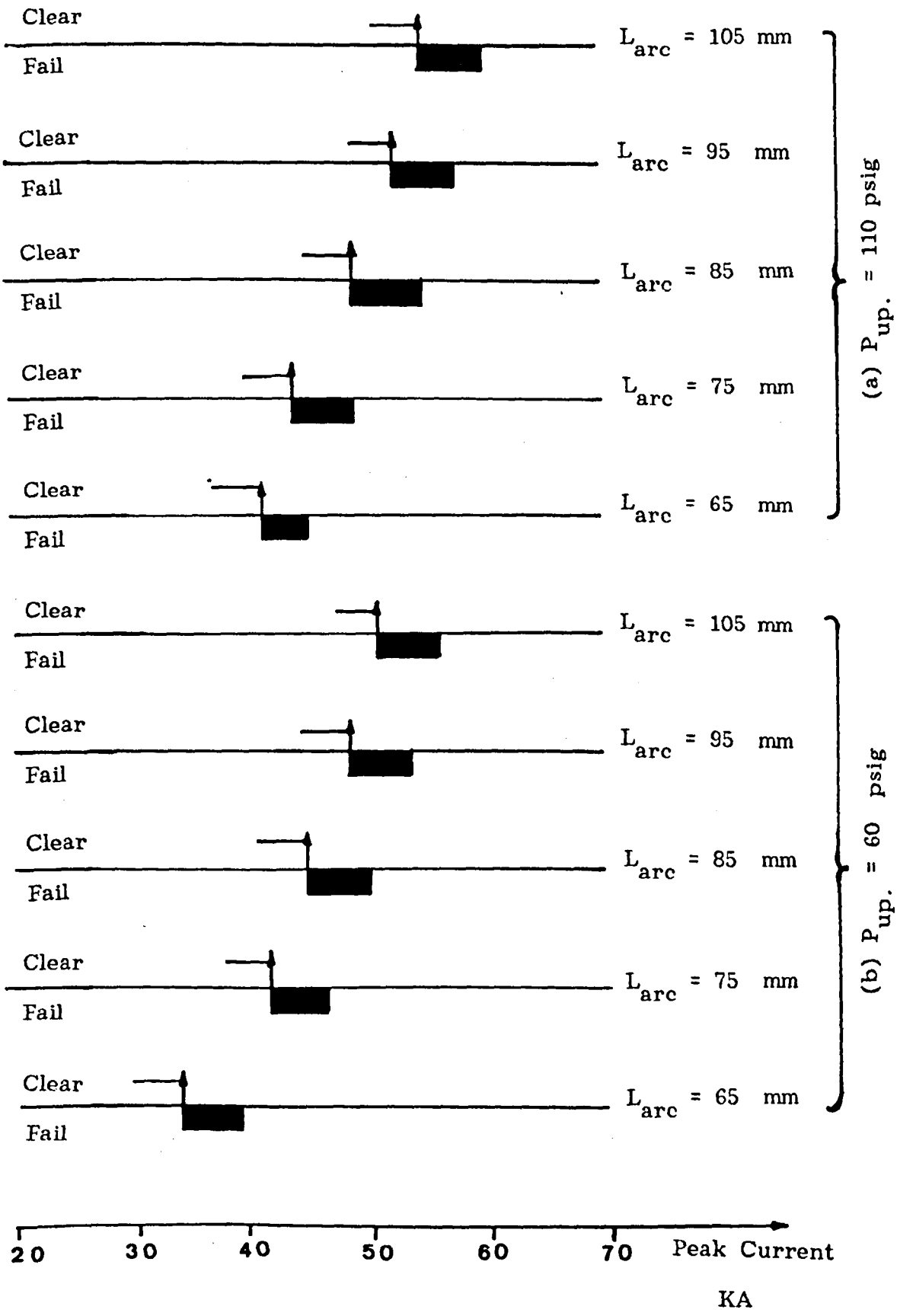

Fig. (6.4) Approximate performance trends, various upstream pressures and various gap between the two electrodes

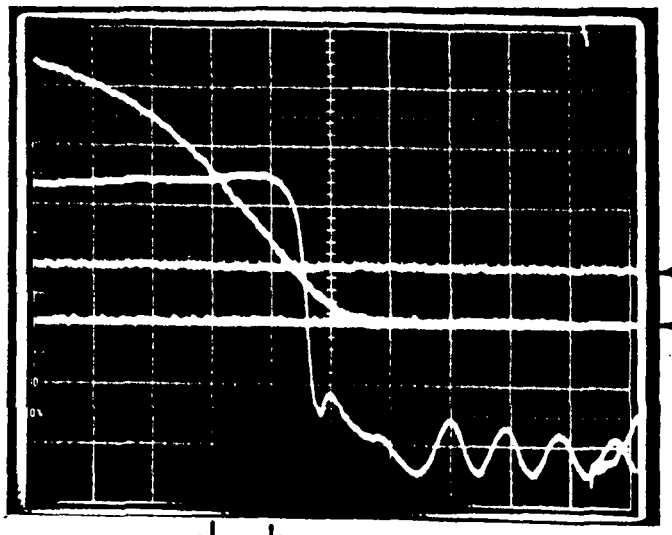

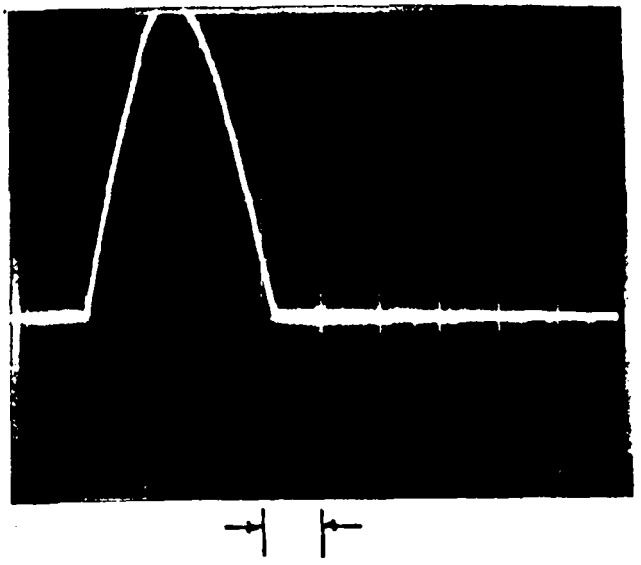

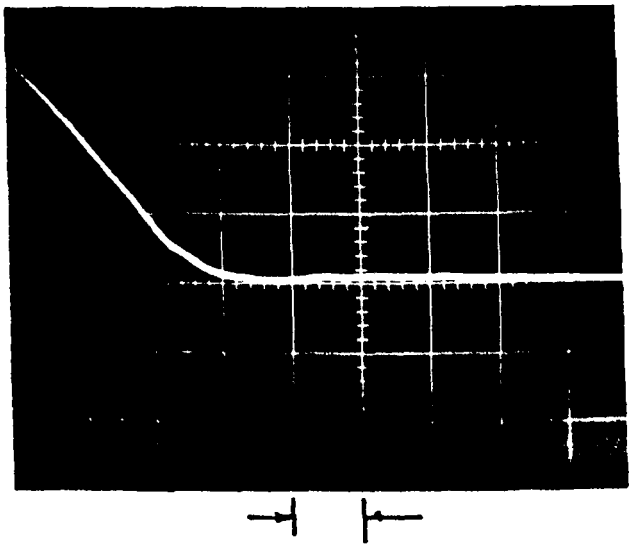

Operating conditions

Exposure time = 1.6 μs Pressure = 110 psig

di/dt = 22 A/μs I_p = 53 KA

(a) P = 110 psig & L_{gap} = 105 mm

Fig. (6.5) Typical records of the time variation of current and voltage with different pressures and different arc lengths

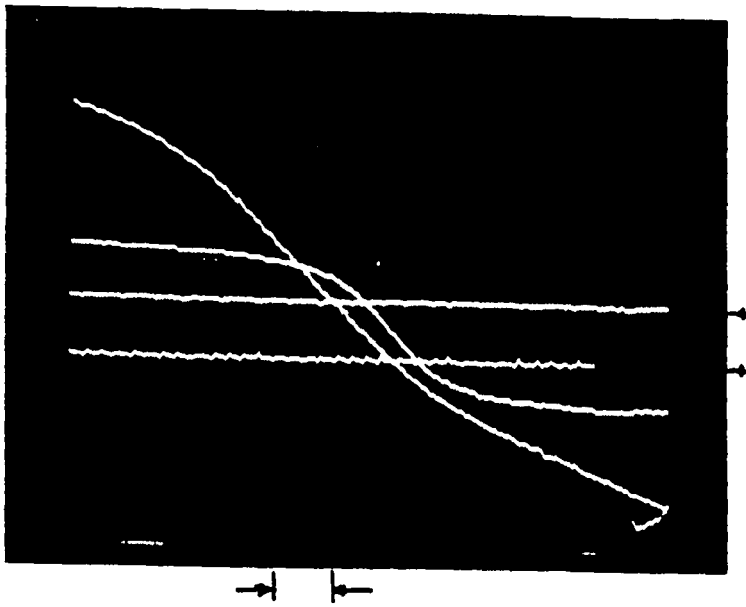

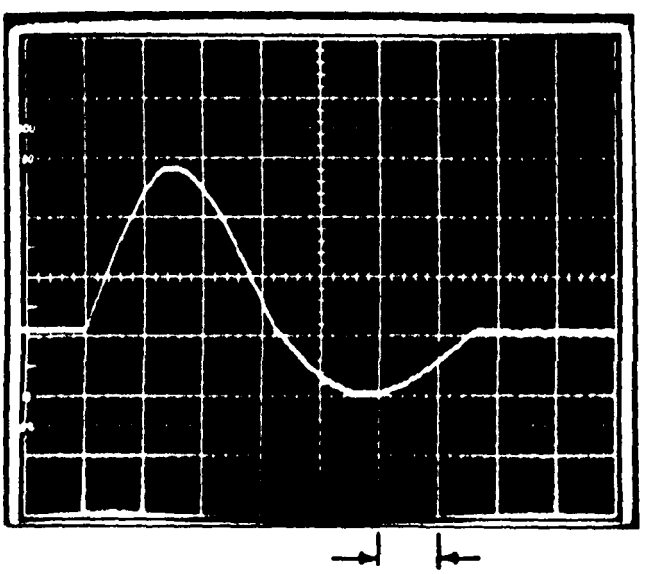

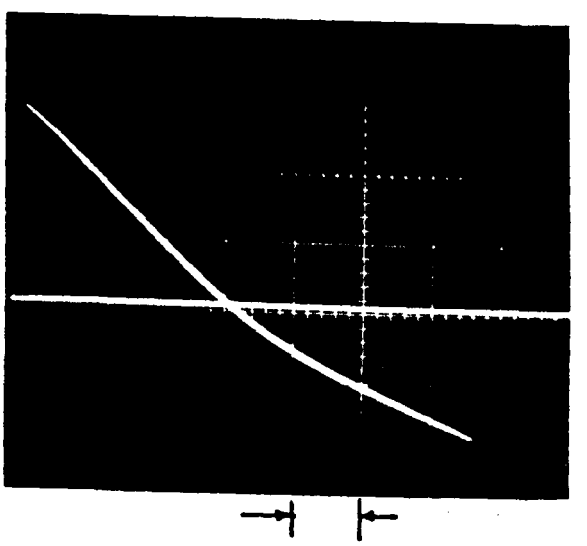

Operating conditions

Exposure time = 1.6 μs Pressure = 60 psig

di/dt = 21 A/μs I_p = 51 KA

Fig. (6.5) (b) P = 60 psig & L_{gap} = 105 mm

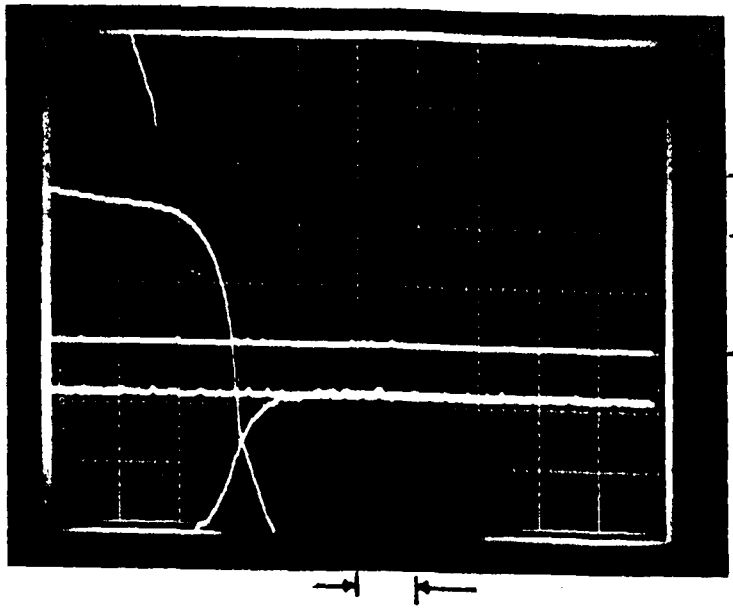

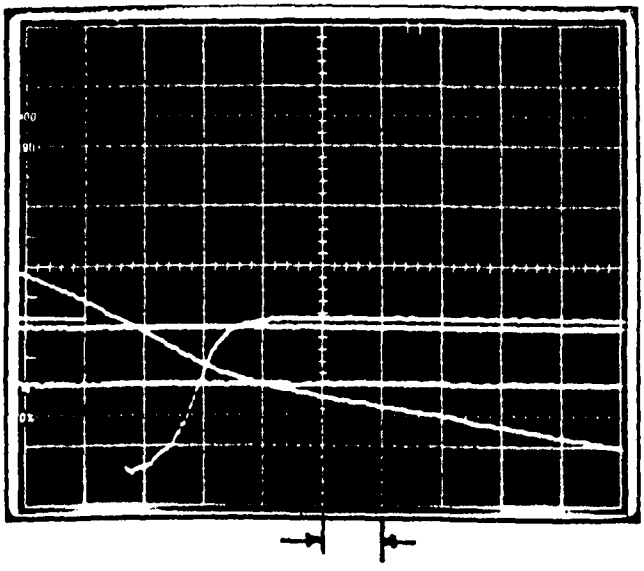

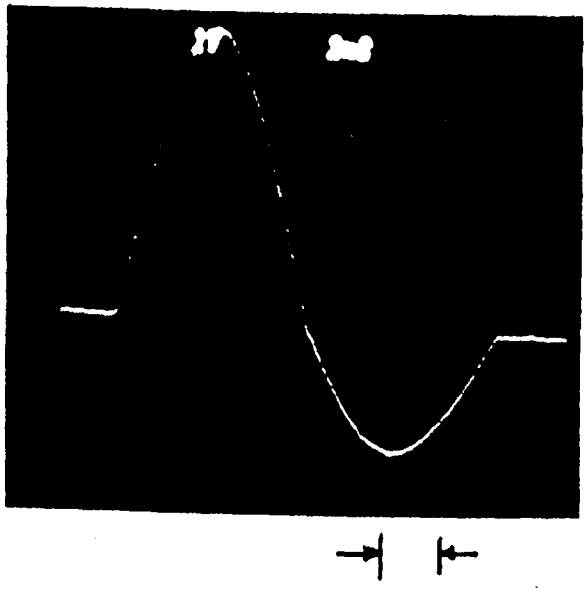

Operating conditions

Exposure time = 1.6 μs Pressure = 110 psig

di/dt =19.5 A/μs I_p = 47 KA

Fig. (6.5) (c) P = 110 psig & L_{gap} = 65 mm

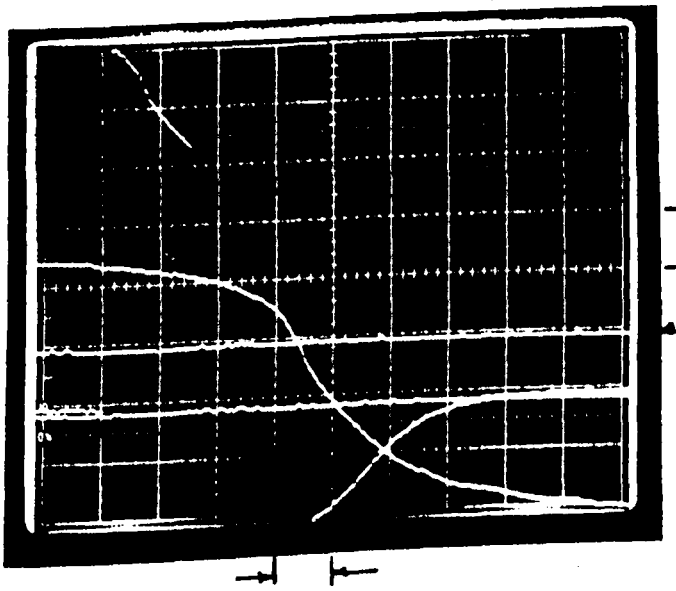

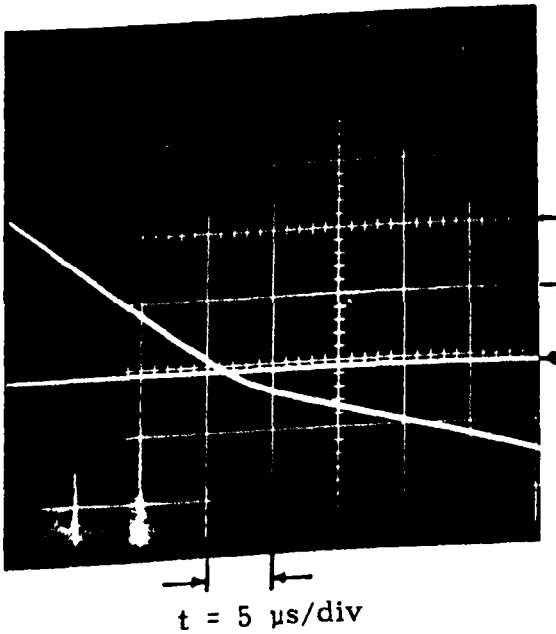

Operating conditions

Exposure time = 1.6 μs Pressure = 60 psig

di/dt = 15 A/μs I_p = 36 KA

Fig. (6.5) (d) P = 60 psig & L_{gap} = 65 mm

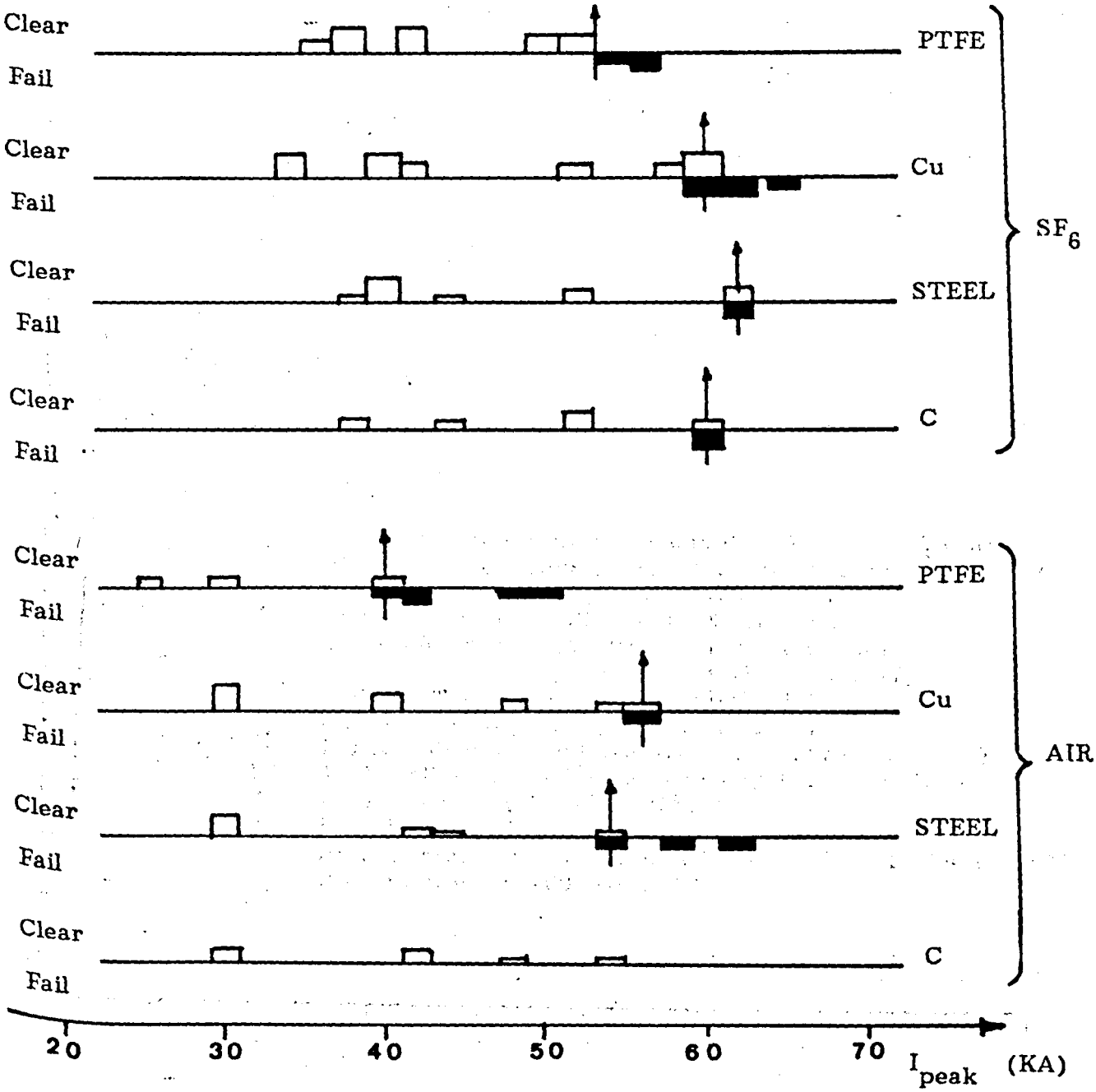

Fig. (6.6) Approximate performance trends, 35 mm throat nozzle, various nozzle materials, SF_6 and air, f = 78 Hz.

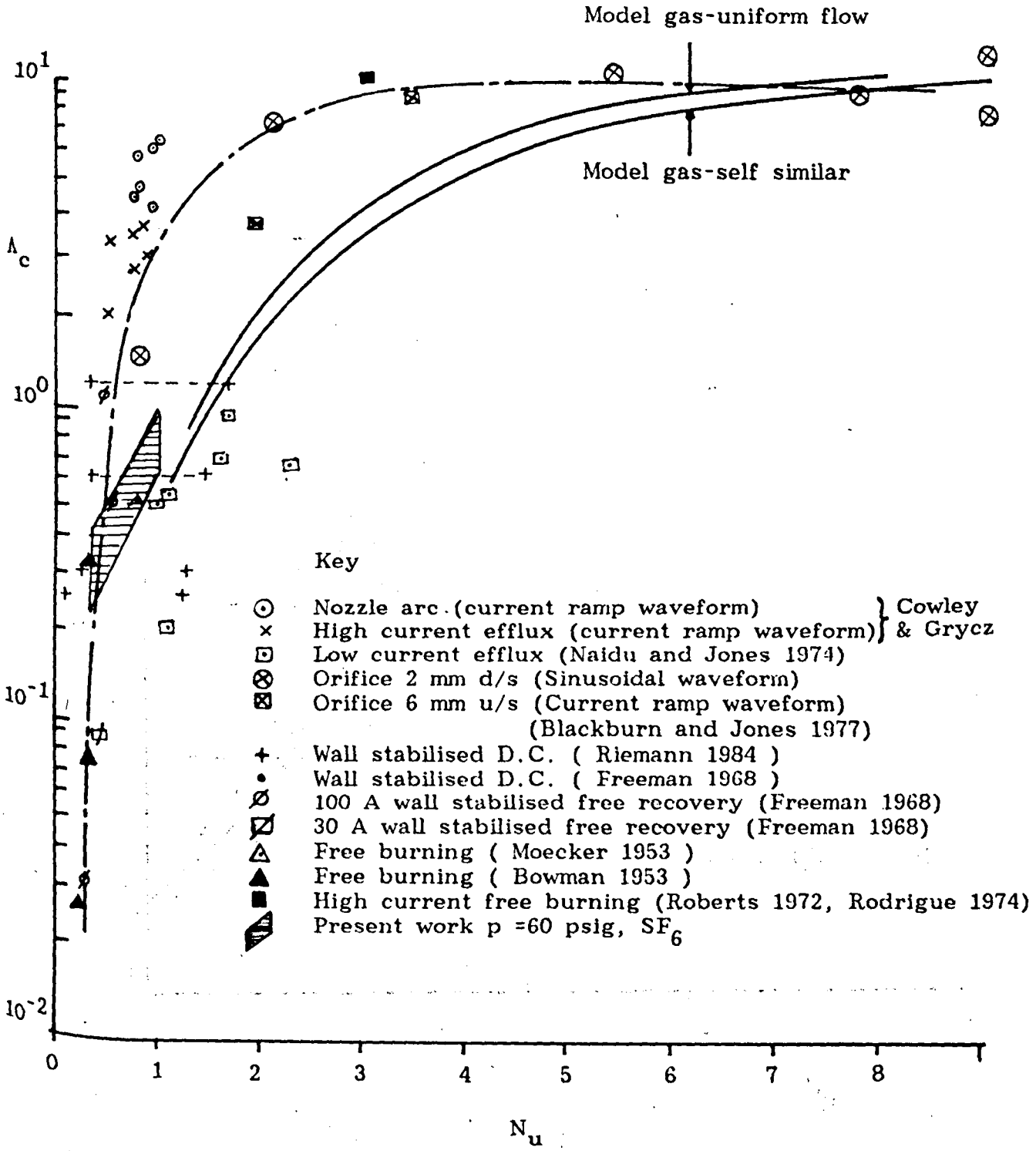

Fig. (6.7) Overall conductance shape factor (Λ_c) as a function of Nusselt number (N_u) for different arc types

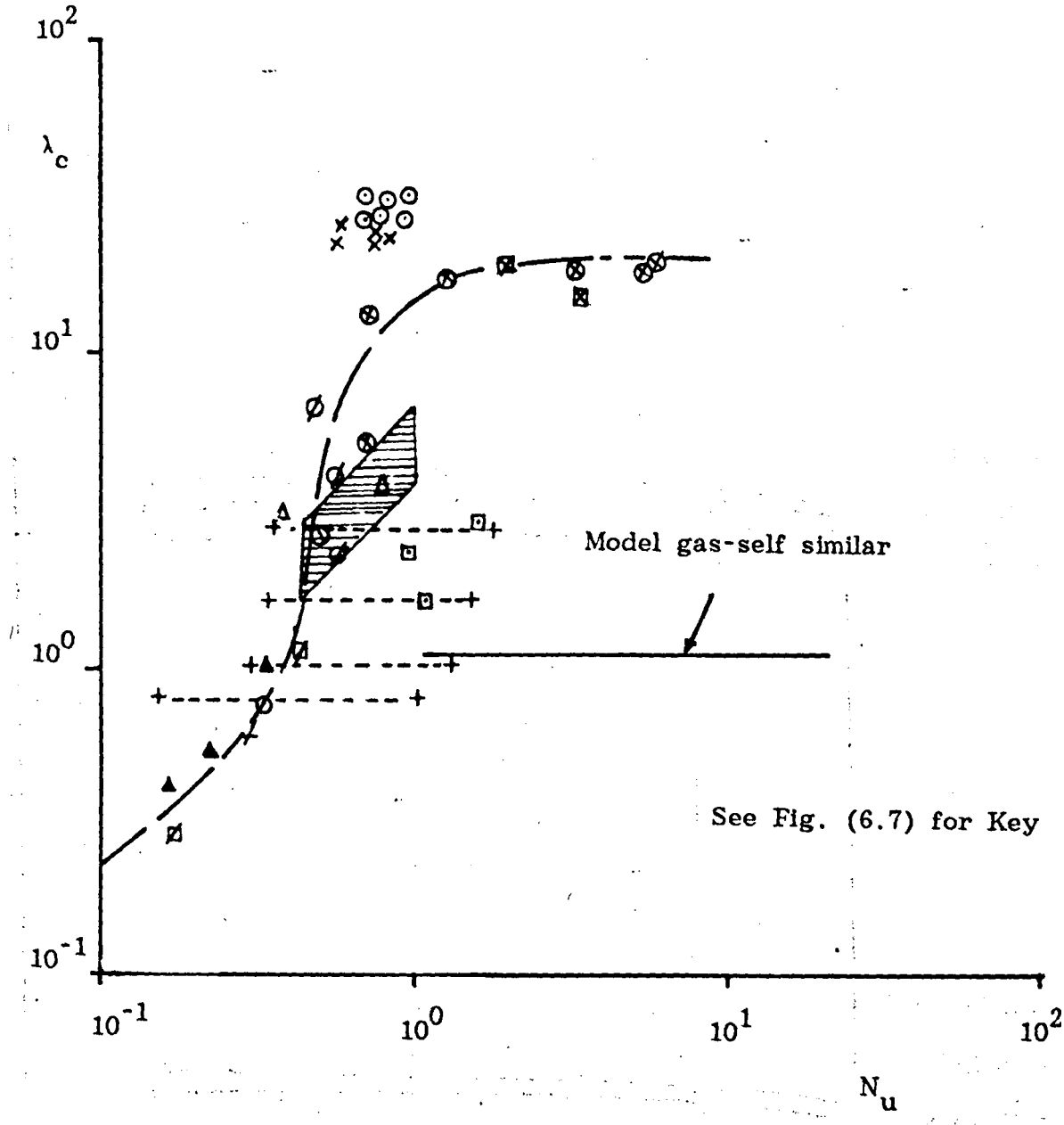

Fig. (6.8) Core conductance shape factor (λ_c) as a function of Nusselt number (N_u) for different arc types

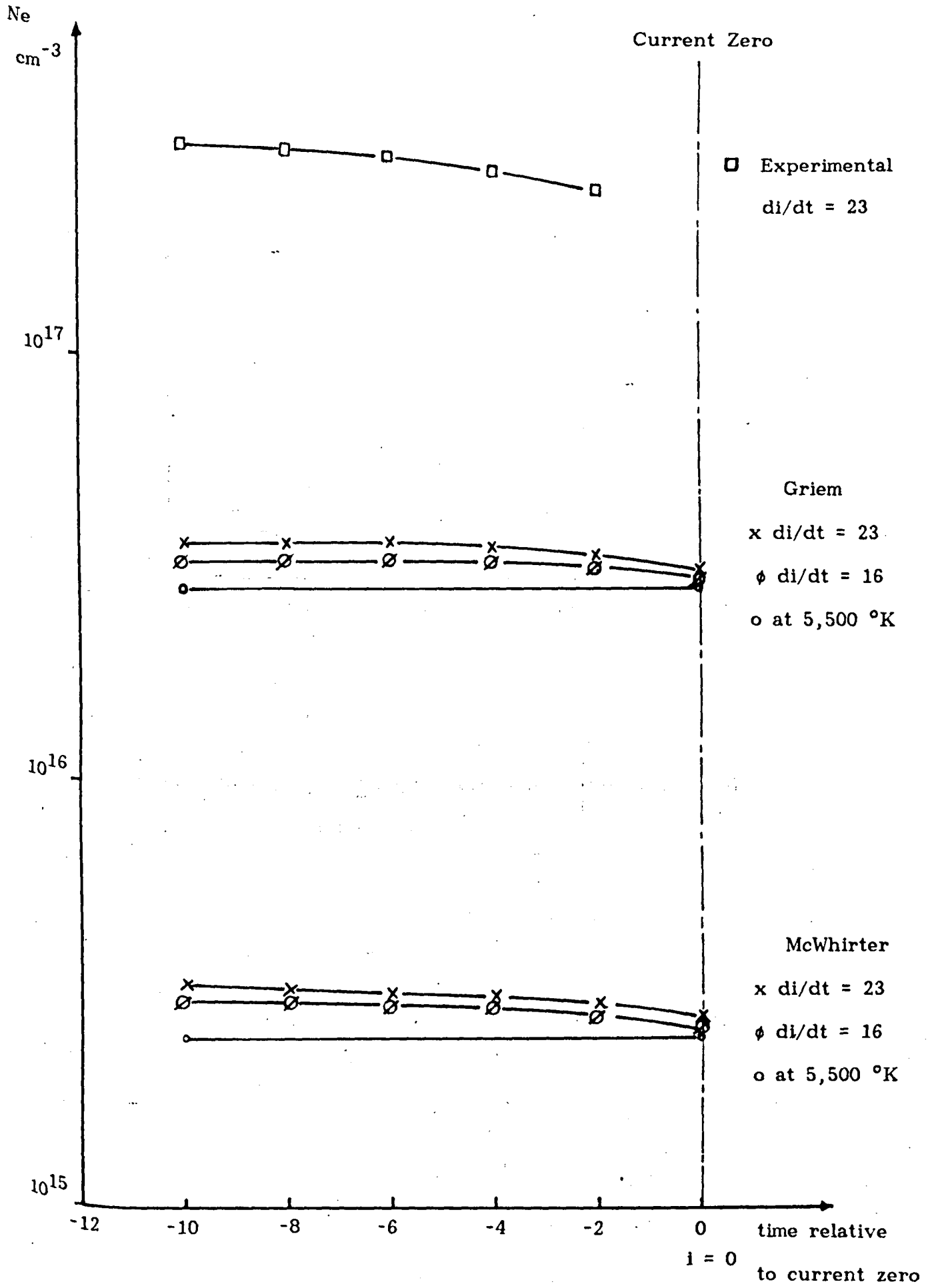

Fig. (6.9) Justification of existance of L.T.E.

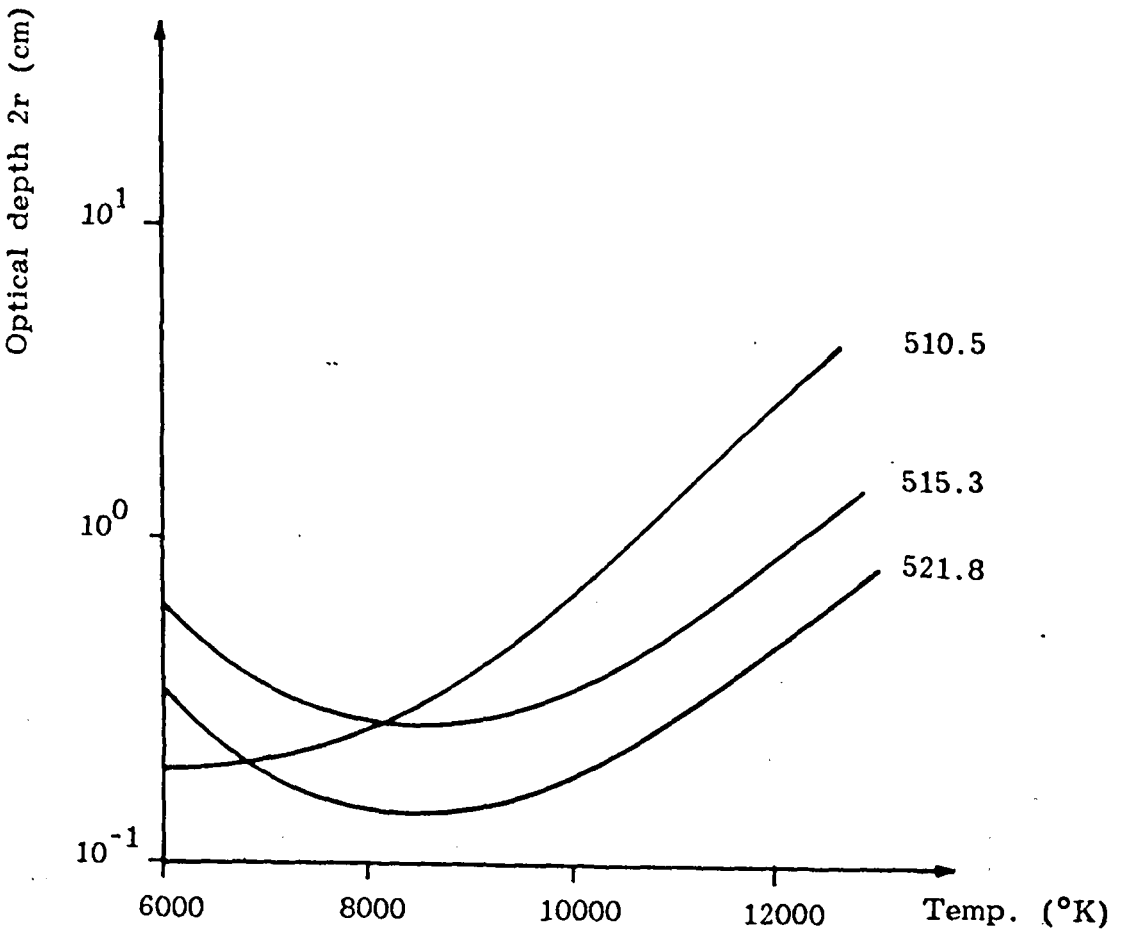

Fig. (6.10) Optical depth versus temperature for CuI diagnostic lines.

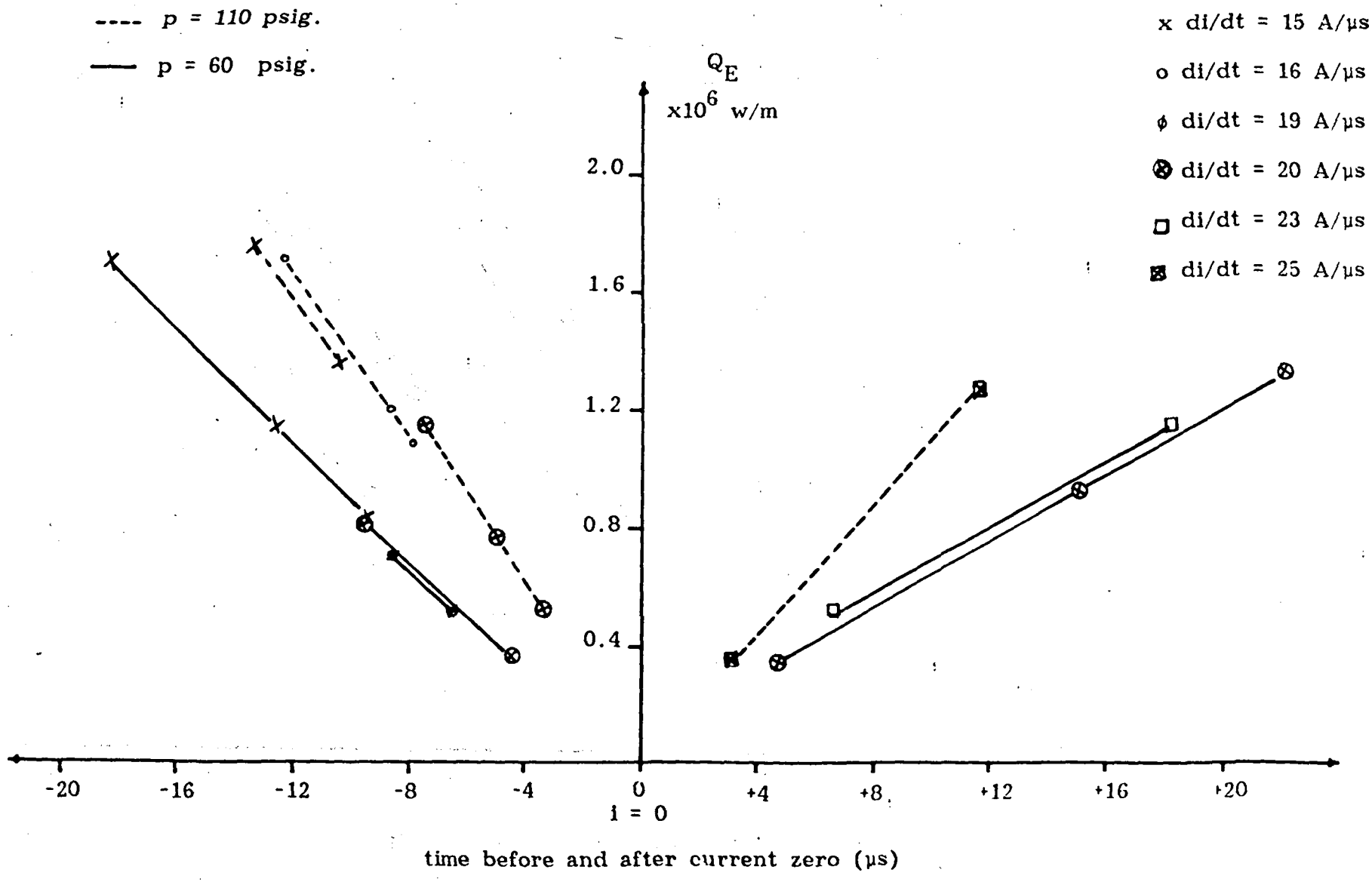

Fig. (6.11) Electrical power input v time before and after current zero

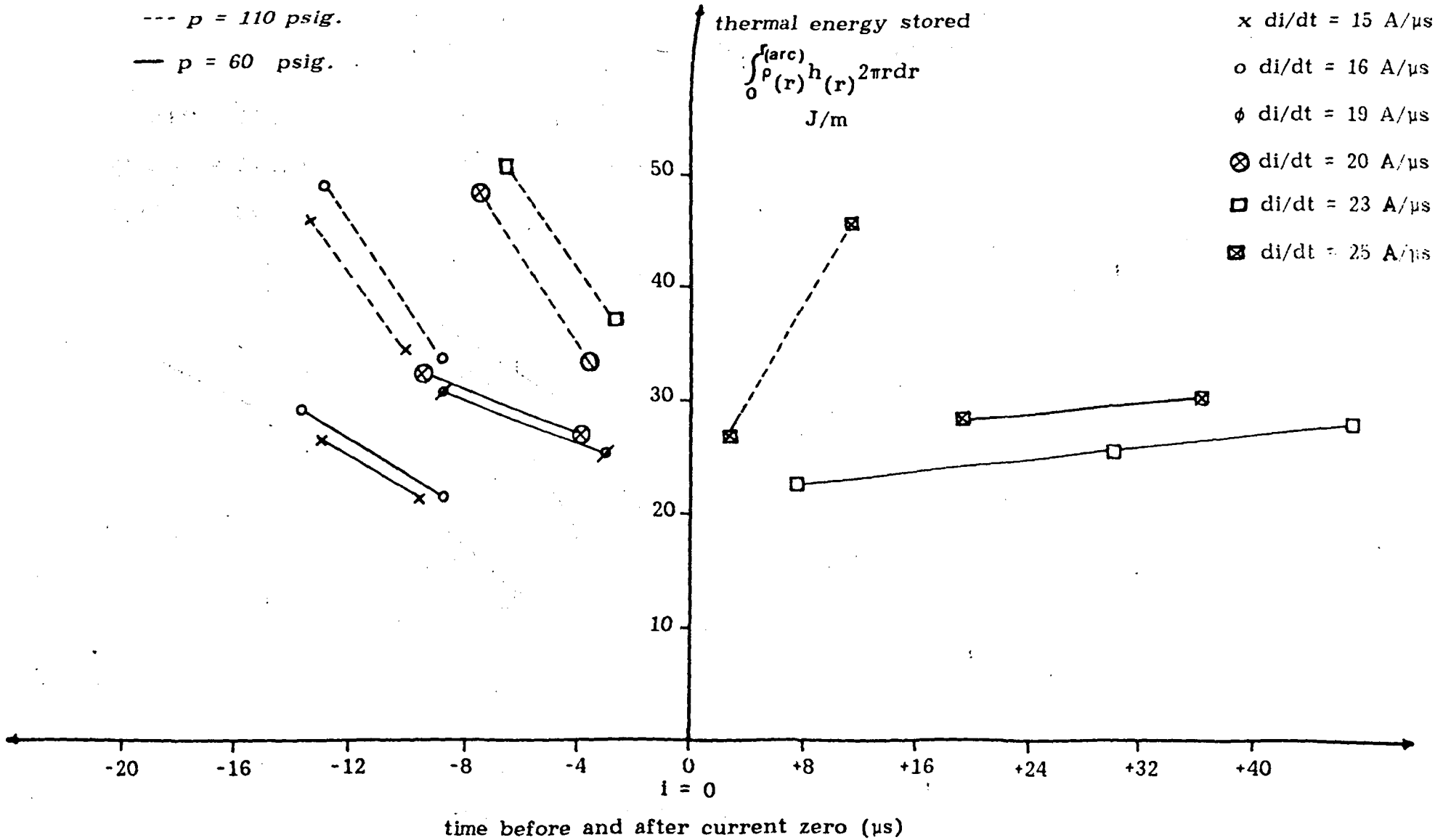

Fig. (6.12) Thermal energy stored v the time before & after current zero

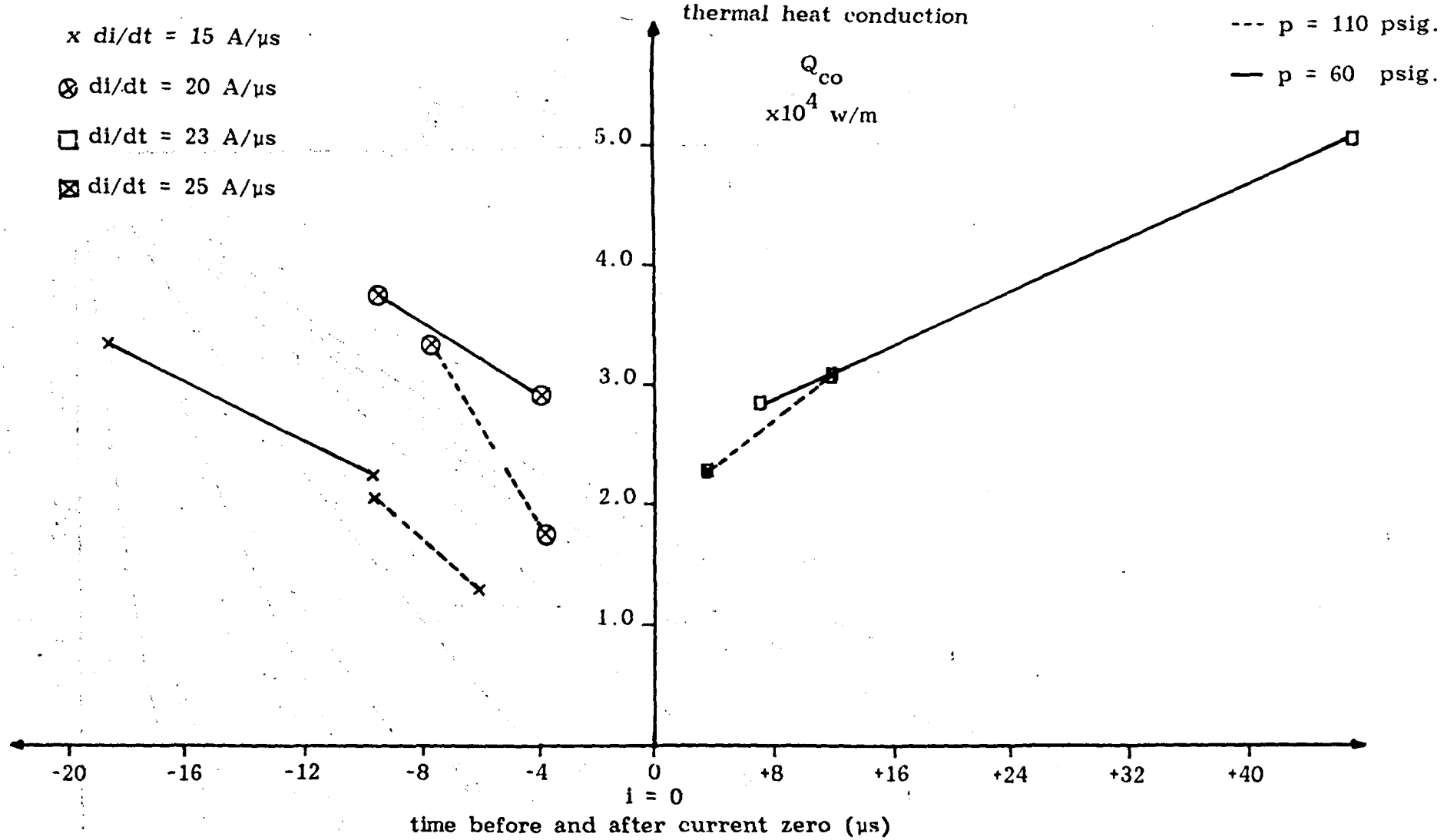

Fig. (6.13) Thermal heat conduction loss v time before and after current zero

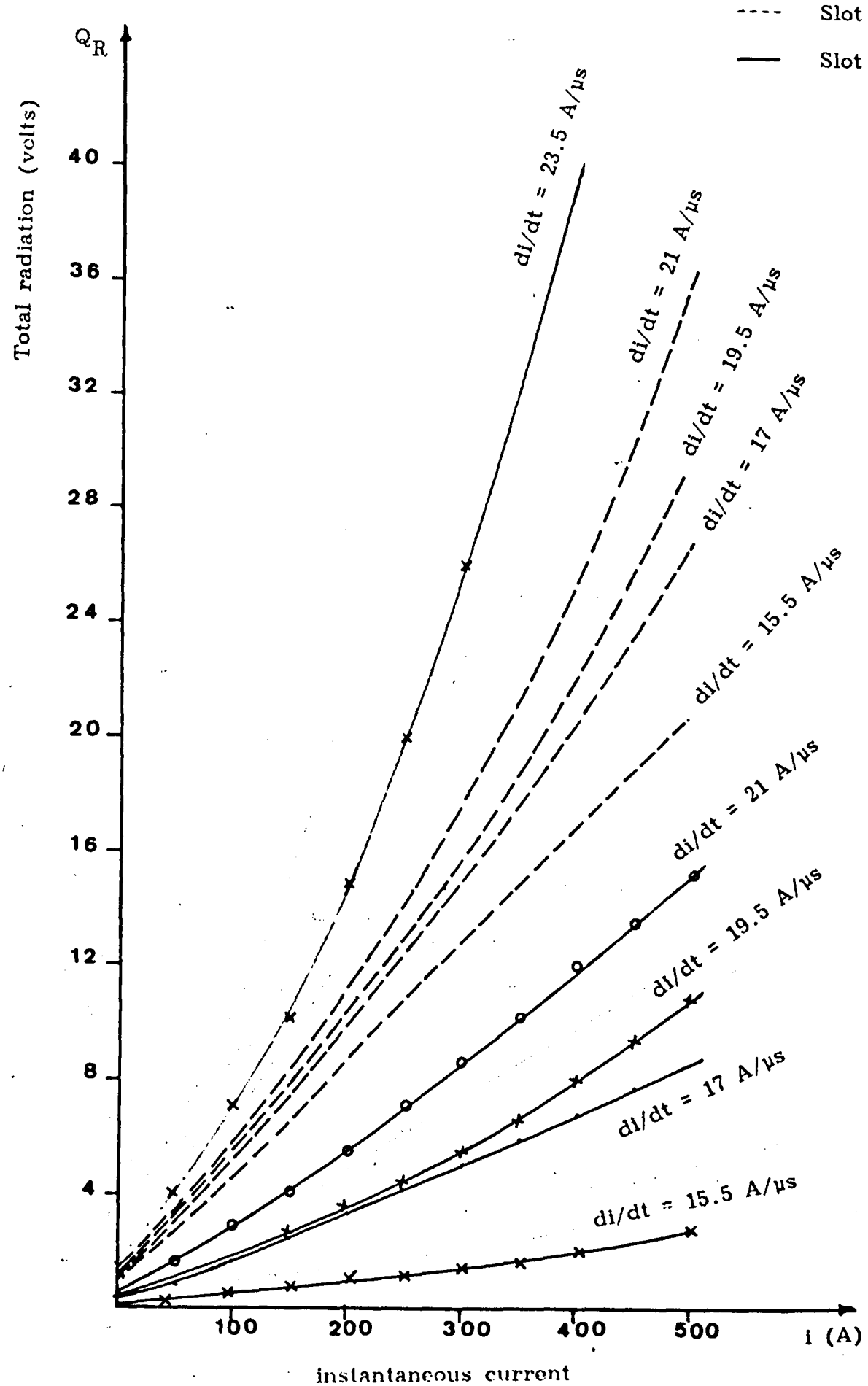

Fig. (6.14) Total radiation v instantaneous current

P=110 psig, Slot 2 & slot 3

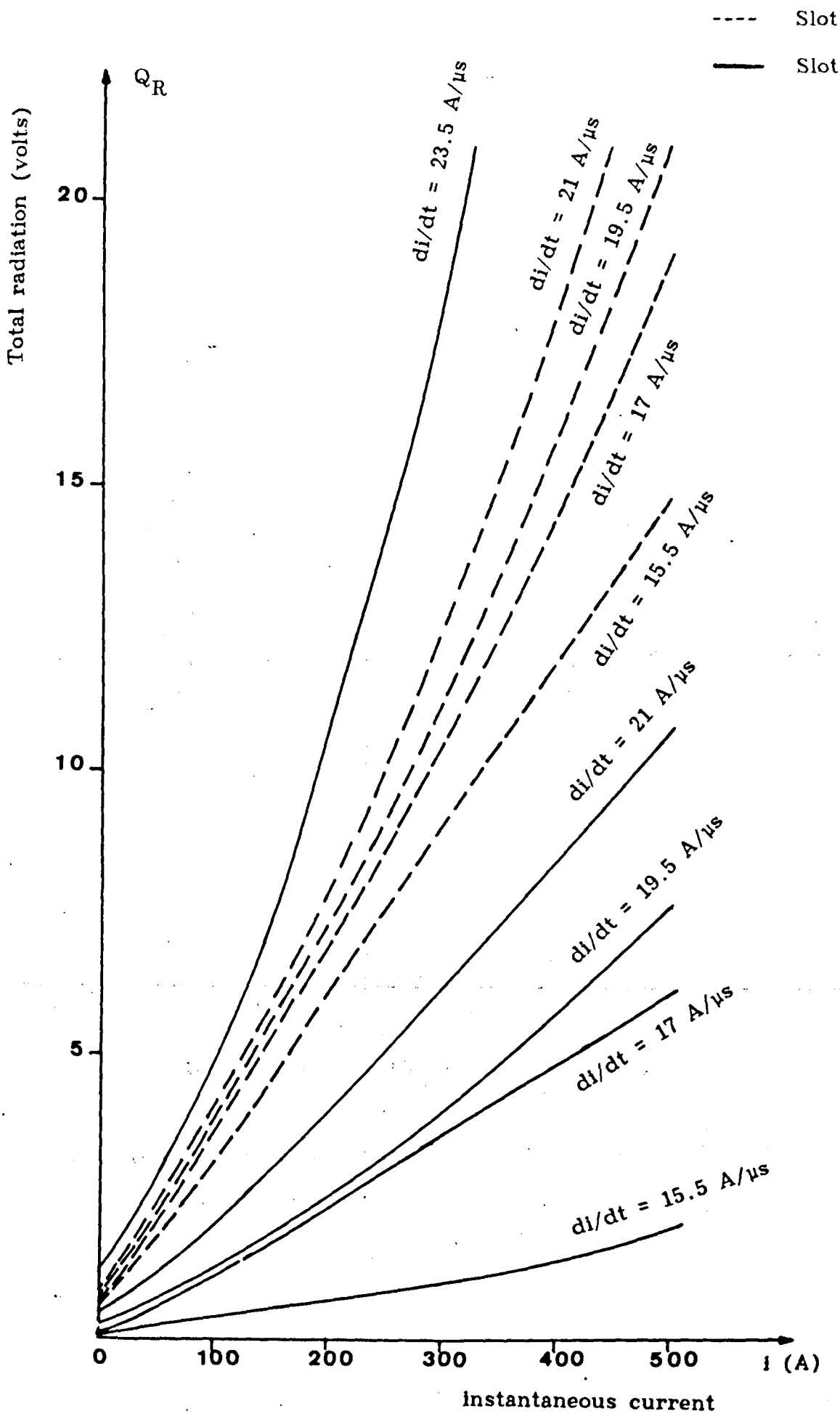

Fig. (6.15) Total radiation v instantaneous current

P = 60 psig, Slot 2 & slot 3

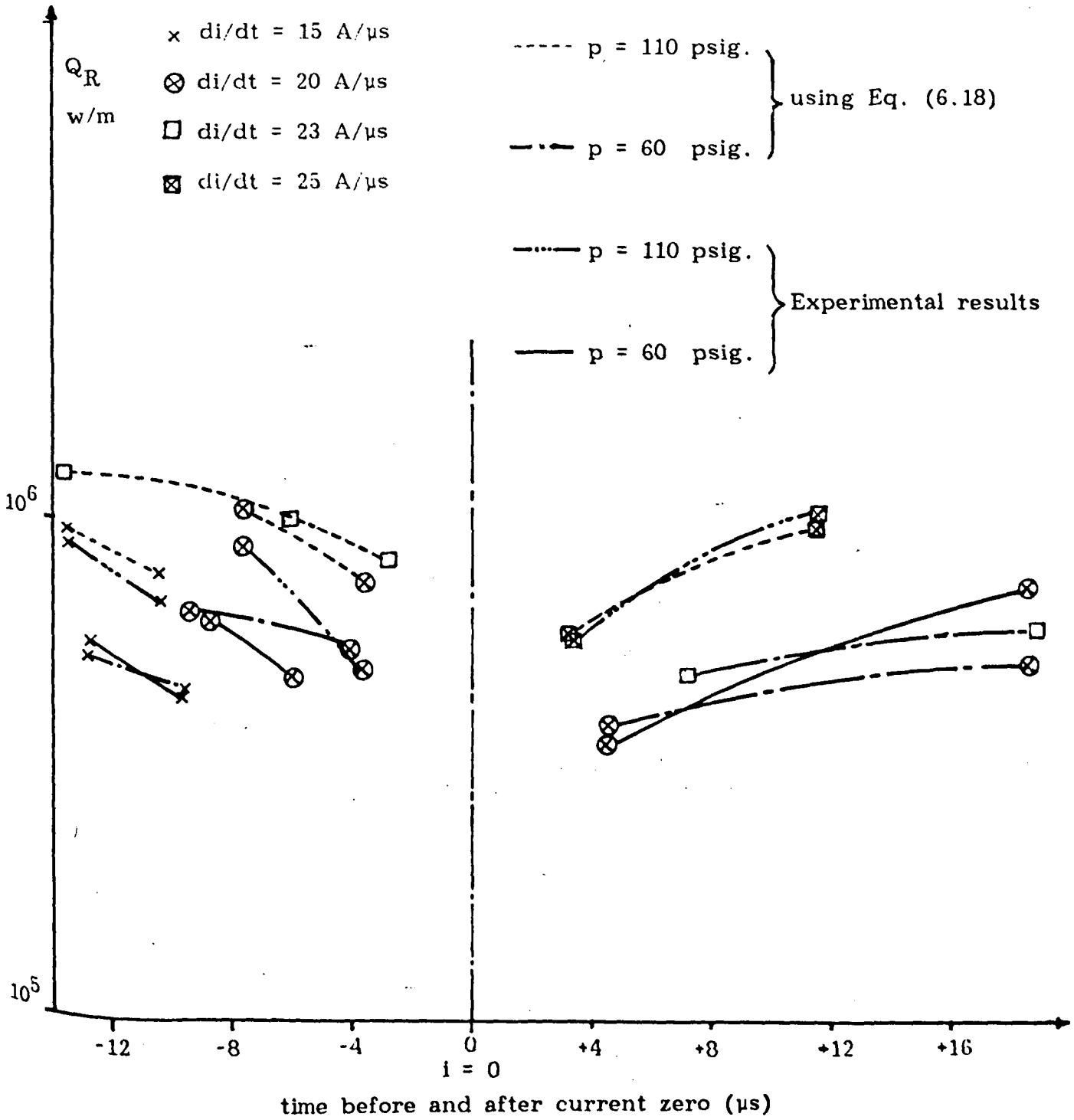

Fig. (6.16) The total radiation loss v time before and after current zero

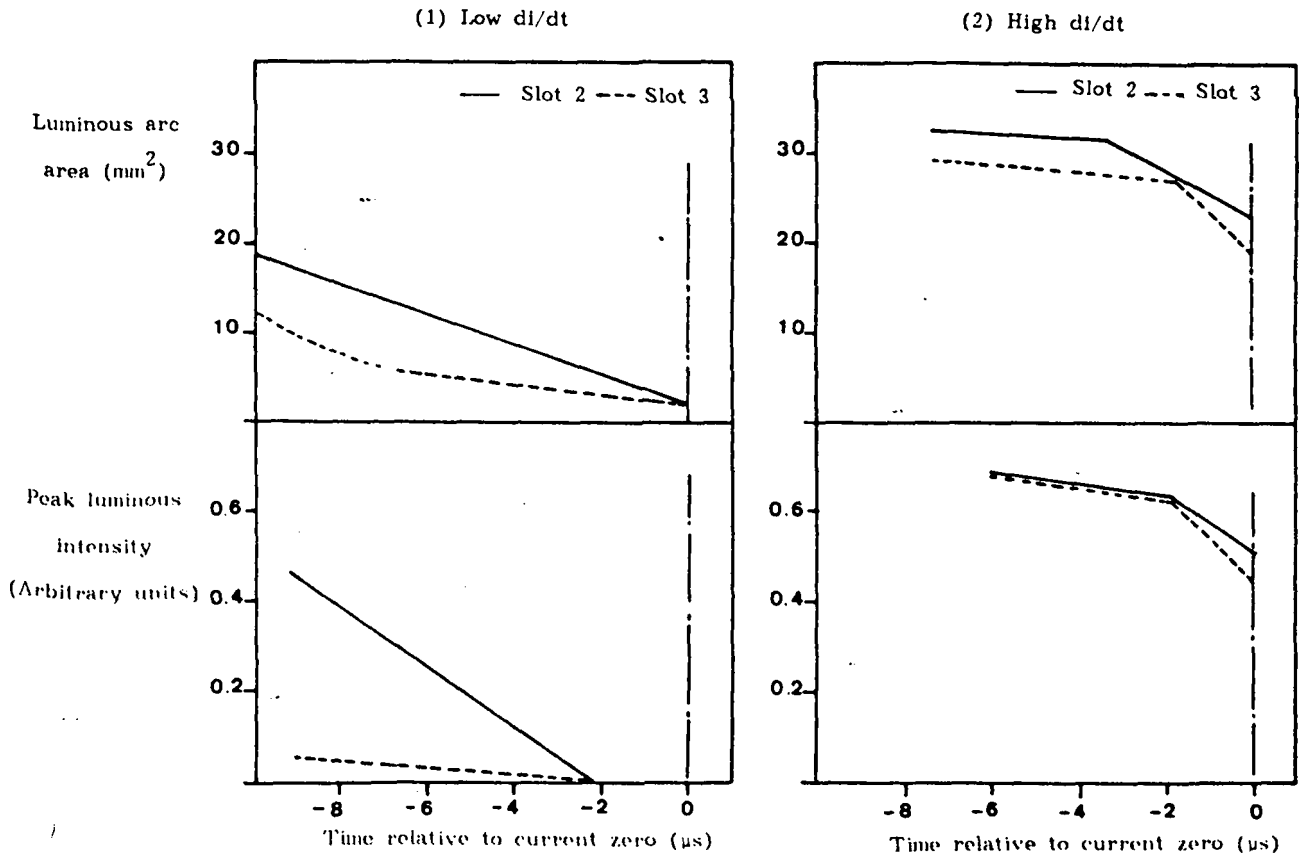

Fig. (6.17) Summary of temporal arc area and intensity decay during the current zero period (source Lewis (1987)).

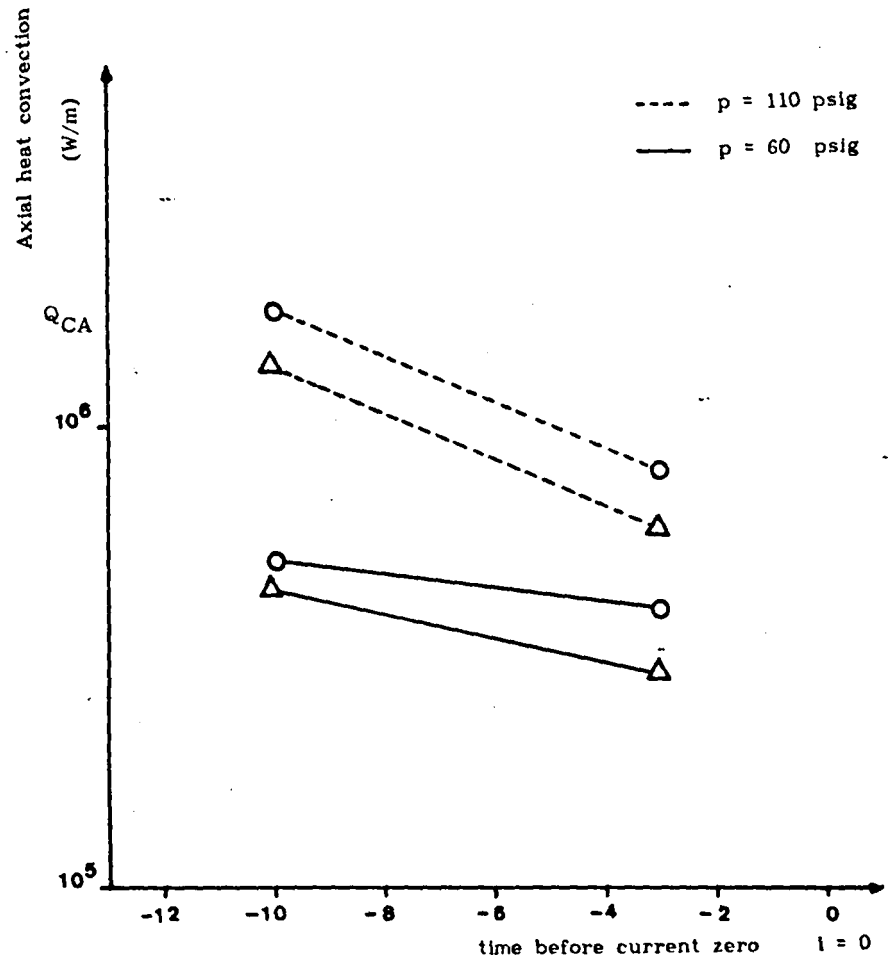

Fig. (6.18) The axial heat convection loss vs. time before current zero at different pressures and different di/dt.

Δ di/dt = 15 A/μs

O di/dt = 20 A/μs

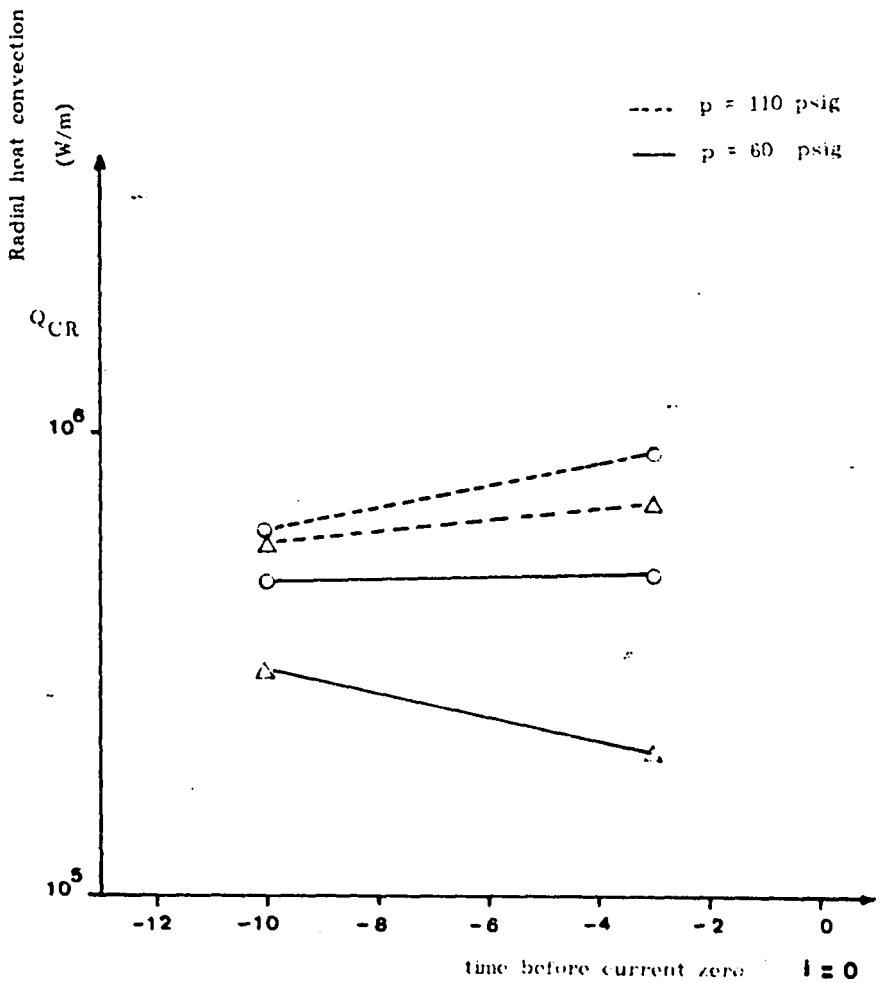

Fig. (6.19) The radial heat convection loss vs. time before current zero at different pressures and different di/dt.

△ di/dt = 15 A μs

○ di/dt = 20 A μs

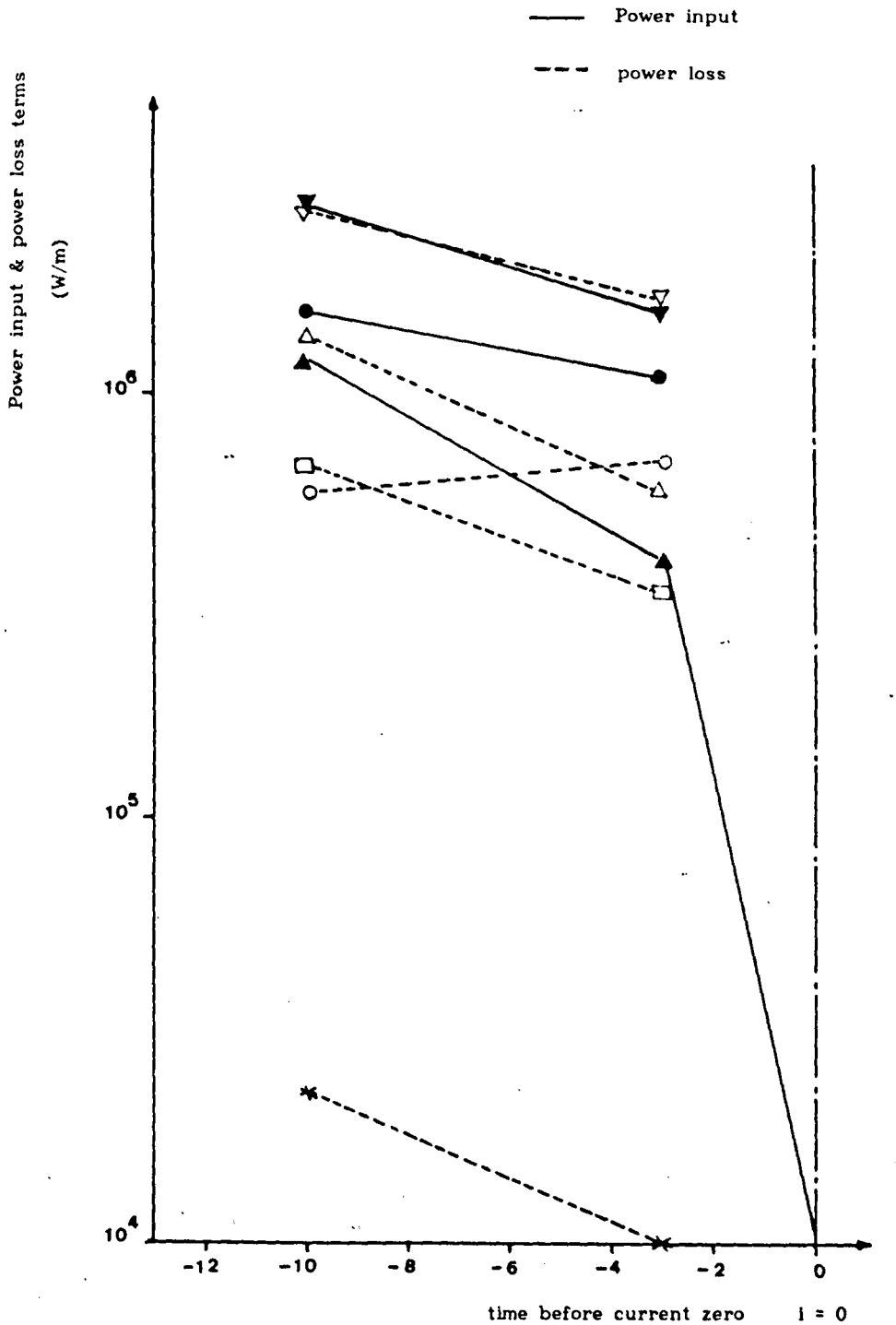

Fig. (6.20) Comparison of the various power loss terms during the current zero period.

(a) p = 110 psig & di/dt = 15 A/μs

▲ Q_E = Electrical power input

● Q_s = Change in thermally stored energy

□ Q_R = Radiation power loss

✱ Q_{co} = Radial conduction loss

Δ Q_{CA} = Axial heat convection

O Q_{CR} = Radial heat convection

▼ Total power input ▽ Total power loss

Key as for Fig. (6.20 a)

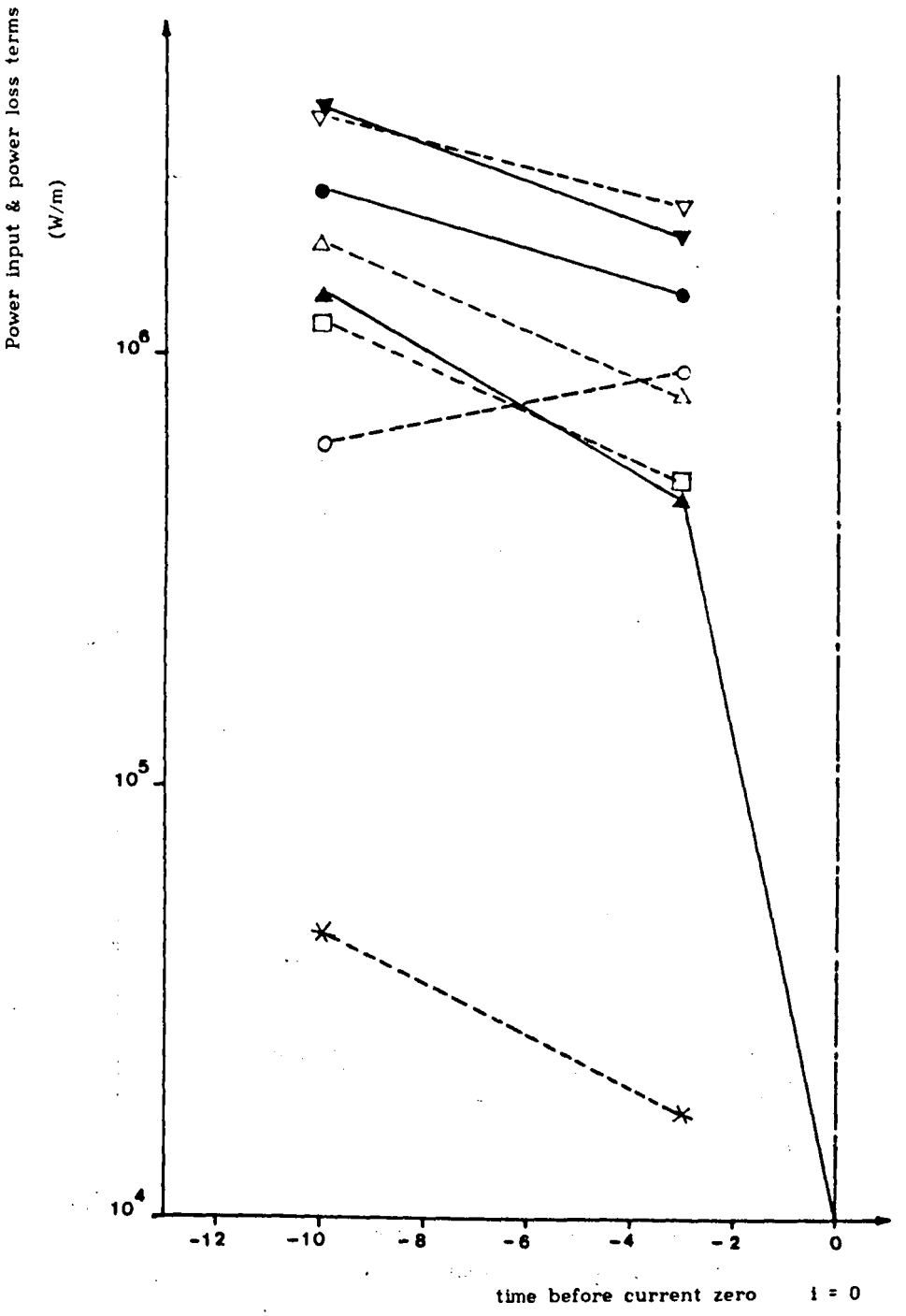

Fig. (6.20) (b) P = 110 psig & di/dt = 20 A/μs

Key as for Fig. (6.20 a)

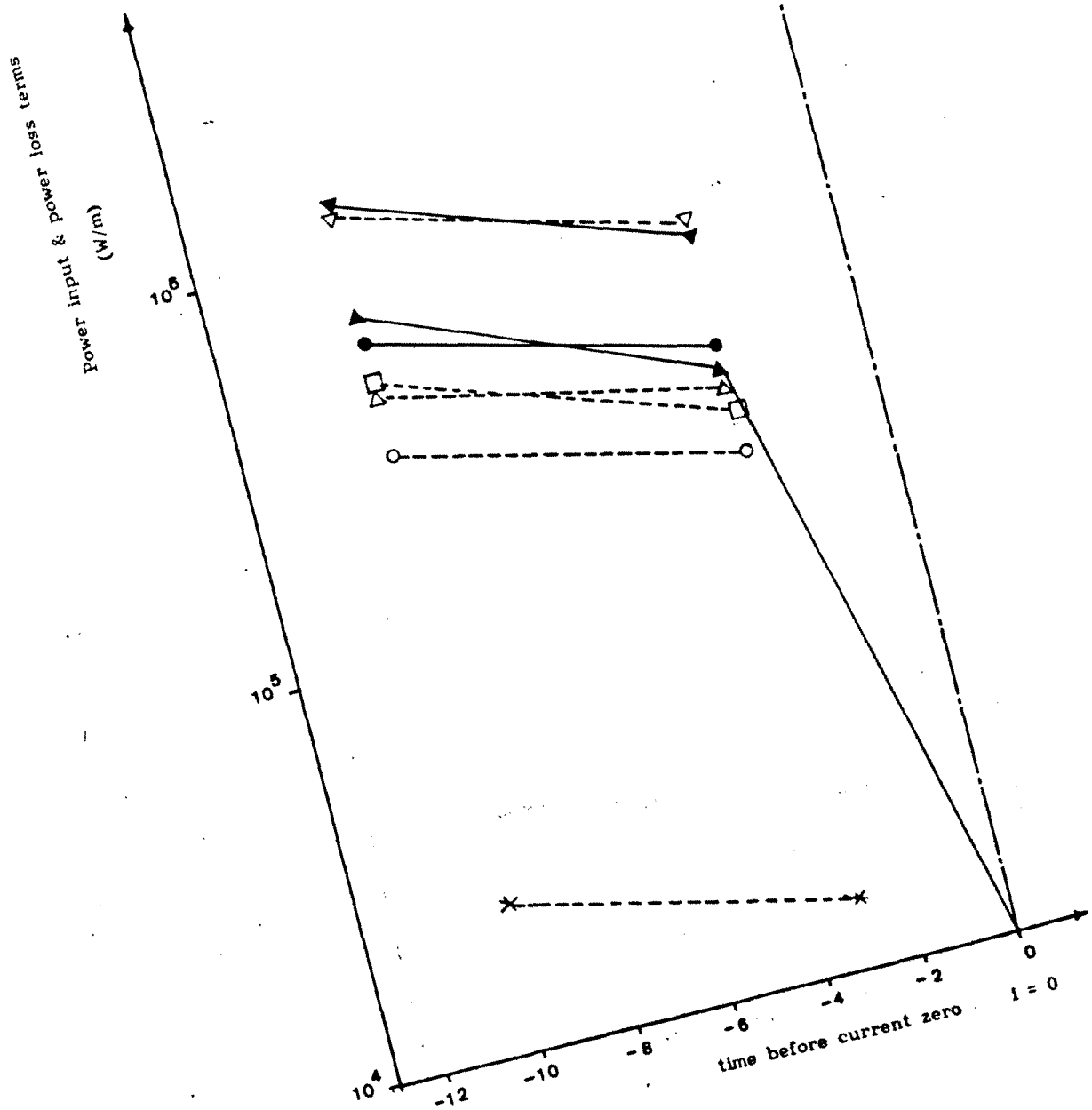

Fig. (6.20) (c) P = 60 psig & dI/dt = 15 A/μs

Key as for Fig. (6.20 a)

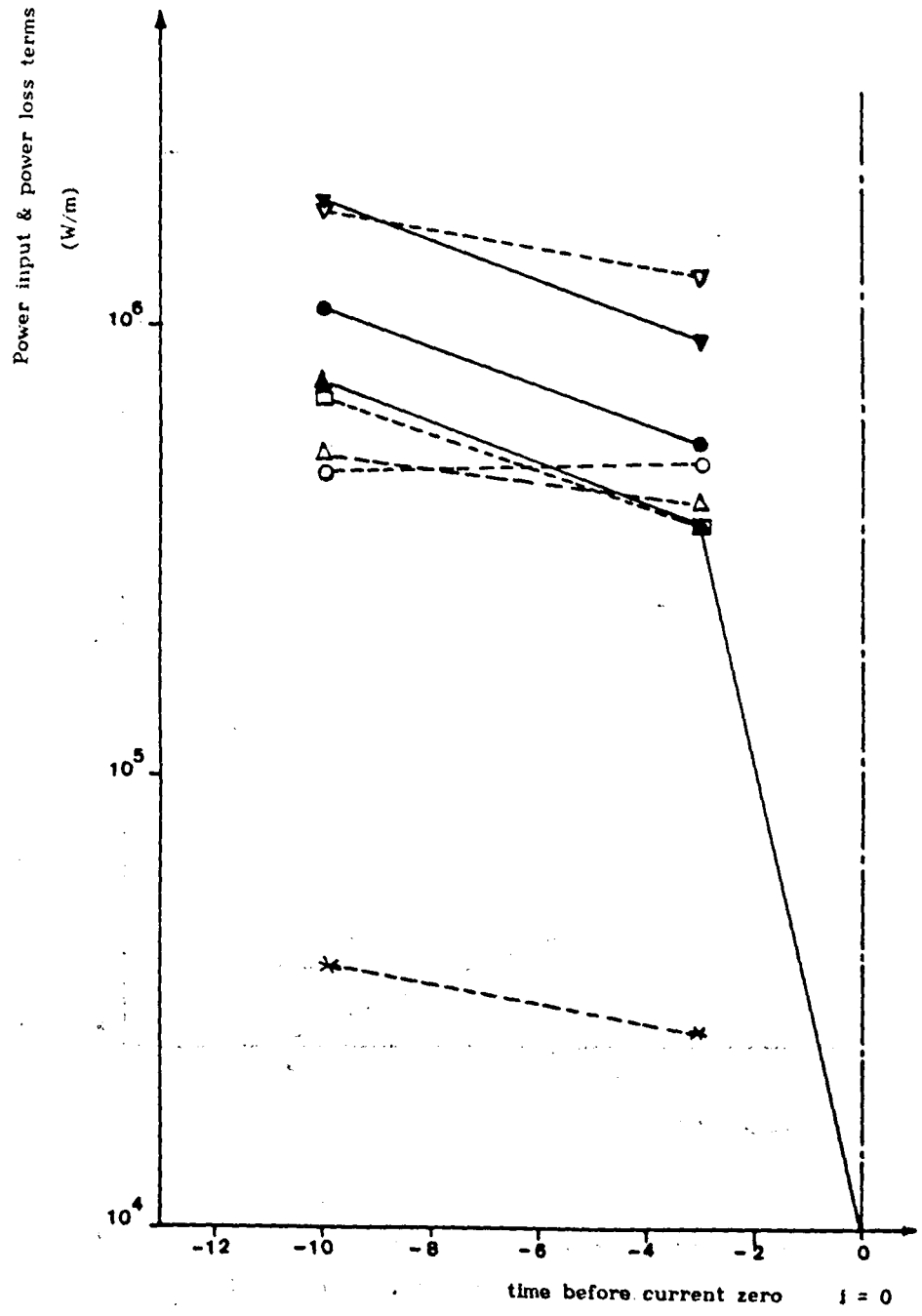

Fig. (6.20) (d) P = 60 psig & di/dt = 20 A/μs

Key as for Fig. (6.20 a)

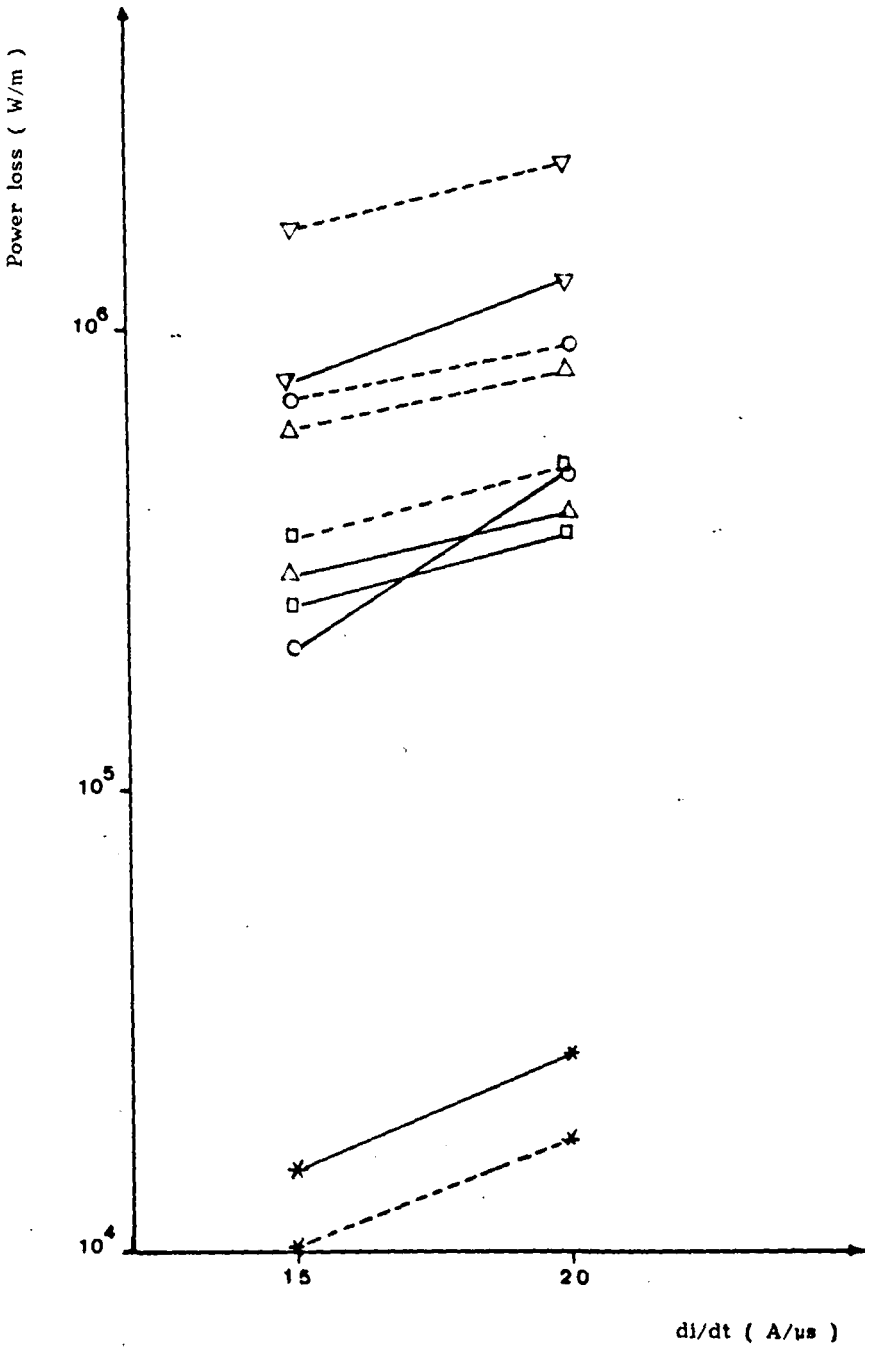

Fig. (6.21) Variation of the power loss terms in the core power balance with di/dt and different pressures at the same time before current zero.

(a) t = -3 μs

- - - p = 110 psig —— p = 60 psig

Key as for Fig. (6.20 a)

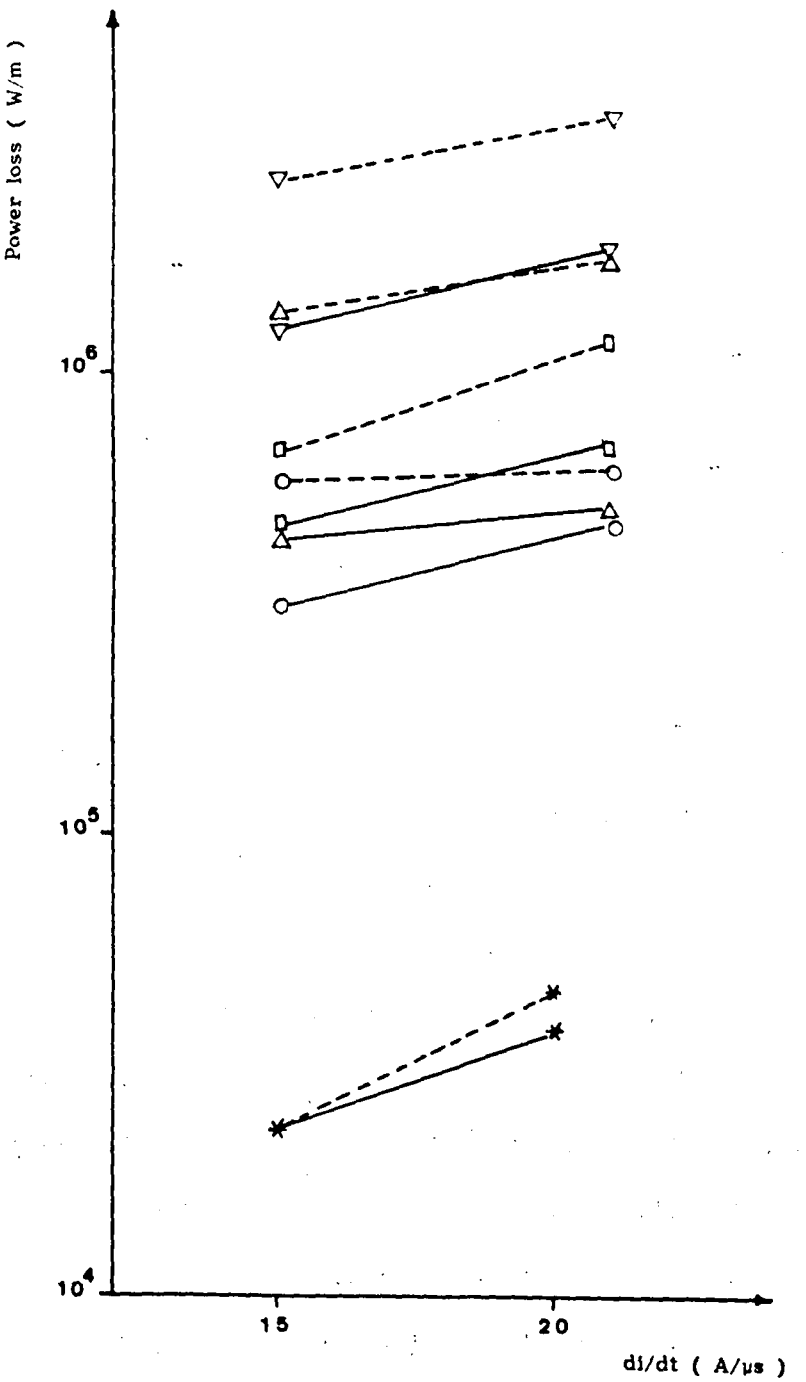

Fig. (6.21) (b) t = -10 μs

— — — p = 110 psig ——— p = 60 psig

CHAPTER 7

SUMMARY AND CONCLUSIONS

Experiments have been performed to investigate the behaviour of an SF_6 circuit breaker under very high power conditions. These investigations have involved time and space resolved spectroscopic measurements to quantify the processes governing arc thermal reignition phenomena. Such investigations of current zero SF_6 arc spectral characteristics in a circuit breaker environment are particularly difficult but provide important information about arc properties. Important parameters such as temperature, electron density, electrical conductivity as well as plasma composition can be obtained from such investigations. All these measurements were taken during the final 10 μs as the fault current flowing through the interrupter decayed naturally to zero. The spectra were obtained with a Monospek 1000 grating spectrometer having a reciprocal dispersion of 0.82 nm/mm and with an entrance slit width of 28.5 μm. The measurement techniques all had fine time resolution (1.6 μs) to allow the transient changes in the optical signals to be faithfully followed. A method was developed whereby the raw spectral data captured by the optical spectrum analyser (OSA 500) could be subjected to computational analysis and converted to a continuous radial temperature profile. Account has been taken of the assymetric nature of the arc plasma column and its random lateral displacement from test to test.

The spectral region studied was between 510 - 517 nm. Besides copper emission lines, randomly occurring tungsten lines from entrained cathode material have also been identified under certain operating conditions. In chapter (5) it was concluded that the tungsten lines appear only at high values of di/dt except for longer time before current zero. In other words the larger the di/dt and t, the higher the probability of appearance of tungsten lines and this implies that this appearance is related to input energy. The ratio of the number density of tungsten to copper atoms in the arc plasma has been determined from the intensities of these lines.

Despite overcoming the practical difficulties and obtaining radially resolved spectral records the analysis of these results still presents problems because of the unstable and irregular nature of the arc column in such environment along with its small lateral dimensions. These investigations are concerned with the evaluation of such experimental results and the derivation from them of an estimate of the plasma conditions within the decaying arc.

The spectra enabled both the radially averaged arc temperature and electron density to be calculated. The spatially resolved spectra also allowed detailed arc temperature profiles to be measured during the current zero period. These temperature profiles have been determined from the ratio of intensities of two copper lines (CuI 515.3 nm and 510.5 nm) and is independent of line profile and whether or not tungsten lines are present. It is of importance that no radial splitting of the arc column effects are in evidence at the localities at

which the arc temperature profile is measured so that energy flow calculations may be applied radially and axially without complication.

Axis temperature estimates for the arc at different pressures indicate that higher pressure arcs possess higher plasma temperatures. It was observed (chapter (5)) that the arc cross-section in the lower pressure arcs has a greater diameter than in the higher pressure arcs.

These temperature estimates and arc diameter measurements have important implications with regard to the presence of tungsten. Firstly no correlation was observed between the tungsten occurrence and axis temperature. Furthermore the more persistent occurrence of tungsten during the current zero period in the larger diameter lower pressure arcs implies that the weaker convection in these arcs plays a dominant role in governing the persistence of tungsten.

The experimental radial temperature profiles also led to an accurate evaluation of the core conductance shape factor and an estimate of the overall conductance shape factors of the integral analysis (e.g Chan et al (1974)). These results have been compared with the work of others which have used widely different operating conditions, through a universal correlation parameter, the Nusselt number. The good agreement found between these results and the shape factors of other workers is an important result since it shows for the first time that the current zero arc column conditions fit the general description established with the boundary layer integral analysis.

A further investigation has also been conducted into the optical thickness of the arc plasma. Two methods for testing and determining the optical depth have been discussed. These have been used in conjunction with the results of chapter (5) to confirm that the arc plasma near current zero is generally optically thin. Also two criteria have been discussed from which the existence of LTE conditions in the plasma can be investigated using the values of electron density and temperature presented in chapter (5).

The temperature profiles measured in this investigation allowed the power balance for the circuit breaker arc plasma column to be determined experimentally for the first time. These results show that (Chapter (6)) the power input term due to the thermally stored energy is about 70 % of the total power input in the case of the higher pressure arc and about 50 % in the case of the lower pressure arc. The rate of release of stored energy is greater in the higher pressure case than the lower pressure case. It was also concluded that the dominant power loss mechanisms during the current zero period are the axial and radial convection (Q_{CA}) & (Q_{CR}) with the radiation loss (Q_R) also contributing significantly. It has been shown that the radial heat conduction term (Q_{co}) is insignificant, contributing only about 1 % of the total power loss in the higher pressure case and about 2 % in the lower pressure case, even close to current zero (figures (6.20 a, b, c and d)). This is an important result which is contrary to conventionally held views. There is some evidence that the most

dominant loss mechanism close to current zero is likely be the radial convection power which has been largely neglected by many researchers.

REFERENCES

Airey D.R.
"Energy balance and transport properties of very high current SF_6 arcs".
Ph.D Thesis, University of Bath, 1977.

Ancilewski M.K., Burlik A.C. and King L.H.A.
"Calculation of SF_6 interrupter performance for thermal reignition criteria".
International conference on large high voltage electrical systems 1984, session Aug/Sept, 13-07.

Barrault M.R., Blackburn T.R., Edels H. and Satanarayana P.
"Investigation of a high current free burning electric arc".
Int. conf. on gas discharges (I.E.E. conf. publ. 90) London, 1972, pp. 221-223.

Biermanns J.
"Arc recovery".
IEE Journal, Vol. 10, 1932, pp. 28-30.

Browne T.E.
"A study of A.C. arc behaviour near current zero by means of mathematical models".
AIEE Transactions, 1948, Vol. 67, pp. 141-153.

Browne T.E.
"An approach to mathematical analysis of a.c. arc extinction in circuit breakers".
AIEE Transactions, 1959, pp. 1508-1517.

Cassie A.M.
"A new theory of arc rupture and circuit severity".
C.I.G.R.E., Vol. 10, 1939, paper 102.

Cassie A.M.
"Introduction to the theory of arc extinction and circuit severity in circuit breakers with post zero conductivity".
ERA report, 1953, No. G/XT134.

Cassie A.M. and Mason F.O.
"Post arc conductivity in gas blast circuit breakers".
C.I.G.R.E., report No. 103, 1956.

Chan S.K., Cowley M.D. and Fang M.T.C.
"Theory of electric arcs in longitudinal flow
Part 6: Correlation of shape factors for integral methods".
Univ. of Liverpool, Elec. Eng., Arc Res. report, ULAP-T26, (1974).

Chan S.K., Cowley M.D. and Fang M.T.C.
"Integral methods of analysing electric arcs :
III Shape factor correlation for low radiation and laminar flow".
J. Phys. D., Appl., Phys., Vol. 9, 1976, pp. 1085-1099.

Chapman A.
"The electrical conductance of a gas blast interrupter arc near current zero".
Ph. D Thesis, View of Liverpool, June 1977.

Chapman A., Jones G.R., and Strachan D.C.
"High current arc in an orifice air flow
5 : The overall electrical behaviour of a.c. arcs particularly near current zero".
Univ. of Liverpool, Elec. Eng., Arc Res. report, ULAP-T36 (1975).

Corliss C.H. and Bozman W.R.
"Experimental transition probabilities of spectral lines of seventy elements".
NBS monograph 53, (1962).

Corliss C.H.
J. Res., Natl. Bur. Stand A, 74 A, 1970, No. 6, pp. 781-790.

Cowley M.D.
"Integral methods of analysing electric arcs : I Formulation".
J. Phys. D., Appl. Phys., Vol. 7, 1974, pp. 2218-2231.

Cowley M.D. and Chan S.K.
"Integral methods of analysing electric arcs : II Examples".
J. Phys. D., Appl. Phys., Vol. 7, 1974, pp. 2232-2245.

El-Kholy S.M., Weilin Hu., Prasad A.N. and Jones G.R.
"Optical spectra of SF_6 circuit breaker arcs during the current zero period".
Proc. Int. Conf. on phenomena in ionized gases ICPIG XVIII Swansea, July 1987, pp. 688-689.

Fang M.T.C. and Brannen D.
"A current zero arc model based on forced convection".
IEEE Trans., Vol. PS7, No. 4, 1979, pp. 217-229.

Flurscheim C.H.
"Some notes on rates of rise of restriking voltage subsequent to interruption of alternating - current power circuits".
Journal IEE, Vol. 76, 1935, pp. 323-337.

Friedrich R.E. and Yeckley R.N.
"A new concept in power circuit breaker design utilising SF_6".
Trans. Am. Inst. Elec. Eng. 76, 1957, pp. 906-909.

Frind G.
"Uber das abklingen von linchtbogen-I Theoretische uberlegungen".
A. Angew, Phys., Vol. 12, No. 5, 1960, pp. 231-237.

Frind G. and Rich J.A.
"Recovery speed of axial flow gas blast interrupter : Dependence on pressure and di/dt for air and SF_6".
IEEE Trans., PAS 93, 1974, pp. 1675-1682.

Frind G., Prescott L.E. and Van Noy H.H.
"Current zero phenomena in an orifice type gas blast interrupter".
IEEE Trans., PAS 99, 1980, pp. 268-278.

Forst L.S. and Liebermann R.W.
"Composition and transport properties of SF_6 and their use in a simplified enthalpy flow arc model".
Proc. IEEE, Vol. 59, 1971, pp. 474-485

Griem H.R.
"Plasma Spectroscopy".
McGraw-Hill Inc., 1964.

Griem H.R.
"Spectral line broadening by plasmas".
Academic press, N. York and London, 1974

Harrison G.R.
"Wavelength table".
New York, Wiley 1952.

Hermann W., Kogelschatz U., Ragaller K., and Schade E.
"Investigation of a cylindrical axially blown high pressure arc".
J. Phys. D., Appl. Phys., Vol. 7, 1974(a), pp. 607- 619.

Hermann W., Kogelschatz U., Niemeyr L., Racaller K. and Schade E.
"Experimental and theoretical study of a stationary high current arc in a supersonic nozzle flow".
J. Phys. D., Appl. Phys., Vol. 7, 1974(b), pp. 1703- 1722.

Hermann W., Kogelschatz U., Niemeyr L., Racaller K. and Schade E.
"Investigation on the physical phenomena around current zero in H.V. gas blast breakers".
IEEE Trans., Vol. PAS 95, No. 4, August 1976, pp. 1165-1176.

Hermann W. and Ragaller K.
"Theoretical description of the current in H.V. gas blast breakers".
I.E.E.E. Trans., Vol. PAS 96, No. 5, Sept/Oct 1977, pp. 1541-1555.

Housby-Smith C. and Jenkins J.E.
"High current arcs in an orifice flow - spectroscopic measurements under quasi-steady state conditions".
Univ. of Liverpool, Elec. Eng., Arc Res. report, ULAP-T54, 1978.

Hudson A.A.
"Effect of arcing on air flow through nozzle of a gas blast circuit breaker".
The Engineer, Vol. 200, 1955, pp. 249-252 and 288-290.

Hudson A.A.
"Mass flow in nozzle of a gas blast circuit breaker - effect of nozzle geometry".
The Engineer, Vol. 217, May 1964, pp. 933-939.

Ikeda H. Jones G.R., Irie M. and Prasad A.N.
"Spectroscopy of very high current convection arcs".
IEE seventh int. conf. on gas discharges and their applications, 1982, pp. 5-8.

Ito T., Ueda Y., Komura H. and Nitta T.
"Spectroscopic study of high current discharges".
IEEE Trans., Vol. 59, No. 4, 1971, pp. 573-578.

Jenkins J.E.
(Private communication, 1984).

Jones G.R., Lidgate D. and Edels H.
"Interaction between a high current arc and the air flow in air blast circuit breaker".
Proc. IEE, Vol. 122, 1975, pp. 1443- 1451.

Jones G.R., Shammas N.Y. and Prasad A.N.
"Radiation induced nozzle ablation in high power circuit interrupters".
Univ. of Liverpool, Elec. Eng., Arc Res. report, ULAP-T84, 1987.

Kinsinger R.E.
"A numerical model for current zero arc interruption processes".
IEEE Trans., PAS 93, No. 4, 1974, pp. 1143-1149.

Kock M. and Richter J.
"Experimentalle Ubergang swahrs heinlichkeiten und die PT72 selare Haufigket des kupfers".
Z fur Astrophysik, 1968, pp. 180-192.

Kopplin H.
"The dynamic behaviour of arcs in alternating current circuits".
Archiv Fur Elektroteckink, Vol. 47, 1962, pp. 47-60.

Kopplin H., Rolff K.P. and Zuckler K.
"Study of the effects of gas flow on the performance of gas blast circuit breakers".
Proc. IEEE, Vol. 59, No. 4, 1971, pp. 518-524.

Lee T.H.
"Physics and engineering of high power switching devices".
M.I.T. press, 1975, pp. 233-235.

Leeds W.M., Browne T.E. and Stram A.P.
"The use of SF_6 for high power arc quenching".
Trans. Am. Int. Elec. Eng. 76, 1957,pp. 906-909.

Lellerc J.L. and Jones G.R.
"The radiative characteristic of gas blast circuit breaker arcs at very high currents".
IEE seventh int. conf. on gas discharges and their applications, London, 1982, pp. 1-3.

Leonard S.L.
"In Plasma Diagnostic Techniques ed. Huddlestone and Leonard". Academic Press, N.Y., 1965, pp. 45-53.

Lewis E., Prasad A.N. and Jones G.R.
"Current zero spectroscopy of a high power SF_6 circuit breaker arc".
Proc. int. conf. on gas discharges and their applications, 1985a, (Oxford), pp. 31-34.

Lewis E., Shammas N.Y. and Jones G.R.
"The current zero SF_6 blast arc at high di/dt"
Proc. int. conf. on gas discharges and their applications, 1985b, (Oxford), pp. 35-38.

Lewis E.
"The thermal properties of an SF_6 circuit breaker arc during the current zero period".
Ph.D Thesis, University of Liverpool, 1987.

Liebermann R.W. and Chen C.L.
"Thermodynamic and transport properties of SF_6".
Westinghouse R and D centre, Pittsburgh, Pennsylvania, 31 May 1977.

Lochte- Holtgreven W.
"in Plasma Diagnostic (Lochte-Holtgreven ed)".
North Holland Publishing Co., Amsterdam, 1968, p.147.

Lochte- Holtgreven W.
"in Plasma Diagnostic (Lochte-Holtgreven ed)".
North Holland Publishing Co., Amsterdam, 1968, pp. 139-141.

Lochte- Holtgreven W.
"Evaluation of plasma parameters pp. 184-188 in Plasma Diagnostic ed."
Lochte-Holtgreven North Holland Publishing Co., Amsterdam, 1968.

Mahajan S.M., Ravi J. and Benenson D.M.
"The thermal boundary layer in dual flow arc plasmas".
IEEE Trans., PS - 12, No. 4, December 1984, pp. 246-250.

Mayr O.
"Contributions to the theory of static and dynamic arcs".

Archive fur Elecktrotechnik, Vol. 37, 1943, pp. 588-608.

Okuda S., Ueda Y., Murai Y., Miyamoto T., Doi Y. and Uenosono c.
"Spectroscopic approach to the analysis of high current arcs in SF_6".
IEEE Trans., on plasma science, Vol. PS-8, No. 4, December 1980, pp. 395-399.

Prince D.C. and Skeats W.F.
"The oil-blast circuit breaker".
Trans. AIEE, Vol. 50, 1931, pp. 506-511.

Ragaller K.
"Current interruption in high voltage networks".
Plenum Press, New York, 1978.

Rieder W.
"Arc circuit interaction near current zero and circuit breaker testing".
IEEE Trans. PAS 91, 1972, pp. 705-715.

Roberts D.E. and Prasad A.N.
"Spectroscopic investigation of the 10 KA free burning arc in air".
Univ. of Liverpool, Elec. Eng., Arc Res. report, ULAP-T8, 1972.

Roberts D.E. and Cowley M.D.
"Spectroscopic investigation of the 10 KA arc in efflux air flow".
Univ. of Liverpool, Elec. Eng., Arc Res. report, ULAP-T18, 1973.

Schlichting H.
"Boundary Layer Theory".
Magraw-Hill, New York, 1958.

Shammas N.Y. and Jones G.R.
"Total radiation losses from SF_6 circuit breaker arcs during the current zero period simulated with current ramps".
Univ. of Liverpool, Elec. Eng., Arc Res. report, ULAP-T70, 1982.

Shammas N.Y.
Private communication (1982).

Shayler P.J. and Fang M.T.C.
"The transport and thermodynamic properties of a copper-nitrogen mixture".
Univ. of Liverpool, Elec. Eng., Arc Res. report, ULAP-T45, 1976.

Shimmin D.W.
"High power short-circuit studies on an SF_6 puffer circuit breaker".
Ph.D Thesis, University of Liverpool, 1986.

Skeats W.F.
"Discussion on the paper presented by Browne (1948)".
AIEE Transactions, 1948, Vol. 67, pp. 141-153.

Slepian J.
"Extinction of an a.c. arc".
AIEE Transactions, 1928, Vol. 47, pp. 1398-1408.

Slepian J.
"Extinction of a long a.c. arc".
AIEE Transactions, 1930, Vol. 49, pp. 521-530.

Slepian J.
"Displacement and diffusion in fluid flow arc extinction".
AIEE Trans., Vol. 60, 1941, pp. 162-167.

Smith M.R., Barrult M.R., Jones G.R., El-Menshawy M.F., Housby-Smith C. and Jenkins J.E.
"Spectroscopic investigations during the current zero period for arcs in an orifice gas flow".
Univ. of Liverpool, Elec. Eng., Arc Res. report, ULAP-T61, 1978.

Strachan D.C.
"Radiation losses from high current free burning arcs between copper electrodes".
Univ. of Liverpool, Elec. Eng., Arc Res. report, ULAP-T14, 1973a.

Strachan D.C.
"Radiation losses from high current free burning arcs between copper electrodes".
J. Phys. D : Appl. Phys., Vol. 6, 1973b, pp. 1712-1723.

Strachan D.C.
"A study of the radiative energy losses from an arc in efflux flow".
Univ. of Liverpool, Elec. Eng., Arc Res. report, ULAP-T23, 1974.

Strachan D.C.
"A study of the radiative energy losses from an arc in jet flow".
J. Phys. D. : Appl. Phys., Vol. 8, 1975(a), pp. 703-713.

Strachan D.C.
"High current arcs in an orifice air flow
4 Radiation loss measurement".
Univ. of Liverpool, Elec. Eng., Arc Res. report, ULAP-T35, 1975(b).

Strachan D.C., Lidgate D. and Jones G.R.
"Radiative energy losses from a high current air blast arc"
Journal of appl. phys., Vol. 48, No. 6, 1977(a), pp. 2324-2330.

Strachan D.C., Jones G.R., Bolton A.W. and Atkinson F.B.
"An experimental test facility for the study of high current arcs in sulphur hexaflouride and air".
Univ. of Liverpool, Elec. Eng., Arc Res. report, ULAP-T46, 1977b.

Swanson B.W. and Roidt R.M.
"Boundary layer analysis of an SF_6 circuit breaker arc".
IEEE Trans., Vol. PAS 90, 1971, pp. 1086-1093.

Swanson B.W. and Roidt R.M.
"Thermal analysis of an SF_6 circuit breaker arc".
IEEE Trans., Vol. PAS 91, 1972, pp. 381-389.

Swanson B.W., Roidt R.M. and Browne T.E. Jnr.
"The effect of gas dynamics and properties of SF_6 and air on short line fault interruption".
IEEE Trans., Vol. PAS 89, No. 8, 1970, pp. 2033-2042.

Swanson B.W., Roidt R.M. and Browne T.E. Jnr.
"Arc cooling and short line fault interruption".
IEEE Trans., Vol. PAS 90, 1971, pp. 1094-1102.

Swanson B.W., Roidt R.M. and Browne T.E. Jnr.

"Some numerical solution of boundary layer equations for SF_6 arcs".
Proc. IEEE, Vol. 59, No. 4, 1971a, pp. 493-501.

Swanson B.W., Roidt R.M. and Browne T.E. Jnr.
"A thermal arc model for short line fault interruption".
ETZ-A, Vol. 93, 1972, pp. 375-380.

Swanson B.W.
"Nozzle arc interruption in supersonic flow".
IEEE Trans., Vol. PAS 96, 1977, pp. 1697-1706.

Taylor S.
"Data acquisition and analysis of circuit breaker arc measurements".
M.Eng. Thesis, University of Liverpool, 1983.

Taylor S., Wang B., Blackburn T.R. and Jones G.R.
"Thermal reignition performance limitations of a model SF_6 circuit breaker under full and scaled power conditions".
Univ. of Liverpool, Elec. Eng., Arc Res. report, ULAP-T72, 1982.

Topham D.R.
"The electric arc in a constant pressure axial flow".
J. Phys. D., Appl. Phys., Vol. 4, 1971, pp. 1114-1125.

Topham D.R.
"The characteristics of axial flow electric arcs subject to pressure gradients".
J. Phys. D., Appl. Phys., Vol. 5, 1972(a), pp. 533-541.

Topham D.R.
"Scaling laws of the interaction of a gas-blast circuit breaker arc with an electric circuit".
Proc. IEE, Vol. 119, 1972(b), pp. 1469-1476.

Topham D.R.
"Measurements of the current zero behaviour of constant pressure axial flow electric arcs in nitrogen".
Proc. IEE, Vol. 120, No. 12, Dec.1973, pp. 1568-1574.

Walmsley H.L., Haji F.H., Strachan D.C. and Jones G.R.
"High current arcs in an orifice flow

8 High speed photography of the luminous core under a.c. conditions".
Univ. of Liverpool, Elec. Eng., Arc Res. report, ULAP-T42, 1976.

Walmsley H.L., Jones G.R. and Barrault M.R.
"Properties of the thermal region of a gas blast a.c. arc particularly near current zero".
Univ. of Liverpool, Elec. Eng., Arc Res. report, ULAP T56, 1978(i).

Walmsley H.L. and Jones G.R.
"Correlation of the integral analysis parameters for gas blast arcs, particularly near current zero".
Univ. of Liverpool, Elec. Eng., Arc Res. report, ULAP-T57, 1978(ii).

Zhang J.
"Theoretical investigation of gas blast arcs".
Ph.D Thesis, University of Liverpool, 1986.

Zuckler K.
"Reciprocal influence of the gas flow and arc in gas blast circuit breakers".
Z. Angew Phys., Vol. 22, 1967, pp. 155-164.

Zuckler K.
"Contribution to the clogging problem in high voltage power breakers".
ETZ-A, Vol. 90, 1969, pp. 711-714.

"Persistent lines of the elements, C.R.C."
Handbook of Chemistry and Physics, 48th Ed. Publ. The Chemical Rubber Co., 1967-1968, pp. E148-151.

APPENDIX (A.1)

COMPUTER PROGRAMS

It is the aim of this section to present some of the software which has been developed and used to interpret the spectral test data. The programs uses have been divided into two categories. Firstly, the software designed to convert the spectral data into radially averaged temperature and half - line widths (for electron density measurement) is presented. Also additional software is presented which deals with the calculation of theoretical spectral line intensities. A second category includes the software which was used to interpret the radially resolved data and convert it to deconvoluted radial intensity profile which can be used to calculate the radial temperature profiles (chapter 5).

Fig. (A.1.1) shows the overall program structure for the interpretation of data into radially averaged temperatures and further calculation of the theoretical line intensity and optical depth. The following programs were developed to implement the above task.

(1) " OSA1 "

The spectral data was input from the Optical Spectrum Analyser OSA 500 in the form of data files, one per arc test. The software in this program is designed to transfer the data from the OSA 500 to the B.B.C. computer using another program "OSA.".

(2) "OSPLT3 "

The software in this program is designed to log the above data onto disc and display it on the VDU for dumping onto a printer etc.

(3) " OSAD "

This program was developed so that the above files may be interrogated. The program calculates the spectral line intensity above the continuum level between two specified wavelength limits. The width of the spectral line at half intensity is also calculated. This task can be performed a number of times per file to facilitate the possibility of a record containing more than one spectral line.

(4) " TEMP "

This program was used to calculate the radially averaged arc temperature using the data from " OSAD " and the formula of equation (3.3).

(5) " OPDEP "

This program uses the data from DATA INT. as well as theoretical data from another program " LOADER " to calculate the theoretical spectral line intensity and the critical optical depth (equation 6.11) for a range of temperatures between 6,000 and 12,000 °K. This data is shown on figures (6.2) and (6.10) respectively.

(6) " IDISP "

This program has been developed to generate a set of predicted radial intensity histograms for a known (parabolic) radial emissivity profile. These intensity histograms are designed to coincide with those measured on the OSA 500 system. "IDISP" also has the facility of calculating such radial histograms for a number of different arc displacements with respect to the central viewing axis through the procedure " proc disp ". A similar program "I515N" used to calculate the radial intensity histograms for the 515.3 nm line and also "I510N" program used for the same purpose for the 510.5 nm line. An output of these two programs are presented at the end of this appendix.

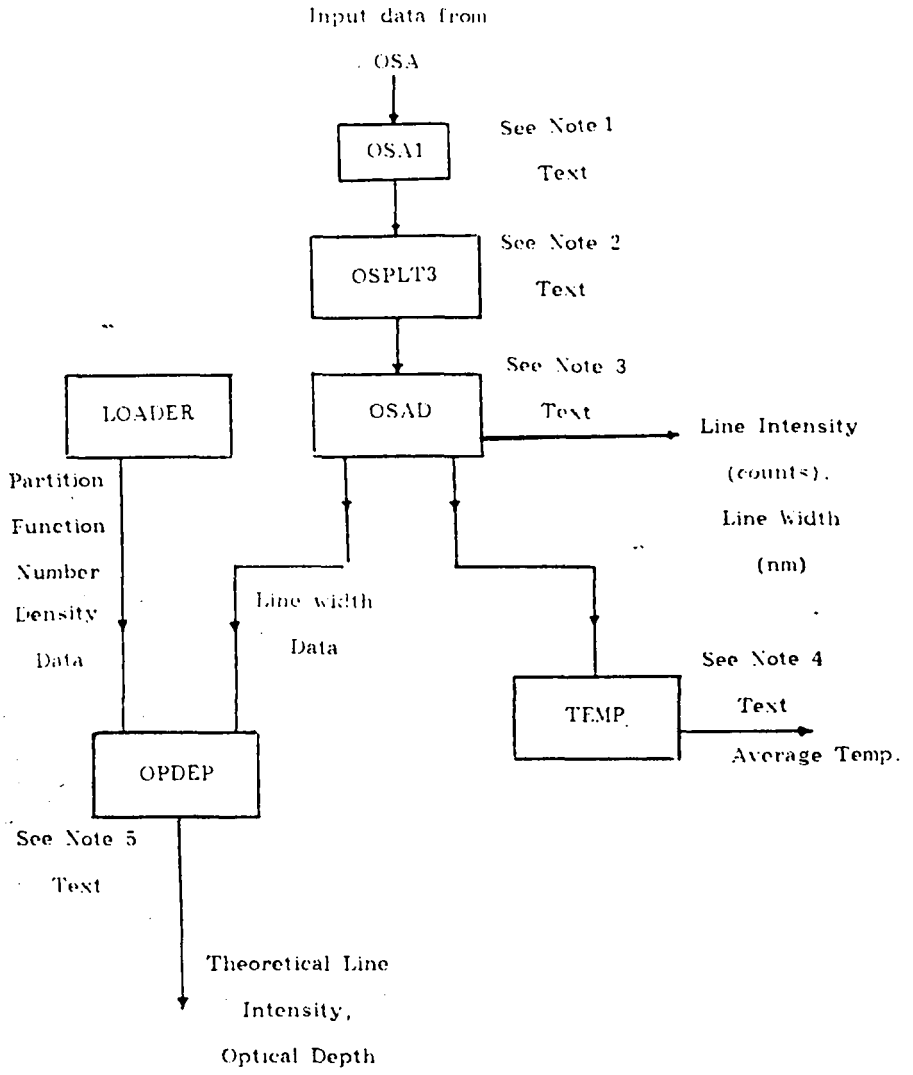

Fig. (A.1.1) Program structure for interpretation of data into radially averaged temperature and evaluation of theoretical line intensity and optical depth.

" OSA1 "

```
 10 REM OSA data transfer
 20
 30 *KEY10 OLD|M MODE3|M
 40 *KEY9 RUN|M
 50 *KEY0 SAVE"OSA1"
 60 *KEY1 LOAD"OSA1"
 70 CSTAT=&FE08:IO=&FE09
 80 TV=&FFEE:OSB=&FFF4
 90 tmpX=&0073:tmpY=&0074
100 ptr=&0076:offset=&0078
110 count_lo=&0079:count_hi=&007A
120 buffer=&0080
130
140 MODE3
150 PRINT "           ********** OSA DATA TRANSFER **********" '
160 INPUT "  filename ? " file$
170
180 *RUN OSA.
190
200 FX=OPENOUT (file$)
210 FOR I% = 0 TO 1995 STEP 4
220   A%=&6000+I%
230   PRINT! FX,!A%
240 NEXT I%
250 CLOSE! FX
260
270 MODE3:VDU 14
280 FX=OPENIN (file$)
290 I% = 0
300 REPEAT
310   I% = I%+1
320   INPUT! FX,A%
330   PRINT I%,A%
340 UNTIL EOF! FX
350 END
360
```

<XXXXXXXXXXX>

" OSPLT3 "

```
 10 REM PLOT ROUTINE FOR OSA Data
 20
 30 MODE0
 40 PROCline(0,0,1023,0)       :REM draw X axis
 50 PROCline(25,0,25,825)       :REM draw Y axis
 70
 90
 91 label$ = "counts"
 92 PROCvertlabel(78,15,label$)
100 label$ ="wavelength (nm)"
101 PROChorizlabel(25,4,label$)
110   VDU30              :REM cursor home
120   PROCerase_line
125 PROCplot
130 PROCinput
135 PROCgrid
140
150 PROCprint
180 END
190
200 DEF PROCplot
210   LOCAL I,X%,Y%
220   INPUT "Filename ? " file$
230   F% = OPENIN (file$)
240   PROCerase_line
250   REPEAT
260      PTR£ F% = 0
270      VDU 31,22,0                          :REM move text cursor
280      INPUT "Scale Factor = " S
290      FOR I=1 TO 899
300        INPUT£ F%,Y%
310        Y%=Y%*S
320        X%=I*2+25
330        PLOT 69,X%,Y%
340      NEXT I
350      PROCerase_line
355 CLOSE£F%
370
380 ENDPROC
400 DEF PROCline(Sx,Sy,Fx,Fy)
410   MOVE Sx,Sy
420   DRAW Fx,Fy
430 ENDPROC
440
450 DEF PROCgrid
460   LOCAL I
470   FOR I = 25 TO 1050 STEP 100
480     PROCline(I,0,I,850)
485     PROChorizcal(I,L)
487     L=L+.7 : REM INCREMENT L FOR PROC horizcal
490   NEXT I
500
510   FOR I = 0 TO 825 STEP 100
520     PROCline(25,I,1023,I)
525     PROCcal (I)
530   NEXT I
540 ENDPROC
550
560 DEF PROCvertlabel(x%,y%,label$)
570   LOCAL i%,line%
580   line%=42
```

```
590    FOR i% = 1 TO LEN(label$)
600      IF i%+y% <= line% THEN PRINT TAB(x%,i%+y%-1);MID$(label$,i%,1)
610    NEXT i%
620 ENDPROC
630
640 DEF PROChorizlabel(x%,y%,label$)
650    PRINT TAB(x%,y%);label$
660 ENDPROC
670
680 DEF PROCerase_line
690    VDU 31,60,0
700    FOR I=60 TO 1 STEP -1:VDU 127:NEXT I
710 ENDPROC
720
730 DEF PROCprint
731 VDU30
740IF ANS$="Y" THEN CHAIN"DUMPO"
750 ENDPROC
770 DEF PROCcal(I)
790 X=I/S
800 MOVE 1100,I+25
805 VDU 5
810 PRINT;X
830 ENDPROC
850 DEF PROChorizcal(I,L)
860 MOVE I-25,850
870 VDU5
880 PRINT;L-3.5
890ENDPROC
950 DEF PROCinput
960 VDU 31,22,0
970 INPUT "Centre Wavelenth = " L
980 PROCerase_line
990 INPUT "Do you want a printout at the end of this program ?" ANS$
1000 PROCerase_line
1010 VDU 30
1110 INPUT "Io - "t0
1120 PROCerase_line
1130 INPUT "  dI/dt = "D
1140 PROCerase_line
1150 INPUT"  Tgate ="Tg
1155 PROCerase_line
1156 INPUT"  Press ="Pt
1157 PROCerase_line
1160 PRINT TAB(2,2);"Io - ";t0;" micS","  dI/dt = ";D;"A/micS","  Tgate =";Tg;'
micS","  Press = ";Pt;"psig"
1165 PRINT TAB(2,1);"filename$ ";file$
1170 VDU30
1180 ENDPROC
```

(XXXXXXXXXXX)

" DUMP0 "

```
 10REM  MODE 0 Screen Dump to Printer
 30
 40VDU30,2
 50VDU1,27,1,65,1,8
 60M0=&8000-633
 70
 80FOR I=0 TO 79
 90VDU1,27,1,&2,1,5,1,0,1,2
100M=M0+(I*8)
110FOR J=0 TO 31
120FOR K=0 TO 7
130VDU1,?M,1,?M
140M=M-1:NEXT K
150M=M-632:NEXT J
160VDU1,13:NEXT I
170VDU1,12,1,27,1,2,1,18,3,7
180END
190
```

(XXXXXXXXXXX)

" OSAD "

```
  50 MODE7
 100 DIM I%(500)    :      DIM A%(500)
 110 CLS
 150 PRINT"FIRST CHOOSE VALUES OF INTENSITY BELOW AND ABOVE WHICH ANY OTHER REC
ORDED VALUES WILL BE IGNORED"
 200 INPUT"THE CHOSEN UPPER THRESHOLD VALUE IS  "Q1%
 250 INPUT"THE CHOSEN LOWER THRESHOLD VALUE IS  "Q0%
 300 PRINT"NOW CHOOSE THE INITIAL CHANNEL (WAVELENTH) LIMITS FOR THE INITIAL RE
GION OF INTEREST . NOTE OTHER REGIONS MAY BE SELECTED LATER "
 350 INPUT"THE CHOSEN LOWER WAVELENTH LIMIT  "L0%
 400 INPUT"THE CHOSEN UPPER WAVELENTH LIMIT  "L1%
 420 INPUT"THE CHOSEN LOWER CHANNEL LIMIT FOR CONTINUUM LEVEL ESTIMATION "X0%
 440 INPUT"THE CHOSEN UPPER CHANNEL LIMIT FOR CONTINUUM LEVEL ESTIMATION "X1%
 445 INPUT"THE CENTRE WAVELENGTH "LAMBDA
 450 INPUT"TIME BEFORE CURRENT ZERO "I0
 460 INPUT"dI/dT"DI
 470 INPUT"Tgate"Tgate
 480 INPUT"filename  "file$
 490 PRINT''''''
 500 MODE7:VDU 14
 520 PROCdatain
 850 C1%=1       : REM SET INITIAL VALUE OF Q
 855 J = 0  : J1 = 0  : REM J AND J1          ARE ARBITRARY COUNTERS
 860 IL = 0 :IR = 0
 870    PROCcontinuum
 900 FOR I = L0% TO L1%
 950   PROCpeakdetect
1000 NEXT I
1010 FOR I = L0% TO L1%
1020   PROClinewidth
1030 NEXT I
1050 PROCprint
1060 W = (INT(LAVR)-INT(LAVL))*4.8/310
1100 END
1150 DEFPROCpeakdetect
1200   C%=A%(I)
1300   IF C%<Q0% OR C%>Q1% THEN GOTO1450   : REM SPECIFY RANGE
1350     IF C% > C1% THEN CMAX% = C%     :     LC%=I%(I)
1400    C1%  = CMAX%
1450 ENDPROC
2000 DEFPROCdatain
2010 F%=OPENIN (file$)
2020 FOR I = 1 TO 499
2030 INPUT# F%,A%
2040 I%(I) = I   :     A%(I) = A%
2050 NEXT I
2060 CLOSE# F%
2070 ENDPROC
3000 DEFPROCcontinuum
3005 SUM = 0
3010 FOR I = X0% TO X1%
3020   SUM% = SUM% + A%(I)
3030 NEXT I
3040 CONT% = SUM%/(X1%-X0%)
3050 ENDPROC
3500 DEFPROClinewidth
3510 Y = A%(I) - CONT%
```

```
3520 IF(Y-(CMAX%-CONT%)/2) > 20 OR (Y-(CMAX%-CONT%)/2) < -20 THEN GOTO 3600
3540 PROClhs
3550 PROCrhs
3600 ENDPROC
4000 DEFPROClhs
4005 IF I > LCX THEN GOTO 4040
4020 J = J + 1  :   IL = IL + I
4030 LAVL = IL/J
4040 ENDPROC
4500 DEFPROCrhs
4505 IF I < LCX THEN GOTO 4540
4520 J1 = J1 + 1  :  IR = IR + I
4530 LAVR = IR/J1
4540 ENDPROC
5000 DEFPROCprint
5005 VDU2
5010 PRINT"filename = ";file$
5015PRINT
5020 PRINT"TIME BEFORE CURRENT ZERO = ";IO;" micS"
5025 PRINT
5030 PRINT"dI/dt =";DI;" Amps/micS"
5035 PRINT
5040 PRINT"Tgate =";Tgate;" micS"
5045 PRINT
5060 PRINT"CENTRE WAVELENGTH = ";LAMBDA;" nm"
5065 PRINT''
5070 W = (INT(LAVR)-INT(LAVL))*4.8/310
5080 @% = &00310
5090 PRINT"PEAK LINE INTENSITY = ";(CMAX%-CONT%);" COUNTS"
5095 PRINT
5100 PRINT"LINE WIDTH = ";W;" nm"
5150 PRINT ''''''''
5170 VDU3
5200 ENDPROC
```

<XXXXXXXXXXXX>

" TEMP "

```
 10 INPUT"UPPER ENERGY LEVEL FOR I1 IN eV    " E1
 20 INPUT"UPPER ENERGY LEVEL FOR I2 IN eV    " E2
 30 INPUT"LINE INTENSITY 1   "I1
 40 INPUT"LINE INTENSITY 2   "I2
 50 INPUT"LINE CENTRE WAVELENGTH 1   "L1
 60 INPUT"LINE CENTRE WAVELENGTH 2   "L2
 70 INPUT"STATISTICAL WEIGHT OF UPPER ENERGY LEVEL OF LINE 1   "GM1
 80 INPUT"STATISTICAL WEIGHT OF UPPER ENERGY LEVEL OF LINE 2   "GM2
 90 INPUT"TRANSITION PROBABILITY FOR LINE 1   "AMN1
100 INPUT"TRANSITION PROBABILITY FOR LINE 2   "AMN2
110 K = 1.38E-23
200 REM NOW CALCULATE THE ARC TEMPERATURE USING THE FOLLOWING EQUATION
210     T = ((E2-E1)/K)*1.6E-19/LN((I1/I2)*(L1/L2)*(GM2*AMN2)/(GM1*AMN1))
220 PRINT T
```

<XXXXXXXXXXXX>

" OPDEP "

```
   5 MODE7  :    @% = &10410
  10 REM PROGRAM TO CALCULATE THE THEORETICAL LINE INTENSITY AND CRITICAL
     OPTICAL DEPTH FOR A KNOWN TEMPERATURE AND PARTICLE DENSITY
  20 REM FIRST INPUT NECASSARY SPECTRAL DATA
  30 PROCinput
  40 PROCcalc
  50 PROCoutput
  60 @% = 10
1000 END
2000 DEFPROCinput
2010  DIM A(8) : DIM G(8) : DIM EM(8) : DIM EMN(8) : DIM L(8) : DIM DL(8)
2015  DIM T(128) : DIM Imn(128) : DIM D(128)
2020      FOR N = 0 TO 7
2030        READ A(N)
2080      NEXT N
2100      FOR N = 0 TO 7
2110        READ G(N)
2120      NEXT N
2150      FOR N = 0 TO 7
2160        READ EM(N)
2170      NEXT N
2200      FOR N = 0 TO 7
2210        READ EMN(N)
2220      NEXTN
2250      FOR N = 0 TO 7
2260        READ L(N)
2270      NEXT N
2280      FOR N = 0 TO 7
2290        READ DL(N)
2295      NEXT N
2300 REM INPUT THE RELEVANT CONSTANTS
2310     C1 = 1.1909E-12 : C2 = 1.4380          : C = 2.998E10
2320 Ne = 6E17  : REM THE AVERAGE                          ELECTRON DENSITY
2330 h = 4.136E-15 * 1.602E-19      :    K = 8.617E-5
2340 CLS
2350 INPUT" INPUT THE ARRAY INDEX NUMBER "X
2500  DATA 7.5E7,6.04E7,0.20E7,0.165E7,0.024E7,1.09E7,3.8E7,3.2E7
2510  DATA 6,4,4,2,4,8,8,6
2520  DATA 6.19,6.19,3.82,3.79,3.82,7.74,7.74,7.8
2530  DATA 2.37,2.40,2.43,2.15,2.18,2.35,2.67,2.7
2540  DATA 521.8,515.3,510.5,578.2,570.0,529.2,465.1,458.6
2550  DATA 0.415,0.458,0.166,0.217,0.217,0.759,0.248,0.31
2600 ENDPROC
3000 DEFPROCcalc
3010 LOCAL I
3020 CLS
3030 INPUT"THE FILENAME FOR THE PARTITION FUNCTION DATA"file$
3040 F = OPENIN(file$)
3050 FOR I = 0 TO 128
3060 INPUT£ F,T,ZT,ST,NZ
3065 PRINT T; ZT; ST; NZ
3070 PROCformulae
3075 T(I)=T : Imn(I)=Imn : D(I)=D
3200 NEXT I
3210 CLOSE£ F
3250 ENDPROC
4000 DEFPROCformulae
4050 IC = ((1/(4*PI))*NZ*G(X)*A(X)*(1/ZT)*h*C*(1/(L(X)*1E-7)))
4060 Imn = (IC)*(EXP(-EM(X)/(K*T)))
4100 B = (C1/(L(X)*1E-7)^5)/(EXP(C2/(L(X)*T*1E-7))-1)
4200 A = A(X)*G(X)*(EMN(X)*1.6E-19)*EXP(-(EM(X))/(K*T))
4300 D = 24*PI*ZT*(DL(X)*1E-7)*B/(NZ*A)
4800 ENDPROC
5000 DEFPROCoutput
5100 LOCAL I
5200 INPUT"THE OUTPUT FILENAME "file1$
5300 A = OPENOUT(file1$)
5350 VDU 2
5400 FOR I = 0 TO 128
5500 PRINT£ A,T(I),Imn(I),D(I)
5600 PRINT;  T(I);  Imn(I);  D(I)
5700 NEXT I
5720 PRINT£ A,L(X)
5730 PRINT; L(X)
5800 CLOSE£ A
5850 VDU 3
5900 ENDPROC
```

" IDISP "

```
  10 REM PROGRAM TO CALCULATE THE OBSERVED INTENSITY FROM A KNOWN RADIAL EMISSI
VITY PROFILE
  30 MODE3
  40   DIM Iy(10)  :  DIM AM(4)
 110 PROCinput
 120 DIM A(R/(10*dY))
 210 M = 0
 410 FOR Y = 0 TO (R - 0.0001) STEP 10*dY
 420 M = ((Y+0.0001)*10) DIV 1
 425 U = Y
 430 FOR S = U  TO M/10 + 0.1001 STEP dY
 440  PROCicalc(Y,Y+10*dY,S)
 450 NEXT S
 460  PROCsimp(Y,Y+10*dY)
 470 A(M) = AREA
 478 AREA1 = 0   :    AREA2 = 0   :   AREA3 = 0
 480 NEXT Y
 482 FOR d = 0 TO 0.5 STEP 0.1
 485 PROCdisp
 490 NEXT d
 905 VDU7
 910 VDU3     :    VDU30
1010 END
1110 DEF PROCinput
1210 INPUT" THE LINE SEPARATION IN mm dY = "dY
1310 INPUT" THE ARC RADIUS R = "R
1610 INPUT" THE MAXIMUM EMISSIVITY e0 = "e0
1710 PRINT''''
1750 AREA1 = 0   :    AREA2 = 0   :   AREA3 = 0
1810 ENDPROC
1910 DEF PROCicalc(Y1,Y2,Y)
1920 L = (100*(S-U+0.001)) DIV 1
1940 IF Y = 0 THEN GOTO 2650
1950 IF Y = R OR Y > R THEN GOTO 2650
2010  I1 = FNRY
2110  I3 = (R^2*FNRY/2 + (R*Y^2)*FNCOSH/2)
2210  I4 = (Y^2*R*FNCOSH - Y^2*FNRY)/2
2310  I5 = (FNRY)^3/3
2320  Iy = 2*e0*I1 - (e0*2/R^2)*(I3 - (I4 - I5))
2330  Iy(L) = Iy
2510 DEF FNRY = (R^2 - Y^2)^0.5
2610 DEF FNCOSH = (LN((R/Y) + ((R/Y)^2 - 1)^.5))
2650 ENDPROC
2700 DEFPROCsimp(Y1,Y2)
2705 N = (Y2-Y1)/dY
2710 IF Y = 0 THEN Iy(0) = Iy(1)
2720 AREA1 = ((Y2 -Y1)/(3*N))*(Iy(0) + Iy(10))
2730 AREA2 = ((Y2 -Y1)/(3*N))*2*(Iy(2) + Iy(4) + Iy(6) + Iy(8))
2740 AREA3 = ((Y2 -Y1)/(3*N))*4*(Iy(1) + Iy(3) + Iy(5) + Iy(7) + Iy(9))
2850  AREA = AREA1 + AREA2 + AREA3
2860 ENDPROC
3000 DEF PROCdisp
3010  ON (d*10 + 1) GOTO 3050,3150,3250,3350,3450,3550
3050     AM(0) = 2*(A(0)+A(1)+A(2)+A(3)+A(4))
3060     AM(1) = (A(5)+A(6)+A(7)+A(8)+A(9)+A(10)+A(11)+A(12)+A(13)+A(14))
3070     AM(2) = (A(15)+A(16)+A(17)+A(18)+A(19)+A(20)+A(21)+A(22)+A(23)+A(24))
3080     AM(3) = AM(1)
```

```
3090      AM(4) = AM(2)
3100     GOTO 3700
3150      AM(0) = A(5) + 2*(A(6)+A(4)+A(2)+A(1)+A(0)) + A(8)
3160      AM(1) = (A(6)+A(7)+A(8)+A(9)+A(10)+A(11)+A(12)+A(13)+A(14)+A(15))
3170      AM(2) = (A(16)+A(17)+A(18)+A(19)+A(20)+A(21)+A(22)+A(23)+A(24))
3180      AM(3) = (A(8)+A(5)+A(6)+A(7)+A(8)+A(9)+A(10)+A(11)+A(12)+A(13))
3190      AM(4) = (A(14)+A(15)+A(16)+A(17)+A(18)+A(19)+A(20)+A(21)+A(22)+A(23))
3200     GOTO 3700
3250      AM(0) = A(6)+A(5)+A(8)+A(3) + 2*(A(2)+A(1)+A(0))
3260      AM(1) = (A(7)+A(8)+A(9)+A(10)+A(11)+A(12)+A(13)+A(14)+A(15)+A(16))
3270      AM(2) = (A(17)+A(18)+A(19)+A(20)+A(21)+A(22)+A(23)+A(24))
3280      AM(3) = (A(3)+A(8)+A(5)+A(6)+A(7)+A(8)+A(9)+A(10)+A(11)+A(12))
3290      AM(4) = (A(13)+A(14)+A(15)+A(16)+A(17)+A(18)+A(19)+A(20)+A(21)+A(22))
3300     GOTO 3700
3350      AM(0) = A(7)+A(6)+A(5)+A(8)+A(3)+A(2) + 2*(A(1)+A(0))
3360      AM(1) = (A(8)+A(9)+A(10)+A(11)+A(12)+A(13)+A(14)+A(15)+A(16)+A(17))
3370      AM(2) = (A(18)+A(19)+A(20)+A(21)+A(22)+A(23)+A(24))
3380      AM(3) = (A(2)+A(3)+A(4)+A(5)+A(6)+A(7)+A(8)+A(9)+A(10)+A(11))
3390      AM(4) = (A(12)+A(13)+A(14)+A(15)+A(16)+A(17)+A(18)+A(19)+A(20)+A(21))
3400     GOTO 3700
3450      AM(0) = A(8)+A(7)+A(6)+A(5)+A(4)+A(3)+A(2)+A(1) + 2*(A(0))
3460      AM(1) = (A(9)+A(10)+A(11)+A(12)+A(13)+A(14)+A(15)+A(16)+A(17)+A(18))
3470      AM(2) = (A(19)+A(20)+A(21)+A(22)+A(23)+A(24))
3480      AM(3) = (A(1)+A(2)+A(3)+A(4)+A(5)+A(6)+A(7)+A(8)+A(9)+A(10))
3490      AM(4) = (A(11)+A(12)+A(13)+A(14)+A(15)+A(16)+A(17)+A(18)+A(19)+A(20))
3500     GOTO 3700
3550      AM(0) = A(9)+A(8)+A(7)+A(6)+A(5)+A(4)+A(3)+A(2)+A(1)+A(0)
3560      AM(1) = (A(10)+A(11)+A(12)+A(13)+A(14)+A(15)+A(16)+A(17)+A(18)+A(19))
3570      AM(2) = (A(20)+A(21)+A(22)+A(23)+A(24))
3580      AM(3) = (A(0)+A(1)+A(2)+A(3)+A(4)+A(5)+A(6)+A(7)+A(8)+A(9))
3590      AM(4) = (A(10)+A(11)+A(12)+A(13)+A(14)+A(15)+A(16)+A(17)+A(18)+A(19))
3600     GOTO 3700
3700     PRINT "ARC DISPLACEMENT d = "d
3710     PRINT'
3800    FOR W = 0 TO 4
3810     PRINT "THE TOTAL INTENSITY AT TRACK ";W;" = ";(AM(W)/AM(0))
3820     NEXT W
3825     PRINT'''
3830   ENDPROC
```

(XXXXXXXXXXX)

```
  10 REM PROGRAM TO CALCULATE THE OBSERVED INTENSITY FROM A KNOWN RADIAL EMISSIV
ITY PROFILE
  30 MODE3
  40   DIM Iy(10)  :  DIM AM(4)
 110 PROCinput
 120 DIM A(R/(10*dY))
 210 M = 0
 410 FOR Y = 0 TO (R - 0.0001) STEP 10*dY
 420 M = ((Y+0.0001)*10) DIV 1
 425 U = Y
 430 FOR S = U  TO M/10 + 0.1001 STEP dY
 440  PROCicalc(Y,Y+10*dY,S)
 450 NEXT S
 460  PROCsimp(Y,Y+10*dY)
 470 A(M) = AREA
 478 AREA1 = 0   :    AREA2 = 0   :   AREA3 = 0
 480 NEXT Y
 482 FOR d = 0 TO 1.0 STEP 0.1
 485 PROCdisp
 490 NEXT d
 905 VDU7
 910 VDU3     :    VDU30
1010 END
1110 DEF PROCinput
1210 INPUT" THE LINE SEPARATION IN mm dY = "dY
1310 INPUT" THE ARC RADIUS R = "R
1610 INPUT" THE MAXIMUM EMISSIVITY e0 = "e0
1710 PRINT''''
1750 AREA1 = 0   :    AREA2 = 0   :   AREA3 = 0
1810 ENDPROC
1910 DEF PROCicalc(Y1,Y2,Y)
1920 L = (100*(S-U+0.001)) DIV 1
1940 IF Y = 0 THEN GOTO 2650
1950 IF Y = R OR Y > R THEN GOTO 2650
2010  I1 = FNRY
2110  I2 =0.5*(R*FNRY + Y^2*FNCOSH)
2210  I3 = R^2*FNRY - 2*((R^2 - Y^2)^1.5)/3
2310  I4 = (3*Y^4*FNCOSH + FNRY*(3*R*Y^2 + 2*R^3))/8
2320  Iy = 2*e0*(I1 - 0.135*I2 + 0.2105*I3 -0.1094*I4)
2330  Iy(L) = Iy
2510 DEF FNRY = (R^2 - Y^2)^0.5
2610 DEF FNCOSH = (LN((R/Y) + ((R/Y)^2 - 1)^.5))
2650 ENDPROC
2700 DEFPROCsimp(Y1,Y2)
2705 N = (Y2-Y1)/dY
2710 IF Y = 0 THEN Iy(0) = Iy(1)
2720 AREA1 = ((Y2 -Y1)/(3*N))*(Iy(0) + Iy(10))
2730 AREA2 = ((Y2 -Y1)/(3*N))*2*(Iy(2) + Iy(4) + Iy(6) + Iy(8))
2740 AREA3 = ((Y2 -Y1)/(3*N))*4*(Iy(1) + Iy(3) + Iy(5) + Iy(7) + Iy(9))
2850  AREA = AREA1 + AREA2 + AREA3
2860 ENDPROC
3000 DEF PROCdisp
3010  ON (d*10 + 1) GOTO 3050,3150,3250,3350,3450,3550,3650,3750,3850,3950,4050
3050     AM(0) = 2*(A(0)+A(1)+A(2)+A(3)+A(4))
3060     AM(1) = (A(5)+A(6)+A(7)+A(8)+A(9)+A(10)+A(11)+A(12)+A(13)+A(14))
3070     AM(2) = (A(15)+A(16)+A(17)+A(18)+A(19)+A(20)+A(21)+A(22)+A(23)+A(24))
3080     AM(3) = AM(1)
3090     AM(4) = AM(2)
3100    GOTO 5000
3150     AM(0) = A(5) + 2*(A(3)+A(2)+A(1)+A(0)) + A(4)
```

```
3160      AM(1) = (A(6)+A(7)+A(8)+A(9)+A(10)+A(11)+A(12)+A(13)+A(14)+A(15))
3170      AM(2) = (A(16)+A(17)+A(18)+A(19)+A(20)+A(21)+A(22)+A(23)+A(24))
3180      AM(3) = (A(4)+A(5)+A(6)+A(7)+A(8)+A(9)+A(10)+A(11)+A(12)+A(13))
3190      AM(4) = (A(14)+A(15)+A(16)+A(17)+A(18)+A(19)+A(20)+A(21)+A(22)+A(23))
3200     GOTO 5000
3250      AM(0) = A(6)+A(5)+A(4)+A(3) + 2*(A(2)+A(1)+A(0))
3260      AM(1) = (A(7)+A(8)+A(9)+A(10)+A(11)+A(12)+A(13)+A(14)+A(15)+A(16))
3270      AM(2) = (A(17)+A(18)+A(19)+A(20)+A(21)+A(22)+A(23)+A(24))
3280      AM(3) = (A(3)+A(4)+A(5)+A(6)+A(7)+A(8)+A(9)+A(10)+A(11)+A(12))
3290      AM(4) = (A(13)+A(14)+A(15)+A(16)+A(17)+A(18)+A(19)+A(20)+A(21)+A(22))
3300     GOTO 5000
3350      AM(0) = A(7)+A(6)+A(5)+A(4)+A(3)+A(2) + 2*(A(1)+A(0))
3360      AM(1) = (A(8)+A(9)+A(10)+A(11)+A(12)+A(13)+A(14)+A(15)+A(16)+A(17))
3370      AM(2) = (A(18)+A(19)+A(20)+A(21)+A(22)+A(23)+A(24))
3380      AM(3) = (A(2)+A(3)+A(4)+A(5)+A(6)+A(7)+A(8)+A(9)+A(10)+A(11))
3390      AM(4) = (A(12)+A(13)+A(18)+A(15)+A(16)+A(17)+A(18)+A(19)+A(20)+A(21))
3400     GOTO 5000
3450      AM(0) = A(8)+A(7)+A(6)+A(5)+A(4)+A(3)+A(2)+A(1) + 2*(A(0))
3460      AM(1) = (A(9)+A(10)+A(11)+A(12)+A(13)+A(14)+A(15)+A(16)+A(17)+A(18))
3470      AM(2) = (A(19)+A(20)+A(21)+A(22)+A(23)+A(24))
3480      AM(3) = (A(1)+A(2)+A(3)+A(4)+A(5)+A(6)+A(7)+A(8)+A(9)+A(10))
3490      AM(4) = (A(11)+A(12)+A(13)+A(14)+A(15)+A(16)+A(17)+A(18)+A(19)+A(20))
3500     GOTO 5000
3550      AM(0) = A(9)+A(8)+A(7)+A(6)+A(5)+A(4)+A(3)+A(2)+A(1)+A(0)
3560      AM(1) = (A(10)+A(11)+A(12)+A(13)+A(14)+A(15)+A(16)+A(17)+A(18)+A(19))
3570      AM(2) = (A(20)+A(21)+A(22)+A(23)+A(24))
3580      AM(3) = (A(0)+A(1)+A(2)+A(3)+A(4)+A(5)+A(6)+A(7)+A(8)+A(9))
3590      AM(4) = (A(10)+A(11)+A(12)+A(13)+A(14)+A(15)+A(16)+A(17)+A(18)+A(19))
3600     GOTO 5000
3650      AM(0) = A(10)+A(9)+A(8)+A(7)+A(6)+A(5)+A(4)+A(3)+A(2)+A(1)
3660      AM(1) = A(11)+A(12)+A(13)+A(14)+A(15)+A(16)+A(17)+A(18)+A(19)+A(20)
3670      AM(2) = A(21)+A(22)+A(23)+A(24)
3680      AM(3) = A(0)+A(0)+A(1)+A(2)+A(3)+A(4)+A(5)+A(6)+A(7)+A(8)
3690      AM(4) = A(9)+A(10)+A(11)+A(12)+A(13)+A(14)+A(15)+A(16)+A(17)+A(18)
3700     GOTO 5000
3750      AM(0) = A(11)+A(10)+A(9)+A(8)+A(7)+A(6)+A(5)+A(4)+A(3)+A(2)
3760      AM(1) = A(12)+A(13)+A(14)+A(15)+A(16)+A(17)+A(18)+A(19)+A(20)+A(21)
3770      AM(2) = A(22)+A(23)+A(24)
3780      AM(3) = A(1)+A(0)+A(0)+A(1)+A(2)+A(3)+A(4)+A(5)+A(6)+A(7)
3790      AM(4) = A(8)+A(9)+A(10)+A(11)+A(12)+A(13)+A(14)+A(15)+A(16)+A(17)
3800     GOTO 5000
3850      AM(0) = A(12)+A(11)+A(10)+A(9)+A(8)+A(7)+A(6)+A(5)+A(4)+A(3)
3860      AM(1) = A(13)+A(14)+A(15)+A(16)+A(17)+A(18)+A(19)+A(20)+A(21)+A(22)
3870      AM(2) = A(23)+A(24)
3880      AM(3) = A(2)+A(1)+A(0)+A(0)+A(1)+A(2)+A(3)+A(4)+A(5)+A(6)
3890      AM(4) = A(7)+A(8)+A(9)+A(10)+A(11)+A(12)+A(13)+A(14)+A(15)+A(16)
3900     GOTO 5000
3950      AM(0) = A(13)+A(12)+A(11)+A(10)+A(9)+A(8)+A(7)+A(6)+A(5)+A(4)
3960      AM(1) = A(14)+A(15)+A(16)+A(17)+A(18)+A(19)+A(20)+A(21)+A(22)+A(23)
3970      AM(2) = A(24)
3980      AM(3) = A(3)+A(2)+A(1)+A(0)+A(0)+A(1)+A(2)+A(3)+A(4)+A(5)
3990      AM(4) = A(6)+A(7)+A(8)+A(9)+A(10)+A(11)+A(12)+A(13)+A(14)+A(15)
4000     GOTO 5000
4050      AM(0) = A(14)+A(13)+A(12)+A(11)+A(10)+A(9)+A(8)+A(7)+A(6)+A(5)
4060      AM(1) = A(15)+A(16)+A(17)+A(18)+A(19)+A(20)+A(21)+A(22)+A(23)+A(24)
4070      AM(2) = 0
4080      AM(3) = A(4)+A(3)+A(2)+A(1)+A(0)+A(0)+A(1)+A(2)+A(3)+A(4)
4090      AM(4) = AM(0)
4100     GOTO 5000
5000     PRINT "ARC DISPLACEMENT d = "d
5100     PRINT'
5200    FOR W = 0 TO 4
5210 IF d>0.5 THEN GOTO 5310
5300     PRINT "THE TOTAL INTENSITY AT TRACK ";W;" = ";(AM(W)/AM(0))
5310     PRINT "THE TOTAL INTENSITY AT TRACK ";W;" = ";(AM(W)/AM(3))
5400     NEXT W
5500     PRINT'''
5600   ENDPROC
```

" ABEL "

```
 5MODE 3
 10 REM PROGRAM TO CALCULATE THE ABEL INVERTED PROFILES WHEN THE
>       MEASURED INTENSITIES ARE KNOWN FOR DIFFERENT ARC DISPLACEMENTS
        WRT RECORDING ZONES
 20 PROCinput
 30 PROCcalc
 35CLS
 40 PROCaload
 50 PROCicalc
 60 END
100 DEF PROCinput
105  DIM R(3) : DIM DC(5)
110  Z = 1    :    REM DEFINE ZONE WIDTH
111 VDU2
112 INPUT "THE OBSERVED INTENSITY AT TRACK 1 = "I1
114 INPUT "THE OBSERVED INTENSITY AT TRACK 2 = "I2
116 INPUT "THE OBSERVED INTENSITY AT TRACK 3 = "I3
120  INPUT "RADIAL ARC DISPLACEMENT BETWEEN -0.5 AND +0.5 = "X
122 VDU3
125GOTO140
130  PROCeraseline
140  FOR N = 1 TO 3
150    READ R(N)
160  NEXT N
170  FOR N = 0 TO 5
180   DC(N) = ((X + (2.5*Z-N))^2)^.5
190  NEXT N
200  DATA 3,2,1
210 ENDPROC
400 DEF PROCcalc
410  PROCacalc(DC(0),R(1))
420 A10 = A
425 PRINT"A10 = ";A
430   PROCacalc(DC(1),R(1))
440 A1A2A0 = A
450 A1A2 = A1A2A0 - A10
460  PROCacalc(DC(1),R(2))
470 A12 = A
480 PRINT"A12 = ";A
490 A11 = A1A2 - A12
500 PRINT" A11 = ";A11
510  PROCacalc(DC(2),R(1))
520 AX = A       : REM AX = (A10+A11+A12) + (A21+A22+A23)
525 A1A2A3 = AX - A1A2A0
530  PROCacalc(DC(2),R(2))
540 A2A2A3 = A
550 A2A3 = A2A2A3 - A12
560 A21 = A1A2A3 -A2A3
570 PRINT" A21 = ";A21
580  PROCacalc(DC(2),R(3))
590 A23 = A
600 PRINT"A23 = ";A23
610 A22 = A2A3 - A23
620 PRINT"A22 = ";A22
630 AT3 = (PI)*(R(3))^2/4
640 A33 = AT3 - A23
650 PRINT"A33 = ";A33
660 AT = PI*(R(1))^2/4 : REM AT IS .25 OF TOTAL AREA OF CIRCLE
670 AT2 = PI*(R(2))^2/4 : REM AT2 IS .25 OF AREA OF RING 2
680 A32 = AT2 - A12 - A2A3 - A33
690 PRINT "A32 = ";A32
700 A31 = AT - A10 - A1A2 - A1A2A3 - A32 - A33
710 PRINT"A31 = ";A31
720  PROCacalc(DC(5),R(1))
730 A50 = A
740  PROCacalc(DC(4),R(1))
750 A5012 = A : REM A5012 = A50 + A51 + A52
760 PROCacalc(DC(4),R(2))
770 A52 = A
```

```
 780 PRINT "A52 = ";A52
 790 A51 = A5012 - A50 -A52
 800 PRINT "A51 = ";A51
 820  PROCacalc(DC(3),R(3))
 830 A43 = A
 840 PRINT "A43 = ";A43
 850  PROCacalc(DC(3),R(2))
 860 A432A5 = A   : REM A432A5 = A43 + A42 + A52
 870 A42 = A432A5 - A43 - A52
 880 PRINT "A42 = ";A42
 890  PROCacalc(DC(3),R(1))
 900 A4TA5T = A    :    REM  A4T5T = A41+A42+A43 + A51+A52+A50
 910 A41 = A4TA5T - A42 - A43 - A5012
 920 PRINT"A41 = ";A41
 930 a33 = AT3 - A43
 935 PRINT "a33 = ";a33
 940 a32 = AT2 - a33 - A42 - A43 - A52
 950 PRINT "a32 = ";a32
 960 a31 = AT - a32 - a33 - A42 - A43 - A41 - A5012
 970 PRINT "a31 = ";a31
 980 ENDPROC
1600 DEF PROCacalc(D,R)
1620  LOCAL Q
1630  Q = 2*ASN((1 - (D/R)^2)^.5)
1640  A = .25*(R)^2*(Q - SIN(Q))
1660 ENDPROC
2000 DEF PROCaload
2010 LOCAL M,N
2015 DIM A(5,3)
2020 A31 = A31 + a31   :   A32 = A32 + a32   :   A33 = A33 + a33
2030 FOR M = 1 TO 5
2040  FOR N = 1 TO 3
2050   READ A(M,N)
2055PRINT TAB(N*15,M*3);  A(M,N)
2060  NEXT N
2070 NEXT M
2200 DATA A11,A12,0
2210 DATA A21,A22,A23
2220 DATA A31,A32,A33
2230 DATA A41,A42,A43
2240 DATA A51,A52,0
2250 ENDPROC
3000 DEF PROCicalc
3010 AP = A(3,2)*A(2,3) - A(2,2)*A(3,3)
3020 AQ = A(3,1)*A(2,3) - A(2,1)*A(3,3)
3040 REM  CALCULATE INVERTED INTESITY OF EACH RING
3050 i1 = (I3*A(2,3)*A(1,2) -I2*A(3,3)*A(1,2) - I1*AP)/(2*(A(1,2)*AQ -A(1,1)*AP
))
3060 i2 = (I1 - 2*i1*A(1,1))/(2*A(1,2))
3070 i3 = (I3 - 2*i1*A(3,1)- 2*i2*A(3,2))/(2*A(3,3))
3072 VDU2
3075 PRINT '''
3080 PRINT "THE ABEL INVERTED INTENSITY OF TRACK 1 ="; i1
3090 PRINT "THE ABEL INVERTED INTENSITY OF TRACK 2 ="; i2
3100 PRINT "THE ABEL INVERTED INTENSITY OF TRACK 3 ="; i3
3110 PRINT ''''''
3120 VDU3
3200 ENDPROC
```

(XXXXXXXXXXX)

```
C     PROGRAM TO CACULATE THE OBSERVED INTENSITY FROM A KNOWN RADIAL
C     EMISSIVITY PROFILE
      REAL BY(0:10),AM(1:5),A(0:50),X(1:5)
      COMMON DY,R,E0,S,U,D,AREA,AREA1,AREA2,AREA3,BY,AM,A
      DY=0.01
      DO 200 R=0.5,2.5,0.5
      WRITE(6,10)R
 10   FORMAT (/,10X,' ARC RADIUS R= ', F5.2/,
     &          10X,'---------------------')
      E0=1.0
      DO 100 Y=0,(R-0.0001),(10*DY)
      M=NINT((Y+0.0001)*10)
      U=Y
      DO 50 S=U,((0.1*M)+0.1001),DY
      CALL ICALC(Y)
 50   CONTINUE
      CALL SIMP(Y,(Y+(10*DY)))
      A(M)=AREA
      AREA1=0.0
      AREA2=0.0
      AREA3=0.0
 100  CONTINUE
      DO 150 D=0,1.0,0.1
      CALL DISP
 150  CONTINUE
 200  CONTINUE
      STOP
      END
      SUBROUTINE ICALC (Y)
      REAL BY(0:10), AM(1:5), A(0:50)
      COMMON DY,R,E0,S,U,D,AREA,AREA1,AREA2,AREA3,BY,AM,A
      L=NINT(100*(S-U+0.001))
      IF (S .EQ. 0) GO TO 2650
      IF (S .GE. R) GO TO 2650
      FNRY = (R**2-Y**2)**1.5
      B1=FNRY
      B2=3.0*R**2
      BI=4.0*E0*B1/B2
      BY(L)=BI
 2650 RETURN
      END
      SUBROUTINE SIMP (Y1,Y2)
      REAL BY(0:10), AM(1:5), A(0:50)
      COMMON DY,R,E0,S,U,D,AREA,AREA1,AREA2,AREA3,BY,AM,A
      C=(Y2-Y1)/DY
      IF (Y .EQ. 0) BY(0)=BY(1)
      AREA1= ((Y2-Y1)/(3.0*C))*(BY(0)+BY(10))
      AREA2= ((Y2-Y1)/(3.0*C))*2*(BY(2)+BY(4)+BY(6)+BY(8))
      AREA3= ((Y2-Y1)/(3.0*C))*4*(BY(1)+BY(3)+BY(5)+BY(7)+BY(9))
      AREA = AREA1 + AREA2 + AREA3
      RETURN
      END
      SUBROUTINE DISP
```

```
      REAL BY(0:10), AM(1:5), A(0:50),X(1:5)
      COMMON DY,R,E0,S,U,D,AREA,AREA1,AREA2,AREA3,BY,AM,A
      N1 = 1 + (D*10)
      GO TO (3050,3150,3250,3350,3450,3550,3650,3750,3850,3950,4050),N1
3050  AM(3) = 2.0*(A(0)+A(1)+A(2)+A(3)+A(4))
      AM(2) = (A(5)+A(6)+A(7)+A(8)+A(9)+A(10)+A(11)+A(12)+A(13)+A(14))
      AM(1) = (A(15)+A(16)+A(17)+A(18)+A(19)+A(20)+A(21)+A(22)+A(23)+
     *A(24))
      AM(4) =AM(2)
      AM(5) = AM(1)
      GO TO 5000
3150  AM(3) = A(5)+2.0*(A(0)+A(1)+A(2)+A(3))+A(4)
      AM(2) = A(6)+A(7)+A(8)+A(9)+A(10)+A(11)+A(12)+A(13)+A(14)+A(15)
      AM(1) = A(16)+A(17)+A(18)+A(19)+A(20)+A(21)+A(22)+A(23)+A(24)
      AM(4) = A(4)+A(5)+A(6)+A(7)+A(8)+A(9)+A(10)+A(11)+A(12)+A(13)
      AM(5) = A(14)+A(15)+A(16)+A(17)+A(18)+A(19)+A(20)+A(21)+A(22)+
     *A(23)
      GO TO 5000
3250  AM(3) = A(6)+A(5)+A(4)+A(3)+2.0*(A(0)+A(1)+A(2))
      AM(2) = A(7)+A(8)+A(9)+A(10)+A(11)+A(12)+A(13)+A(14)+A(15)+A(16)
      AM(1) = A(17)+A(18)+A(19)+A(20)+A(21)+A(22)+A(23)+A(24)
      AM(4) = A(3)+A(4)+A(5)+A(6)+A(7)+A(8)+A(9)+A(10)+A(11)+A(12)
      AM(5) = A(13)+A(14)+A(15)+A(16)+A(17)+A(18)+A(19)+A(20)+A(21)+
     *A(22)
      GO TO 5000
3350  AM(3) = A(7)+A(6)+A(5)+A(4)+A(3)+A(2)+2.0*(A(0)+A(1))
      AM(2) = A(8)+A(9)+A(10)+A(11)+A(12)+A(13)+A(14)+A(15)+A(16)+A(17)
      AM(1) = A(18)+A(19)+A(20)+A(21)+A(22)+A(23)+A(24)
      AM(4) = A(2)+A(3)+A(4)+A(5)+A(6)+A(7)+A(8)+A(9)+A(10)+A(11)
      AM(5) = A(12)+A(13)+A(14)+A(15)+A(16)+A(17)+A(18)+A(19)+A(20)+
     *A(21)
      GO TO 5000
3450  AM(3) = A(8)+A(7)+A(6)+A(5)+A(4)+A(3)+A(2)+A(1)+2.0*(A(0))
      AM(2) = A(9)+A(10)+A(11)+A(12)+A(13)+A(14)+A(15)+A(16)+A(17)+
     *A(18)
      AM(1) = A(19)+A(20)+A(21)+A(22)+A(23)+A(24)
      AM(4) = A(1)+A(2)+A(3)+A(4)+A(5)+A(6)+A(7)+A(8)+A(9)+A(10)
      AM(5) = A(11)+A(12)+A(13)+A(14)+A(15)+A(16)+A(17)+A(18)+A(19)+
     *A(20)
      GO TO 5000
3550  AM(3) = A(9)+A(8)+A(7)+A(6)+A(5)+A(4)+A(3)+A(2)+A(1)+A(0)
      AM(2) = A(10)+A(11)+A(12)+A(13)+A(14)+A(15)+A(16)+A(17)+A(18)+
     *A(19)
      AM(1) = A(20)+A(21)+A(22)+A(23)+A(24)
      AM(4) = A(0)+A(1)+A(2)+A(3)+A(4)+A(5)+A(6)+A(7)+A(8)+A(9)
      AM(5) = A(10)+A(11)+A(12)+A(13)+A(14)+A(15)+A(16)+A(17)+A(18)+
     *A(19)
      GO TO 5000
3650  AM(3) = A(10)+A(9)+A(8)+A(7)+A(6)+A(5)+A(4)+A(3)+A(2)+A(1)
      AM(2) = A(11)+A(12)+A(13)+A(14)+A(15)+A(16)+A(17)+A(18)+A(19)+
     *A(20)
      AM(1) = A(21)+A(22)+A(23)+A(24)
      AM(4) = A(0)+A(0)+A(1)+A(2)+A(3)+A(4)+A(5)+A(6)+A(7)+A(8)
      AM(5) = A(9)+A(10)+A(11)+A(12)+A(13)+A(14)+A(15)+A(16)+A(17)+
     *A(18)
      GO TO 5000
```

```
3750 AM(3) = A(11)+A(10)+A(9)+A(8)+A(7)+A(6)+A(5)+A(4)+A(3)+A(2)
     AM(2) = A(12)+A(13)+A(14)+A(15)+A(16)+A(17)+A(18)+A(19)+A(20)+
    *A(21)
     AM(1) = A(22)+A(23)+A(24)
     AM(4) = A(1)+A(0)+A(0)+A(1)+A(2)+A(3)+A(4)+A(5)+A(6)+A(7)
     AM(5) = A(8)+A(9)+A(10)+A(11)+A(12)+A(13)+A(14)+A(15)+A(16)+
    *A(17)
     GO TO 5000
3850 AM(3) = A(12)+A(11)+A(10)+A(9)+A(8)+A(7)+A(6)+A(5)+A(4)+A(3)
     AM(2) = A(13)+A(14)+A(15)+A(16)+A(17)+A(18)+A(19)+A(20)+A(21)+
    *A(22)
     AM(1) = A(23)+A(24)
     AM(4) = A(2)+A(1)+A(0)+A(0)+A(1)+A(2)+A(3)+A(4)+A(5)+A(6)
     AM(5) = A(7)+A(8)+A(9)+A(10)+A(11)+A(12)+A(13)+A(14)+A(15)+
    *A(16)
     GO TO 5000
3950 AM(3) = A(13)+A(12)+A(11)+A(10)+A(9)+A(8)+A(7)+A(6)+A(5)+A(4)
     AM(2) = A(14)+A(15)+A(16)+A(17)+A(18)+A(19)+A(20)+A(21)+A(22)+
    *A(23)
     AM(1) = A(24)
     AM(4) = A(3)+A(2)+A(1)+A(0)+A(0)+A(1)+A(2)+A(3)+A(4)+A(5)
     AM(5) = A(6)+A(7)+A(8)+A(9)+A(10)+A(11)+A(12)+A(13)+A(14)+
    *A(15)
     GO TO 5000
4050 AM(3) = A(14)+A(13)+A(12)+A(11)+A(10)+A(9)+A(8)+A(7)+A(6)+A(5)
     AM(2) = A(15)+A(16)+A(17)+A(18)+A(19)+A(20)+A(21)+A(22)+A(23)+
    *A(24)
     AM(1) = 0.0
     AM(4) = A(4)+A(3)+A(2)+A(1)+A(0)+A(0)+A(1)+A(2)+A(3)+A(4)
     AM(5) = AM(3)
     GO TO 5000
5000 WRITE (6,6000)D
     WRITE (6,6001)
6000 FORMAT (' ARC DISPLACEMENT D= ', F5.2)
6001 FORMAT (' --------------------')
     DO 5010 I=1,5,1
     IF(D-0.5) 99,99,999
99   RATIO = AM(I)/AM(3)
     GO TO 9999
999  RATIO = AM(I)/AM(4)
9999 WRITE(1,5555) RATIO
     WRITE (6,6010)I,RATIO
5010 CONTINUE
     WRITE(6,*)
     WRITE(6,*)
6010 FORMAT (' THE TOTAL INTENSITY AT TRACK ',I2,' = ', E15.5)
5555 FORMAT(2F6.3)
     RETURN
     END
```

xxxxxxxxxxxxx

" I515N OUT "

ARC RADIUS R= 0.50

ARC DISPLACEMENT D= 0.00

THE TOTAL INTENSITY AT TRACK 1 = 0.00000E+00
THE TOTAL INTENSITY AT TRACK 2 = 0.00000E+00
THE TOTAL INTENSITY AT TRACK 3 = 0.10000E+01
THE TOTAL INTENSITY AT TRACK 4 = 0.00000E+00
THE TOTAL INTENSITY AT TRACK 5 = 0.00000E+00

ARC DISPLACEMENT D= 0.10

THE TOTAL INTENSITY AT TRACK 1 = 0.00000E+00
THE TOTAL INTENSITY AT TRACK 2 = 0.00000E+00
THE TOTAL INTENSITY AT TRACK 3 = 0.10000E+01
THE TOTAL INTENSITY AT TRACK 4 = 0.32428E-01
THE TOTAL INTENSITY AT TRACK 5 = 0.00000E+00

ARC DISPLACEMENT D= 0.20

THE TOTAL INTENSITY AT TRACK 1 = 0.00000E+00
THE TOTAL INTENSITY AT TRACK 2 = 0.00000E+00
THE TOTAL INTENSITY AT TRACK 3 = 0.10000E+01
THE TOTAL INTENSITY AT TRACK 4 = 0.11839E+00
THE TOTAL INTENSITY AT TRACK 5 = 0.00000E+00

ARC DISPLACEMENT D= 0.30

THE TOTAL INTENSITY AT TRACK 1 = 0.00000E+00
THE TOTAL INTENSITY AT TRACK 2 = 0.00000E+00
THE TOTAL INTENSITY AT TRACK 3 = 0.10000E+01
THE TOTAL INTENSITY AT TRACK 4 = 0.27846E+00
THE TOTAL INTENSITY AT TRACK 5 = 0.00000E+00

ARC DISPLACEMENT D= 0.40

THE TOTAL INTENSITY AT TRACK 1 = 0.00000E+00
THE TOTAL INTENSITY AT TRACK 2 = 0.00000E+00
THE TOTAL INTENSITY AT TRACK 3 = 0.10000E+01
THE TOTAL INTENSITY AT TRACK 4 = 0.54939E+00
THE TOTAL INTENSITY AT TRACK 5 = 0.00000E+00

ARC DISPLACEMENT D= 0.50

THE TOTAL INTENSITY AT TRACK 1 = 0.00000E+00
THE TOTAL INTENSITY AT TRACK 2 = 0.00000E+00
THE TOTAL INTENSITY AT TRACK 3 = 0.10000E+01
THE TOTAL INTENSITY AT TRACK 4 = 0.10000E+01
THE TOTAL INTENSITY AT TRACK 5 = 0.00000E+00

ARC DISPLACEMENT D= 0.60

THE TOTAL INTENSITY AT TRACK 1 = 0.00000E+00
THE TOTAL INTENSITY AT TRACK 2 = 0.00000E+00
THE TOTAL INTENSITY AT TRACK 3 = 0.54939E+00
THE TOTAL INTENSITY AT TRACK 4 = 0.10000E+01
THE TOTAL INTENSITY AT TRACK 5 = 0.00000E+00

ARC DISPLACEMENT D= 0.70

THE TOTAL INTENSITY AT TRACK 1 = 0.00000E+00
THE TOTAL INTENSITY AT TRACK 2 = 0.00000E+00
THE TOTAL INTENSITY AT TRACK 3 = 0.27846E+00
THE TOTAL INTENSITY AT TRACK 4 = 0.10000E+01
THE TOTAL INTENSITY AT TRACK 5 = 0.00000E+00

ARC DISPLACEMENT D= 0.80

THE TOTAL INTENSITY AT TRACK 1 = 0.00000E+00
THE TOTAL INTENSITY AT TRACK 2 = 0.00000E+00
THE TOTAL INTENSITY AT TRACK 3 = 0.11839E+00
THE TOTAL INTENSITY AT TRACK 4 = 0.10000E+01
THE TOTAL INTENSITY AT TRACK 5 = 0.00000E+00

ARC DISPLACEMENT D= 0.90

THE TOTAL INTENSITY AT TRACK 1 = 0.00000E+00
THE TOTAL INTENSITY AT TRACK 2 = 0.00000E+00
THE TOTAL INTENSITY AT TRACK 3 = 0.32428E-01
THE TOTAL INTENSITY AT TRACK 4 = 0.10000E+01
THE TOTAL INTENSITY AT TRACK 5 = 0.00000E+00

ARC RADIUS R= 1.00

ARC DISPLACEMENT D= 0.00

THE TOTAL INTENSITY AT TRACK 1 = 0.00000E+00
THE TOTAL INTENSITY AT TRACK 2 = 0.19990E+00
THE TOTAL INTENSITY AT TRACK 3 = 0.10000E+01
THE TOTAL INTENSITY AT TRACK 4 = 0.19990E+00
THE TOTAL INTENSITY AT TRACK 5 = 0.00000E+00

ARC DISPLACEMENT D= 0.10

THE TOTAL INTENSITY AT TRACK 1 = 0.00000E+00
THE TOTAL INTENSITY AT TRACK 2 = 0.13046E+00
THE TOTAL INTENSITY AT TRACK 3 = 0.10000E+01
THE TOTAL INTENSITY AT TRACK 4 = 0.28805E+00

THE TOTAL INTENSITY AT TRACK 5 = 0.00000E+00

ARC DISPLACEMENT D= 0.20

THE TOTAL INTENSITY AT TRACK 1 = 0.00000E+00
THE TOTAL INTENSITY AT TRACK 2 = 0.76644E-01
THE TOTAL INTENSITY AT TRACK 3 = 0.10000E+01
THE TOTAL INTENSITY AT TRACK 4 = 0.40025E+00
THE TOTAL INTENSITY AT TRACK 5 = 0.00000E+00

ARC DISPLACEMENT D= 0.30

THE TOTAL INTENSITY AT TRACK 1 = 0.00000E+00
THE TOTAL INTENSITY AT TRACK 2 = 0.37008E-01
THE TOTAL INTENSITY AT TRACK 3 = 0.10000E+01
THE TOTAL INTENSITY AT TRACK 4 = 0.54532E+00
THE TOTAL INTENSITY AT TRACK 5 = 0.00000E+00

ARC DISPLACEMENT D= 0.40

THE TOTAL INTENSITY AT TRACK 1 = 0.00000E+00
THE TOTAL INTENSITY AT TRACK 2 = 0.11337E-01
THE TOTAL INTENSITY AT TRACK 3 = 0.10000E+01
THE TOTAL INTENSITY AT TRACK 4 = 0.73756E+00
THE TOTAL INTENSITY AT TRACK 5 = 0.00000E+00

ARC DISPLACEMENT D= 0.50

THE TOTAL INTENSITY AT TRACK 1 = 0.00000E+00
THE TOTAL INTENSITY AT TRACK 2 = 0.00000E+00
THE TOTAL INTENSITY AT TRACK 3 = 0.10000E+01
THE TOTAL INTENSITY AT TRACK 4 = 0.10000E+01
THE TOTAL INTENSITY AT TRACK 5 = 0.00000E+00

ARC DISPLACEMENT D= 0.60

THE TOTAL INTENSITY AT TRACK 1 = 0.00000E+00
THE TOTAL INTENSITY AT TRACK 2 = 0.00000E+00
THE TOTAL INTENSITY AT TRACK 3 = 0.73756E+00
THE TOTAL INTENSITY AT TRACK 4 = 0.10000E+01
THE TOTAL INTENSITY AT TRACK 5 = 0.11337E-01

ARC DISPLACEMENT D= 0.70

THE TOTAL INTENSITY AT TRACK 1 = 0.00000E+00
THE TOTAL INTENSITY AT TRACK 2 = 0.00000E+00
THE TOTAL INTENSITY AT TRACK 3 = 0.54532E+00
THE TOTAL INTENSITY AT TRACK 4 = 0.10000E+01
THE TOTAL INTENSITY AT TRACK 5 = 0.37008E-01

ARC DISPLACEMENT D= 0.80

THE TOTAL INTENSITY AT TRACK 1 = 0.00000E+00
THE TOTAL INTENSITY AT TRACK 2 = 0.00000E+00
THE TOTAL INTENSITY AT TRACK 3 = 0.40025E+00
THE TOTAL INTENSITY AT TRACK 4 = 0.10000E+01
THE TOTAL INTENSITY AT TRACK 5 = 0.76644E-01

ARC DISPLACEMENT D= 0.90

THE TOTAL INTENSITY AT TRACK 1 = 0.00000E+00
THE TOTAL INTENSITY AT TRACK 2 = 0.00000E+00
THE TOTAL INTENSITY AT TRACK 3 = 0.28805E+00
THE TOTAL INTENSITY AT TRACK 4 = 0.10000E+01
THE TOTAL INTENSITY AT TRACK 5 = 0.13046E+00

ARC RADIUS R= 1.50

ARC DISPLACEMENT D= 0.00

THE TOTAL INTENSITY AT TRACK 1 = 0.00000E+00
THE TOTAL INTENSITY AT TRACK 2 = 0.47180E+00
THE TOTAL INTENSITY AT TRACK 3 = 0.10000E+01
THE TOTAL INTENSITY AT TRACK 4 = 0.47180E+00
THE TOTAL INTENSITY AT TRACK 5 = 0.00000E+00

ARC DISPLACEMENT D= 0.10

THE TOTAL INTENSITY AT TRACK 1 = 0.00000E+00
THE TOTAL INTENSITY AT TRACK 2 = 0.38686E+00
THE TOTAL INTENSITY AT TRACK 3 = 0.10000E+01
THE TOTAL INTENSITY AT TRACK 4 = 0.56355E+00
THE TOTAL INTENSITY AT TRACK 5 = 0.48463E-02

ARC DISPLACEMENT D= 0.20

THE TOTAL INTENSITY AT TRACK 1 = 0.00000E+00
THE TOTAL INTENSITY AT TRACK 2 = 0.31180E+00
THE TOTAL INTENSITY AT TRACK 3 = 0.10000E+01
THE TOTAL INTENSITY AT TRACK 4 = 0.66087E+00
THE TOTAL INTENSITY AT TRACK 5 = 0.18176E-01

ARC DISPLACEMENT D= 0.30

THE TOTAL INTENSITY AT TRACK 1 = 0.00000E+00
THE TOTAL INTENSITY AT TRACK 2 = 0.24540E+00
THE TOTAL INTENSITY AT TRACK 3 = 0.10000E+01
THE TOTAL INTENSITY AT TRACK 4 = 0.76461E+00
THE TOTAL INTENSITY AT TRACK 5 = 0.42486E-01

ARC DISPLACEMENT D= 0.40

THE TOTAL INTENSITY AT TRACK 1 = 0.00000E+00
THE TOTAL INTENSITY AT TRACK 2 = 0.18682E+00
THE TOTAL INTENSITY AT TRACK 3 = 0.10000E+01
THE TOTAL INTENSITY AT TRACK 4 = 0.87667E+00
THE TOTAL INTENSITY AT TRACK 5 = 0.80468E-01

ARC DISPLACEMENT D= 0.50

THE TOTAL INTENSITY AT TRACK 1 = 0.00000E+00
THE TOTAL INTENSITY AT TRACK 2 = 0.13562E+00
THE TOTAL INTENSITY AT TRACK 3 = 0.10000E+01
THE TOTAL INTENSITY AT TRACK 4 = 0.10000E+01
THE TOTAL INTENSITY AT TRACK 5 = 0.13562E+00

ARC DISPLACEMENT D= 0.60

THE TOTAL INTENSITY AT TRACK 1 = 0.00000E+00
THE TOTAL INTENSITY AT TRACK 2 = 0.80468E-01
THE TOTAL INTENSITY AT TRACK 3 = 0.87667E+00
THE TOTAL INTENSITY AT TRACK 4 = 0.10000E+01
THE TOTAL INTENSITY AT TRACK 5 = 0.18682E+00

ARC DISPLACEMENT D= 0.70

THE TOTAL INTENSITY AT TRACK 1 = 0.00000E+00
THE TOTAL INTENSITY AT TRACK 2 = 0.42486E-01
THE TOTAL INTENSITY AT TRACK 3 = 0.76461E+00
THE TOTAL INTENSITY AT TRACK 4 = 0.10000E+01
THE TOTAL INTENSITY AT TRACK 5 = 0.24540E+00

ARC DISPLACEMENT D= 0.80

THE TOTAL INTENSITY AT TRACK 1 = 0.00000E+00
THE TOTAL INTENSITY AT TRACK 2 = 0.18176E-01
THE TOTAL INTENSITY AT TRACK 3 = 0.66087E+00
THE TOTAL INTENSITY AT TRACK 4 = 0.10000E+01
THE TOTAL INTENSITY AT TRACK 5 = 0.31180E+00

ARC DISPLACEMENT D= 0.90

THE TOTAL INTENSITY AT TRACK 1 = 0.00000E+00
THE TOTAL INTENSITY AT TRACK 2 = 0.48463E-02
THE TOTAL INTENSITY AT TRACK 3 = 0.56355E+00
THE TOTAL INTENSITY AT TRACK 4 = 0.10000E+01
THE TOTAL INTENSITY AT TRACK 5 = 0.38686E+00

ARC RADIUS R= 2.00

ARC DISPLACEMENT D= 0.00

THE TOTAL INTENSITY AT TRACK 1 = 0.78230E-01
THE TOTAL INTENSITY AT TRACK 2 = 0.67784E+00
THE TOTAL INTENSITY AT TRACK 3 = 0.10000E+01
THE TOTAL INTENSITY AT TRACK 4 = 0.67784E+00
THE TOTAL INTENSITY AT TRACK 5 = 0.78230E-01

ARC DISPLACEMENT D= 0.10

THE TOTAL INTENSITY AT TRACK 1 = 0.48795E-01
THE TOTAL INTENSITY AT TRACK 2 = 0.61666E+00
THE TOTAL INTENSITY AT TRACK 3 = 0.10000E+01
THE TOTAL INTENSITY AT TRACK 4 = 0.73928E+00
THE TOTAL INTENSITY AT TRACK 5 = 0.11587E+00

ARC DISPLACEMENT D= 0.20

THE TOTAL INTENSITY AT TRACK 1 = 0.26898E-01
THE TOTAL INTENSITY AT TRACK 2 = 0.55535E+00
THE TOTAL INTENSITY AT TRACK 3 = 0.10000E+01
THE TOTAL INTENSITY AT TRACK 4 = 0.80152E+00
THE TOTAL INTENSITY AT TRACK 5 = 0.16255E+00

ARC DISPLACEMENT D= 0.30

THE TOTAL INTENSITY AT TRACK 1 = 0.11945E-01
THE TOTAL INTENSITY AT TRACK 2 = 0.49362E+00
THE TOTAL INTENSITY AT TRACK 3 = 0.10000E+01
THE TOTAL INTENSITY AT TRACK 4 = 0.86518E+00
THE TOTAL INTENSITY AT TRACK 5 = 0.21934E+00

ARC DISPLACEMENT D= 0.40

THE TOTAL INTENSITY AT TRACK 1 = 0.32891E-02
THE TOTAL INTENSITY AT TRACK 2 = 0.43147E+00
THE TOTAL INTENSITY AT TRACK 3 = 0.10000E+01
THE TOTAL INTENSITY AT TRACK 4 = 0.93104E+00
THE TOTAL INTENSITY AT TRACK 5 = 0.28764E+00

ARC DISPLACEMENT D= 0.50

THE TOTAL INTENSITY AT TRACK 1 = 0.00000E+00
THE TOTAL INTENSITY AT TRACK 2 = 0.36930E+00
THE TOTAL INTENSITY AT TRACK 3 = 0.10000E+01
THE TOTAL INTENSITY AT TRACK 4 = 0.10000E+01
THE TOTAL INTENSITY AT TRACK 5 = 0.36930E+00

ARC DISPLACEMENT D= 0.60

THE TOTAL INTENSITY AT TRACK 1 = 0.00000E+00
THE TOTAL INTENSITY AT TRACK 2 = 0.28764E+00
THE TOTAL INTENSITY AT TRACK 3 = 0.93104E+00
THE TOTAL INTENSITY AT TRACK 4 = 0.10000E+01
THE TOTAL INTENSITY AT TRACK 5 = 0.43147E+00

ARC DISPLACEMENT D= 0.70

THE TOTAL INTENSITY AT TRACK 1 = 0.00000E+00
THE TOTAL INTENSITY AT TRACK 2 = 0.21934E+00
THE TOTAL INTENSITY AT TRACK 3 = 0.86518E+00
THE TOTAL INTENSITY AT TRACK 4 = 0.10000E+01
THE TOTAL INTENSITY AT TRACK 5 = 0.49362E+00

ARC DISPLACEMENT D= 0.80

THE TOTAL INTENSITY AT TRACK 1 = 0.00000E+00
THE TOTAL INTENSITY AT TRACK 2 = 0.16255E+00
THE TOTAL INTENSITY AT TRACK 3 = 0.80152E+00
THE TOTAL INTENSITY AT TRACK 4 = 0.10000E+01
THE TOTAL INTENSITY AT TRACK 5 = 0.55535E+00

ARC DISPLACEMENT D= 0.90

THE TOTAL INTENSITY AT TRACK 1 = 0.00000E+00
THE TOTAL INTENSITY AT TRACK 2 = 0.11587E+00
THE TOTAL INTENSITY AT TRACK 3 = 0.73928E+00
THE TOTAL INTENSITY AT TRACK 4 = 0.10000E+01
THE TOTAL INTENSITY AT TRACK 5 = 0.61666E+00

ARC RADIUS R= 2.50

ARC DISPLACEMENT D= 0.00

THE TOTAL INTENSITY AT TRACK 1 = 0.25705E+00
THE TOTAL INTENSITY AT TRACK 2 = 0.78766E+00
THE TOTAL INTENSITY AT TRACK 3 = 0.10000E+01
THE TOTAL INTENSITY AT TRACK 4 = 0.78766E+00
THE TOTAL INTENSITY AT TRACK 5 = 0.25705E+00

ARC DISPLACEMENT D= 0.10

THE TOTAL INTENSITY AT TRACK 1 = 0.20554E+00
THE TOTAL INTENSITY AT TRACK 2 = 0.74578E+00
THE TOTAL INTENSITY AT TRACK 3 = 0.10000E+01
THE TOTAL INTENSITY AT TRACK 4 = 0.82933E+00
THE TOTAL INTENSITY AT TRACK 5 = 0.31319E+00

ARC DISPLACEMENT D= 0.20

THE TOTAL INTENSITY AT TRACK 1 = 0.16046E+00
THE TOTAL INTENSITY AT TRACK 2 = 0.70344E+00
THE TOTAL INTENSITY AT TRACK 3 = 0.10000E+01
THE TOTAL INTENSITY AT TRACK 4 = 0.87109E+00
THE TOTAL INTENSITY AT TRACK 5 = 0.37284E+00

ARC DISPLACEMENT D= 0.30

THE TOTAL INTENSITY AT TRACK 1 = 0.12143E+00
THE TOTAL INTENSITY AT TRACK 2 = 0.66038E+00
THE TOTAL INTENSITY AT TRACK 3 = 0.10000E+01
THE TOTAL INTENSITY AT TRACK 4 = 0.91323E+00
THE TOTAL INTENSITY AT TRACK 5 = 0.43568E+00

ARC DISPLACEMENT D= 0.40

THE TOTAL INTENSITY AT TRACK 1 = 0.88200E-01
THE TOTAL INTENSITY AT TRACK 2 = 0.61636E+00
THE TOTAL INTENSITY AT TRACK 3 = 0.10000E+01
THE TOTAL INTENSITY AT TRACK 4 = 0.95608E+00
THE TOTAL INTENSITY AT TRACK 5 = 0.50171E+00

ARC DISPLACEMENT D= 0.50

THE TOTAL INTENSITY AT TRACK 1 = 0.60555E-01
THE TOTAL INTENSITY AT TRACK 2 = 0.57117E+00
THE TOTAL INTENSITY AT TRACK 3 = 0.10000E+01
THE TOTAL INTENSITY AT TRACK 4 = 0.10000E+01
THE TOTAL INTENSITY AT TRACK 5 = 0.57117E+00

ARC DISPLACEMENT D= 0.60

THE TOTAL INTENSITY AT TRACK 1 = 0.36668E-01
THE TOTAL INTENSITY AT TRACK 2 = 0.50171E+00
THE TOTAL INTENSITY AT TRACK 3 = 0.95608E+00
THE TOTAL INTENSITY AT TRACK 4 = 0.10000E+01
THE TOTAL INTENSITY AT TRACK 5 = 0.61636E+00

ARC DISPLACEMENT D= 0.70

THE TOTAL INTENSITY AT TRACK 1 = 0.19584E-01
THE TOTAL INTENSITY AT TRACK 2 = 0.43568E+00
THE TOTAL INTENSITY AT TRACK 3 = 0.91323E+00
THE TOTAL INTENSITY AT TRACK 4 = 0.10000E+01
THE TOTAL INTENSITY AT TRACK 5 = 0.66038E+00

ARC DISPLACEMENT D= 0.80

THE TOTAL INTENSITY AT TRACK 1 = 0.84069E-02
THE TOTAL INTENSITY AT TRACK 2 = 0.37284E+00
THE TOTAL INTENSITY AT TRACK 3 = 0.87109E+00
THE TOTAL INTENSITY AT TRACK 4 = 0.10000E+01
THE TOTAL INTENSITY AT TRACK 5 = 0.70344E+00

ARC DISPLACEMENT D= 0.90

THE TOTAL INTENSITY AT TRACK 1 = 0.22319E-02
THE TOTAL INTENSITY AT TRACK 2 = 0.31319E+00
THE TOTAL INTENSITY AT TRACK 3 = 0.82933E+00
THE TOTAL INTENSITY AT TRACK 4 = 0.10000E+01
THE TOTAL INTENSITY AT TRACK 5 = 0.74578E+00

xxxxxxxxxxxxxx

```
C     FOR TEMP AXIS 8000
      REAL BY(0:10),AM(1:5),A(0:50),X(1:5)
      COMMON DY,R,E0,S,U,D,AREA,AREA1,AREA2,AREA3,BY,AM,A
      DY=0.01
      DO 200 R=0.5,2.5,0.5
      WRITE(6,10)R
   10 FORMAT (/,10X,' ARC RADIUS R= ', F5.2/,
     &          10X,'--------------------')
C     E0=1.0
C     E0=0.94
C     E0=0.85
C     E0=0.77
C     E0=0.72
C     E0=0.65
C     E0=0.61
C     E0=0.56
      E0=0.52
C     E0=0.49
C     E0=0.45
C     E0=0.43
C     E0=0.40
      T=0.0001
      DO 100 Y=T,(R-0.0001),(10*DY)
      M=NINT((Y+0.0001)*10)
      U=Y
      DO 50 S=U,((0.1*M)+0.1001),DY
      CALL ICALC(Y)
   50 CONTINUE
      CALL SIMP(Y,(Y+(10*DY)))
      A(M)=AREA
      AREA1=0.0
      AREA2=0.0
      AREA3=0.0
  100 CONTINUE
      DO 150 D=0,1.0,0.1
      CALL DISP
  150 CONTINUE
  200 CONTINUE
      STOP
      END
      SUBROUTINE ICALC (Y)
      REAL BY(0:10), AM(1:5), A(0:50)
      COMMON DY,R,E0,S,U,D,AREA,AREA1,AREA2,AREA3,BY,AM,A
      L=NINT(100*(S-U+0.001))
      IF (S .EQ. 0) GO TO 2650
      IF (S .GE. R) GO TO 2650
      FNRY =SQRT(R**2-Y**2)
      B1=FNRY
      B=LOG((R/Y)+SQRT((R**2/Y**2)-1))
      B2=0.5*(R*FNRY+Y**2*B)
      B3=R**2*FNRY-2.0*((R**2-Y**2)**1.5)/3.0
      B4=(3.0*Y**4*B+FNRY*(3.0*R*Y**2+2.0*R**3))/8.0
C     BI=2.0*E0*(B1-0.071*B2+0.085*B3-0.066*B4)
```

```
C      BI=2.0*E0*(B1-0.023*B2-0.064*B3-0.0148*B4)
C      BI=2.0*E0*(B1-0.128*B2+0.176*B3-0.095*B4)
C      BI=2.0*E0*(B1+0.006*B2-0.07*B3-0.017*B4)
C      BI=2.0*E0*(B1-0.135*B2+0.2105*B3-0.1094*B4)
C      BI=2.0*E0*(B1+0.0007*B2-0.005*B3-0.044*B4)
C      BI=2.0*E0*(B1+0.045*B2-0.013*B3-0.048*B4)
C      BI=2.0*E0*(B1+0.0399*B2+0.0317*B3-0.065*B4)
       BI=2.0*E0*(B1-0.0535*B2+0.295*B3-0.155*B4)
C      BI=2.0*E0*(B1-0.058*B2+0.256*B3-0.138*B4)
C      BI=2.0*E0*(B1-0.149*B2+0.477*B3-0.211*B4)
C      BI=2.0*E0*(B1-0.055*B2+0.434*B3-0.208*B4)
C      BI=2.0*E0*(B1-0.188*B2+0.716*B3-0.298*B4)
       BY(L)=BI
 2650 RETURN
       END
       SUBROUTINE SIMP (Y1,Y2)
       REAL BY(0:10), AM(1:5), A(0:50)
       COMMON DY,R,E0,S,U,D,AREA,AREA1,AREA2,AREA3,BY,AM,A
       C=(Y2-Y1)/DY
       IF (Y .EQ. 0) BY(0)=BY(1)
       AREA1= ((Y2-Y1)/(3.0*C))*(BY(0)+BY(10))
       AREA2= ((Y2-Y1)/(3.0*C))*2*(BY(2)+BY(4)+BY(6)+BY(8))
       AREA3= ((Y2-Y1)/(3.0*C))*4*(BY(1)+BY(3)+BY(5)+BY(7)+BY(9))
       AREA = AREA1 + AREA2 + AREA3
       RETURN
       END
       SUBROUTINE DISP
       COMMON DY,R,E0,S,U,D,AREA,AREA1,AREA2,AREA3,BY,AM,A
       REAL BY(0:10), AM(1:5), A(0:50)
       N1 = 1 + (D*10)
       GO TO (3050,3150,3250,3350,3450,3550,3650,3750,3850,3950,4050),N1
 3050 AM(3) = 2.0*(A(0)+A(1)+A(2)+A(3)+A(4))
       AM(2) = (A(5)+A(6)+A(7)+A(8)+A(9)+A(10)+A(11)+A(12)+A(13)+A(14))
       AM(1) = (A(15)+A(16)+A(17)+A(18)+A(19)+A(20)+A(21)+A(22)+A(23)+
     *A(24))
       AM(4) =AM(2)
       AM(5) = AM(1)
       GO TO 5000
 3150 AM(3) = A(5)+2.0*(A(0)+A(1)+A(2)+A(3))+A(4)
       AM(2) = A(6)+A(7)+A(8)+A(9)+A(10)+A(11)+A(12)+A(13)+A(14)+A(15)
       AM(1) = A(16)+A(17)+A(18)+A(19)+A(20)+A(21)+A(22)+A(23)+A(24)
       AM(4) = A(4)+A(5)+A(6)+A(7)+A(8)+A(9)+A(10)+A(11)+A(12)+A(13)
       AM(5) = A(14)+A(15)+A(16)+A(17)+A(18)+A(19)+A(20)+A(21)+A(22)+
     *A(23)
       GO TO 5000
 3250 AM(3) = A(6)+A(5)+A(4)+A(3)+2.0*(A(0)+A(1)+A(2))
       AM(2) = A(7)+A(8)+A(9)+A(10)+A(11)+A(12)+A(13)+A(14)+A(15)+A(16)
       AM(1) = A(17)+A(18)+A(19)+A(20)+A(21)+A(22)+A(23)+A(24)
       AM(4) = A(3)+A(4)+A(5)+A(6)+A(7)+A(8)+A(9)+A(10)+A(11)+A(12)
       AM(5) = A(13)+A(14)+A(15)+A(16)+A(17)+A(18)+A(19)+A(20)+A(21)+
     *A(22)
       GO TO 5000
 3350 AM(3) = A(7)+A(6)+A(5)+A(4)+A(3)+A(2)+2.0*(A(0)+A(1))
       AM(2) = A(8)+A(9)+A(10)+A(11)+A(12)+A(13)+A(14)+A(15)+A(16)+A(17)
       AM(1) = A(18)+A(19)+A(20)+A(21)+A(22)+A(23)+A(24)
       AM(4) = A(2)+A(3)+A(4)+A(5)+A(6)+A(7)+A(8)+A(9)+A(10)+A(11)
```

```
      AM(5) = A(12)+A(13)+A(14)+A(15)+A(16)+A(17)+A(18)+A(19)+A(20)+
     *A(21)
      GO TO 5000
3450  AM(3) = A(8)+A(7)+A(6)+A(5)+A(4)+A(3)+A(2)+A(1)+2.0*(A(0))
      AM(2) = A(9)+A(10)+A(11)+A(12)+A(13)+A(14)+A(15)+A(16)+A(17)+
     *A(18)
      AM(1) = A(19)+A(20)+A(21)+A(22)+A(23)+A(24)
      AM(4) = A(1)+A(2)+A(3)+A(4)+A(5)+A(6)+A(7)+A(8)+A(9)+A(10)
      AM(5) = A(11)+A(12)+A(13)+A(14)+A(15)+A(16)+A(17)+A(18)+A(19)+
     *A(20)
      GO TO 5000
3550  AM(3) = A(9)+A(8)+A(7)+A(6)+A(5)+A(4)+A(3)+A(2)+A(1)+A(0)
      AM(2) = A(10)+A(11)+A(12)+A(13)+A(14)+A(15)+A(16)+A(17)+A(18)+
     *A(19)
      AM(1) = A(20)+A(21)+A(22)+A(23)+A(24)
      AM(4) = A(0)+A(1)+A(2)+A(3)+A(4)+A(5)+A(6)+A(7)+A(8)+A(9)
      AM(5) = A(10)+A(11)+A(12)+A(13)+A(14)+A(15)+A(16)+A(17)+A(18)+
     *A(19)
      GO TO 5000
3650  AM(3) = A(10)+A(9)+A(8)+A(7)+A(6)+A(5)+A(4)+A(3)+A(2)+A(1)
      AM(2) = A(11)+A(12)+A(13)+A(14)+A(15)+A(16)+A(17)+A(18)+A(19)+
     *A(20)
      AM(1) = A(21)+A(22)+A(23)+A(24)
      AM(4) = A(0)+A(0)+A(1)+A(2)+A(3)+A(4)+A(5)+A(6)+A(7)+A(8)
      AM(5) = A(9)+A(10)+A(11)+A(12)+A(13)+A(14)+A(15)+A(16)+A(17)+
     *A(18)
      GO TO 5000
3750  AM(3) = A(11)+A(10)+A(9)+A(8)+A(7)+A(6)+A(5)+A(4)+A(3)+A(2)
      AM(2) = A(12)+A(13)+A(14)+A(15)+A(16)+A(17)+A(18)+A(19)+A(20)+
     *A(21)
      AM(1) = A(22)+A(23)+A(24)
      AM(4) = A(1)+A(0)+A(0)+A(1)+A(2)+A(3)+A(4)+A(5)+A(6)+A(7)
      AM(5) = A(8)+A(9)+A(10)+A(11)+A(12)+A(13)+A(14)+A(15)+A(16)+
     *A(17)
      GO TO 5000
3850  AM(3) = A(12)+A(11)+A(10)+A(9)+A(8)+A(7)+A(6)+A(5)+A(4)+A(3)
      AM(2) = A(13)+A(14)+A(15)+A(16)+A(17)+A(18)+A(19)+A(20)+A(21)+
     *A(22)
      AM(1) = A(23)+A(24)
      AM(4) = A(2)+A(1)+A(0)+A(0)+A(1)+A(2)+A(3)+A(4)+A(5)+A(6)
      AM(5) = A(7)+A(8)+A(9)+A(10)+A(11)+A(12)+A(13)+A(14)+A(15)+
     *A(16)
      GO TO 5000
3950  AM(3) = A(13)+A(12)+A(11)+A(10)+A(9)+A(8)+A(7)+A(6)+A(5)+A(4)
      AM(2) = A(14)+A(15)+A(16)+A(17)+A(18)+A(19)+A(20)+A(21)+A(22)+
     *A(23)
      AM(1) = A(24)
      AM(4) = A(3)+A(2)+A(1)+A(0)+A(0)+A(1)+A(2)+A(3)+A(4)+A(5)
      AM(5) = A(6)+A(7)+A(8)+A(9)+A(10)+A(11)+A(12)+A(13)+A(14)+
     *A(15)
      GO TO 5000
4050  AM(3) = A(14)+A(13)+A(12)+A(11)+A(10)+A(9)+A(8)+A(7)+A(6)+A(5)
      AM(2) = A(15)+A(16)+A(17)+A(18)+A(19)+A(20)+A(21)+A(22)+A(23)+
     *A(24)
      AM(1) = 0.0
      AM(4) = A(4)+A(3)+A(2)+A(1)+A(0)+A(0)+A(1)+A(2)+A(3)+A(4)
```

```
      AM(5) = AM(3)
      GO TO 5000
 5000 WRITE (6,6000)D
      WRITE (6,6001)
 6000 FORMAT (' ARC DISPLACEMENT D= ', F5.2)
 6001 FORMAT (' --------------------')
      DO 5010 I=1,5,1
      IF(D-0.5) 99,99,999
 99   RATIO = AM(I)/AM(3)
      GO TO 9999
 999  RATIO = AM(I)/AM(4)
9999  WRITE(1,5555) RATIO
      WRITE (6,6010)I,RATIO
 5010 CONTINUE
      WRITE(6,*)
      WRITE(6,*)
 6010 FORMAT (' THE TOTAL INTENSITY AT TRACK ',I2,' = ', E15.5)
 5555 FORMAT(2F6.3)
      RETURN
      END
```

xxxxxxxxxxxxx

ARC RADIUS R= 0.50

ARC DISPLACEMENT D= 0.00

THE TOTAL INTENSITY AT TRACK 1 = 0.00000E+00
THE TOTAL INTENSITY AT TRACK 2 = 0.00000E+00
THE TOTAL INTENSITY AT TRACK 3 = 0.10000E+01
THE TOTAL INTENSITY AT TRACK 4 = 0.00000E+00
THE TOTAL INTENSITY AT TRACK 5 = 0.00000E+00

ARC DISPLACEMENT D= 0.10

THE TOTAL INTENSITY AT TRACK 1 = 0.00000E+00
THE TOTAL INTENSITY AT TRACK 2 = 0.00000E+00
THE TOTAL INTENSITY AT TRACK 3 = 0.10000E+01
THE TOTAL INTENSITY AT TRACK 4 = 0.77212E-01
THE TOTAL INTENSITY AT TRACK 5 = 0.00000E+00

ARC DISPLACEMENT D= 0.20

THE TOTAL INTENSITY AT TRACK 1 = 0.00000E+00
THE TOTAL INTENSITY AT TRACK 2 = 0.00000E+00
THE TOTAL INTENSITY AT TRACK 3 = 0.10000E+01
THE TOTAL INTENSITY AT TRACK 4 = 0.19855E+00
THE TOTAL INTENSITY AT TRACK 5 = 0.00000E+00

ARC DISPLACEMENT D= 0.30

THE TOTAL INTENSITY AT TRACK 1 = 0.00000E+00
THE TOTAL INTENSITY AT TRACK 2 = 0.00000E+00
THE TOTAL INTENSITY AT TRACK 3 = 0.10000E+01
THE TOTAL INTENSITY AT TRACK 4 = 0.37527E+00
THE TOTAL INTENSITY AT TRACK 5 = 0.00000E+00

ARC DISPLACEMENT D= 0.40

THE TOTAL INTENSITY AT TRACK 1 = 0.00000E+00
THE TOTAL INTENSITY AT TRACK 2 = 0.00000E+00
THE TOTAL INTENSITY AT TRACK 3 = 0.10000E+01
THE TOTAL INTENSITY AT TRACK 4 = 0.63191E+00
THE TOTAL INTENSITY AT TRACK 5 = 0.00000E+00

ARC DISPLACEMENT D= 0.50

THE TOTAL INTENSITY AT TRACK 1 = 0.00000E+00
THE TOTAL INTENSITY AT TRACK 2 = 0.00000E+00
THE TOTAL INTENSITY AT TRACK 3 = 0.10000E+01
THE TOTAL INTENSITY AT TRACK 4 = 0.10000E+01

THE TOTAL INTENSITY AT TRACK 5 = 0.00000E+00

ARC DISPLACEMENT D= 0.60

THE TOTAL INTENSITY AT TRACK 1 = 0.00000E+00
THE TOTAL INTENSITY AT TRACK 2 = 0.00000E+00
THE TOTAL INTENSITY AT TRACK 3 = 0.63191E+00
THE TOTAL INTENSITY AT TRACK 4 = 0.10000E+01
THE TOTAL INTENSITY AT TRACK 5 = 0.00000E+00

ARC DISPLACEMENT D= 0.70

THE TOTAL INTENSITY AT TRACK 1 = 0.00000E+00
THE TOTAL INTENSITY AT TRACK 2 = 0.00000E+00
THE TOTAL INTENSITY AT TRACK 3 = 0.37527E+00
THE TOTAL INTENSITY AT TRACK 4 = 0.10000E+01
THE TOTAL INTENSITY AT TRACK 5 = 0.00000E+00

ARC DISPLACEMENT D= 0.80

THE TOTAL INTENSITY AT TRACK 1 = 0.00000E+00
THE TOTAL INTENSITY AT TRACK 2 = 0.00000E+00
THE TOTAL INTENSITY AT TRACK 3 = 0.19855E+00
THE TOTAL INTENSITY AT TRACK 4 = 0.10000E+01
THE TOTAL INTENSITY AT TRACK 5 = 0.00000E+00

ARC DISPLACEMENT D= 0.90

THE TOTAL INTENSITY AT TRACK 1 = 0.00000E+00
THE TOTAL INTENSITY AT TRACK 2 = 0.00000E+00
THE TOTAL INTENSITY AT TRACK 3 = 0.77212E-01
THE TOTAL INTENSITY AT TRACK 4 = 0.10000E+01
THE TOTAL INTENSITY AT TRACK 5 = 0.00000E+00

ARC RADIUS R= 1.00

ARC DISPLACEMENT D= 0.00

THE TOTAL INTENSITY AT TRACK 1 = 0.00000E+00
THE TOTAL INTENSITY AT TRACK 2 = 0.36377E+00
THE TOTAL INTENSITY AT TRACK 3 = 0.10000E+01
THE TOTAL INTENSITY AT TRACK 4 = 0.36377E+00
THE TOTAL INTENSITY AT TRACK 5 = 0.00000E+00

ARC DISPLACEMENT D= 0.10

THE TOTAL INTENSITY AT TRACK 1 = 0.00000E+00
THE TOTAL INTENSITY AT TRACK 2 = 0.27406E+00
THE TOTAL INTENSITY AT TRACK 3 = 0.10000E+01

THE TOTAL INTENSITY AT TRACK 4 = 0.46164E+00
THE TOTAL INTENSITY AT TRACK 5 = 0.00000E+00

ARC DISPLACEMENT D= 0.20

THE TOTAL INTENSITY AT TRACK 1 = 0.00000E+00
THE TOTAL INTENSITY AT TRACK 2 = 0.19179E+00
THE TOTAL INTENSITY AT TRACK 3 = 0.10000E+01
THE TOTAL INTENSITY AT TRACK 4 = 0.56945E+00
THE TOTAL INTENSITY AT TRACK 5 = 0.00000E+00

ARC DISPLACEMENT D= 0.30

THE TOTAL INTENSITY AT TRACK 1 = 0.00000E+00
THE TOTAL INTENSITY AT TRACK 2 = 0.11722E+00
THE TOTAL INTENSITY AT TRACK 3 = 0.10000E+01
THE TOTAL INTENSITY AT TRACK 4 = 0.69061E+00
THE TOTAL INTENSITY AT TRACK 5 = 0.00000E+00

ARC DISPLACEMENT D= 0.40

THE TOTAL INTENSITY AT TRACK 1 = 0.00000E+00
THE TOTAL INTENSITY AT TRACK 2 = 0.51930E-01
THE TOTAL INTENSITY AT TRACK 3 = 0.10000E+01
THE TOTAL INTENSITY AT TRACK 4 = 0.83148E+00
THE TOTAL INTENSITY AT TRACK 5 = 0.00000E+00

ARC DISPLACEMENT D= 0.50

THE TOTAL INTENSITY AT TRACK 1 = 0.00000E+00
THE TOTAL INTENSITY AT TRACK 2 = 0.00000E+00
THE TOTAL INTENSITY AT TRACK 3 = 0.10000E+01
THE TOTAL INTENSITY AT TRACK 4 = 0.10000E+01
THE TOTAL INTENSITY AT TRACK 5 = 0.00000E+00

ARC DISPLACEMENT D= 0.60

THE TOTAL INTENSITY AT TRACK 1 = 0.00000E+00
THE TOTAL INTENSITY AT TRACK 2 = 0.00000E+00
THE TOTAL INTENSITY AT TRACK 3 = 0.83148E+00
THE TOTAL INTENSITY AT TRACK 4 = 0.10000E+01
THE TOTAL INTENSITY AT TRACK 5 = 0.51930E-01

ARC DISPLACEMENT D= 0.70

THE TOTAL INTENSITY AT TRACK 1 = 0.00000E+00
THE TOTAL INTENSITY AT TRACK 2 = 0.00000E+00
THE TOTAL INTENSITY AT TRACK 3 = 0.69061E+00
THE TOTAL INTENSITY AT TRACK 4 = 0.10000E+01
THE TOTAL INTENSITY AT TRACK 5 = 0.11722E+00

ARC DISPLACEMENT D= 0.80

THE TOTAL INTENSITY AT TRACK 1 = 0.00000E+00
THE TOTAL INTENSITY AT TRACK 2 = 0.00000E+00
THE TOTAL INTENSITY AT TRACK 3 = 0.56945E+00
THE TOTAL INTENSITY AT TRACK 4 = 0.10000E+01
THE TOTAL INTENSITY AT TRACK 5 = 0.19179E+00

ARC DISPLACEMENT D= 0.90

THE TOTAL INTENSITY AT TRACK 1 = 0.00000E+00
THE TOTAL INTENSITY AT TRACK 2 = 0.00000E+00
THE TOTAL INTENSITY AT TRACK 3 = 0.46164E+00
THE TOTAL INTENSITY AT TRACK 4 = 0.10000E+01
THE TOTAL INTENSITY AT TRACK 5 = 0.27406E+00

ARC RADIUS R= 1.50

ARC DISPLACEMENT D= 0.00

THE TOTAL INTENSITY AT TRACK 1 = 0.00000E+00
THE TOTAL INTENSITY AT TRACK 2 = 0.75780E+00
THE TOTAL INTENSITY AT TRACK 3 = 0.10000E+01
THE TOTAL INTENSITY AT TRACK 4 = 0.75780E+00
THE TOTAL INTENSITY AT TRACK 5 = 0.00000E+00

ARC DISPLACEMENT D= 0.10

THE TOTAL INTENSITY AT TRACK 1 = 0.00000E+00
THE TOTAL INTENSITY AT TRACK 2 = 0.66196E+00
THE TOTAL INTENSITY AT TRACK 3 = 0.10000E+01
THE TOTAL INTENSITY AT TRACK 4 = 0.82018E+00
THE TOTAL INTENSITY AT TRACK 5 = 0.37729E-01

ARC DISPLACEMENT D= 0.20

THE TOTAL INTENSITY AT TRACK 1 = 0.00000E+00
THE TOTAL INTENSITY AT TRACK 2 = 0.57003E+00
THE TOTAL INTENSITY AT TRACK 3 = 0.10000E+01
THE TOTAL INTENSITY AT TRACK 4 = 0.87262E+00
THE TOTAL INTENSITY AT TRACK 5 = 0.90345E-01

ARC DISPLACEMENT D= 0.30

THE TOTAL INTENSITY AT TRACK 1 = 0.00000E+00
THE TOTAL INTENSITY AT TRACK 2 = 0.48184E+00
THE TOTAL INTENSITY AT TRACK 3 = 0.10000E+01
THE TOTAL INTENSITY AT TRACK 4 = 0.91896E+00

THE TOTAL INTENSITY AT TRACK 5 = 0.15506E+00

ARC DISPLACEMENT D= 0.40

THE TOTAL INTENSITY AT TRACK 1 = 0.00000E+00
THE TOTAL INTENSITY AT TRACK 2 = 0.39742E+00
THE TOTAL INTENSITY AT TRACK 3 = 0.10000E+01
THE TOTAL INTENSITY AT TRACK 4 = 0.96202E+00
THE TOTAL INTENSITY AT TRACK 5 = 0.23064E+00

ARC DISPLACEMENT D= 0.50

THE TOTAL INTENSITY AT TRACK 1 = 0.00000E+00
THE TOTAL INTENSITY AT TRACK 2 = 0.31628E+00
THE TOTAL INTENSITY AT TRACK 3 = 0.10000E+01
THE TOTAL INTENSITY AT TRACK 4 = 0.10000E+01
THE TOTAL INTENSITY AT TRACK 5 = 0.31628E+00

ARC DISPLACEMENT D= 0.60

THE TOTAL INTENSITY AT TRACK 1 = 0.00000E+00
THE TOTAL INTENSITY AT TRACK 2 = 0.23064E+00
THE TOTAL INTENSITY AT TRACK 3 = 0.96202E+00
THE TOTAL INTENSITY AT TRACK 4 = 0.10000E+01
THE TOTAL INTENSITY AT TRACK 5 = 0.39742E+00

ARC DISPLACEMENT D= 0.70

THE TOTAL INTENSITY AT TRACK 1 = 0.00000E+00
THE TOTAL INTENSITY AT TRACK 2 = 0.15506E+00
THE TOTAL INTENSITY AT TRACK 3 = 0.91896E+00
THE TOTAL INTENSITY AT TRACK 4 = 0.10000E+01
THE TOTAL INTENSITY AT TRACK 5 = 0.48184E+00

ARC DISPLACEMENT D= 0.80

THE TOTAL INTENSITY AT TRACK 1 = 0.00000E+00
THE TOTAL INTENSITY AT TRACK 2 = 0.90345E-01
THE TOTAL INTENSITY AT TRACK 3 = 0.87262E+00
THE TOTAL INTENSITY AT TRACK 4 = 0.10000E+01
THE TOTAL INTENSITY AT TRACK 5 = 0.57003E+00

ARC DISPLACEMENT D= 0.90

THE TOTAL INTENSITY AT TRACK 1 = 0.00000E+00
THE TOTAL INTENSITY AT TRACK 2 = 0.37729E-01
THE TOTAL INTENSITY AT TRACK 3 = 0.82018E+00
THE TOTAL INTENSITY AT TRACK 4 = 0.10000E+01
THE TOTAL INTENSITY AT TRACK 5 = 0.66196E+00

ARC RADIUS R= 2.00

ARC DISPLACEMENT D= 0.00

THE TOTAL INTENSITY AT TRACK 1 = 0.23755E+00
THE TOTAL INTENSITY AT TRACK 2 = 0.88053E+00
THE TOTAL INTENSITY AT TRACK 3 = 0.10000E+01
THE TOTAL INTENSITY AT TRACK 4 = 0.88053E+00
THE TOTAL INTENSITY AT TRACK 5 = 0.23755E+00

ARC DISPLACEMENT D= 0.10

THE TOTAL INTENSITY AT TRACK 1 = 0.17303E+00
THE TOTAL INTENSITY AT TRACK 2 = 0.84736E+00
THE TOTAL INTENSITY AT TRACK 3 = 0.10000E+01
THE TOTAL INTENSITY AT TRACK 4 = 0.90982E+00
THE TOTAL INTENSITY AT TRACK 5 = 0.30885E+00

ARC DISPLACEMENT D= 0.20

THE TOTAL INTENSITY AT TRACK 1 = 0.11589E+00
THE TOTAL INTENSITY AT TRACK 2 = 0.80949E+00
THE TOTAL INTENSITY AT TRACK 3 = 0.10000E+01
THE TOTAL INTENSITY AT TRACK 4 = 0.93601E+00
THE TOTAL INTENSITY AT TRACK 5 = 0.38649E+00

ARC DISPLACEMENT D= 0.30

THE TOTAL INTENSITY AT TRACK 1 = 0.67007E-01
THE TOTAL INTENSITY AT TRACK 2 = 0.76602E+00
THE TOTAL INTENSITY AT TRACK 3 = 0.10000E+01
THE TOTAL INTENSITY AT TRACK 4 = 0.95989E+00
THE TOTAL INTENSITY AT TRACK 5 = 0.47027E+00

ARC DISPLACEMENT D= 0.40

THE TOTAL INTENSITY AT TRACK 1 = 0.27701E-01
THE TOTAL INTENSITY AT TRACK 2 = 0.71567E+00
THE TOTAL INTENSITY AT TRACK 3 = 0.10000E+01
THE TOTAL INTENSITY AT TRACK 4 = 0.98233E+00
THE TOTAL INTENSITY AT TRACK 5 = 0.56019E+00

ARC DISPLACEMENT D= 0.50

THE TOTAL INTENSITY AT TRACK 1 = 0.00000E+00
THE TOTAL INTENSITY AT TRACK 2 = 0.65516E+00
THE TOTAL INTENSITY AT TRACK 3 = 0.10000E+01
THE TOTAL INTENSITY AT TRACK 4 = 0.10000E+01
THE TOTAL INTENSITY AT TRACK 5 = 0.65516E+00

ARC DISPLACEMENT D= 0.60

THE TOTAL INTENSITY AT TRACK 1 = 0.00000E+00
THE TOTAL INTENSITY AT TRACK 2 = 0.56019E+00
THE TOTAL INTENSITY AT TRACK 3 = 0.98233E+00
THE TOTAL INTENSITY AT TRACK 4 = 0.10000E+01
THE TOTAL INTENSITY AT TRACK 5 = 0.71567E+00

ARC DISPLACEMENT D= 0.70

THE TOTAL INTENSITY AT TRACK 1 = 0.00000E+00
THE TOTAL INTENSITY AT TRACK 2 = 0.47027E+00
THE TOTAL INTENSITY AT TRACK 3 = 0.95989E+00
THE TOTAL INTENSITY AT TRACK 4 = 0.10000E+01
THE TOTAL INTENSITY AT TRACK 5 = 0.76602E+00

ARC DISPLACEMENT D= 0.80

THE TOTAL INTENSITY AT TRACK 1 = 0.00000E+00
THE TOTAL INTENSITY AT TRACK 2 = 0.38649E+00
THE TOTAL INTENSITY AT TRACK 3 = 0.93601E+00
THE TOTAL INTENSITY AT TRACK 4 = 0.10000E+01
THE TOTAL INTENSITY AT TRACK 5 = 0.80949E+00

ARC DISPLACEMENT D= 0.90

THE TOTAL INTENSITY AT TRACK 1 = 0.00000E+00
THE TOTAL INTENSITY AT TRACK 2 = 0.30885E+00
THE TOTAL INTENSITY AT TRACK 3 = 0.90982E+00
THE TOTAL INTENSITY AT TRACK 4 = 0.10000E+01
THE TOTAL INTENSITY AT TRACK 5 = 0.84736E+00

ARC RADIUS R= 2.50

ARC DISPLACEMENT D= 0.00

THE TOTAL INTENSITY AT TRACK 1 = 0.44968E+00
THE TOTAL INTENSITY AT TRACK 2 = 0.91228E+00
THE TOTAL INTENSITY AT TRACK 3 = 0.10000E+01
THE TOTAL INTENSITY AT TRACK 4 = 0.91228E+00
THE TOTAL INTENSITY AT TRACK 5 = 0.44968E+00

ARC DISPLACEMENT D= 0.10

THE TOTAL INTENSITY AT TRACK 1 = 0.37604E+00
THE TOTAL INTENSITY AT TRACK 2 = 0.88761E+00
THE TOTAL INTENSITY AT TRACK 3 = 0.10000E+01
THE TOTAL INTENSITY AT TRACK 4 = 0.93418E+00

```
THE TOTAL INTENSITY AT TRACK  5 =     0.51680E+00


ARC DISPLACEMENT D=  0.20
--------------------
THE TOTAL INTENSITY AT TRACK  1 =     0.30787E+00
THE TOTAL INTENSITY AT TRACK  2 =     0.85978E+00
THE TOTAL INTENSITY AT TRACK  3 =     0.10000E+01
THE TOTAL INTENSITY AT TRACK  4 =     0.95377E+00
THE TOTAL INTENSITY AT TRACK  5 =     0.58100E+00


ARC DISPLACEMENT D=  0.30
--------------------
THE TOTAL INTENSITY AT TRACK  1 =     0.24551E+00
THE TOTAL INTENSITY AT TRACK  2 =     0.82844E+00
THE TOTAL INTENSITY AT TRACK  3 =     0.10000E+01
THE TOTAL INTENSITY AT TRACK  4 =     0.97162E+00
THE TOTAL INTENSITY AT TRACK  5 =     0.64193E+00


ARC DISPLACEMENT D=  0.40
--------------------
THE TOTAL INTENSITY AT TRACK  1 =     0.18932E+00
THE TOTAL INTENSITY AT TRACK  2 =     0.79335E+00
THE TOTAL INTENSITY AT TRACK  3 =     0.10000E+01
THE TOTAL INTENSITY AT TRACK  4 =     0.98832E+00
THE TOTAL INTENSITY AT TRACK  5 =     0.69962E+00


ARC DISPLACEMENT D=  0.50
--------------------
THE TOTAL INTENSITY AT TRACK  1 =     0.13933E+00
THE TOTAL INTENSITY AT TRACK  2 =     0.75259E+00
THE TOTAL INTENSITY AT TRACK  3 =     0.10000E+01
THE TOTAL INTENSITY AT TRACK  4 =     0.10000E+01
THE TOTAL INTENSITY AT TRACK  5 =     0.75259E+00


ARC DISPLACEMENT D=  0.60
--------------------
THE TOTAL INTENSITY AT TRACK  1 =     0.95274E-01
THE TOTAL INTENSITY AT TRACK  2 =     0.69962E+00
THE TOTAL INTENSITY AT TRACK  3 =     0.98832E+00
THE TOTAL INTENSITY AT TRACK  4 =     0.10000E+01
THE TOTAL INTENSITY AT TRACK  5 =     0.79335E+00


ARC DISPLACEMENT D=  0.70
--------------------
THE TOTAL INTENSITY AT TRACK  1 =     0.59197E-01
THE TOTAL INTENSITY AT TRACK  2 =     0.64193E+00
THE TOTAL INTENSITY AT TRACK  3 =     0.97162E+00
THE TOTAL INTENSITY AT TRACK  4 =     0.10000E+01
THE TOTAL INTENSITY AT TRACK  5 =     0.82844E+00
```

ARC DISPLACEMENT D= 0.80

THE TOTAL INTENSITY AT TRACK 1 = 0.31365E-01
THE TOTAL INTENSITY AT TRACK 2 = 0.58100E+00
THE TOTAL INTENSITY AT TRACK 3 = 0.95377E+00
THE TOTAL INTENSITY AT TRACK 4 = 0.10000E+01
THE TOTAL INTENSITY AT TRACK 5 = 0.85978E+00

ARC DISPLACEMENT D= 0.90

THE TOTAL INTENSITY AT TRACK 1 = 0.11722E-01
THE TOTAL INTENSITY AT TRACK 2 = 0.51680E+00
THE TOTAL INTENSITY AT TRACK 3 = 0.93418E+00
THE TOTAL INTENSITY AT TRACK 4 = 0.10000E+01
THE TOTAL INTENSITY AT TRACK 5 = 0.88761E+00

xxxxxxxxxxxxxxx

APPENDIX (A.2)

DIAGNOSTIC INSTRUMENTATION

The sequence of operation of the OSA 500 in order to obtain a radially averaged arc spectrum is as follows :

(1) Before the test

(a) Choose an available memory M (e.g. 5)

(b) Preset the number of scans N (usually N = 3)

(c) CALL 0 ENTER M ENTER = initialise OSA for recording

(2) During the test

The OSA is triggered externally

(3) After the test

(a) Make a dark scan in an available memory

CALL 0 ENTER X ENTER - START

The dark current of the vidicon is scanned by the preset (1(b)) amount

(b) Subtract the dark current from the signal

CALL 1 ENTER M ENTER X ENTER

The result is in memory M and displayed

(c) The information can be transferred to the external computer using the following instructions

DEFINE 3 ENTER 9600 ENTER

CALL 6 ENTER M ENTER

In this case the external computer is the BBC which has to be initialised before this transmission using a separate program (OSA1) (app.1).

The sequence of operation of the OSA in order to obtain a radially resolved arc spectrum is as follows :

(1) Before the test

(a) The 2D initialisation must be executed if not already done so. Usually the parameters for the 2D0 routine are as follows

2D0 ENTER 15 ENTER 5 ENTER 6 ENTER 10 ENTER 1

(b) A dark scan must be made. This is achieved by invoking the 2D2 routine as follows

2D2 ENTER START

The dark current is stored in memories 1 to 5 . This must be shifted out to other available memories by using the 2D8 routine as follows

2D8 ENTER 1 ENTER 5 ENTER X ENTER

The dark scan is now stored in memories X to (X + 4).

(c) The first 5 memories must be cleared for storage of arc spectra as follows

2D6 ENTER

(d) The accumulation program is invoked again, thus

2D2 ENTER

The OSA is ready for triggering externally to receive the DATA.

(2) During the test

The OSA is triggered externally.

(3) After the test

(a) The dark current is subtracted from each of memories 1 to 5 to obtain the true spectrum. The dark current records are stored in memories X to (X + 4), (1(b)) and can be subtracted from the corresponding data in 1 to 5 by repeated use of the CALL 1 routine.

(b) The spectra with dark current subtracted are shifted out to other memories using the 2D8 routine.

(c) These spectra can be transmitted to the external computer using CALL 6 with DEFINE 3 again set to 9600.

Operating instruction for CALL, 2D and DEFINE programs

(i) CALL Programmes

CALL 0 : Accumulation Program

Entry : CALL 0 ENTER X ENTER START possibly STOP.

Result : In memory X, after pressing the start key the preselected number of scans on the display screen will be accumulated. Whilst the accumulation proceeds, the red LED over the START key will light. Memory X will be automatically displayed on the XY display during and after the accumulation.

After initialisation with CALL 0 the accumulation can be effected as often as desired by pressing the START key, until a new instruction is entered.

The X-Y display control keys are blocked until the entry of a new instruction.

CALL 1 : Subtraction Program

Entry : CALL 1 ENTER X ENTER Y ENTER
Result : Memory Y is subtracted from memory X and the result is stored in memory X and automatically shown on the display.

CALL 2 : Accumulations and Subtractions Programs

Entry : CALL 2 ENTER X ENTER START
Result : After pressing the START key the preselected number of presets will be accumulated in memory X (e.g. a signal spectrum). If the START key is again pressed, then the same number of presets will be subtracted from the contents of memory X with the scanned spectrum (e.g. dark spectrum). Memory X will now contain the signal spectrum corrected by the dark spectrum. If on the display values around 0 and also around 65525 are held, then the Y offset must be shifted by the key until all points of the results spectrum are over 0 (the correction is necessary since the computer calculates without using sign so as not to lose dynamics i.e. for example, 2-3 = 65535).

Call 3 : Alternative Presentation

Entry : CALL 3 ENTER X ENTER

Result : Alternative presentation of real time and memory X on the display, i.e. both spectra are shown in succession and therefore appear at the same time on the display. The intensities of the cursor channels are given alternatively for both spectra on the screen display.

Call 4 : Standardisation

Entry : CALL 4 ENTER X ENTER

Result : Memory X is standardised at 12 bits, i.e. maxima of the spectra are set to 4095 and all other values to corresponding values, so that the values are multiplied by the same factor as the maximum value, or divided by the same factor as the maximum value.

Call 5 : Addition Program

Entry : CALL 5 ENTER X ENTER Y ENTER

Result : Memory Y and memory X are added and the result stored in memory X and automatically shown on display XY.

Call 6 : Serial Outputs

Entry : CALL 6 ENTER X ENTER

Result : Memory X between UG and OG (see define 0/I) is output through the serial interface. Here in one line first the channel number, then the intensity, and finally Carriage Return are output. In addition, in the first "Memory X" as well as at the end the current integral and mean values are output. The coding of the individual symbols is in the ASCII code.

Call 7 : Integral

Entry : CALL 7 ENTER

Result : Between UG and OG the integral of the spectrum shown on the display is calculated and given on the screen after Integral. The integral is calculated by adding the intensity values from UG to OG. The figure after the E gives the power of 10; e.g. 35,000E2 = $35,000 \times 10^2$.

Call 8 : Number of channels

Entry : CALL 8 ENTER X00 ENTER

Result : By call 8, the number of channels by which the target is scanned, is altered. Possible values : 100, 200, 300, 400, 500. After entry of one value, the X axis is shortened to the display of n/5 where n = number of channels / 100. Exactly as shown on the display, the target is now scanned from channel 1 as far as only n/5. It must be remembered here that the dwell time of the electron beam per diode (64 µs) remains the same (i.e. the same amount of information collected as with 500 points), but the integration time of the light be-

tween scans is reduced to n/5 of 32 ms (i.e. for steady state excitation - the same illumination strength) in real time the intensity of the spectral lines will be less.

If the scanning field is reduced, it is no longer possible to call X expand by the key operation. It is better in this case to set the optimum picture size by means of the Expand potentiometer adjacent to the X-Y display. Against the disadvantage of the reduced target area, the smaller number of channels has two advantages: the number of memories is increased to 150/n memories, i.e. for 100 channels a maximum of 150 memories is now possible. Then also in the 2D mode 150 tracks can be simultaneously stored in memory.

Call 9 : Alternative Program

Entry : CALL 9 ENTER X ENTER Y ENTER
Result : Alternative presentation as for program Call 3, but presentation of two memories X and Y.

Call 10 : Cushion correction

Entry : CALL 10 ENTER X ENTER
Result : This program corrects the memories X and Y by the values of a correction spectrum.

Call 11 : Multiplication program :

Entry : CALL 11 ENTER X ENTER Y ENTER

Result : Memory X is multiplied by memory Y, the result stored in memory X and automatically displayed on the XY display. Since the result can be output over the 16 bit range, in such a case the result is shifted by so many bits that the maximum can be covered by 16 bits.

CAUTION

Memory 0 is needed for the multiplication and for this reason neither be mulplicant nor multiplier.

Call 12 : Division Program

Entry : CALL 12 ENTER X ENTER Y ENTER

Result : Memory X is divided by memory Y, the result is stored in memory X and automatically displayed on the XY display. In order to attain full accuracy, the result is shifted to the right by so many bits that the maximum no longer contains any leading zero figures.

CAUTION

Memory 0 is needed for the division, and this reason should neither be dividend nor divisor.

Call 13 : Erase all memories

Entry : CALL 13 ENTER

Result : Memory 0 to memory 30 are erased.

Call 14 : ASCII Output

Entry : CALL 14 ENTER

Result : An ASCII symbol is output as control symbol through the serial interface. This control symbol can be programmed in to customer's requirements.

Call 15 : Average value

Entry : CALL 15 ENTER

Result : Between UG and OG the intensity average value of the spectrum shown on the screen is calculated and output in the penultimate line of the screen.

Call 16 : Delay and accumulation program

Entry : CALL 16 ENTER X ENTER START

Result : Call 16 is used after, by DELAY N ENTER the number of seconds was entered during which light is to be collected at the target. Then CALL 16 can be called and by X the memory in which accumulation is to be effected after the delay time is entered. After pressing START, the target will be exposed for the given number of seconds and the result stored in memory. It is possible to use START again as often as desired without re-initialisation.

Call 17 : Dark keying

Entry : CALL 17 ENTER

This programme is at present only in software, but not available in hardware.

Call 18 : Real-time Plot Program

(only for systems with Floppy Disc Option)

Entry : CALL 18 ENTER S ENTER

By this program it is possible to have a real-time spectrum plotted out at specific intervals of time. S is the time period in seconds between the plotting of two real-time spectra. By pressing a command key the program is stopped.

CAUTION

The spectrum is plotted which is at that moment on the X-Y display, so that the real-time spectrum must be visible there.

Call 19 : Arithmetic with constants

Entry : CALL 19 ENTER Z ENTER V xxxx ENTER

Result : Memory A, according to the sign V (+, -, *, /) is automatically logically associated with the constants xxxxx (up to 5 places) and the result is stored in Z

(ii) 2D PROGRAMMES

(only possible for detectors with 2D option)

Generally for the two dimensional scanning of the detector : By the 2D initialisation the target area scanned will be split into the preselected number of tracks and each track in succession scanned by the electron beam, the scanning time for each track being 32 ms, so that the total scanning time for the target is given by n-32, where n = number of tracks.

In 2D images with several tracks on the display the function X - expand and Y - offset are not capable of alteration. Only for 2D4 (real full track) can Y expand be selected. If it is desired to show a stored track with spread, the memory in which the track is held must be selected as a sole image by DISPLAY X ENTER

2D Initialisation

Entry : 2D0 ENTER U ENTER W ENTER X ENTER Y ENTER Z ENTER
Result : A 2D image is initialised by this entry with the following specification :

U - PT = Possible tracks = number of segments, in which the target is split in the Y direction.

W - NT = Number of tracks = number of tracks which are really to be scanned by the camera and then shown on the X-Y display. NT must always = PT

X - ST = Start track = Number of track (as seen from above) which is to be scanned first. If PT = NT, then ST must equal 1.

Y - OT = offset track = Distance between two tracks to be scanned. If FT = NT then OT must = 1.

Z - IT = Intensified track = That track of which the intensity value on the display screen is to be shown for the corresponding cursor value. This track is scanned more brightly on the XY display.

The initialised value for PT, NT, ST, OT and IT, after completing the last entry, are shown on the display screen (lines 7 and 8).

If a 2D target picture is to be stored in memory, then NT should not be greater than 30, since only 30 memories are available. If, however, the number of channels is less than 500, the possible figure for NT is increased to the maximum number of memories then available.

2D 1 : Real-time

Entry : 2D 1 ENTER

Result : A 2D real-time image with the tracks shown on the screen. For the intensified track the cursor and intensity value are displayed.

The tracks are scanned in succession on the target, each track in 32 ms.

2D 2 : 2D Accumulation

Entry : 2D 2 ENTER START

Result : 2D accumulation in the memory predetermined by the tracks with the predetermined number of scans. Here every track initialised by 2D is accumulated in the memory having the same number as that representing the track i.e. Track 1 in memory 1 etc.

CAUTION

After Press START Key appears in the second line, there should be a wait of at least 10 seconds before pressing START, since the discharge of the target to 2D scan must have decayed.

2D 3 : 2D Plot Program

Entry : 2D 3 ENTER

Result : 2D program for an XY recorder in which the initialised tracks are plotted starting at the top and working down. The tracks are automatically recorded over each other and the pen lift switched at the end of each track, so that at the start of the next track it can be dropped again. Starting and finishing channels for the recording process are determined by UG and OG. By pressing a command key the recording process can be stopped. Care must then be taken that

with more than 16 tracks which are to be recorded on one sheet, the tracks overlap since the amplitude for one track on the display and on the plotter cannot be set smaller than for 16 tracks. Change of recorder speed see under Define 2.

2D 4 : Presentation of one track only in real time

Entry : 2D 4 ENTER X ENTER

Result : Only the track X is shown in real time on the display. Track X is now alone scanned in its correct position on the target. As against 2D real-time the track will now be scanned every 32 ms. (less dark current than with 2D real-time).

2D 5 : 2D Memory image

Entry : 2D 5 ENTER

Result : A 2D memory picture with the track of corresponding memories, i.e. Track 1 in memory 2, track 2 in memory 2 etc.

2D 6 : 2D clear

Entry : 2D 6 ENTER

Result : All the memories initialised by 2D 0 for track storage are erased.

2D 7 : 2D Delay and Accumulation

Entry : 2D 7 ENTER START

Result : As a linkage of the programmes 2D 2 (2D Accumulation) and call 16 (1D Delay and accumulation), after a certain delay time the target will be two dimensionally scanned and memorised.

Firstly, with DELAY N ENTER, the delay time should be entered (N = number of seconds).

Before the start of the delay time the target is scanned with NT. The start of the delay time (suppression of the beam) is recognisable by the stationary holding of the base line at the lower edge of the display.

2D 8 : Shift 2D images

Entry : 2D 8 ENTER X ENTER Y ENTER Z ENTER

With this program two 2D images which have been fed into the first memory, can be shifted by one command into the memory space behind. The parameters to be called signify :

X - ST Start track of the 2D memory image to be shifted.

Y - NT Number of tracks (memories) to be shifted.

Z - DT Destination track = 1st memory of the memory range into which the 2D image is to be shifted.

(iii) DEFINE PROGRAMMES

Define 0 = Lower Limit (UG or LL)

Entry : DEFINE 0 ENTER Z ENTER

Result : The lower limit for integral, plot, average value, and serial output is set at Z. Z must lie between 1 and 499.

Z is set to 1 in the initialisation program.

Define 1 : Upper limit (OG or UL)

Entry : DEFINE 1 ENTER W ENTER

Result : The upper limit for integral, plot, average value, and serial output is set to W. W must lie between 1 and 499, and in addition, W must be > Z. W is set to 499 in the initialisation program.

Define 2 : Plot speed

Entry : DEFINE 2 ENTER V ENTER

Result : The plot speed for plot and 2D plot is set to V. The greater V, the slower the plot speed. V is set to 2 in the initialisation program. The smallest value for V is V = 1.

Define 3 : Baud rate

Entry : DEFINE 3 ENTER S ENTER

Result : The Baud rate for the serial interface is set to S. S can have any value between 1 and 9600. The initialisation value for S is set at 300 Baud.

Define 4 : Lambda (Wavelength)

Entry : DEFINE 4 ENTER 1 ENTER

Result : By setting define 4 to 1, in line 3 of the screen display instead of the intensity the wavelength for the set channel (cursor position) is shown provided that the wavelength recorder option is incorporated in the instrument. Switching back to intensity by entering 0

Define 5 : Y Offset

Entry : DEFINE 5 ENTER Z ENTER

Result : By entry of a value for Z between -32767 and 32767 the Y offset is set to this value i.e. the zero line on the XY display is shifted by this value.

Define 6 : Heating off, Plot Relay, Dark scan of camera

Entry : DEFINE 6 ENTER W ENTER

Result : Setting of functions by input of the following values :

Function		Value
Switch in recorder output X-Y		65519
Plot relay (Pen down)	on	65503
Plot relay and recorder output	on	65487
Dark scan - camera	on	65471
Vidicon heating (filament)	off	64511

All functions are reset by input of 65535

Define 7 : Delay scans

Entry : DEFINE 7 ENTER N ENTER

Result : The target is both in real time and in 2D real time operating dark-scanned between every N scans i.e. the light integration time per diode column is raised from 32 ms to (N-U), U = 32 ms. In the programs call 0 and 2D 2, after pressing the START key the target is scanned dark N.32 ms before the read-out starts. The number N is seen on the display screen (line 12).

Define 8 : Accu. + memory erasure

Entry : DEFINE 8 ENTER 1 ENTER

Result : If the variable 8 is set to 1, the accumulation memory in which accumulation is to be effected on calling Call 0 is erased on each of Call 0 before pressing the START Key. Reset of the function by entry of 0.

Define 14 : 2D variable

Entry : DEFINE 14 ENTER R ENTER

Result : The intensified track is changed to the value R.

Define 20-49 : Track number

Entry : DEFINE 20 ENTER P ENTER

Result : From Define 20 to Define 49, 30 tracks can be defined which order of their entry from define 20 on are then scanned on the target. In this way it is possible from 256 tracks to select any 30 which, also by means of 2D 2, can be accumulated in the appropriate memory track of Define 20 in memory 1, track of define 21 in memory 2, etc.

APPENDIX (A.3)

OPTICAL DEPTH

In order to derive the optical depth, the black body radiation function (e.g. Smith et al (1978)),

$$\beta_0(\lambda,T) = (C_1/\lambda^5)\ [\exp(C_2/\lambda T)-1]^{-1} \qquad (1)$$

Where

λ = the wavelength

T = the temperature

$C_1 = 1.1909 \times 10^{-12}$ wcm^{2}sr^{-1}

$C_2 = 1.4380$ cm°K

is compared with the intensity of a given line

$$I_{mn} = (1/4\pi)(Ng_mA_{mn}/Z(T))(e^{-(Em/KT)})\ (hc/\lambda) \qquad (2)$$

Where

N = number density

Z(T) = partition function

Equation (1) has units of surface area and per unit wavelength, whereas equation (2) has units of volume alone. But for a sphere of radius r and a full line half width of $\Delta\lambda_{mn}$:

$$\beta_0^* = 4\pi r^2 \Delta\lambda_{mn}\ (C_1/\lambda^5)[\exp(C_2/\lambda T)-1]^{-1}$$

and

$$I_{mn}^* = (4\pi r^3/3)(Ng_mA_{mn}/Z(T))\ (hc/4\pi\lambda)(e^{-(Em/KT)})$$

Where the superscript * indicates that the values are normalised to units of power alone.

The optical depth 2r is therefore given by equating I_{mn}^{*} and β_0^{*} to give :

$$2r = [24\pi Z(T)\Delta\lambda_{mn}((C_1/\lambda^5)(\exp(C_2/\lambda T)-1)^{-1})]/(Nz(T)A_{mn}g_m \Delta E_{mn}e^{-(Em/KT)}) \quad (cm) \qquad (3)$$

Fig.(A.3.1) shows the variation of CuI species and electron density for various SF_6 and Cu plasma compositions (e.g. Kinsinger, unpublished). The data of Fig.(A.3.1) was used in the calculation of the optical depth in chapter (6).

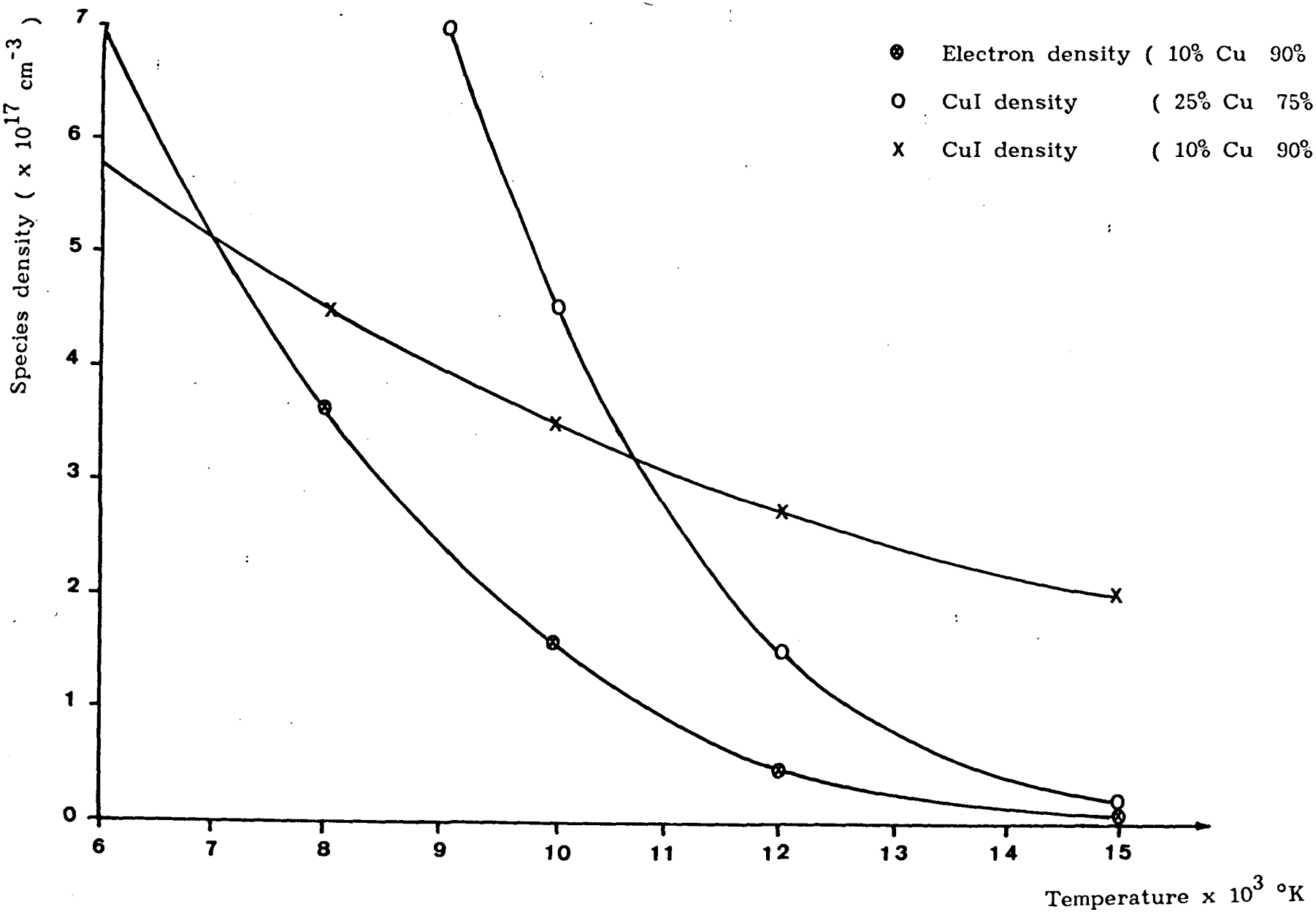

Fig (A.3.1) CuI and electron densities for different plasma composition (Source : Kinsinger unpublished)

APPENDIX (A.4)

TRANSPORT PROPERTIES OF SF_6

The thermal transport properties of SF_6 used in the evaluation of the arc energy conservation were obtained form Frost and Liebermann (1971), table (6.3). The variation of the electrical conductivity (σ), thermal conductivity (K), enthalpy (h) and density (ρ) with temperature in the range 5,000 to 11,000 °K for the pressures of 4 atm and 2 atm are shown on Figs. (A.4.1, 2). The variation of sonic velocity with temperature in the range 5,000 to 11,000 °K for the pressures of 4 atm and 2 atm are shown on Figure (A.4.3).

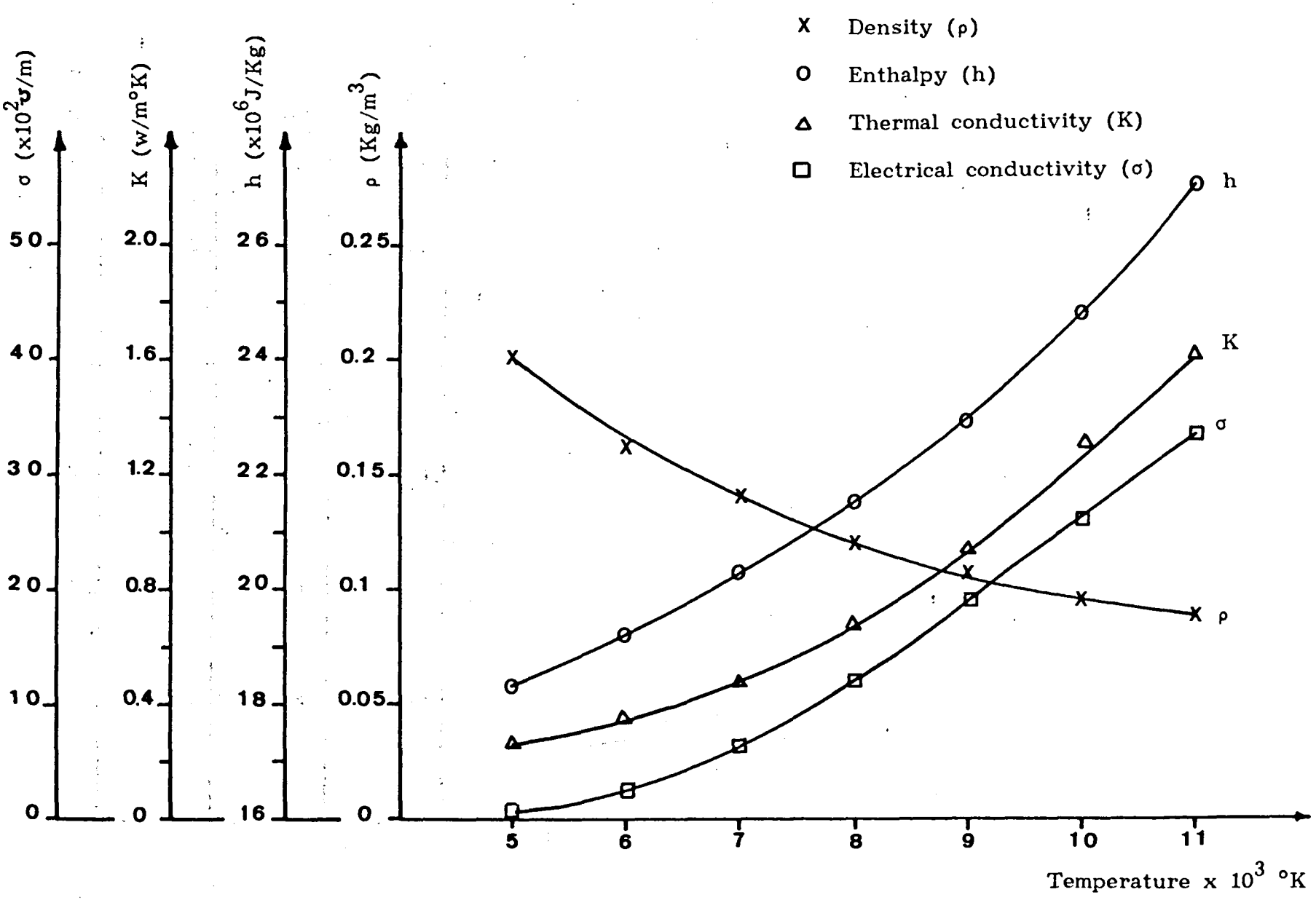

Fig. (A.4.1) The transport properties of SF_6 (p = 4 atm)

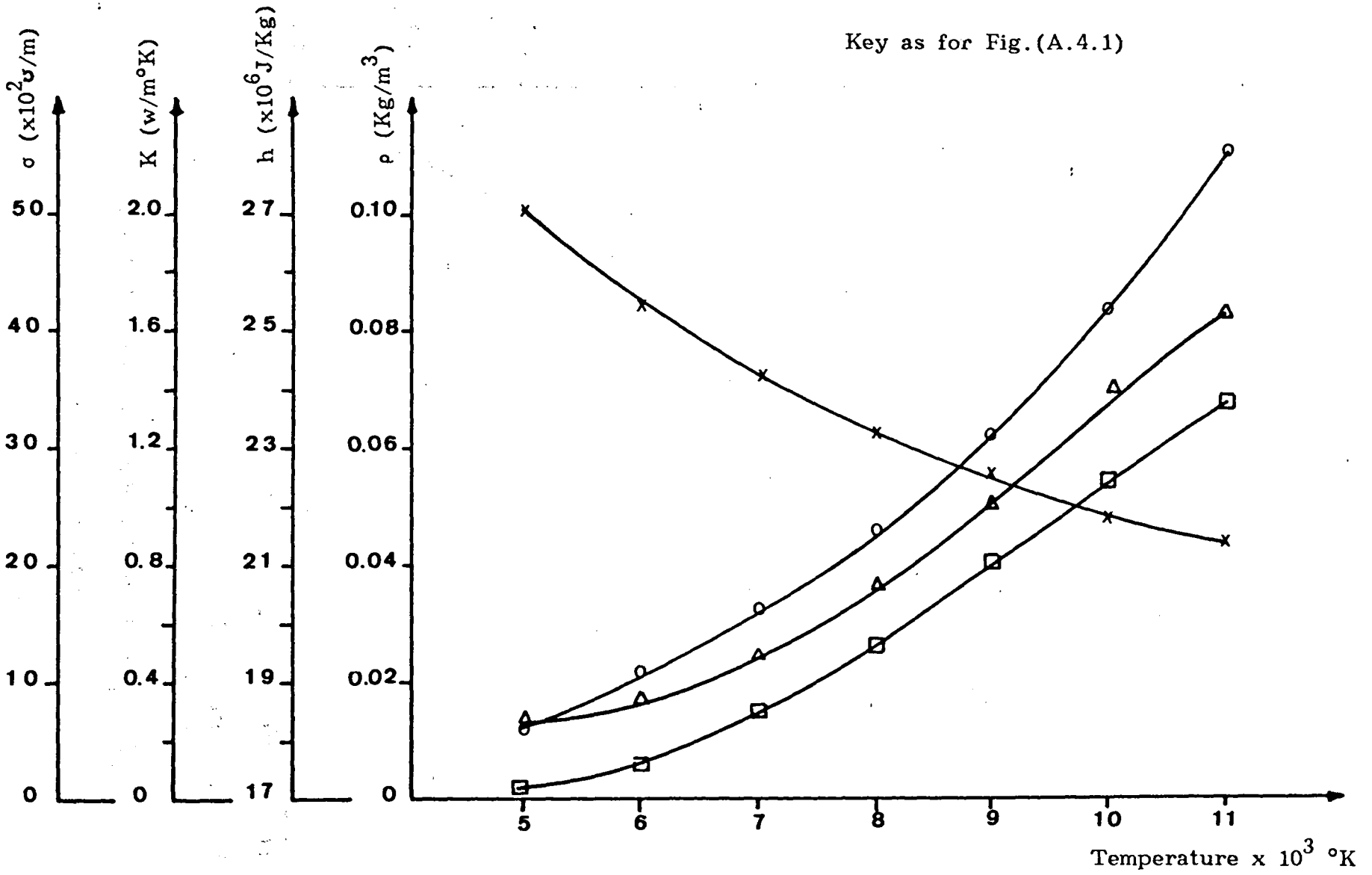

Fig.(A.4.2) The transport properties of SF_6 (p = 2 atm)

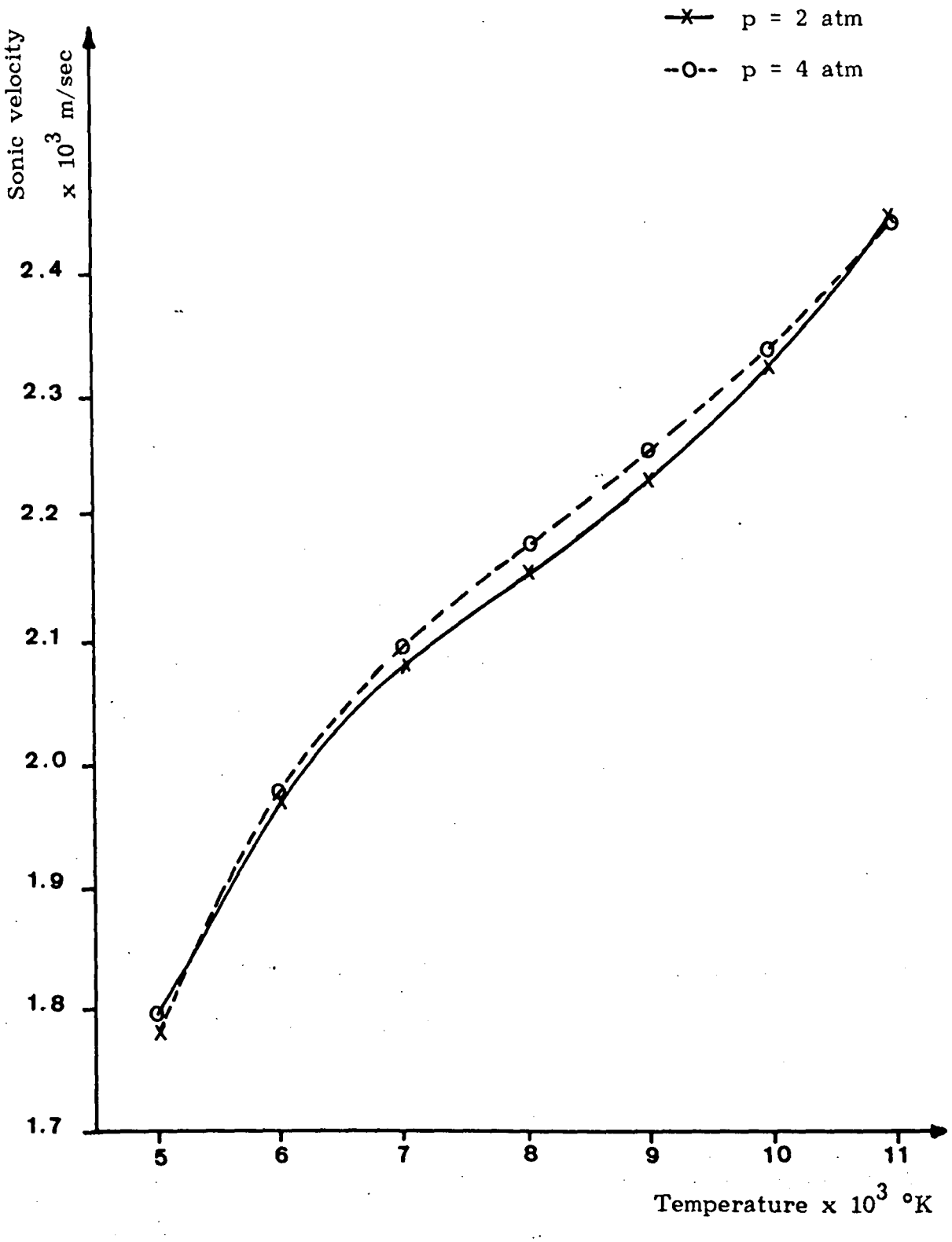

Fig.(A.4.3) Variation of sonic velocity in SF_6 with temperature at different pressures.

APPENDIX (A.5)

PUBLISHED PAPERS

1- El-Kholy S.M., Weilin Hu, Prasad A.N. and Jones G.R.

"Optical spectra of SF_6 circuit breaker during the current zero period".

Proc. Int. Conf. on phenomena in ionized gases ICPIG XVIII Swansea, July 1987, pp. 688-689.

2- El-Kholy S.M., Jones G.R., Lewis E. and Prasad A.N.

"Evaluation of the spectra of decaying arcs in gas blast circuit breakers".

To be presented at the IX Int. Conf. on Gas Discharges and their Applications (Venice) September 1988.

3- Lewis E., Jones G.R. and El-Kholy S.M.

"Power dissipating processes in the current zero circuit breaker arc".

To be presented at the IX Int. Conf. on Gas Discharges and their Applications (Venice) September 1988.

4- Jones G.R., El-Kholy S.M., Weilin Hu.

"Spectral emission from copper and tungsten following high current arcing".

Accepted for publication in J. Phys. D : Appl. Phys.

OPTICAL SPECTRA OF SF_6 CIRCUIT BREAKER ARCS DURING THE CURRENT ZERO PERIOD

S.M. El-Kholy*, Hu Weilin+, A.N. Prasad°, G.R. Jones°

*Department of Electrical Eng., El-Minufiyah University, Shebien El-Kom, Egypt.
+Department of Eng. Mechanics, Tsinghua University, Beijing, China.
oDepartment of Electrical Eng. & Electronics, University of Liverpool, Liverpool. U.K.

Abstract

Optical Spectra of model SF_6 circuit breaker arcs (having a peak current up to 64 KA) during current the zero period have been investigated. Under certain experimental conditions tungsten lines are apparent in the arc spectra in addition to the more well established copper lines. In this contribution some typical spectra are given and conditions under which tungsten lines appear are identified and discussed.

Introduction

A preliminary investigation of the optical spectra of a high power SF_6 circuit breaker during the current zero period of a A.C. sustained arc has been made by Lewis et.al [1]. The present contribution reports a continuation of the above work. Such investigations of current zero SF_6 arc spectral characteristics in a circuit breaker environment is particularly difficult but provides important information about arc properties. Important parameters such as temperature, electron density, conductivity as well as plasma composition can be obtained from such investigations. In [1] only copper lines were identified in the spectrum of the arc. Experiments conducted over a wider range of operating conditions show that sometimes not only copper but also tungsten lines appear in the arc spectrum. This paper seeks to identify these lines and explain under what conditions the tungsten lines will appear.

Experimental Facilities

The model circuit breaker, the power supply circuit and the measuring system employed were identical to those used by Lewis et al [1,2]. The power supply circuit provided peak sinusoidal currents in the range 34-64 KA at a frequency of 78 Hz. The model circuit breaker was of the two pressure monoflow SF_6 type using an upstream pressure of both 7.8 bar and 4.25 bar, and downstream pressure of 1 bar. The contacts of the circuit breaker were made from copper-tungsten, and the nozzle was made from PTFE. A 3 mm high slot situated at the nozzle throat permitted the arc radiation to be focussed at the entrance slit of a monochromator which had a 1 m focal length and 8.2 A/mm reciprocal dispersion. The width of the entrance slit of the monochromator was 28.5 μm. The spectrum on the exit plane of the monochromator was detected and recorded by an Optical Spectral Analyser 500 with Vidicon Camera SIT500. The moment of recording the spectrum was selected in the range -30 - +67 μs around current zero (minus sign means before current zero, plus sign after current zero) and most experiments were conducted within ±20 μs. The exposure time was 1.6 or 3 μs.

Experimental Results

Fig. 1 shows two recorded spectra within a selected wavelength range of the arc radiation emitted from a diametric strip including the arc axis. The horizontal axis in these figures represents wavelength (in nm) whilst the vertical axis represents the intensity of the radiation (in counts, relative intensity). The experimental conditions corresponding to curve a were as follows: upsteam pressure 7.8 bar peak current 40 KA, current zero value of di/dt = 18 A/μs, instant of recording 10 μs before current zero, exposure time 3 μs. The two peaks on curve a are the two copper lines CuI5 10.5 and CuI5 15.3. The wavelength region between these two copper lines is devoid of any other spectral lines of significant intensity. The experimental conditions relevent to curve b were: upstream pressure 4.25 bar, peak current 45 KA current zero value of di/dt = 20 A/μs, instant of recording 7.2 μs before current zero, exposure time 3 μs. In Fig. 1 curve b, besides the two copper lines apparent on figure 1 curve a, there are a group of tungsten lines . The intensity of these lines may be equal or even stronger than the two copper lines. Through a statistical analysis of 150 experiments it was found that the appearance of the tungsten lines depends mainly on two factors: the rate of decay of current at current zero di/dt and the time t, at which the spectrum was recorded. Fig. 2 summarises the occurrence or absence tungsten lines from a series of 95 experiments at a pressure of 7.8 bar. The horizontal axis in this figure represents the instant of time at which the spectrum was recorded (t=0 indicates current zero) whilst the vertical axis represents di/dt. In this figure the plus sign represents cases in which tungsten lines appear whilst the minus sign represents cases in which tungsten lines are absent. Results for conditions when the arc was extinguished at current zero are of course confined to the sector before current zero (to the left of the vertical axis corresponding to t=0).

The results shown on figure 2 may be divided into three zones as indicated by the two dashed lines. In the zone above the two dashed lines tungsten lines are always identifiable in the spectrum. In the zone below the two dashed lines, no tungsten lines have been identified in the spectrum. In the zone between the two dashed lines, the occurrence or absence of tungsten lines varies from one experiment to another. The existance of this zone of uncertainty is due to the following reasons: Firstly, there is no absolute standard for judging the appearance of any tungsten lines, but simply to decide approximately by comparing the relative intensities of the tungsten and copper lines. Thus it is not clear whether on some records, the noisy nature of the spectrum between the two copper lines (e.g. curve a) is due to instrument noise or due to low intensity tungsten lines. Secondly, there are error limitations in the measurement of di/dt and t. The error of di/dt is about 0.4 [A/μs] whilst the error of t is about 0.2 μs. Thirdly, some random factors may occur during testing which may also affect the appearance of the tungsten lines. For instance, tungsten lines are not usually apparent even at high currents when the circuit breaker contacts are new. This is because the vaporization of copper from the copper-tungsten sintered contact material occurs preferentially and as a result the temperature of contacts is prevented from rising sufficiently to promote tungsten evaporation. For contacts which have suffered arcing several times, the tungsten content in the surface layer may be greatly increased, so that tungsten evaporation is enhanced. This behaviour is consistent with the observation from the present experimentation that the tungsten lines appear in the approximate order W514.5, W513.8, W513.0, W512.4, W511.7 nm. As the various lines appear progressively, the intensity of the W514.5 nm line increases whilst the intensity of two copper lines decrease gradually. Sometimes the situation exists whereby the intensities of the CuI515.3 and W514.5 nm are approximately identical and the lines overlap each other so as to be individually indistinguishable.

The dashed lines on Fig. 2 show that the tungsten lines appear only at high values of di/dt except for longer times before current zero. Experimental results similar to those shown on figure 2 but for an upsteam pressure of 4.25 bar rather than 7.8 bar, show a similar trend in the boundaries between appearance and non appearance of the tungsten lines. However in the lower pressure case the occurrence boundaries are shifted to lower values of di/dt implying that the tungsten entrainment persists more extensively in the latter case. Temperature estimates for the arcs at both these pressures indicate that the high pressure arc to possess a higher plasma temperature. A simple correlation between the occurrence of tungsten in the arc with a higher plasma temperature therefore does not exist.

Arc cross-section estimate indicates the lower pressure arcs to have a greater diameter than the higher pressure arcs so suggesting less severe axial convection effects possibly enhanced by more severe flow throttling due to nozzle blocking. This suggests that the occurrence or otherwise of the tungsten in the arc plasma is more strongly dependent upon reduced convection being incapable of removing the persisting tungsten following entrainment during the peak current phase.

References

[1] Lewis, E., Prasad, A.N. and Jones, G.R. 8th Int. Conf. on Gas Discharges and their applications (1985), (Oxford) p. 31 - 35.

[2] Lewis, E., Shammas, N.Y. and Jones, G.R. 8th Int. Conf. on Gas Discharges and their applications (1985), (Oxford) p. 35 - 39.

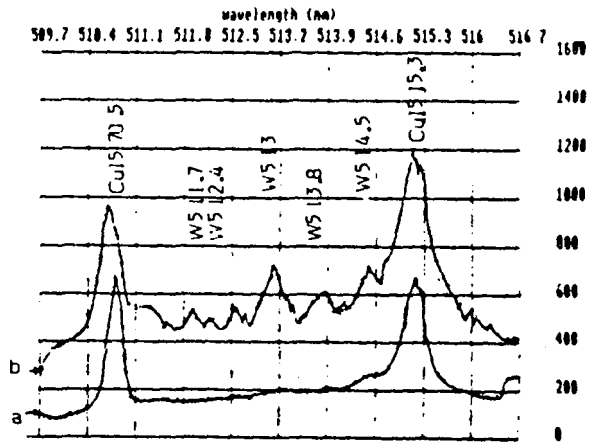

Figure 1. Curve (a) arc spectrum Cu lines only
Curve (b) arc spectrum Cu and W lines.

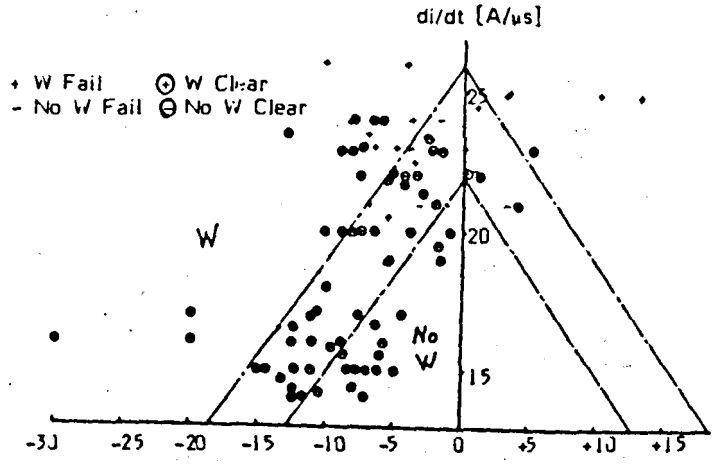

Figure 2. Correlated results showing occurrence of W lines (Pressure = 110 psig)

EVALUATION OF THE SPECTRA OF DECAYING ARCS IN GAS BLAST CIRCUIT BREAKERS

El-Kholy, S.M.I.*, Jones, G.R.♦, Lewis, E.♦, and Prasad, A.N.♦

Department of Electrical Engineering & Electronics, University of Liverpool, U.K.

1. INTRODUCTION

The performance of a gas blast circuit breaker is governed by the extinction of the arc discharge which is formed between the contacts of the interrupter. The arc exists within the confines of a nozzle used to tailor a flow of gas for achieving the control and eventual extinction of the discharge. It has been long appreciated that measurements of the arc properties during its extinction in such a circuit breaker are important for understanding the role of various fundamental processes in causing arc extinction. However the inaccessible nature of the circuit breaker nozzle throat and the complexity of the operating conditions have limited the use of sophisticated diagnostics in realistic interrupter test heads. Recently these difficulties have been overcome (e.g. Lewis et al (1985)) (1)(2) and spectroscopic measurements have been made during the few microseconds of the arc extinction period at the nozzle throat location where it is believed that the plasma recovery is most critical. This has been achieved through the use of an optical spectrum analyser capable of detecting low level light emission with microsecond exposure and with five simultaneously recorded line of sight measurements. Optical access into the confines of the interrupter nozzle without affecting the circuit breaker performance was achieved via a slot in the nozzle wall made gas tight by a window and gasket on the side remote from the arc.

Despite overcoming the practical difficulties and obtaining radially resolved spectral records the anlysis of these results still presents problems because of the unstable and irregular nature of the arc column in such an environment along with its small lateral dimensions. This contribution is concerned with the evaluation of such experimental results and the derivation from them of an estimate of the plasma conditions within the decaying arc.

2. Experimental Conditions

The experimental conditions - model circuit breaker power supply circuit and the optical measuring system - have already been described by Lewis et al [1][2]. Sinusoidal currents of peak values in the range 34 - 65 kA at a frequency of 78 Hz have been used. The model circuit breaker was of the two pressure monoflow type using an upstream pressure of 7.8 or 4.25 bar and a downstream pressure of one bar absolute. The circuit breaker contacts were made from copper-tungsten and the nozzle from PTFE.

Optical access to the throat of the circuit breaker nozzle was achieved via a 3 mm high slot. The emitted radiation transmitted through this slot was focussed on the entrance slit of a Monochromator (1m focal length, 8.2 Å/mm reciprocal dispersion, entrance slit width 28.5 μm). The spectrum on the exit plane of the monochromator was recorded with an Optical Spectrum Analyser using a Vidicon Camera for registering the optical image.

3. Experimental Results

The spectral range investigated (510 - 517 nm) covers two prominent CuI spectral lines at 510.5 and 515.3 nm. These lines may be utilised in principle for the derivation of plasma temperature by the method of relative line intensity (e.g. Lewis et al (1),(2)). Since both lines lie within the recorded spectral range they may be observed simultaneously on the same record from a single test, so avoiding errors arising from test to test variations.

These type of records could be recorded along five separate line of sights simultaneously with the optical spectrum analyser (figure 1). There is therefore the possibility of achieving some radial resolution from results taken during a single test so again avoiding errors due to test to test variations. However there is the consequence that the five line of sight records represent the maximum number of spectral data points obtainable across the arc column diameter and so governs the accuracy with which the radial variation of properties may be determined. This manifests itself as, for example, a radial intensity profile degenerating into a discontinuous, staircase distribution as depicted on the top of figure 1.

Continuous radial profiles of intensity in the vicinity of the 515.3 nm spectral line peak have however been obtained in seperate experiments from short exposure photographic records. These were registered with an image converter camera viewing the arc through an appropriate narrow band filter.

These records have shown that the arc plasma column may vary from test to test in the following respects

(i) the peak intensity within the waveband of the filter may vary from test to test

(ii) the radial intensity profile is occasionally assymmetric

(iii) for the axisymmetric records the intensity profile shape at the 515.3 nm wavelength is always similar although the amplitude may vary

(iv) the arc column suffers latteral displacements from test to test, away from the nozzle axis, which are of the same order as the arc diameter.

The implications of (i) is that evaluation of radially resolved properties e.g. temperature, which rely on the ratio of intensities taken from photographs from two seperate tests, will be unreliable. The implication of (iv) is that for the present line of sight spectral measurements a compromise is required between arranging for the line of sights to be close together to give a fine resolution and at the other extreme ensuring that

*Menoufia University, Egypt

♦Department of Electrical Engineering and Electronics, University of Liverpool, U.K.

they are sufficiently far apart to capture the entire arc crossection even if it suffers an extreme latteral displacement.

As a result of this latter requirement the staircase intensity profile may superficially lead to an interpretation that the intensity profile is assymmetric. This is illustrated on figure 2 which shows two staircase profiles obtained along the same fixed line of sights from the same parabolic profile but which is latterally displaced by different amounts with respect to the line of sights. The difference in the displacements is only about 10% of the arc diameter but it has a substantial influence upon the shape and symmetry of the staircase profile.

The problem of analysing the experimental results from such experiments is therefore complicated because the limited number of radially resolved data points makes it difficult to distinguish between symmetric profiles latterally displaced (iv) and truly assymmetric profiles (iii) which although rarer may still occur.

The purpose of this contribution is to evolve an analytical strategy for achieving this identification so that radially resolved temperature profiles of the arc plasma can be derived from such measurements. Advantage is taken of the reproducible shape of the well behaved 515.3 nm profiles as indicated photographically ((iii) above).

4. Analysis of Results

A scheme for anlysing these spectral results taking account of possible lateral displacements of the arc column and assymetries in the distributions is shown in the form of a flow diagram on figure 3. A computer programme based upon this flow diagram was used in the anlysis of the results.

The spectral records obtained along each line of sight (figure 1) are first inspected and the intensity of each of the spectral lines (515.3, 510.5 nm) are noted. These are plotted as a staircase type radial profile as shown on figure 2 and form the basis of the analysis which follows.

Inspection of high speed photographs (section 3) (narrow band filtered) allows an Abel inverted intensity profile to be derived as indicated on figure 4. This has been found experimentally to be representative of the intensity profiles observed throughout the arc extinction phase. The Abel inverted distribution is quite closely similar to a parabolic curve which permits a simplification of the computational analysis.

The staircase profile corresponding to the observation of this Abel inverted profile along the five lines of sights (as viewed by the optical spectrum analyser (figure 1)) may be constituted as shown on figure 2. As already discussed a slight shift of the parabolic profile with respect to the line of sights produces an assymmetric distortion of the staircase profile (figure 2). Calculations have therefore been made for a series of displacements of the basic parabolic profile to derive a family of corresponding staircase profiles, each of which may differ from the others. This then forms the basis of a profile data bank.

These calculations - the formation of staircase profiles corresponding to various displacements of the basic parabolic profiles - have been repeated for a number of parabolic profiles corresponding to different arc radii in the range 0.5 to 2.5 mm.

The members of this family of profiles are then compared with the experimentally measured staircase profile of the 515.3 nm line. Should no match be obtained between experiment and theory the implication is that the profile is truly assymmetric. In the present investigations this occurred only rarely and the analysis of these few profiles was not pursued further. For the remaining profiles the particular continuous parabolic profile corresponding to the experimental staircase was established. The axis temperature was then varied to produce a further series of intensity profiles.

From these latter profiles the radial variation of the emissivity for the 510.5 nm spectral line (which differs from that of the 515.3 nm line, figure 5) was constructed (3). The radial intensity profiles corresponding to these 510.5 nm emissivity profiles are then constructed and the corresponding staircase profiles deduced. These are then compared with the experimentally measured staircase profiles for the 510.5 nm line. The absence of a correlation between the experimental and theoretical profiles again implies the existence of an assymmetric arc column. Otherwise a continuous intensity profile may be determined from the staircase profile transformation procedure.

In this manner smooth profiles for both the 515.3 and 510.5 nm are obtained from the limited number of line of sight measurements. These profiles are already Abel inverted and may therefore be directly used to determine the plasma temperature profile from their ratio (relative line intensity measurement).

5. Experimental Results

Examples of two temperature profiles determined using the analytical approach described above are shown on figure 6. These profiles correspond to current decay rates of 15 A/μs with an upstream pressure of 7.8 bar absolute and an exposure time of 1.6 μs. The broader profile corresponds to an instant 13.4 μs before current zero whilst the narrower profile is for an instant 6 μs before current zero.

The results show clearly the typical radial displacement of the arc column which can occur during the arc extinction phase. In this case the displacement between the two profiles is about 0.8 mm compared with the 4 mm width of the profiles themselves.

Once such profiles have been derived their implications may of course be considered: The particular results shown on figure 6 indicate that the decay of the arc temperature profile during extinction, proceeds through both a decrease in the magnitude of the temperature profile as well as a contraction of its radial extent.

6. Conclusion

It has been shown that useful experimental results may be derived from the analysis of a limited number of line of sight spectral records in combination with high speed photographs using narrow band filtering. Using such an approach, data from a wide range of operating conditions has been processed and analysed. As a result the effect of different operating conditions e.g. peak arc fault current, upstream pressure upon the extinction of the arc discharges has been obtained. These results are allowing theoretical predictions of the arc behaviour close to extinction to be examined more closely in a circuit breaker environment where real operating conditions have not been compromised in order to use more sophisticated investigative methods.

Acknowledgements

The authors acknowledge the support provided by the Science and Engineering Research Council. S.M.I. El-Kholy is also grateful to the Egyptian Government whose support enabled him to participate in the research.

References

1. Lewis, E., Prasad, A.N. and Jones, G.R., 8th Int.Conf. on Gas Discharges and their Applications (1985), Oxford, pp. 31-35.

2. Lewis, E., Shammas, N.Y. and Jones, G.R., 8th Int.Conf. on Gas Discharges and their Applications (1985), Oxford, pp. 35-39.

3. Smith, M.R., Barrault, M.R., Jones, G.R., El Menshawy, M.F., Housby Smith, C. and Jenkins J.E., "Spectroscopic investigations during the current zero period for arcs in an orifice gas flow", University of Liverpool, Electrical Engineering, Arc Research Report, ULAP-T61, 1978.

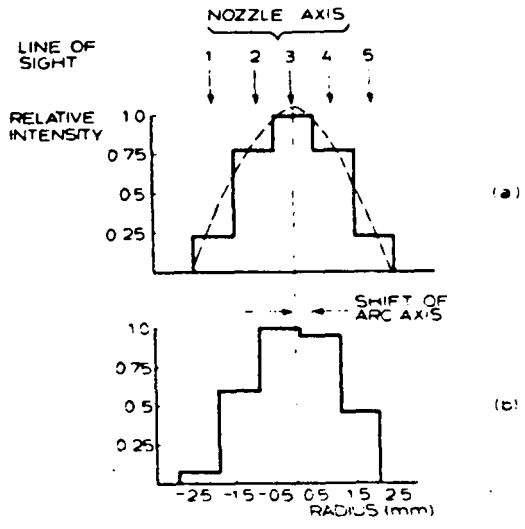

Figure 2. Examples of staircase profiles observed along two fixed line of sights for two different lateral displacements of the arc column.
(a) Lateral shift zero
(b) Lateral shift 0.4 mm.

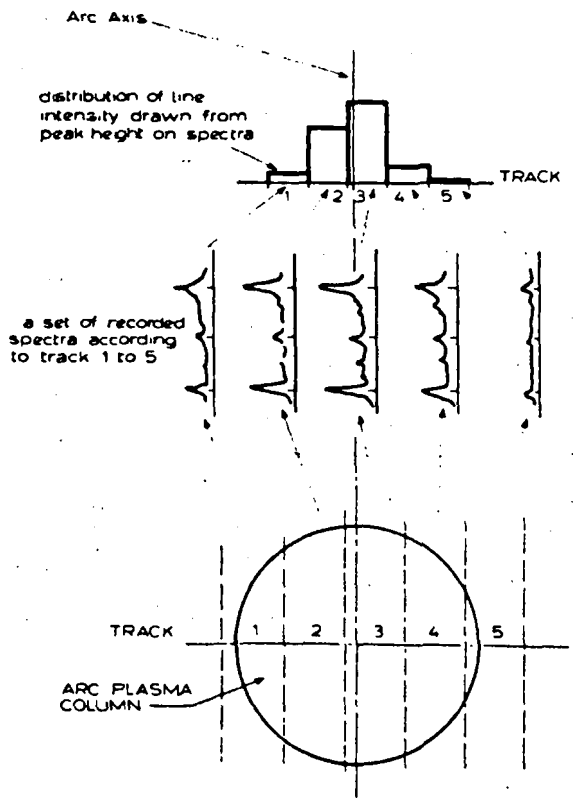

Figure 1 An illustration of recorded spectra and derived intensity distribution.

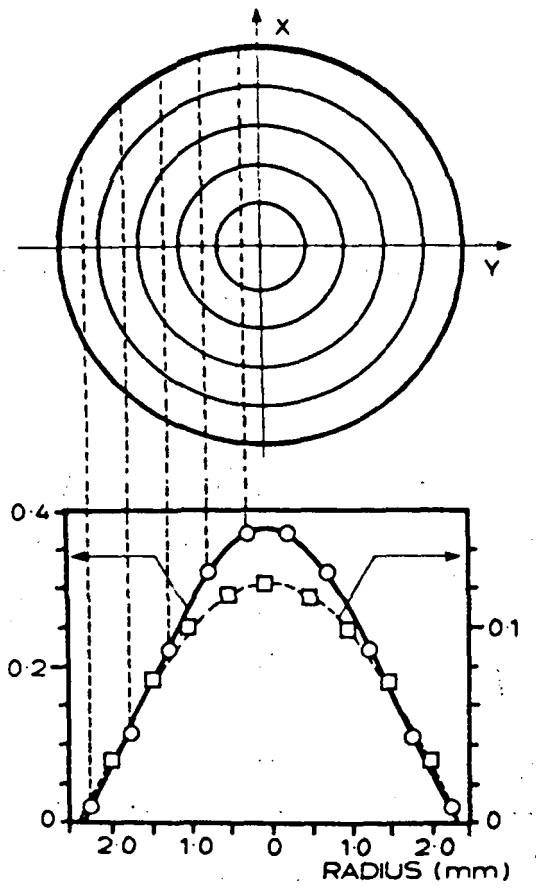

Figure 4. Measured and Abel inverted intensity profiles

O Measured (Arbitrary Units)

Abel Inverted (Arbitrary Units)

$[I(r) = 0.12\ (1 - r/2.35)^2)]$

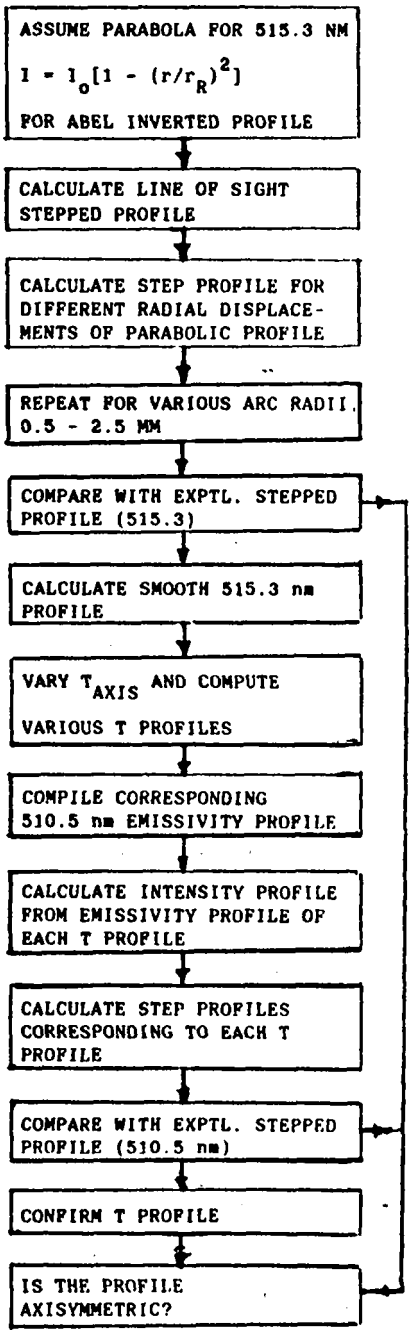

FIGURE 3. FLOW DIAGRAM FOR THE ANALYSIS OF LATTERALLY SHIFTED SPECTRAL LINE DISTRIBUTIONS.

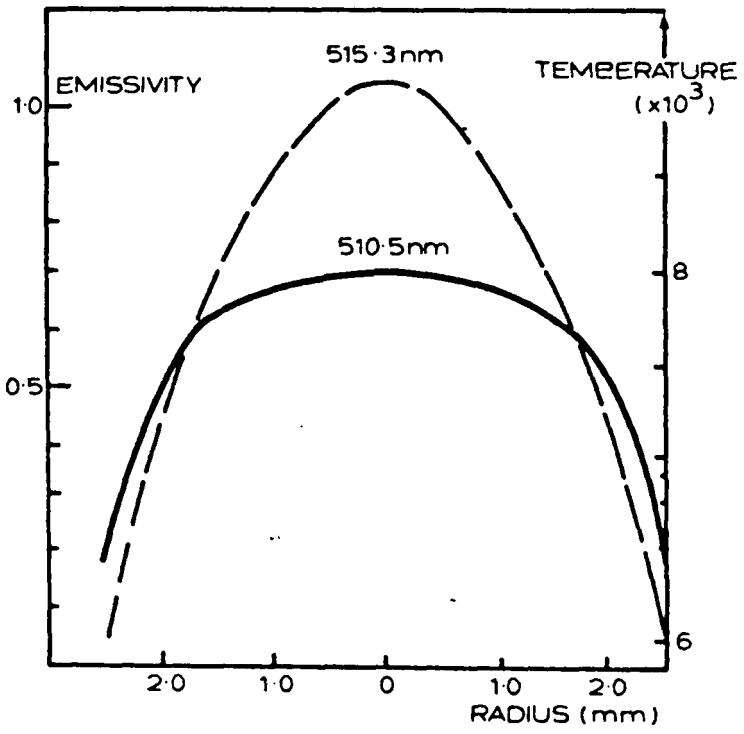

Figure 5. Radial profiles of emissivity and temperature for the two CuI lines 515.3nm, 510.5nm.

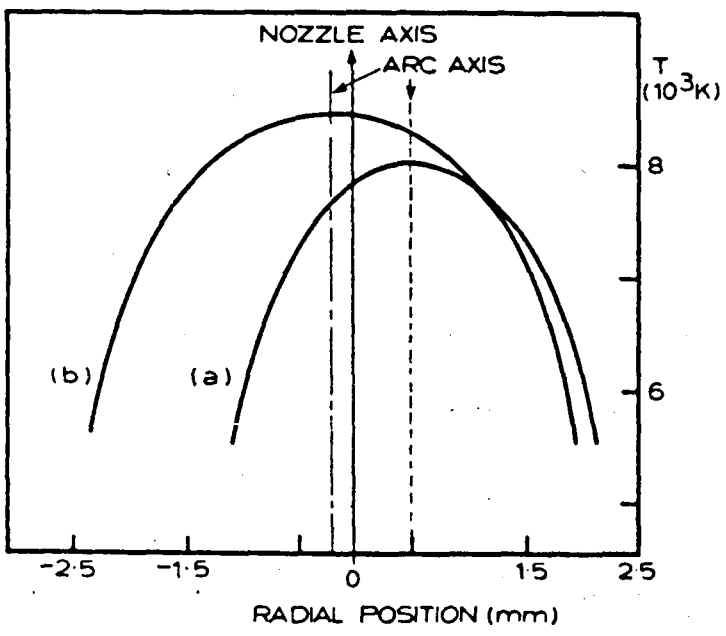

Figure 6. Radial temperature profiles during arc extinction [di/dt = 16A/μs, 7.8 Bar ABS.]

(a) 6μs before current zero

(b) 13.4μs before current zero

POWER DISSIPATING PROCESSES IN THE CURRENT ZERO CIRCUIT BREAKER ARC

Lewis, E.[Φ], Jones, G.R.[Φ], and El-Kholy, S.M.I.[*]

ΦDepartment of Electrical Engineering & Electronics, University of Liverpool, U.K.
*Menoufia University, Egypt.

1. INTRODUCTION

Although extensive experimental investigations have improved our knowledge of the behaviour of electric arc columns in the environment of gas blast circuit breakers, little direct information exists about the arc extinction phase at the end of a half cycle of fault current under real circuit breaker conditions. This is mainly because of the experimental difficulty of obtaining the relevant measurements, and their subsequent analysis. Some progress is now being made in the acquisition and analysis of such information and some results recently obtained are described in this contribution.

The results described relate to optical measurements made at a series of locations along the axis of the nozzle of a model interrupter. The measurements undertaken have involved high speed image converter photographs of the radial extent of the luminous column of the arc and of the maximum intensity of light from the arc axis. Similar photographs have been taken through a narrow band filter centred on a copper I emission line. Total radiation measurements have been taken with a flat wavelength response photomultiplier and spectral distribution measurements have been obtained using an optical spectrum analyser. All these measurements have been taken during the final 10 μs as the fault current flowing through the interrupter decayed naturally to zero. The measurement techniques all had fine time resolution (1 μs or less) to allow the transient changes in the optical signals to be faithfully followed. The basic results of these types of measurements have already been reported by Lewis et al (1985 (i),(ii)), Lewis (1987), Shammas and Jones (1982).

The present contribution seeks to exploit the results of these measurements to gain an improved understanding of the role of various physical processes during the arc extinction phase in the model interrupter.

Experimental Conditions

The experimental conditions investigated are those already described by Lewis et al (1985) (i),(ii)). The arc was confined to burn in a shaped PTFE nozzle of throat crossection 35 mm. Optical access to the arc column was obtained through a series of latteral slots in the nozzle wall, all gas sealed so as not to affect the performance of the interrupter (Lewis et al (1985) (i),(ii)).

The arc column was sustained by an alternating current at a frequency of 78 Hz provided by a ringing LC circuit. The interrupter contacts remained stationary throughout the arcing half cycle in order to avoid any complicated influences due to their movement. Peak currents in the range 34 - 53 kA were investigated with SF_6 as the host arcing medium. The interrupter contacts were made from a sintered mixture of copper and tungsten.

The behaviour of the arc during the few microseconds when the current reduced to zero at the end of the current half cycle has been investigated. Because of the high peak currents which preceed this current zero, substantial electrode evaporation occurs and the electrode material entrained into the arc plasma persists until the current zero instant (e.g. El-Kholy et al (1987)). Indeed the spectral specy monitored during the current zero period is the copper vapour from the upstream contact.

Some typical experimental results for the time variation of the luminous arc crossection and peak emitted intensity on the arc axis are shown on figure 1. Results for two axial locations close to the nozzle throat and separated from each other by an axial distance of 10 mm are shown. Also shown is the time variation of a radially averaged plasma temperature determined from the intensity variation at a wavelength corresponding to a CuI line emission (Lewis et al (1985)). The results shown on this figure correspond to a pre current zero current decay rate of 15 A/μs. Similar results have been obtained for other current decay rates.

Radially resolved temperature profiles have also been derived from spectral measurements with an optical spectrum analyser of the form discussed by El-Kholy elsewhere in these proceedings.

Arc Governing Equations

The power transfer processes which govern the behaviour of the arc plasma column as distinct from the entire thermally affected volume may be summarised as

The Electrical Power Input

$$Q_E = E \cdot i \qquad (1)$$

where E is the electric field strength, i is the instantaneous arc current.

The change in thermal energy stored in the arc plasma

$$Q_s = \frac{d}{dt}\left[\int_o^R \rho(r)h(r)\,2\pi r dr\right] \qquad (2)$$

where ρ,h are the gas density and enthalpy respectively, R is the radius of the arc column.

The Radial heat conduction at the arc column boundary

$$Q_{co} = \int_o^R \frac{1}{r}\frac{\partial}{\partial r}\left[Kr\frac{\partial T}{\partial r}\right] 2\pi r dr \qquad (3)$$

where K is the coefficient of thermal conductivity, T is temperature.

The axial convection in the arc core

$$Q_{ca} = \frac{\partial}{\partial z}\left[\int_0^R \rho(r)h(r)\, v(r)\, 2\pi r dr\right] \qquad (4)$$

where v(r) is the axial component of the flow velocity.

The radiated power loss Q_R may be measured separately as a total power loss and which as such probably underestimates the radiated loss at the arc column boundary on account of the additional absorption which occurs in the surrounding heated gas.

The radial convection losses

$$Q_{CR} = m_e\, h \qquad (5)$$

where m_e is the radial mass flow rate which may be determined from the mass conservation equation (e.g. Pang and Brannen (1979)).

$$\frac{\partial}{\partial t}\left[\int_0^R \rho(r)2\pi r dr\right] + \frac{\partial}{\partial z}\left[\int_0^R \rho(r)v2\pi r dr\right] - m_e = 0 \qquad (6)$$

The power balance for the arc core may then be written

$$Q_E = Q_{CA} + Q_s - Q_{CR} - Q_{CO} - Q_R \qquad (7)$$

A power balance equation for the entire arc gap may also be written, using suitable approximations, in terms of the electrical conductance of the overall gap (g = I/V) and the total electrical power dissipated in the gap (P = IV). If as a result the parameter [(1/g) dg/dt] is plotted against P the intercepts of the tangent to the curve on the (1/g dg/dt) axis yield the Mayr time constants of the gap (e.g. Lewis (1987)). A localised form of the Mayr time constant may be derived by writing g = σA, where A is the crossectional area of the arc column and σ is an average electrical conductivity.

Evaluation of Individual Power Loss Terms

Each of the power loss terms (equations 1 to 5) may be evaluated from the present optical measurements. The evaluations have been made from the luminous crossection results and the mean temperature values of the type shown on figure 1, the temperature profiles of the type given by El-Kholy et al elsewhere in these proceedings and the total radiation results of (Lewis (1987)). Values for the material properties of SF_6 (σ,K,ρ,h, etc.) have been taken from Frost and Libermann (1971). The calculations have been performed at two time intervals before current zero (10 and 7.9 μs) and at two different values of current decay rates (14.2 and 21 A/μs).

The electrical power input per unit arc length (equation (1)) was determined as an average value by dividing the overall arc voltage by the arc length L (i.e. $Q_E = VI/L$).

Evaluation of the change in stored thermal energy (equation (2)) involves a knowledge of the radial temperature profile and its time variation. Since temperature profiles have only been measured at a limited number of instants before current zero reliance has been placed on the use of the more continuously monitored luminous arc records for estimating the time dependence. Thus a knowledge of a single radial temperature profile coupled with the time wise variation of the average arc temperature and crossection (figure 1) allows the term of equation 2 to be evaluated on the assumption that the shape of the temperature profile remains fixed. A pressure of 4 bar was assumed at the nozzle throat (Taylor (1983)).

The power loss due to radial thermal conduction (equation 3) was evaluated from the measured radial temperature gradient at the core boundary.

The power loss due to axial heat convection (equation 4) requires a value of the local flow velocity (v (r)) as well as the evaluation of the axial gradient of the heat flux flow rate (d/dz). Since under normal operating conditions sonic flow was arranged downstream of the nozzle throat (e.g. Taylor (1983)), the gas velocity was assumed sonic across the section of the arc at the nozzle throat during the current zero period under investigation. In order to estimate the axial gradient, use was made of results obtained through two adjacent viewing slots which were 10 mm apart. However since temperature profiles have only been measured at one of these axial locations recourse was made to the high speed photographic records for the second axial position. These results were used to estimate changes in both the luminous crossection of the arc (yielding the diameter of the 6000 K isotherm) and the peak (axial) intensity of the optical emission (indicating approximately changes in the axis temperature through approximate calibration). Account also needs to be taken of the pressure difference between the two axial locations and this was obtained from the axial pressure distribution results of Taylor (1983).

The power loss due to radiative transfer at the arc plasma boundary is difficult to determine since the detailed emission and absorption characteristics of the boundary layer gas are not known. Consequently a lower limit was used corresponding to the total radiation measured remote from the arc column in the wavelength range 400 to 900 nm. These measurements were made simultaneous to the other optical measurements using a calibrated flat wavelength response photomultiplier (Shammas and Jones (1982)).

The radial convection power transfer (equation 5) involves both a time derivative term and an axial derivative term (equation 6). These terms were evaluated in a similar manner to that described above for the axial convection term (equation 4) and the change in stored thermal energy (equation 2).

Discussion of Results

Some results of the calculations of the various power loss terms (equations 1 to 6) as described above are shown on figures 2 and 3. Figure 2 shows the values calculated at two instants (~ 9 μs and 2.2 μs) before current zero following a peak arc current of 40 kA (di/dt = 18.5 A/μs). These results show that the dominant power loss mechanisms during this period are the axial and radial convection (Q_{CA}) (Q_{CR}) with the radiation loss (Q_R) also contributing significantly. On the other hand the thermal conduction term (Q_{CO}) is insignificant contributing only about 1% of the total power loss. Furthermore the convection and radiation losses decrease significantly within the time period studied but the conduction losses remain almost constant.

Also shown on figure 2 are the power input terms Q_E and Q_S (equations (1),(2)). The change in stored thermal energy Q_S is greater than the electrical power input Q_E close to current zero although both are of the same order of magnitude. Of course at current zero itself the electrical input must decrease significantly to zero.

Inspection of the results of figure 2 also shows that the total power input ($Q_E + Q_S$) balances to

within a factor of two, the total power loss (Q_{CO} + Q_{CA} + Q_{CR} + Q_R).

Figure 3 shows the values calculated for the power loss terms as a function of pre current zero current decay rate (di/dt) which for the present work is synonimous with peak current. Values at 14.2 A/μs and 21 A/μs are given, the former corresponding to an instant 10 μs before current zero and the latter at 7.9 μs. Axial convection losses are dominant with radial convection and radiation being significant. Thermal conduction is again insignificant. However the results shown on figure 3 suggest that the axial convection losses decrease by about an order of magnitude as di/dt changes from 14 to 21 A/μs whilst the radiation loss remains almost constant and the radial convection loss increases. Thus at the higher di/dt values the radiation and radial convection losses assume increased importance compared with axial convection.

Also shown on figure 3 are the evaluated power input terms. The electrical inputs at both values of di/dt are of a similar magnitude but the rate of change of stored energy is less by over an order of magnitude at the higher di/dt.

The agreement between the total power input (Q_E + Q_s) with the total losses (Q_{CO} + Q_{CA} + Q_{CR} + Q_R) at both values of di/dt is good so confirming the self consistency of the calculations.

The present experimental results also allow some comparisons to be made for the decay time of the arc plasma column. The arc response has normally been considered in terms of the Mayr time constant, τ, as defined above. These values may be estimated directly from measured electrical parameters (current, voltage) or indirectly from the arc crossection and electrical conductivity (equation (11)). Directly estimated values (e.g. Lewis (1987)) are compared on figure 4 with the indirectly estimated values from the present results using equation (11). The latter were calculated with mean values of electrical conductivity σ corresponding to a mean temperature (figure 1) and with the measured luminous crossections (figure 1). The directly measured time constants (which refer to the behaviour of the arc gap as a whole) and the indirectly estimated values (which refer to the local conditions at the nozzle throat) show good agreement with each other. This implies that the decay controlling section of the arc gap resides at the nozzle throat as has been generally acknowledged.

A futher comparison for the arc recovery time may be made using the power loss terms evaluated on figures 2 and 3. Thus the time required for the dissipation of the energy thermally stored in the arc plasma volume is given by

$$\tau_s = \text{Energy stored} / (Q_{CO} + Q_{CA} + Q_{CR} + Q_R) \quad (8)$$

where the energy stored $= \int_0^R \rho(r)\, h(r)\, 2\pi r dr$

Values of these time scales at different times before current zero are compared with the Mayr time constants on figure 4 and are seen to be self consistent within experimental uncertainties.

Conclusions

The present calculations have shown that the combination of axial and radial convection losses dominate the recovery of the arc plasma column even close to the instant when the fault current passes through zero. As a consequence, these results provide a means against which theoretical models for predicting circuit breaker behaviour may be critically assessed.

References

1. El-Kholy, S.M., Hu Weilin, Prasad, A.N. and Jones G.R. (1987). "Optical spectra of SF_6 circuit breaker arcs during the current zero period", Proc. XVIII Int. Conf. on Phenomena in Ionised Gases (Swansea). p. 688-9.

2. Fang, M.T.C. and Brannen, D. (1979). "A current zero arc model based upon forced convection", IEEE Plasma Trans. PS-7, No. 4. pp. 217-29.

3. Frost, L.S. and Liebermann, R.W. (1971). "Composition and transfer properties of SF_6 and their use in a simplified enthalpy flow arc model", Proc. IEEE 59, PP. 474-85.

4. Lewis, E. (1987) "The thermal properties of an SF_6 circuit breaker arc during the current zero period", Ph.D. Thesis, University of Liverpool.

5. Lewis, E., Shammas, N.Y. and Jones, G.R. (1985) (i). "The current zero SF_6 blast arc at high di/dt", Proc. Int. Conf. on gas discharges and their applications, (Oxford). pp. 35-8.

6. Lewis, E., Prasad, A.N. and Jones, G.R. (1985). (ii) "Current zero spectroscopy of a high power SF_6 circuit breaker arc", Proc. Int. Conf. on Gas discharges and their applications, (Oxford), pp. 31-4.

7. Shammas, N.Y. and Jones, G.R. (1982), "Total radiation losses from SF_6 circuit breaker arcs during the current zero period simulated with current zero ramps", University of Liverpool, Arc Research Report ULAP-T70.

8. Taylor, S. (1983) "Data acquisition and analysis of circuit breaker arc measurements", M.Eng. Thesis, University of Liverpool.

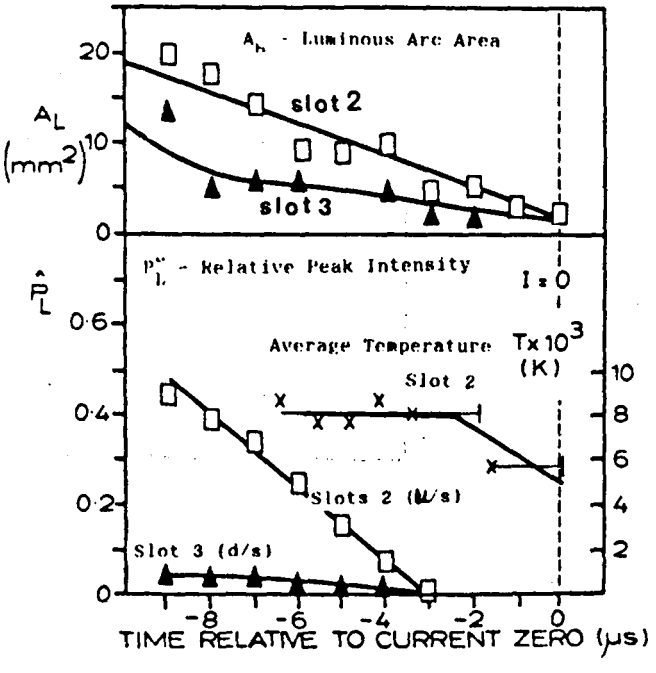

Figure 1 Time variation of arc column properties (di/dt) = 15 A/μs).

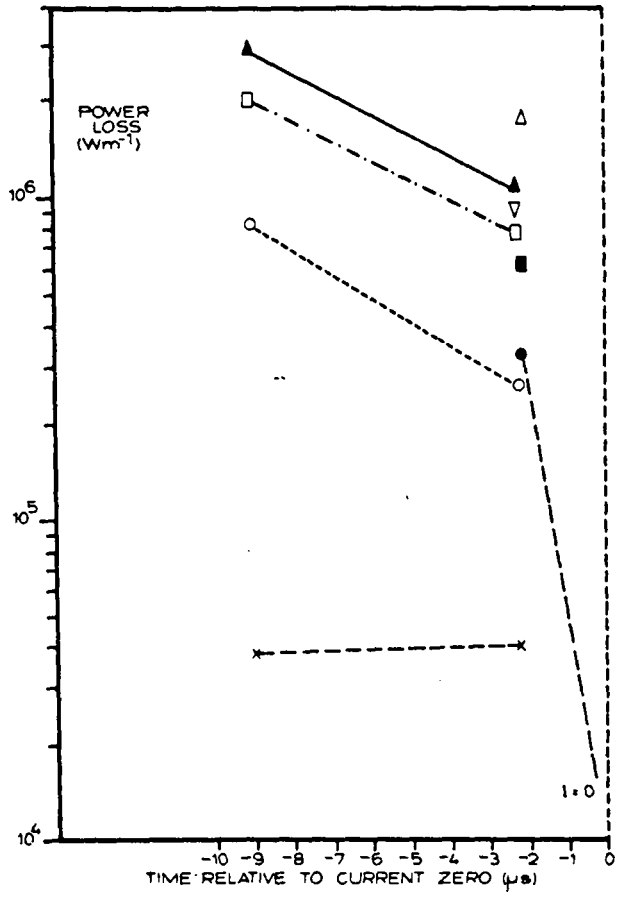

Figure 2 Time variation of power loss tems
Power Input: ● Q_E, # Q_S, ▲ Total
Power Loss : X Q_{CO}, □ Q_{CA}, ▽ Q_{CR},
O QR, Δ Total.

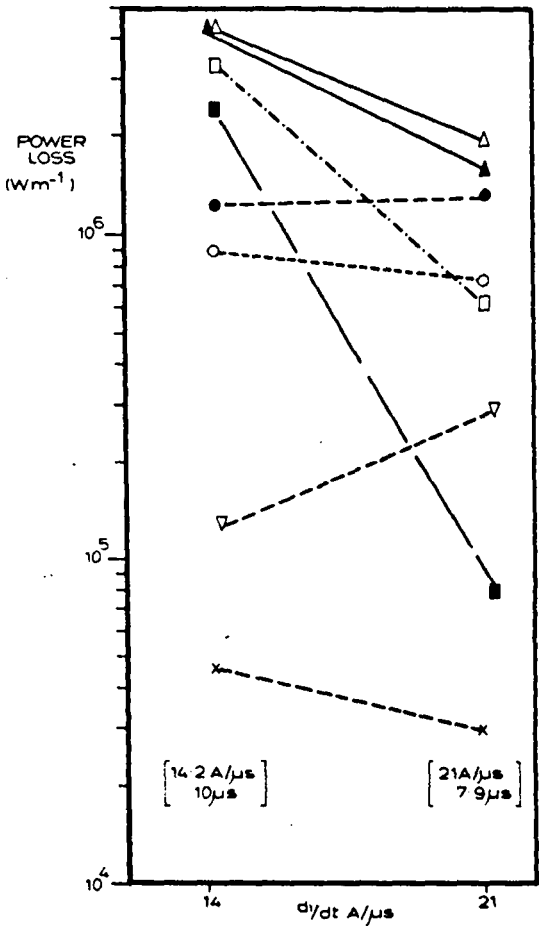

Figure 3 Power loss terms vs dI/dt
(Key as for Figure 2).

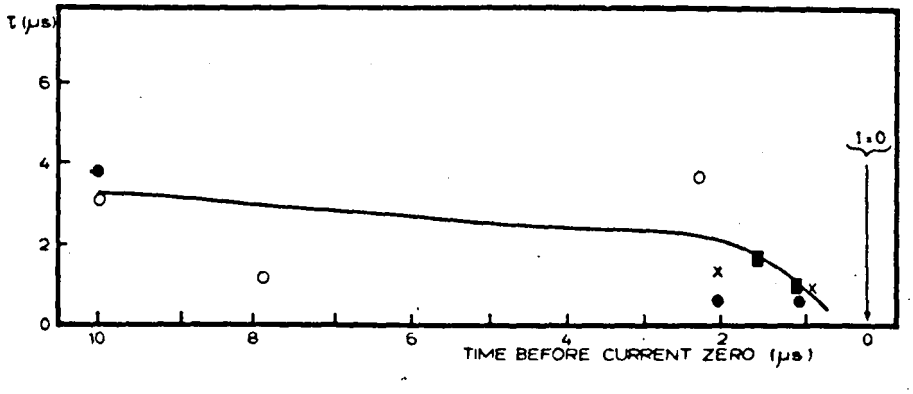

Figure 4 Mayr time constants (τ) and energy dissipation time scales
● Mayr time constants, low dI/dt
■ Mayr time constants, high dI/dt
O Present results
X Lewis (1987).